UNIVERSITÀ DEGLI STUDI DI MILANO
SCUOLA DI DOTTORATO
TERRA, AMBIENTE E BIODIVERSITÀ

Dottorato di Ricerca in Scienze della Terra
Ciclo XXV

The character and spatial distribution of Holocene and Pleistocene hydrothermal travertines (Albegna Valley, southern Tuscany, central Italy).

Ph.D. Thesis

Federica Barilaro
Matricola R08690

Tutore	**Anno accademico**	*Coordinatore*
Dr. Giovanna Della Porta	**2011/2012**	**Prof. Elisabetta Erba**

Alla mia famiglia,

motivo di orgoglio e

grande punto di forza.

Contents

Chapter 1

General Introduction: The character and spatial distribution of Holocene and Pleistocene hydrothermal travertines (Albegna Valley, Southern Tuscany, Central Italy).

Scientific interest in hydrothermal spring deposits has been low during the last decades. Renewed attention in the products and processes of continental carbonate formation has been promoted by the recent hydrocarbon discoveries in non-marine carbonates in the South Atlantic. These discoveries have generated a large interest for both the oil industry and the earth scientists with a consequent awareness that non-marine carbonate depositional processes lack a clear understanding. The understanding of continental carbonates faces many challenges when confronted with the knowledge and the fundamental concepts on marine carbonates. In particular there is the need of improving the knowledge regarding the mechanisms and the conditions that lead to the precipitation of continental carbonates and concerning the development of non-marine depositional models applicable to subsurface. Other issues that require revision are related to the terminology currently in use in the available literature about continental carbonates. In fact, in the published literature, an adequate textural classification of non-marine carbonates is lacking. Standardized definitions of terminology and distinguishable parameters for the different variety of continental carbonates have still to be developed.

Of the different terrestrial environments in which carbonate deposits precipitate, this research focuses on limestone accumulated in hydrothermal systems, defined travertine (sensu Pedley, 1990; Ford and Pedley, 1996). One of the most controversial issue in the study of hydrothermal travertine deposits is the mechanisms of precipitation involved in the formation of these continental carbonates. univocal generally accepted terminology based on the classical classifications of carbonates able to provide information about the components and texture of the

fabric types and also on the depositional mechanisms that acted during their deposition is lacking in literature. Thus, in order to improve the understanding of the nature, the processes of formation, the products, porosity types, diagenetic pathways and depositional environments of hydrothermal travertines, a multi-scale study of the Albegna Valley (Southern, Tuscany, Central Italy) travertine deposits is presented. This study has the purpose a) to propose a revised terminology for travertine fabrics, b) to suggest univocal new classification of the carbonate fabrics based on the classical terminology of carbonates (cf. Dunham 1962; Embry and Klovan, 1971), and c) to provide the first comprehensive evaluation of the reservoir properties (porosity and permeability) of hydrothermal spring carbonates.. The investigation of this research focuses on a fossil Pleistocene travertine unit, well exposed along an active quarry (situated on the Pianetti terrace of the Albegna Valley), and on an actively forming travertine deposit at Bagni di Saturnia (12 km far-away from the fossil counterpart). The goals of this project, funded by BG Group (UK), Repsol (Brasil) and Statoil (Norway), are several and range from academic to economic. The academic goals include: 1) the definition of carbonate fabric varieties, their diagenesis and porosity; 2) the understanding of abiotic vs. microbially induced processes that control calcium carbonate precipitation and their link to the fabric types; 3) the evaluation of the relationship between water chemistry and inorganic and biogenic carbonate fabrics in hydrothermal settings, and 4) the definition of the depositional settings, their fabric character and spatial distribution. From the economic point of view, the travertine research in the Albegna Valley may essentially be considered as guide to help to understand the relationship between depositional environment, diagenesis/porosity and the reservoir properties of continental travertines as a guide to the South Atlantic reservoirs.

The research of the Albegna Valley travertine will be summarized in the following chapters. Chapter 2 gives a brief summary about general concepts of travertine carbonates based on the review of the published literature. In Chapter 3, the background information about the geological setting of the study area is presented including the distribution and description of hydrothermal travertine deposits at Albegna Valley. Chapter 4 focuses on the Pleistocene Pianetti travertine deposit. Travertine units, architectural pattern, fabric types (comprising also micro-fabrics and nano-scale descriptions) and their relative porosity and permeability, diagenesis, geochemical composition and isotopic values are described and interpreted.. In particular this chapter includes a proposed hydrothermal travertine classification based on the variety of fabric types, which appear strictly related to an interplay between abiotic and biotic processes, depositional

environments and diagenesis. In addition, the first comprehensive evaluation of porosity and permeability of hydrothermal travertines is included in this chapter.

Chapter 5 investigates the formation of present-day travertines at Bagni di Saturnia. Analyses and successive interpretations of the chemistry of flowing water, depositional systems, microbial mats and microbial community, fabric types (including nano-scale observations), porosity and geochemistry of the present-day carbonate precipitates are presented. Bagni di Saturnia ecosystem provides an important opportunity to study the biogeochemical and physical interactions that produce travertine deposits similar to those of the past and improve the interpretation of ancient travertines. A model of carbonate precipitation in hydrothermal setting is proposed on the basis of up-to-date studies about marine and non-marine microbialites (biologically induced and influenced carbonates). In hydrothermal systems, a complex interaction between depositional environments and physicochemical and biotic processes drives carbonate precipitation and influences the development of fabric types.

The implications and final conclusions of this research are summarised in Chapter 6.

Chapter 2
Hydrothermal travertine: general concepts based on literature reviews

2.1 Introduction

The literature available about continental carbonates requires a standardization of the confused terminology currently in use, lacks of parameters to distinguish clearly between ambient temperature cool-water deposits (tufa), hydrothermal deposits (travertines) and lacustrine deposits. The available literature does not provide an adequate textural classification of non-marine carbonates. In addition, the mechanism of mineral precipitation that have been proposed to explain continental carbonate and in particular travertine formation is still debated. In order to improve the understanding of the nature, the formation processes, and the products of continental carbonates and with the aim of acquiring the appropriate terminology and classification schemes, an extended literature research has been performed. This was fundamental for the progress of the research presented in this study. With the aim to capture the essential characters of the studies available in the published literature, a database of selected papers about non marine carbonates has been organized (Appendix in DVD). This database is includes a selection of publications relative to case studies of Recent and ancient hydrothermal travertine and fresh water calcareous. This chapter contains a selected information relative to the general concept of hydrothermal travertines deriving from the literature review. Some aspects mainly related to mode of travertine precipitation, depositional systems and geochemistry will be discussed in detailed in the following chapters.

2.2 Terminology clarification

There is lack of clarity regarding the terminology applied to describe continental carbonates. In fact, several definitions of travertine can be found in the literature. The term “travertine”, in its

broadest sense, refers to all non-marine carbonates formed around seepages, springs, along streams and rivers, occasionally in lakes and consisting of calcite or aragonite, of low to moderate inter-crystalline porosity and often high mouldic or framework porosity within vadose or occasionally shallow phreatic environmental (Pentecost, 1994, 2005). Another definition distinguishes travertine and calcareous tufa on the basis of the physical properties of calcium carbonate-rich water from which these deposits are precipitated. Travertine and calcareous tufa deposits are then considered the product of calcium carbonate precipitation under thermal-hydrothermal and near ambient temperature conditions, respectively, in continental areas (Pedley, 1990; Ford and Pedley, 1996; Faccenna et al., 2008; Gandin and Capezzuoli, 2008). According to Pedley (1990) and Ford and Pedley (1996) the term travertine addresses the product of calcium carbonate precipitation under hydrothermal flowing water in continental areas. In particular, travertines are here defined as continental calcium carbonate deposits precipitated by warm to hot water (> 20°C) supersaturated with respect to calcium bicarbonate, degassing CO_2 while out-flowing from a tectonically controlled hydrothermal vent. The wide range of depositional settings where hydrothermal vents occurred includes both sub-aerial flowing-water systems and subaqueous lacustrine settings.

2.3 Fundamental reactions and processes that govern travertine precipitation

The fundamental reactions that govern calcium-carbonate precipitation of flowing-water system of hydrothermal travertines are the following (Pentecost, 2005):

$$1) CaCO_3 + CO_2 + H_2O \Leftrightarrow (HCO_3^-)_2 + Ca^{2+}$$

$$2) CO_2 + H_2O \Leftrightarrow H_2CO_3 \Leftrightarrow H^+ + HCO_3^-$$

Precipitation of calcium carbonate in spring systems usually occurs when CO_2 degasses from CO_2-rich groundwater. Most of the hydrothermal travertines form from the degassing of surfacing carbon dioxide-rich groundwater containing > 2mmol L^{-1} (ca. 80 ppm) calcium (Pentecost, 2005). When groundwater, rich in dissolved carbon dioxide, attacks carbonate rocks, it forms a solution containing calcium and bicarbonate ions (Eq. 1). This solution emerges on the surface through faults and fractures; the calcium bicarbonate rich-water entering in contact

with the atmosphere loses carbon dioxide and precipitation occurs. Travertine deposition is the reverse of the reaction in Eq. 1. Different linked factors control calcium carbonate precipitation. The rate of CO_2-degassing from spring water is controlled by: 1) the pCO_2 of the spring water when discharged at its vent (Herman and Lorah, 1987, 1988; Chafetz and Lawrence, 1994); 2) the area and depth of water on the discharge apron (Dandurand et al., 1982); 3) the amount of water agitation and turbulence (Jacobson and Usdowski, 1975; Herman and Lorah, 1988); 4) aeration, jet-flow, and low-pressure effects (Zhang et al., 2001).

Carbon dioxide loss from water leads to an increase in pH due to the consumption of H^+ and HCO_3^-, and to an increase in CO^{2-}_3 favouring carbonate precipitation (Arenas et al., 2010).

Mechanical CO_2 loss is considered the most important CO_2 removal agent that contributes to calcite precipitation. Turbulent flow and agitation over the lips of pools on discharge aprons, for example, commonly cause increased CO_2 degassing that raises the saturation levels and thereby promotes $CaCO_3$ precipitation at the pool margins (Jones and Renaut, 2010). Aeration and jet-flow effects are significant contributors to CO_2 loss (Chen et al., 2004). Evaporation is induced by high temperature of the water at the air/water interface and it can be an important process in CO_2 transfer (Pentecost, 2005; Jones and Renaut, 2010). Nevertheless, precipitation is not purely a consequence of physical processes; calcium carbonate precipitation might be biologically influenced by the presence of microbial biofilms, common in such high temperature environments. Precipitation of calcium carbonate has been proven in association with the activity of complex microbiological communities ('biofilms') in a wide variety of contexts (Pedley, 1990; Buczynski and Chafetz, 1991; Reid et al., 2000; Riding and Liang, 2005; Andrews and Brasier, 2005; Benzerara et al., 2009; Dupraz et al., 2009). Biological precipitation of carbonates might be the result of activity of different groups of microorganisms (Wolicka and Borkowski, 2008). This process can be induced by photosynthesis, which is conducted by cyanobacteria and phototrophic bacteria. Photosynthetic CO_2-uptake and other physiological activities of plants (e.g. HCO_3^- assimilation) also enhance calcite precipitation, but appear to contribute to a lesser extent as compared to physico-chemical processes (Pentecost, 1996; Merz-Preiß and Riding, 1999; Pazdur et al., 2002). In anaerobic condition, the activity of sulphate reducing bacteria may be responsible for the formation of carbonates (Dupraz and Visscher, 2005). Bacterial colonies settle in lower energy microhabitats/niches sheltered from the tractive flow, and incorporate carbonate particles in the mucilaginous biofilm (Extracellular Polymeric Substances, EPS) they produce (Merz-Preiß and Riding, 1999). EPS provide a cohesive matrix where many biogeochemical reactions take place. Temperature is one of the factors with most influence on

the seasonal growth of plants and hence on photosynthetic process (Vazquez-Urbez et al., 2009). Plants provide sites for calcite nucleation and precipitation, and for trapping calcite particles.

Travertine precipitation can also be related to CO_2 ingassing rather than outgassing. As suggested by Pentecost (2005), these uncommon travertines are formed by the following reaction that occurs between atmospheric carbon dioxide and hyperalkaline groundwater:

3) $Ca(OH)_2 + CO_2 = CaCO_3 + H_2O$

This groundwater most frequently occurs in regions undergoing serpentinization (O'Neil and Barnes, 1971) or those in contact with natural or industrially produced calcium hydroxide (Pentecost, 2005). Travertine precipitation confined to alkaline and saline lakes is observed when groundwater rich in calcium mixes with alkaline surface water. This process is described by Pentecost (2005) as groundwater alkalization and occurs when hydroxyl ions in the lake water react with bicarbonate (HCO_3^-) to form carbonate (CO_3^{2-}) followed by precipitation of calcium carbonate. The reaction related to the ground water alkalization is the following:

4) $Ca(HCO_3)_2 + OH^- = CaCO_3 + HCO_3^- + H_2O$

2.4 Travertine mineralogy

Thermal travertines are an archive of CO_2 sources and sinks in hydrothermal systems (Moore et al., 2005). The most abundant travertine deposits are carbonate bodies, although silica and minor amounts of Fe-Mn oxides are also common (Gibert et al., 2009).

Travertine deposits are variably formed by aragonite and calcite. The mineralogy of these deposits is controlled by a complex set of parameters that may act alone or combined. Calcite has been commonly attributed to precipitation from water temperature below 40-45°C while aragonite forms at temperature > 40-45°C. However, studies conducted by Jones and Renaut (1995, 1996) demonstrate that calcite precipitation occurs also from water with temperature of < 90°C; this could be related to the high turbulence of the flow water that increases the degassing and the saturation level. Aragonite precipitation, as opposed to calcite, has generally been associated with water that has attained very high levels of supersaturation with respect to $CaCO_3$ (Jones and Renaut, 2010). Aragonite also forms at considerable low temperatures under condition of rapid precipitation from highly supersaturated waters (Chafetz et al., 1991; Chafetz et al., 1998). Similarly, the precipitation of aragonite instead of calcite in lakes and cool springs has commonly been attributed to a high Mg/Ca ratio (Müller et al., 1972; Kelts and Hsu, 1978;

Popp and Wilkinson, 1983). The Mg/Ca ratio needed to trigger aragonite rather than calcite precipitation is debatable. Folk (1994) suggested that aragonite would precipitate from any water that has a Mg/Ca ratio 2:1, irrespective of water temperature.

Silica is widespread in hydrothermal systems. It can be supplied by thermal water. The silica supersaturation of the thermal fluid necessary for silica precipitation is achieved by its cooling when it reaches the surface. Calcite travertine co-precipitates with silica in some hydrothermal springs (Jones et al., 1996), but silicification does not always occur. Hydrothermal silica is deposited by the cooling and evaporation of Si-rich solutions, usually neutral in pH and low in Ca (Pentecost, 2005). Mixing and changes in the pH of hydrothermal water, evaporation and/or steam loss after discharge could cause the silicification of continental carbonates formed in hot springs (Jones and Renaut, 2010). Silicification might occur during diagenesis. Melezhik et al. (2004) described hot-water travertines with dolomite travertine crusts and mounds separated by internal dissolution surfaces, all veneered with 1–5 mm-thick crystalline silica sinters. The corrosive relationships between the dolomite travertines and the lower contact of the silica sinters, the desiccated and fragmented silica sinters, and the interlayered detrital sediments suggest silicification occurred prior to burial (Jones and Renaut, 2010).

2.5 Travertine fabric types

Several studies about travertine can be found in the published literature. However, the first innovative study on the petrography and origin of travertine deposits was by Chafetz and Folk (1984). In a second phase, authors such as Guo and Riding (1992), Guo & Riding (1998), Chafetz and Guidry (1999), recognized and described travertine fabric types (Fig. 2.1) that can be regrouped as follows.

Crystalline crust travertine: generally dense, dazzling white, and coarsely fibrous crusts (Fig. 2.1A) consisting of elongate (feather) calcite crystals perpendicular to the depositional surface (Guo and Riding, 1998). These calcite crystals are termed ray crystals (Chafetz and Folk, 1984; Folk et al., 1985). Crystalline crusts typically form thick, laterally extensive deposits on slopes and cliffs and reflect rapid precipitation from fast flowing waters (Folk et al., 1985; Guo and Riding, 1992).

Shrub travertine: This fabric type consists of porous travertines dominated by small shrub-like growths (Chafetz and Folk, 1984; Pentecost, 1990). Shrub travertine (Fig. 2.1B) is characterized by an upward expanding, irregular dendrite morphology (Chafetz and Meredith, 1983; Chafetz and Folk, 1984; Guo and Riding, 1994, 1998; Chafetz and Guidry, 1999) and typically grows in terrace pools and depressions (Guo and Riding, 1998). Such shrubs, formed of micrite and spar-rhombs or needle crystals (Guo and Riding, 1994, 1998), have been attributed to abiogenic (Pentecost, 1990) and biogenic (Chafetz and Meredith, 1983; Chafetz and Folk, 1984; Chafetz and Guidry, 1999) precipitation processes. Mn- and Fe-rich black shrubs have been found in travertines in southern Morocco (Chafetz et al., 1998). Chafetz and Guidry (1999) distinguished three kinds of shrub: bacterial, crystal and ray crystal. These range from highly irregular forms (bacterial shrubs) to features that display regular geometric patterns (crystal shrubs and ray-crystal crusts). The bacterial and crystal shrubs were considered to be bacterially mediated while ray crystal crusts were thought to be formed by a combination of bacterial and abiotic processes. Petrographic (Chafetz and Folk, 1984; Guo & Riding, 1994) and stable isotope studies (Guo et al., 1996) support the view that they formed mainly under microbial influence, but with a component of inorganic precipitation. Pentecost (1990) proposed an abiotic origin for all the shrub formation.

Pisoid travertine: Travertine pisoids (Fig. 2.1C) range in shape from spherical, to irregularly rounded, to irregular (shrub-like, hemispherical), depending on water energy and microbial involvement (Guo and Riding, 1998). Three types can be distinguished based on the microstructure ranging from concentrically laminated (Folk and Chafetz, 1983), radial shrub (Folk and Chafetz, 1983) to stromatolitic mammillated (Guo and Riding, 1998). Concentrically laminated pisoids form in splashing and turbulent water (Guo and Riding, 1998). They are rarely transported and show little abrasion. This fabric has been regarded as inorganic (Folk and Chafetz, 1983), but formation of this and the other types of pisoids may be partly influenced by biotic processes. Radial shrub pisoids have a distinctly different dendritic microstructure, resembling that of the stratiform shrub travertine (Guo and Riding, 1998). Radial shrub pisoids form in intermittently agitated microterrace pools where they are closely associated with abundant bacteria, cyanobacteria and diatoms (Guo and Riding, 1994). Stromatolitic mammillated pisoids have mainly been found in older travertines and show irregular nodular outgrowths (Guo and Riding, 1998). These may be mediated by cyanobacteria (Kosun et al., 2005).

Paper-thin raft travertine: Rafts formed of calcite or aragonite develop at the water surface of stagnant pools where surface degassing of CO2 causes an increase in saturation that leads to calcite or aragonite precipitation (Folk et al., 1985; Chafetz et al., 1991; Guo and Riding, 1998). Paper-thin rafts (Fig. 2.1D) are thin, delicate, brittle crystalline layers occurring widely as a few individual sheets representing water films (Guo and Riding, 1998). Dense concentrations are more localized, representing accumulations on the floor of small stagnant pools and sheets of still water.

Coated bubble travertine: Coated bubble travertine (Fig. 2.1E) consists of individual bubbles preserved by rapid precipitation on gas bubbles in standing water (Guo and Riding, 1998). The gas bubbles are produced by microbial activity in microbial mats or sediment on the floor of spring pools (Chafetz and Folk, 1984; Chafetz et al., 1991).

Reed travertine: Guo and Riding (1999) suggested that reed travertine (Fig. 2.1F) consists of plant stems and roots coated by micritic travertine. These create cylindrical moulds up to 3 mm in diameter. The interiors mostly remain empty or are partly filled by fine sediment or spar crystals, and part of the original outer tissue may be replaced by micrite. Reed preservation as moulds is largely responsible for the high porosity of these deposits.

Lithoclast travertine: It is typically dark grey or brown and dominated by silt sand grade detritus (Fig. 2.1A) derived from the break-up of adjacent light-coloured travertine slope deposits, such as crystalline crust and shrub travertine. Lithoclast travertine also contains a high proportion of reed or other plant fragments and, locally, gastropods, ostracodes and quartz silt matrix (Guo and Riding, 1998).

The described fabric types characterize the different travertine deposits and depositional systems.

2.6 Travertine deposits and depositional systems

Travertine deposits are preferentially located along fracture lineaments, either immediately above extensional fissures or in the hanging walls of normal faults (Hancock et al., 1999). Structurally controlled thermal springs aligned along the traces of relevant faults represent the superficial display of a deep geothermal system (Brogi et al., 2010). In those areas characterized by anomalous geothermal gradients, faulting guaranties the opening of fractures in the bedrock favouring the circulation and upwelling of hydrothermal fluids (Bellani et al., 2004

andreferences therein). For this reason, fault intersections are considered to be particular favourable sites for spring (Pecsi et al., 1982). Hancock et al. (1999) suggested that most travertine bodies accumulate close (within 1-2 km) to active faults. According to these authors, the sites of many travertine deposits coincide with the locations of either step-over zones (relay ramps) or the lateral tips of fault zones; both these settings are those within which complex strains can lead to the development of networks of intersecting tensional fissures that enhance the sub-surface flow of hydrothermal fluids.

The occurrence of thermal springs can produce different travertine body morphologies (Fig. 2.2). According to the location and the type of the orifices (aligned or punctual) the discharge of the calcium carbonate rich-water builds ridge, mound, pinnacle and tower-shaped carbonate deposits (Fig. 2.2). However, Hancock et al. (1999) suggest that the morphology of travertine deposits overlying tensional fissures is controlled by the rheology of the underlying materials. The morphology of travertine deposits can be strictly controlled by the geometric setting and kinematics of faults and related damage zones (Altunel and Hancock, 1993a, Hancock et al., 1999; Brogi and Capezzuoli, 2009; Brogi et al., 2010).

Travertine deposits accumulate around springs along fractures such as joints or faults forming elongate, wedge-like structures termed fissure ridges (Pentecost, 2005). Fissure-ridge (Fig. 2.2A) travertines comprise vertical fissures occupied by banded travertine, and inclined (from 5° to 90°) bedded travertine flanking the fissures (Bargar, 1978; Chafetz and Folk, 1984; Pentecost, 2005). Ridges can be straight or curved in plan view and range from about 100 m to 2000 m long, 5 m to 400 m wide and 1 m up to 20 m high (Hancock et al., 1999; Ozkul et al., 2002; Pentecost, 2005). A fissure-ridge expresses a line of springs situated along an extensional fracture. Hancock et al. (1999) suggested that fissure-ridges develop where fissures cut bedrocks at the surface.

Travertine mounds (Fig. 2.2C) consist of travertine domes ranging from a few centimetres up to 100 m in height and from a few centimetres up to 90 cm in diameter, situated at spring orifices. Mounds are the result of instantaneous precipitation from thermal spring water that issues from point sources within segments of active faults and then flows down a slope to build a mound of travertine (Hancock et al., 1999). Travertine mounds can be characterized by low angle walls. These walls in general vary from smooth or stepped morphologies. However, Pentecost (2005) suggested that many mounds are of low relief and consist of sheet-like layers of travertine with a dip of just a few degrees. In these cases, the mound outlines become irregular, presumably in response to minor differences in ground level surrounding the springs.

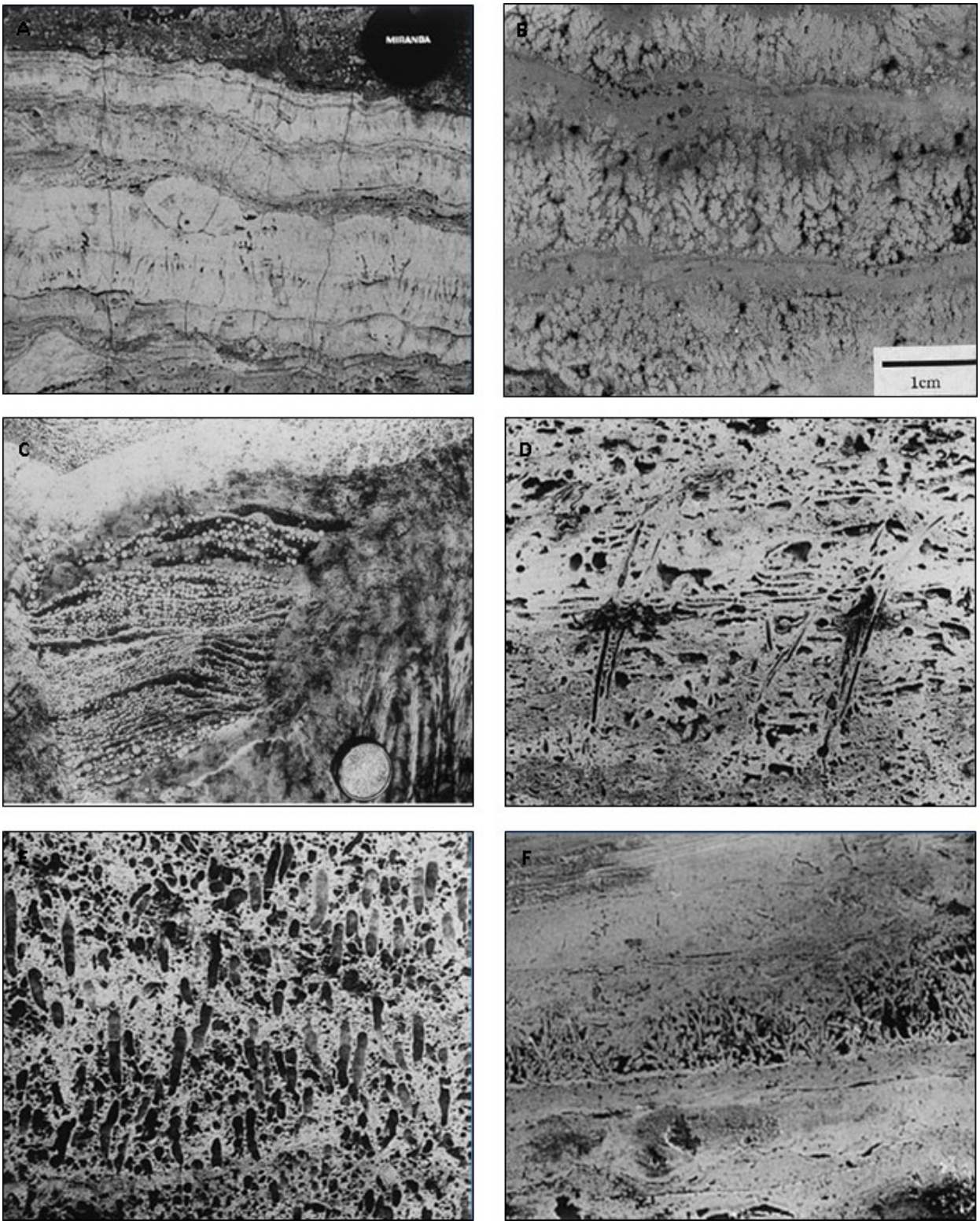

Fig. 2.1 Main travertine fabric types. A) Dense crystalline crusts, typical of rapid precipitation on slopes, overlain by lithoclast travertine. Lens cap 6 cm (from Guo and Riding, 1998). B) Three layers of bacterial shrubs separated by laminae of silt-sized micritic aggregates. Each shrubs/micritic aggregate pair is a yearly accumulation (from Chafetz and Guidry, 1999). C) Pisoid travertine in small terrace pool. Pisoids are spherical and concentrically laminated in this highly agitated environment. Lens cap 6 cm (from Guo and Riding, 1998). D) Paper-thin rafts associated with reeds. Initially, rafts are thin delicate sheets precipitated on the surface of still pools. Field of view 12.5 cm (from Guo and Riding, 1998). E) Coated bubble travertine characterized by a hollow centre and a dense micritic rim. Field of view 20 cm(from Guo and Riding, 1998). F) Reed travertine. The precipitation of finely crystalline carbonate preserves reeds and coarse grasses as moulds that locally form *in situ* clumps. Field of view 80 cm (from Guo and Riding, 1998).

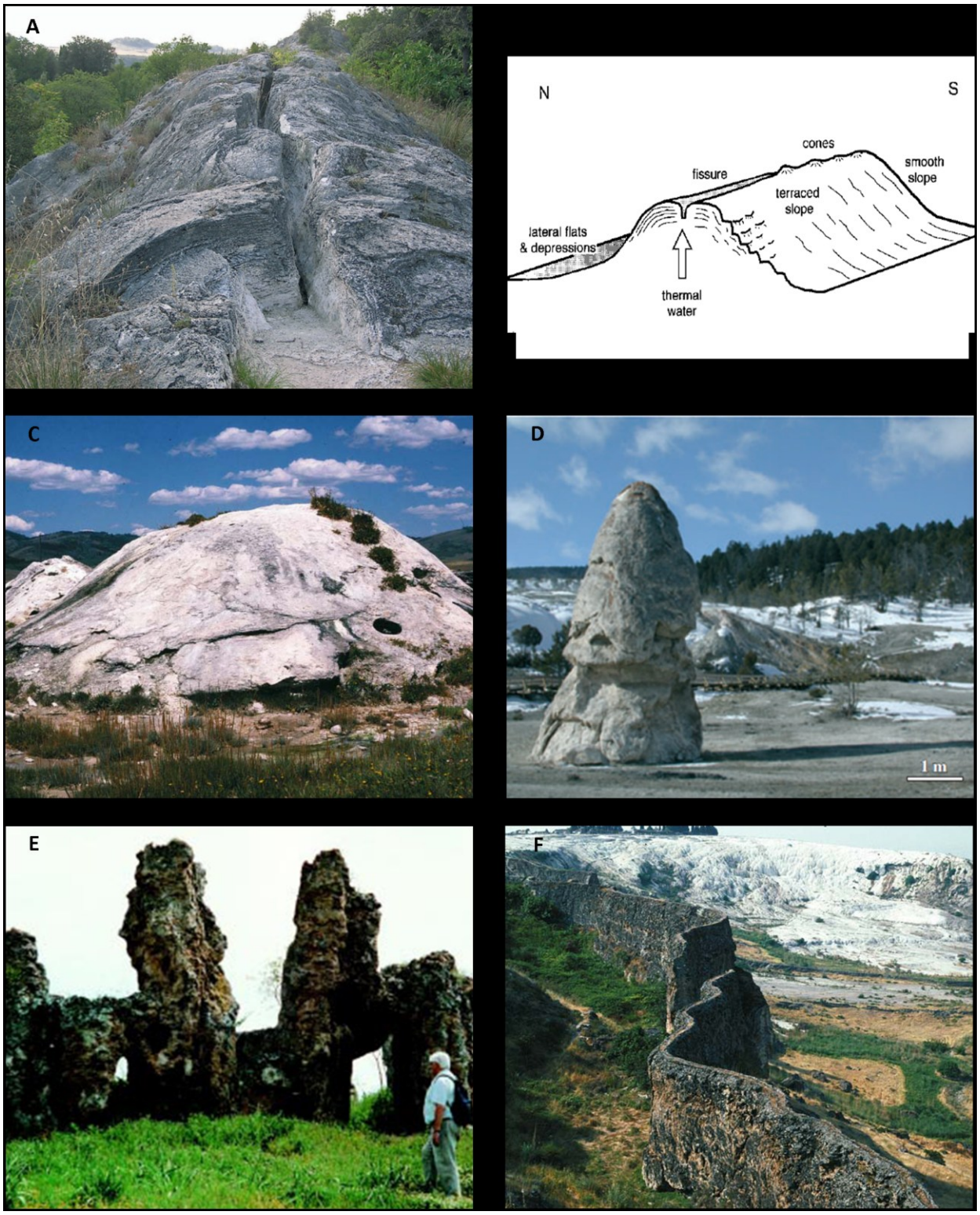

Fig. 2.2 Main travertine deposit morphologies. A) Fissure ridge, Rapolano Terme, Tuscany, Italy. (from Pedley, 2009). B) Schematic section of the Terme di San Giovanni fissure ridge (up to 10 m high and an overall width of 20- 40 m) at Rapolano Terme, Tuscany, Italy. Terraced slope and smooth slope depositional systems characterize the walls of the of fissure ridge. Lateral flat and depression are adjacent to the fissure ridge (from Guo and Riding, 1999). C) A pair of small (5 m high) recently active mounds near Auburn, Wyoming, USA. (from Pentecost, 2005). D) Pinnacle at Mammoth Hot Springs (from Fouke, 2011). E) Towers rising above an area underlain by unconsolidated sediments between Lakes Volvi and Lagada, northern Greece (from Hancock et al., 1999). F) One of the self-built channels at Pamukkale, Turkey. Note break in the canal wall caused by earthquakes and the main travertine mound in the background (from Pentecost, 2005).

Travertine pinnacles (Fig. 2.2D) consist of particular cone-shaped structures formed by instantaneous precipitation from springs emerging with hydrostatic pressures sufficient to build domes more developed in height than in width; these pinnacles can reach heights exceeding 20 m.

Tower-shaped travertines (tufa towers) (Fig. 2.2E) are similar in morphology to spring pinnacles. The travertine tower deposits originate at sub-lacustrine thermal springs; these travertine structures usually result from the mixing of Ca-rich spring waters with saline, alkaline carbonate-rich lake water leading to the rapid precipitation of calcium carbonate (Pentecost, 2005). Travertine towers are characteristic deposits in present-day and former lakes into which carbonate-rich spring waters are or were being discharged into unconsolidated lake-bottom sediments (Hancock et al., 1999). They range in height from a few tens of centimetres to a few tens of metres (Hancock et al., 1999; Pentecost, 2005). These tower-shaped deposits are often aligned reflecting an underlying control by faults and fractures.

Self-built channel deposits (Fig. 2.2F) are linear travertine masses built up by spring waters along the flow direction (Ozkul et al., 2002). The channels are restricted from both sides by rims developing along the points where precipitation is the highest (Ozkul et al., 2002).

Terraced slopes (Fig. 2.3A) are high energy flow systems consisting of terrace walls (several centimetres up to 2 m high), pools (a few centimetres up to 20 m wide), pool rims (a few centimetres to 1 m high) and waterfalls (a few metres high; Guo and Riding, 1998). However, pools are the only zones of the terraced slopes where the flow energy is reduced.

Smooth slopes (Fig. 2.3B) consist of non-terraced and low-angle slopes (dipping less than 10^0 to ca. 50°) on which the terrace pools did not developed (Guo and Riding, 1998; Ozkul et al., 2002). They present reduced surface roughness and less fluctuations in water flow/supply than the terraced slope. However, also smooth slopes are high-energy deposits.

Flat ponds consist of horizontal to sub-horizontal areas (Ozkul et al., 2002) several metres wide. These represent areas of low topography and relative low energy flow water (Fig. 2.3D).

Terraced, smooth and flat morphologies characterize also the walls of fissure ridges and travertine mounds (Fig. 2.2B and 2.3).

Crystalline crusts (from centimetres to a few decimetres thick) are common of rims and walls, vertical surfaces of waterfalls of the terrace pools. These are also characteristic of smooth slopes, where water supply and flow velocity are fast (Guo and Riding, 1998; Ozkul et al., 2002).

Shrubs are typical components of pools of terraced slopes (relatively low energy areas; Guo and Riding, 1998; Ozkul et al., 2002). In horizons of reduced topographic relief (ponds) and of low-

angle dip of smooth slope systems, centimetre-scale alteration of different fabrics occurs including: shrubs (from a few millimetres to 20 cm thick), a few millimetres to centimetres elongated rafts, undulated sub-millimetre micrite/microspar laminae, pisoids, and rounded and elongated gas bubbles (Guo and Riding, 1998; Ozkul et al., 2002).

Fig. 2.3 Travertine depositional systems. A) Terraced slope consisting of pools with raised rims and walls. South side of western part of Rapolano Terme fissure ridge, Tuscany, Italy (from Guo and Riding, 1999). B) Steep smooth slope on the south side of the eastern end of the Rapolano Terme fissure ridge. The lateral flats to the right are farm fields (from Guo and Riding, 1999). C) Canary Terrace, Mammoth Hot Springs, Wyoming, USA. Note the smooth surface in the background (from Pentecost, 2005). D) Lateral flat and depression at Rapolano Terme (from Guo and Riding, 1999).

Chapter 3
Geological setting

3.1 Introduction

The Pleistocene Pianetti travertine deposits and the actively forming Bagni di Sarurnia system are located in the Neogene basin of the Albegna River in Southern Tuscany, Central Italy. Southern Tuscany represents the inner portion of the Northern Apennine chains (Fig. 3.1A).

3.2 Regional geological outline

The Northern Apennine (Fig. 3.1A) is a long arch-shaped, mountain chain originated from the convergence, collision and subsequent emplacement of tectonic units (Cretaceous–early Miocene) between the Adria microplate, the European plate (here represented by the Sardinia-Corsica massif) and the interposed Ligurian-Piedmont oceanic basin (Vai and Martini, 2001; Carmignani, 2004; Billi and Tiberti, 2003, 2004; Brogi et al., 2005). Convergence occurred first with the anti-clockwise rotation of the Sardinia-Corsica block and the opening of the back-arc basin of the Balearic Sea, then followed by the opening of the Tyrrhenian Sea initially as a fore-arc basin and then as a back-arc one (Castellarin et al., 1992; Faccenna et al., 2001; Brogi, 2004). The collision led to the formation of a tectonic unit composed by several stacked thrust sheets derived from oceanic and epi-continental palaeogeographic domains of the inner Northern Apennine (Sagri et al., 2004; Brogi and Liotta, 2008).

After the emplacement, extensional tectonic migrating eastward affected the Inner Northern Apennine (Elter et al., 2011) with a resulting “Basins and Range-type” structural architecture (Martini and Sagri, 1993) developed since the Middle Miocene (Bartole, 1995; Carmignani et al., 1995; Argnani et al., 1997), where high-angle normal and orthogonal transfer zones dissected the previous compressional features and the extensional structures (Brogi, 2004, 2008; Brogi et al., 2005). Minor structures related to the transfer zone were active until the latest Pleistocene and are considered to have controlled the hydrothermal circulation (Brogi & Fulignati, 2012; Brogi et

al., 2010, 2012). The extensional basins formed on a thinned continental crust (Calcagnile and Panza, 1981; Locardi and Nicolich, 1992) and were coeval with widespread anatectic magmatism which gave rise to magmatic intrusions emplaced at shallow depth, volcanism (Serri et al., 1993; Ferrari et al., 1996; Poli et al., 2002; Peccerillo, 2003; Dini et al., 2005; Rossetti et al., 2008) and an important widespread post-Pliocene uplift, testified by Middle Pliocene marine deposits up to 700 m above sea level (Pasquarè et al., 1983; Marinelli et al., 1993; Bossio et al., 1995). The Albegna Basin represents one of these extensional basins. It is a broad tectonic depression oriented NNE–SSW, located East of the Middle-Tuscan Ridge and its southern extension ends close to the M. Argentario (Fig. 3.1A).

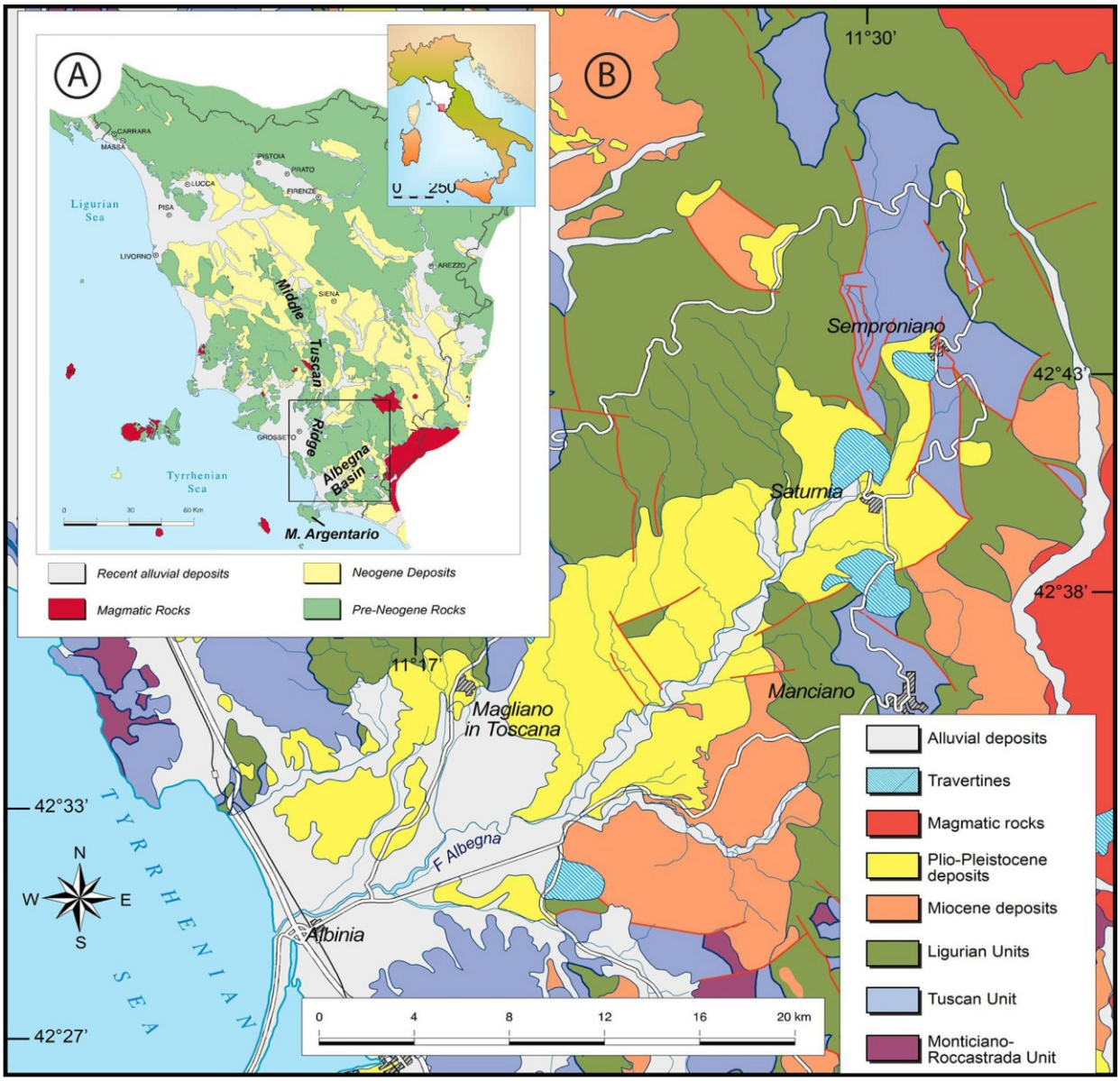

Fig. 3.1 Geological setting of the study area. A) Simplified geological sketch map of Tuscany; B) Geological map of the Albegna Basin. Redrafted after Carmignani and Lazzarotto (2004)

3.3 Geological setting of the Albegna Valley

The Neogene Basin of the Albegna River is disposed along a significant anti-Apennine structural lineament, oriented SSW-NNE instead of following the NW-SE trend of the Northern Apennine arc and of several other extensional basins in Tuscany (Fig. 3.1).

The existence of an Albegna "lineament", that is probably the most remarkable element of previous formed crustal weakness zone, was confirmed by Zanchi and Tozzi (1987). Field evidence and photogeological structural analyses conducted by these authors demonstrate the effect of extensional tectonics in the Albegna Valley.

The tectonic activity of this lineament seems to have been present since the Early Pliocene and during most of the Quaternary.

The substrate of the Albegna Basin is composed of several metamorphic and non-metamorphic tectonic units stacked during the Northern Apennine evolution. They are, from the top (Fig. 3.2A): a) Ophiolitic Unit (the uppermost tectonic unit belonging to the Ligurian Complex–LU1) consisting of remnants of the Jurassic oceanic crust (peridotites, gabbros and basalts), and the sedimentary cover, mainly composed of Jurassic radiolarite and Cretaceous shale, clayey marl and limestone; b) S. Fiora Unit (LU1) composed of Cretaceous–Eocene clayey-marly and anenitic succession deposited on the oceanic crust of the Neotethys; c) Canetolo Unit (Argille e calcari Auct.; SU) composed of Eocene clayey carbonate succession deposited in a transition crustal sector passing from the oceanic crust to the Adria continental margin; c) Tuscan Nappe representing the deepest non-metamorphic tectonic unit of the Northern Apennines, composed of a succession ranging from Middle-Upper Triassic evaporites to Jurassic platform carbonates, Cretaceous-Oligocene pelagic deposits and upper Oligocene–lower Miocene turbiditesd) Monticiano–Roccastrada Unit consisting of a metamorphic succession here composed mainly of the Triassic Verrucano siliciclastics Group. Stratigraphic and sedimentological studies on the deposits filling the Albegna Basin (Fig.3.2B) have been carried out by many authors (Bonazzi et al., 1980, 1982; Pasquarè et al., 1983; Tozzi and Zanchi, 1987; Bossio et al., 2003-2004). According to Bosi et al. (1996), the evolution of this extensional basins was complex, due to the fact that the orientation of the main tectonic structures, the localization of structural highs and lows, and regional uplift varied from the Messinian through time. The oldest Neogene formations crop out in the eastern part of the basin, where they are represented by dominantly lacustrine massive clays (Lignitiferous Unit-T Unit-Tortonian) evolving into brackish conditions

(Acquabona-Spicchiaiola Unit-M1-early Messinian). These deposits are unconformably covered by conglomerates and clays of a late Messinian fluvio-lacustrine system (Lago-Mare Unit-M3-late Messinian) testifying for a morphological renewal of the area (probably accompanied by tilting of the previous Miocene strata according to Tozzi and Zanchi, 1987). All these Miocene formations were deposited in an Apennine oriented, NNW-SSE trending depositional basin (Bonazzi et al., 1992). Only from the Pliocene, due to the uplift of the Scansano and Argentario-Manciano highs, the Neogene Albegna Basin assumed the present anti-Apenninic arrangement (SSW-NNE; Bonazzi et al., 1992). Pliocene deposits rest on the Miocene deposits and are mainly represented by marine clays (Pliocene I Unit-P1-Zanclean) unconformably overlain by coarser marine sediments (Pliocene II Unit-P2-Piacenzian) locally evolving in continental limestones and clays of lacustrine environment (Pliocene III Unit-P3-Piacenzian). During the Pleistocene a strong uplift occurred in all Tuscany and, consequently, even in the Albegna area (Tozzi and Zanchi, 1987; Bonazzi et al., 1992; Bossio et al., 2003-2004). Due to this uplift, according to Bossio et al. (2003-2004), Pleistocene sedimentary events are discontinuous and extensively reported only in the southwestern part of the basin. The widespread travertine deposits occurring in the Albegna Valley are generally unconformable over all these Neogene-Pleistocene deposits (Martelli et al., 1982; Zanchi and Tozzi, 1987; Bosi et al., 1996).

3.3.1 Distribution of travertine deposits in the Albegna Valley

The circulation of low-enthalpy fluids (related to brittle fracture systems) is responsible of the deposition of different types of mineral deposits of hydrothermal origin consisting mainly of oxides and sulphides of mercury and antimony and of extended travertine deposits (Zanchi and Tozzi, 1987). Travertine deposits are a common feature of the Albegna Valley (Fig. 3.3) and were deposited in various phases and over a long time interval (Bosi et al., 1996).

In the study area travertines are present in several deposits, distributed along faults and fractures differently oriented (Zanchi and Tozzi, 1987). Travertine deposits are mostly widespread in the Saturnia zone of the Albegna Valley, a north-south elongated area comprised between Manciano and Semproniano (Zanchi and Tozzi, 1987). Manciano, Montemerano, Saturnia, Pian di Palma, Poggio Capalbiaccio, La Marsiliana, and Semproniano are the localities where travertine deposits occur, frequently associated with well-defined tectonic structures (Martelli et al., 1989).

All the travertine deposits are generally attributed to Early Pleistocene-Holocene times for the morphological and stratigraphic position (Martelli et al., 1982; Zanchi and Tozzi, 1987). However, Bosi et al. (1996) suggested that the lower limit of the travertine deposition in the Albegna Valley could even be the Messinian time.

According to Bosi et al. (1996) in the Albegna Valley there are at least five travertine units (Fig. 3.4) of different ages from the Messinian to present day. These travertine units were named by Bosi et al. (1996) as: Tr5 (Messinian in age, travertine cropping out at Marsiliana and Poggio Capalbiaccio); Tr4 (Pliocene, cropping out at Semproniano/Samprugnano), Tr3 (Middle Pleistocene, travertine cropping out at Saturnia village and Colle Lupo); Tr2 (Middle-Late Pleistocene cropping out at Montemerano, I Pianetti, Pian di Palma, Manciano), Tr1 (Holocene at Bagni di Saturnia and the thermal spa Terme di Saturnia).

The travertine outcrops in the Albegna Valley area can be classified in two morphological groups (Fig. 3.4; Bosi et al., 1996). These includes: 1) the first group includes travertines with typical horizontal stratification, which gives flat morphologies variably hanging over the valleys.

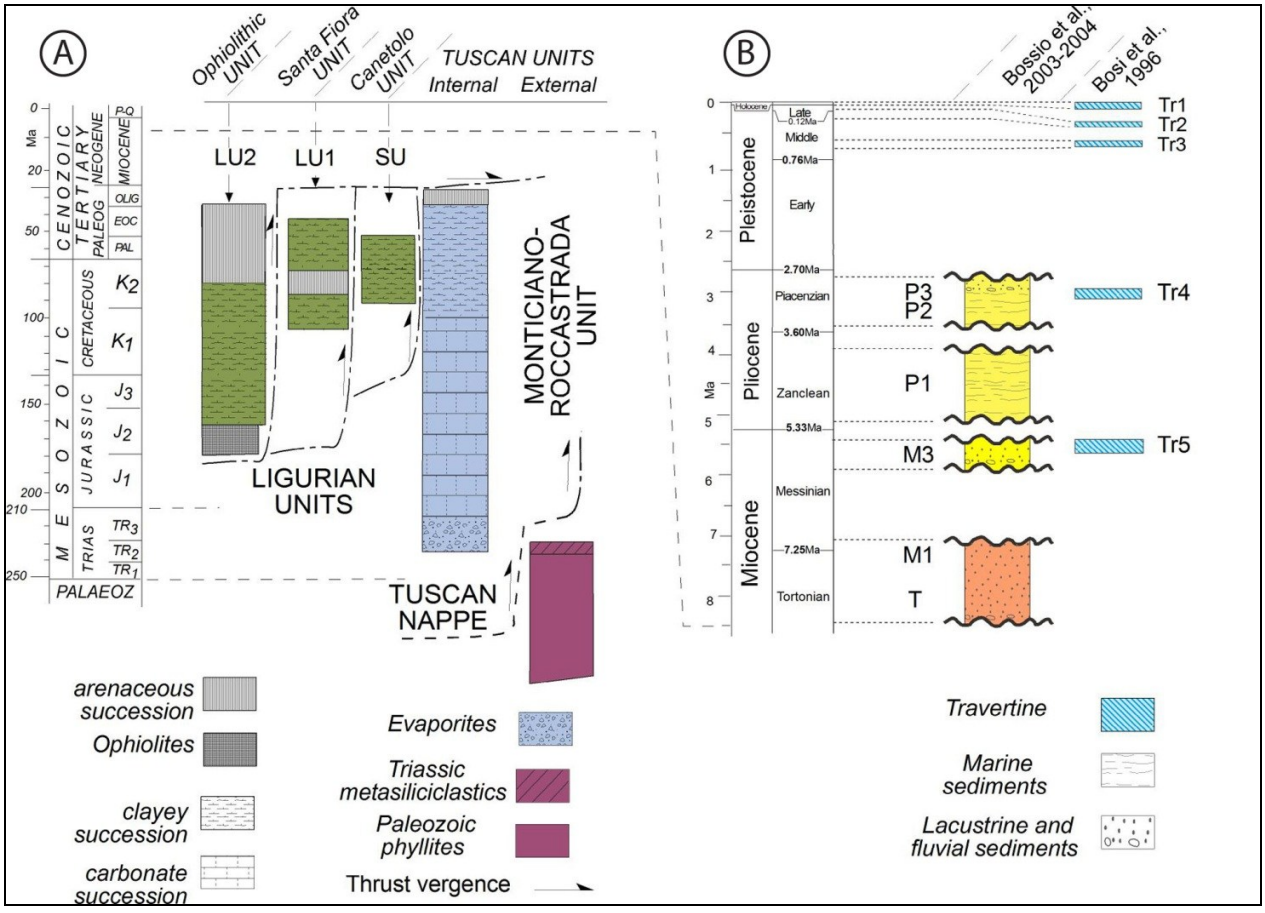

Fig 3.2 A) Relationship among the different tectonic units of Northern Apennines present in the Albegna Basin; B) Stratigraphy of the Neogene to Holocene succession cropping out in the Albegna Basin.

These travertines are the product of sedimentary events occurred in well distinct periods. Travertine deposits of the Units Tr1, Tr2, Tr3, Tr4 are part of this group (Fig. 3.4B); 2) the second group includes stratified, usually tilted (with dips up to 60-70°) travertine deposits; they present also faults, in some cases with a marked horizontal component, and their dip/strike is similar to those of the Messinian units which form their substrate. Travertines of the Unit Tr5 belong to this group (Fig. 3.4).

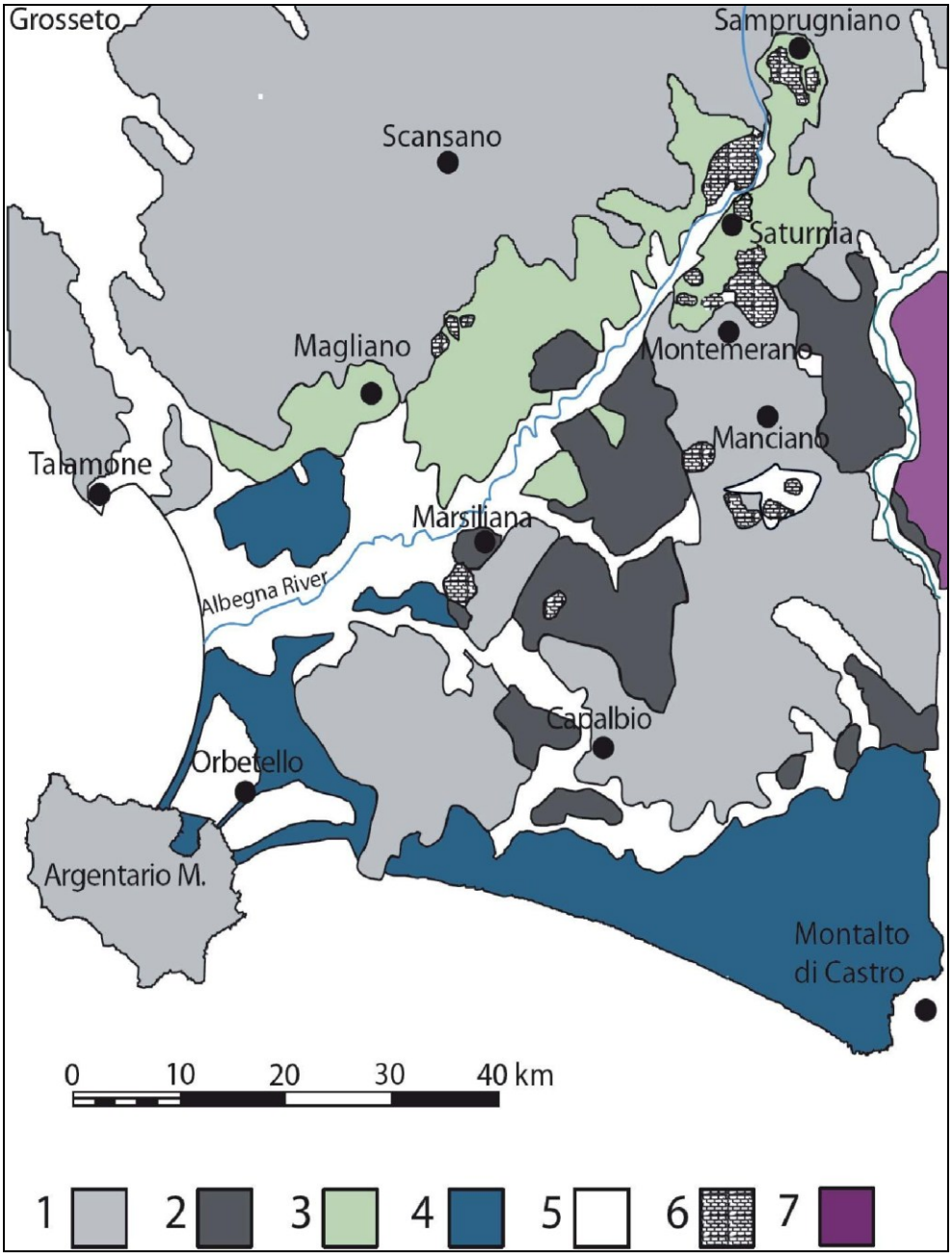

Fig. 3.3 Simplified geological map of the Albegna Valley. Legend: 1) Tuscan Nappe and allochthonous units; 2) Messinian continental, brackish and marine deposits; 3) Pliocene marine deposits; 4) Pleistocene marine and coastal deposits; 5) alluvial-colluvial sediment; 6) Miocene to Holocene Travertines; 7) Volcanic deposits of Vulsini Mountains (map modified after Bosi et al., 1996).

Bosi et al. (1996) determined the relative ages of the travertine bodies on the basis of morpho-lithostratigraphic features such as the fluvial/alluvial terraces. The alluvial terraces were divided in three orders according to their elevation: 1) A1 terrace from 25 m to 80 m above sea level (including the Tr 1 travertine); 2) A2 terrace from 80 to 160 m a.s.l (comprising the Tr 2 travertine), and 3) A3 terrace from 100 m up to 190 m (with the travertines deposits Tr 3, 4 and 5 older than this terrace).

In particular, the present-day unit of travertine Tr1 consists of still precipitating travertine or associated to the terrace A1 (Bagni di Saturnia, Terme di Saturnia). The terrace A2 contains some volcanic intercalations referred to the Volsinian volcanites, with an age between 400 and 100 kyrs (Barberi et al., 1990), and is correlated to the travertine Tr2 on the base of their similar lower erosive stratigraphic surface.

However, the age dating of the travertine deposits proposed by Bosi et al. (1996) is debated. The Tr 5 deposits cropping out at the Marsiliana and Poggio Capalbiaccio were attributed to the Messinian by Bosi et al. (1996). According to these authors, the morphological configuration of these travertines is substantially similar to that of the Meso-Cenozoic bedrock, they never overlie deposits younger than Messinian, and the Messinian deposits are locally interbedded with travertine-bearing thin strata. The Tr4 travertine deposits cropping out at Semproniano were dated as Pliocene by Bosi et al. (1996), whereas other authors considered them as Early Pleistocene in age (Zanchi and Tozzi, 1987 and references therein). Poggio Semproniano deposits represent the highest travertines, resting on Pliocene deposits up to an altitude of 700 m. The Tr3 travertines are those on which the village of Saturnia is located and they probably are Middle Pleistocene in age (as the Colle Lupo outcrop-Bosi et al., 1996). The Tr 2 travertine deposits are the most laterally extensive and/or better preserved from erosion being younger. Bosi et al. (1996) indicated that the travertine of Pianetti (Montemerano) and Pian di Palma terraces are Middle to Late Pleistocene in age, while according to Zanchi and Tozzi (1987) these travertines are Late Pleistocene-Early Holocene in age.

In the Manciano sector, travertine deposits fill Pleistocene grabens and are also associated with volcanic deposits (Zanchi and Tozzi, 1987). In particular, travertines cropping out on the eastern sector of the Manciano graben contain reworked pyroclastic material covered by alluvial and recent travertine deposits (Martelli et al., 1989). The Tr1 present–day travertine system is located in the Bagni di Saturnia and Terme di Saturnia area, at about 14 km from the Pleistocene travertine counterparts that, as suggested by Bosio et al. (1996), is part of the first group of

travertines. Therefore, travertine deposits of the Neogene Albegna Valley are located from about less 20 m up to 700 m a.s.l and some of these deposits are still active.

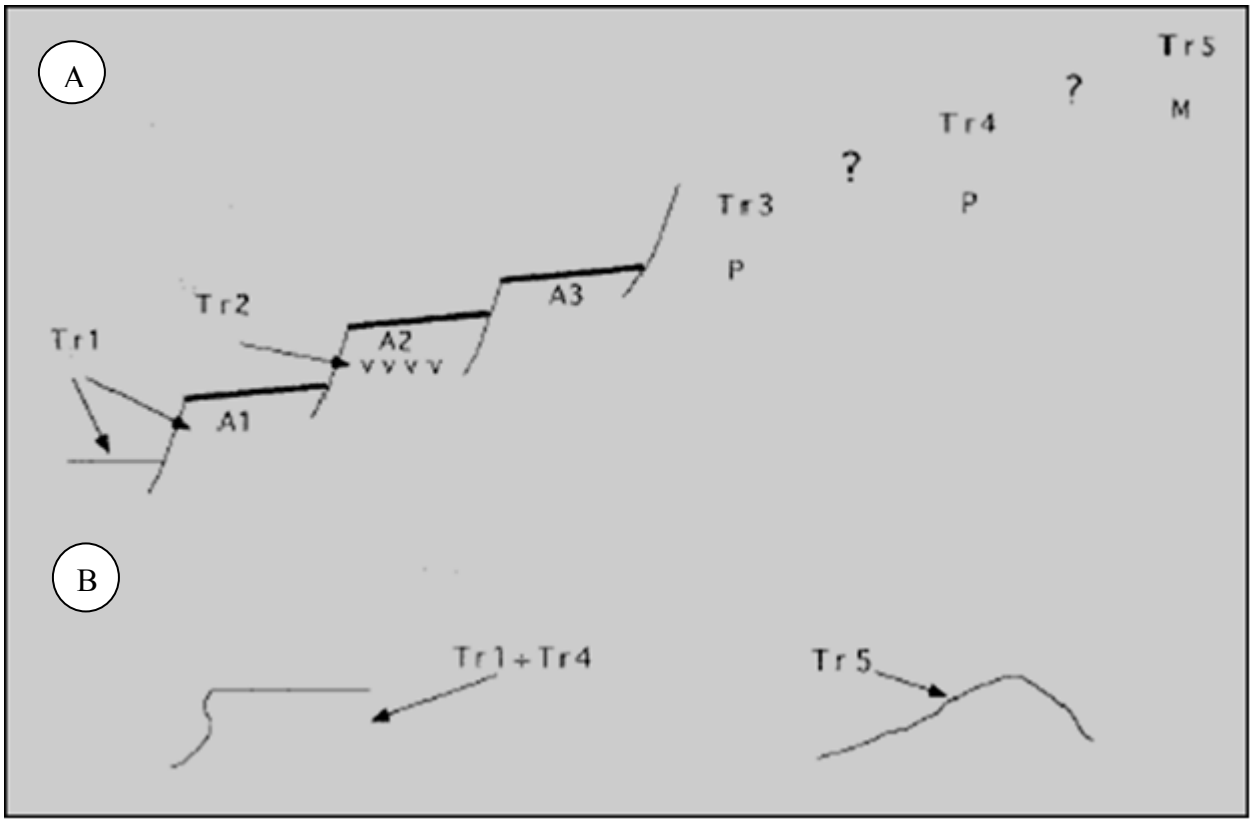

Fig. 3.4 Scheme of the morpho-lithostratigraphic relationships (Bosi et al., 1996) between travertine bodies and fluvial/alluvial terraces. A) (Tr1 to Tr5) travertine lithosomes: Tr1) active Holocene travertines of Terme di Saturnia, associated in age to A1; Tr2) upper-middle Pleistocene travertines of Montemerano, Pian di Palma, Grinzano, Podere Romitorio, associated in age to A2 terrace; Tr3) middle Pleistocene travertines of Saturnia Village, Colle Lupo, older than A3; Tr4) lower Pliocene-Pleistocene travertines of Semproniano/Samprugnano; Tr5) Messinian travertines of Poggio Capalbiaccio, Marsiliana, Fonte della Morcola. (A1 to A3) flood terraces; (vvv) main volcanic intercalations; (M) bedrock older than Messinian; (P) bedrock lower Pliocene; (thick line) upper surfaces of the fluvial terraces.

Chapter 4

Characterization of Pleistocene hydrothermal travertine deposits in the Albegna Valley, Southern Tuscany, Central Italy.

Abstract

A Pleistocene travertine body, cropping out on the Pianetti Terrace, central-eastward area of the Neogene Albegna Basin (Southern Tuscany, central Italy) was investigated: 1) to define the geometry of the sedimentary body and depositional environments, including their lateral and vertical evolution; 2) to characterize the varieties of hydrothermal travertine carbonate fabrics; 3) to improve the understanding of the abiotic and microbially mediated processes that control calcium carbonate precipitation in hot-spring settings; 4) to establish the link between fabric types and travertine depositional environments. The Pianetti travertine body, well exposed within an active quarry, exhibits a wedge shape differentiated into three decametre scale travertine units. Exposure surfaces represented by claystone layers separate the deposit in three travertine units and constitute the travertine sequence boundaries, suggesting an intermittent accretion of the travertine system. Different architectural patterns including clinoforms, stepped and sub-horizontal layers corresponding to smooth slope, terraced slope and pond depositional environments, respectively, were individuated within the travertine units. The geometry and the relative depositional systems of each unit are controlled by different factors such as the location, typology and activity (water supply, hydrostatic pressure of the spring) of the hydrothermal vents, roughness of pre-existing surface and topography along which hydrothermal water flew and mixing with meteoric water. A large variety of fabric types characterize the Pianetti travertine body. Eight main categories of fabric types and the relative sub-categories can be essentially classified into three classes: 1) travertine boundstone and cementstone s.l. in which

the original components are directly precipitated from hydrothermal thermal water; 2) encrusted travertine in which original components (acting as substrate) are directly encrusted by carbonate precipitated by flowing hydrothermal water; 3) carbonate grains packstone/grainstone to floatstone/rudstone formed by fragments of already lithified travertine precipitates (intraclasts) and other lithoclasts.

Pore structure (ranging from depositional to secondary porosity) is an important component of travertine fabrics. Porosity and permeability investigations (Helium techniques, microCT scanning and image analysis software AVIZO) shows that travertines display a wide range in porosity and permeability that is a direct function of: 1) primary fabric orientation; 2) diagenesis; 3) travertine fabric.

The distinguished fabric types reflect the precipitation processes due to an interplay of abiotic and biotic processes (biologically induced by microbial metabolic process or simply influenced by nucleation on microbial biofilm substrate) and subsequent diagenesis. The physical-chemical and biological interaction is also registered in travertine isotopic geochemistry. Organic matter remains and organomineral nano-globules within the Pianetti travertine suggest that for some precipitates the biologic influence is fundamental. However, even for the biologically induced mineralization, abiotic processes and physical-chemical characteristic of the precipitating thermal water are necessary for travertine formation. A relationship between fabric types and velocity/turbulence and discharged volumes of the flowing water is suggested. In addition, fabrics occurring in low energy areas might be more biologically influenced than fabrics occurring in fast flowing dipping surface for which the abiotic processes of physical degassing might prevail. Many fabrics seem to represent transitional forms of a continuum between the two end-members of purely abiotic and microbially mediated (influenced/induced) precipitates.

4.1 Introduction

Hydrothermal travertines are a category of continental carbonate deposits forming under thermal-hydrothermal conditions (Ford and Pedley, 1996). Travertine precipitation occurs by discharging calcium and bicarbonate enriched groundwater at temperatures > 20°C (Pedley, 2009) from a tectonically controlled hydrothermal vent (Hancock et al., 1999; Brogi et al., 2010). Hydrothermal vents occurred in a wide range of depositional settings including both subaerial flowing-water and subaqueous lacustrine systems, especially related to extensional tectonics

(Hancock et al., 1999; Shipton et al., 2004; Altunel, 2005). The occurrence of thermal springs can produce different travertine body morphologies. According to the location and the typology of the orifices (aligned or punctual) the discharge of the calcium carbonate rich-water builds ridges, mounds, pinnacles, tower-shaped and self-built channel carbonate deposits (Chafetz and Folk, 1984; Pentecost and Viles, 1994; Pentecost, 1995; Guo and Riding, 1998; Hancock et al., 1999; Ozkul et al., 2002; Pentecost, 2005). However, Hancock et al. (1999) suggest that the morphology of travertine deposits overlying tensional fissures is controlled by the rheology of the underlying materials and can also be strictly controlled by the geometric setting and kinematics of faults and related damage zones (Altunel and Hancock, 1993a, Hancock et al., 1999; Brogi and Capezzuoli, 2009; Brogi et al., 2010). The flowing of the water from the spring to the lower morphology areas creates different depositional environments ranging essentially from terraced and smooth slopes to flat ponds (Chafetz and Folk, 1984; Guo and Riding, 1998; Ozkul et al., 2002; Pentecost, 2005).

Considerable interest in travertine has been enhanced in the last decades by suggestions that these carbonates can be used as a tool for paleo-climatic, neotectonic and paleo-hydrological conditions (Hancock et al., 1999; Fouke et al., 2000; Moore et al., 2005; Brogi et al., 2009; Gilbert et al., 2009). Geochemical analyses of presently forming travertines have been performed on samples collected from several thermal localities as the Yellowstone Park hydrothermal spring systems (Friedman, 1970; Fouke et al., 2000); in Italy Le Zitelle springs near Viterbo and Bagni San Filippo on the Monte Amiata (Siena), related to volcanic complexes (Gonfiantini et al., 1968; Chafetz and Lawrence, 1994) and the Rapolano/Acqua Borra (Siena) geothermal springs (Guo et al., 1996). Several researches are performed at hydrothermal field in order to identify the response of the hydrothermal system to climatic change. Travertine deposits have been considered as indicators of warm climatic phases in the continental environment (Pentecost,1995; Boch et al., 2000; Frank et al., 2000; Horvatincic et al., 2000). Soligo et al. (2002), on the basis of six travertine bodies outcropping along the Middle Velino Valley (Central Italy) argue that travertines could be considered as climatic proxies in continental environment, in the same way as oxygen marine records from planktonic foraminifer assemblages.

Contrary to the marine carbonates, and even though the ever-increasing interest in hot springs, travertine lack of clear understanding. The scientific community working on hydrothermal travertine is in agreement regarding the morphologies of the deposits and their depositional systems; however, the processes that govern the travertine formation are still debated. Travertine are potential data repositories for unravelling questions about the modes of mineral precipitation

in continental settings. Several mechanisms of mineral precipitation have been proposed to explain travertine formation and these vary from abiotic to biogenic processes (Chafetz and Folk, 1984; Folk, 1994; Guo and Riding, 1996; Chafetz and Guidry, 1999; Tekin et al., 2000; Jones and Renaut, 2010; Fouke, 2011); however, it is necessary to gain a more complete understanding of the mechanisms and the conditions that lead to the precipitation of these continental carbonates. The abiotic physicochemical control on mineral precipitation is driven by CO2 degassing and evaporation of the water outflowing from the spring, resulting in supersaturation with respect to calcium carbonate (Kitano, 1963; Jones et al., 2005; Pentecost, 2005; Pentecost and Coletta, 2007; Dupraz et al., 2009; Jones and Renaut, 2010). Turbulence and velocity of water flow cause physical CO2 loss that provides passive calcification of any type of substrate (Pentecost, 2005; Dupraz et al., 2009). Nevertheless, research on carbonate hot springs around the world has documented that precipitation is not purely a consequence of physical processes: calcium carbonate precipitation might be biologically influenced/induced by the presence of organic components (Chafetz and Folk, 1984; Folk, 1994; Guo and Riding, 1994; 1998; Pentecost, 1995, 2005; Ford & Pedley, 1996; Farmer, 2000; Fouke et al., 2000; Riding, 2000; Renaut and Jones, 2000; Fouke, 2011). Although the possibility that microbes contribute to the mineral formation at hydrothermal setting was revealed more than a century ago (Weed, 1889 and references therein), the role played by the microbial communities in travertine precipitation is still controversial. Microbial mats found at hot springs have a profound impact on travertine by providing substrates for mineralization, even though precipitation is due to vigorous CO2 degassing (Farmer, 2000; Fouke et al., 2000). Cyanobacteria, heterotrophic bacteria and diatoms can play a role in calcite and aragonite nucleation (Chafetz and Folk, 1984; Folk et al., 1985; Guo and Riding, 1992; Chafetz and Guidry, 1999), and through photosynthesis and other biochemical processes may mediate mineral precipitations (Renaut and Jones, 2000). Guo et al. (1996) suggest a possible effect of bacteria-cyanobacteria photosynthetic metabolism on stable carbon isotopes in hot-spring travertines of Rapolano Terme (Central, Italy). Pentecost (1996) estimated that up to 20% of the CaCO3 precipitated at a hot spring may be attributed to biological activity. Precipitation in hot spring context may be extracellular or replacive, and may affect unicells, filaments, sheaths, biofilms and extracellular polymeric substances (Renaut and Jones, 2000). Photosynthetic CO2-uptake and other physiological activities of plants (e.g. HCO3- assimilation) also enhance calcite precipitation (Merz-Preiß and Riding, 1999) but appear to contribute to a lesser extent as compared to physico-chemical processes (Jones and Renaut, 2010). Pentecost and Coletta (2007) showed that microbial photosynthesis and

respiration had a negligible effect on Le Zitelle travertine deposition (Central Italy) and suggested that photosynthesis could provide a carbon sink of no more than 10% of the measured CO_2 evasion rate at the studied site. Fouke (2011) advocates an interaction between spring-water chemistry, physical processes (temperature changes, degassing, boiling, steaming, evaporation and dilution), hydrology (flow rates, flux and surface area) and biotic activities (metabolism, microbial photosynthesis, respiration and biochemical effects) as primary control for the travertine precipitation. Microbes affect travertine fabrics. Fenestral and mouldic porosity, rod-shaped bacteria and peculiar fabric morphology are the evidences of microbe remains (Chafetz and Folk, 1984; Folk et al, 1985; Renaut and Jones, 2000). Dupraz et al. (2009) assume that although the alkalinity engine, responsible for carbonate precipitation in hydrothermal-spring settings, results from an abiotic source, precipitation is initiated on organic substrates. Pentecost et al. (1997) suggest that cyanobacteria locally influenced the travertine microfabric by providing sites for the trapping and nucleation of calcite at the cell surface, but the bulk of the travertine did not appear to be influenced by the presence of these microbes.

Travertines offer a sensitive record of complex interactions between abiotic vs. microbially induced processes and the depositional environment (Chafetz and Folk, 1984; Folk, 1993, 1994; Pentecost, 1995, 2005; Ford and Pedley, 1996; Fouke 2011). Hydrothermal deposits have been identified as important targets for planetary exploration and the search of extra-terrestrial life (NASA, 1995; Allen et al., 2000; Farmer, 2000) and have been recognized as location in the search for evidence of ancient microbial fossils that formed on the early Earth (Riding, 2000; Pentecost, 2005; Fouke, 2011). Microbialites formed by different organo-mineralization processes (Dupraz et al., 2009) have been studied in non-marine and marine deposits (Pedley, 2000;Sprachta et al., 2001; Van Lith et al., 2003; Dupraz et al., 2004; Dupraz. and Visscher, 2005; Turner and Jones, 2005; Perri and Tucker, 2007; Pedley et al., 2009; Spadafora et al., 2010; Manzo et al., 2012; Perri et al., 2012) but fundamentally remain unidentified in travertine deposits. Studies of travertine deposits are often deficient in both micro-fabrics and nano-scale descriptions that are fundamental tools for the understanding of role of organisms and the processes in travertine formation. Even though the first study innovative on the petrography of travertine was done by Chafetz and Folk (1984) and in a second phase, the recognition and description of travertine fabric types were made by authors such as Guo and Riding (1998), into the scientific community a clear and detailed travertine classification is lacking. It is considered necessary a univocal classification essentially based on the classical terminology of carbonates that immediately give information on the components and morphology of the fabric types and

also on the mechanisms that acted during their deposition. For that reason a travertine classification developed using some terms of classical classifications of carbonate textures is proposed. In order to improve the understanding of the nature, the formation processes, depositional environments, products of hydrothermal travertine and also with the purpose to establish a link between fabric types and travertine depositional environment a multi-scale study of the Pianetti travertine deposit (Albegna Valley, Southern, Tuscany, Central Italy) is presented. All the above findings might be the key to elucidate the environmental conditions and the processes responsible for the hydrothermal travertine through geologic time and can have implications for comparable carbonate reservoirs in the subsurface.

4.2 Materials and methods

The study of the Albegna River Basin travertine provides also fundamental information in terms of geometry and lateral and vertical evolution of the sedimentary bodies. Travertine geometry, depositional systems and fabric types have been distinguished not only by means of field and petrographic and SEM observations but also by stable isotope analyses. This study provides the first comprehensive evaluation of the reservoir properties of hot-spring carbonates. Seventy horizontally and vertically drilled plugs were measured for porosity and permeability. The pore structure of ten samples was quantified using microCT scanning and AVIZO has proved to be an excellent visualization tool in the travertine sample. Observations of travertine outcrops on saw-cut quarry walls had represented the base for the studied Pleistocene travertine body. Aerial photograph and satellite image observations were used to document the extension of the quarry with the aid of the published geological maps of the area.

Field data were obtained by macro-scale observations, detailed stratigraphic sections and mapping (field sketches). Stratigraphic sections, varying from 2 m up to 4 m in thickness, were logged to characterize the different fabric types and their vertical alternation from the meso- (millimetre to decimetre) to macro- (metre) to mega-scale (decametre). Hundreds samples of travertine deposits were collected in the field and returned to the Milan University laboratory facilities. More than 320 samples were embedded in resin and then thin sectioned with a thickness of approximately 30 μm, varying in dimensions from 28 × 48 mm and 43 × 55 mm to 55 × 95 mm. The thin sections were analysed by optical and reflected light microscopy. A limited number of these thin sections was analysed to determine the property of the samples to

emit light when excited by ultraviolet light. The variation of the auto-fluorescence was observed using incident light emitted by Hg high-pressure vapours attached to a Zeiss optical polarizing microscope (Zeiss, Gottingen, Germany), equipped with high-performance wide band-pass filters. Cathodoluminescance analyses were done on a selected set of thin sections using a luminoscope CITL (model MK 5-2 operating system at 10 KV with a beam current between 4-6 MA, and vacuum gauge 50-70 millitor). Scanning electron microscope (SEM) and electron microprobe (EDS) analyses were made using an a Cambridge Stereoscan 360. Also, WDS microanalysis was performed using EOL 8200 Super Probe. The Pleistocene studied samples/thin sections for SEM observation were gold coated, while the specimens for microanalysis were coated with carbon. The duration of coating varied according to the porosity of the samples but it was always in the range of 30-60 seconds in order to prevent possible coating artefacts. Some of the SEM samples were etched with hydrochloric acid. To avoid the alteration of real features of the travertines, the etching of the samples was carried-out with diluted HCL 1% at different time intervals (from a few seconds up to 1 minute).

The mineralogical composition of selected travertine fabrics and claystone samples was determined using a X-RAY Powder Diffractometer Philips X'Pert MPD with high temperature chamber. Selected elements were quantified on Inductively Coupled Plasma Spectrometry (ICP). Stable isotopes (Oxygen and Carbon) analyses were performed using a MAT253 mass spectrometer with automated carbonate preparation device (Gas bench II) at the University of Bochum, Institute for Geology, Mineralogy und Geophysics stable isotope facility. Stable isotope results were calibrated to the PDB scale by the international standards CO^{-1} and CO^{-8}. The analytical precision is better than 0.07 ‰ for $\delta^{13}C$ and 0.13 ‰ for $\delta^{18}O$.

Seventy horizontal and vertical (with respect to stratigraphic way up) drilled plugs were measured for porosity and permeability properties at the Weatherford Laboratories, Norway using gas expansion (helium) technique. The results were integrated with petrography and SEM observation of the correspondent plug thin sections focusing the attention on pore genesis and architecture. The pore structure of selected samples was quantified using microCT scanning (CTAN SkyScan-1172) (). Morphometric parameters were calculated on 3D based surface-rendered volume models and on 2D binarized cross-section images Micro-tomography is a powerful method to create 3D models, which can be used to visualize and quantify pore and rock structures. The necessary steps for using the X-ray micro-tomography technology are three: 1) Scanning: selection of the type of scanning that is composed of three different resolutions (Low 34μm; Medium 17μm; High 7μm). 2) Reconstruction: removal of errors (when possible)

produced by acquisition. 3) Analysis CT-An elaboration of scanned images for evaluation of image quality and selection of the correct threshold. AVIZO software was applied to elaborate the CT-An image scanning and to rebuild the pore network (Figs. 4.14D, 4.15B and F, 4.16D) Image analysis software (AVIZO) allows a detailed understanding of the Pore Network pore distribution (pores and pore throat). AVIZO has proved to be an excellent visualization tool in the travertine sample.

4.3 Geological setting

A fossil travertine body, cropping out in an active quarry(called Saturnia Travertine Quarry) on the Pianetti Terrace (Montemerano sector), central-eastward area of the Neogenic Albegna Basin (Fig. 4.1) (Southern Tuscany, Central Italy) is the object of the present study. A detailed description of the geological setting of the area under study is reported in Chapter 3. According to Bosi et al. (1996), the travertine deposit should have accumulated during the Pleistocene. It is assumed that this deposit was part of a wider travertine unit (Fig. 4.2) arranged in a N-S direction and extending from Pian di Palma (on the right bank of the Albegna river) to the Montemerano area. This travertine body, probably ca. 8 cm long and ca. 2.5 km wide, was subsequently eroded by the Albegna river; therefore the single unit was divided into Pian di Palma and Pianetti travertine deposits. Saturnia travertine quarry with an area of 38 hectares and with a depth of excavation of 30-35 m allows the investigation of the travertines in terms of carbonate fabrics, geometry of the sedimentary bodies and lateral and vertical evolution".

4.4 Data description

4.4.1 Travertine units and their internal architectures

The travertine quarrying for commercial purposes allows the observation of the vertical and lateral evolution of the travertine sedimentary bodies (Fig. 4.3). The quarry walls exhibit a wedge-shaped travertine body differentiated into three decametre-scale travertine sequences defined as Unit I, II, and III from the oldest (lowermost) to the most recent (uppermost) (Fig.

4.3B-E). Each travertine unit shows different internal architectural patterns (Fig. 4.3B) ranging from: 1) metre-scale columnar convex shaped structure (Fig. 4.4A); 2) Clinoformal beds (less than 1 m nearly 8 m thick) dipping from circa 4° to 45° that can expand laterally over tens of metres (up to 80 m) across the quarry walls (Fig. 4.4B); 3) Stepped topography (Fig. 4.4C-D) differentiated into different stratal orientations showing i) vertical to overhanging (several centimetres to 2 m high), ii) sub-horizontal to concave (a few centimetres to 15 m wide), iii) raised and also convex (few centimetres to 1 m high) morphologies; 4) Flat sub-horizontal layers (Fig. 4.4E-F), laterally continuous (overs tens of metres) and vertically alternated (for 2-5 metres). Travertine unit sequence boundaries are represented by two claystone layers respectively named "clay layer 1" between Unit I and II and "clay layer 2" between Unit II and III (Fig. 4.3).

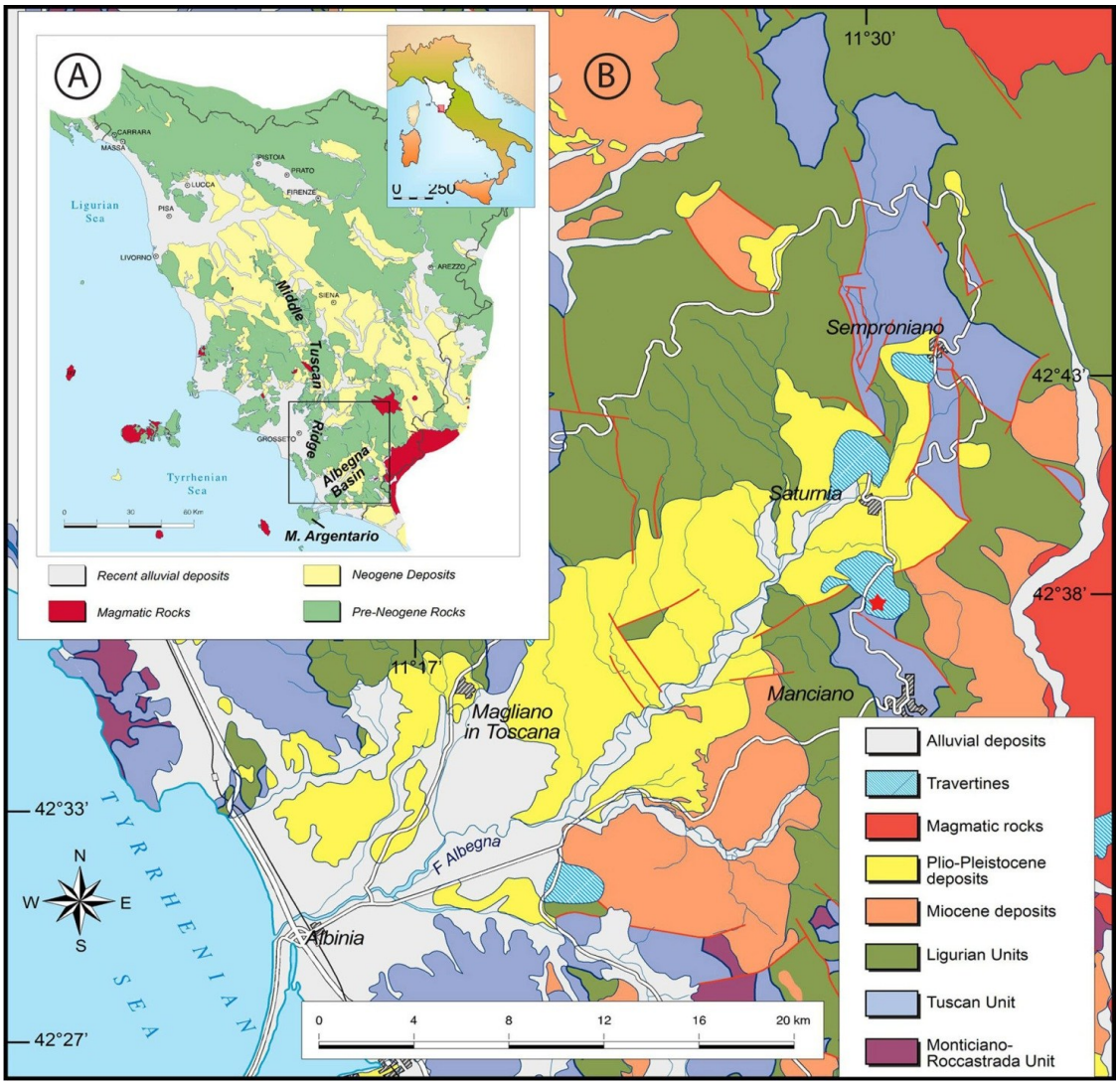

Fig. 4.1 Geological setting of the study area. A) Simplified geological sketch map of Tuscany; B) Geological map of the Albegna Basin. The red star indicates the location of the studied Pianetti travertine body, well exposed along an active quarry.Redrafted after Carmignani and Lazzarotto (2004).

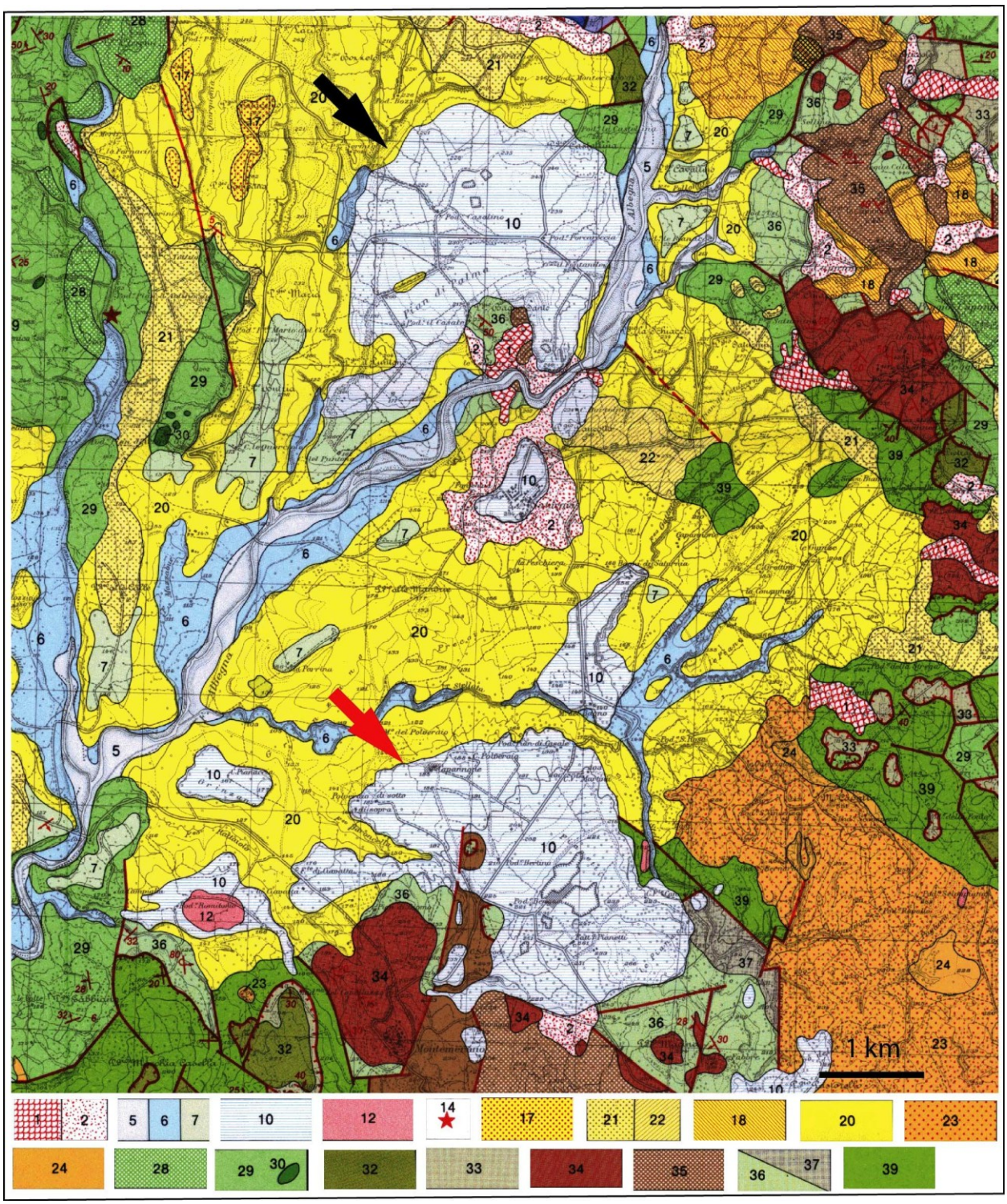

Fig. 4.2 Geological map of Albegna Valley (Betelli et al., 1990) showing the Pian di Palma travertine body (black arrow) of probable comparable age to the Saturnia/Pianetti travertine (red arrow) according to Bosi et al. (1996). Legend: 1) Landslide and 2) Quaternary deposits; 5) 6) and 7) alluvial deposits; 10) Travertine deposits; 12) Tuff and ignimbrite deposits; 14) Vulcanic dikes; 17) Early Pliocene sand and gravel deposists; 18) Early Pliocene sandstones; 20) Early Pliocene claystone; 21) and 22)Early Pliocene sands and conglomerates; 23) Messinian conglomerates; 24) Messinian claystones; 28) Late Cretaceous quartz-sandstones; 29) Late Cretaceous limestone-shale deposits; 30) Ophiolites; 32) Late Cretaceous turbidites; 33) Aptian-Albian and Late Cretaceous shales; 34) Late Eocene-Early Oligocene sandstones; 35) Late Eocene calcareous sandstones; 36) and 37) Eocene claystones and limestones; 39) Late Cretaceous calcareous turbidites.

Fig. 4.3 Field views and diagram of the travertine geometry of Pianetti travertine body. A) Panoramic view of the active Saturnia travertine quarry (photo from Puliti Manuel). Scale bar 7 m. B) Interpretative diagram of the Pianetti travertine geometry showing lateral and vertical transitions between the internal architectures that characterized the travertine deposit. Travertine Units are numbered I, II and III. Unit boundaries are marked by two claystone layers (1-2). Brecciated interval divides Unit II in Unit IIa and Unit IIb. Clinoformal (CT), stepped (ST) and sub-horizontal (H) topography are individuated within the travertine Units. C) Enlarged view of A showing the three stacked travertine units separated by two claystone layers 1 and 2. Scale bar 2 m. D) Outcrop image showing claystone layer 1 (yellow line) which unconformably overlies and entirely drapes travertine Unit I and claystone layer 2 (green line) overlying the top of Unit II. Note that Unit I thins-up towards the NE contrary to the travertine Unit II that thickens towards NE. In blue is indicated a metre scale columnar convex shaped structure. The orange square is enlarged in E. E) Enlarged view of D showing the travertine Units and claystone layer relationship in the SW. Unit II is 2 m thick in the SW direction.

Unit I

Unit I, ca. 50 to 300 m in width and ca. 250 m in length, thins-up towards NE ranging from nearly 20 m to 5 m in thickness (Fig. 4.3B, D-E). The thickest part of Unit I displays at the top a metre-scale columnar convex shaped structure more developed in height than in width (Fig. 4.3D and 4.4A). Unit I is characterized by clinoforms (mainly low angle ca. 10-15^0, 1-3 m high, tens of metres laterally extended) that gradually aggrade and prograde towards the NE into stepped (a few centimetres up to 15 m thick, from a few centimetre up to 50 m laterally extended) and sub-horizontal morphology (3-5 m thick, extending laterally over tens of metres) (Fig. 4.3B). Discontinuities characterized by intraclastic floatstone to rudstone with a grey matrix are observed within the described travertine units. The carbonate layers of Unit I are intensively fractured. Some of these fractures are filled-up by more recent carbonate cement and sediment while others are filled by cement of hydrothermal origin. The top of Unit I is karstified displaying multi-scale sinkholes, incisions, caves and dissolution vugs. "Clay layer 1" unconformably overlies and entirely drapes travertine Unit I (Fig. 4.3C-D). This layer shows significant thickness variability from ca. 60 cm to 3 m and consists mainly of massive and grey clays. However, centimetre-thick strata with detrital grains of quartz and K-feldspar are interbedded with massive clay at the base of this claystone layer. XRD diffraction analysis reveals that illite is the main components of the claystone of layer 1; however, the clay contains also smectite, quartz and feldspars. The described claystone layer 1 divides Unit I from the overlying Unit II.

Unit II

Travertine Unit II thickens towards the NE from 2 to 15 m (Fig. 4.3B, D and E). This travertine Unit ranges ca. 300 m in width and ca. 300 m in length. The geometry of Unit II is controlled by the underlying Unit I: where Unit I becomes thinner in the distal part further from the vent, Unit II reaches the greatest thickness. Unit II mainly starts with prograding clinoforms (2 m nearly 8 m thick, from few metres up to 80 m wide, planar to convex upward clinoforms dipping 15°-45°; Fig. 4.4B and E) passing up-wards and laterally into stepped stratified layers (from a few centimetre up to 5 m thick, extending laterally over tens of metres) that evolve into sub-horizontal deposits (3-5 m thick, extending laterally over tens of metres) showing a decimetre to centimetre scale stepped morphology (Fig. 4.4E). A brecciated interval divides the clinoforms

and stepped stratified layers (Unit IIa) from a sub-horizontal one (Unit IIb; Fig. 4.4B and 4.4E). The brecciated surface consists of lithoclastic rudstone/floatstone of poorly sorted, angular to sub-rounded fragments of already lithified travertine (from a few microns to a few decimetres in size) embedded into grey silty matrix. Although less common, extraclasts may occur. The stratified travertine sub-unit (IIb) onlaps the discontinuity surface (Fig. 4.4B and E). The upper part of travertine Unit II forms an aggradational and progradational wedge. Metre-scale caves are widespread within Unit II. These are filled by carbonate precipitated by meteoric water at the transition of vadose/phreatic zones (e.g. speleothemes) related to claystone layer 2 sitting at the top of the Unit II and to the present-day meteoric exposure. Different fossils were found associated with the karstic caves such as bones of mammals, probably deers. Claystone layes 2 consists of less than one metre-thick green-brown clay layer composed by illite and quartz.

Unit III

Unit III sits above claystone layer 2 and represents the top travertine unit (Fig. 4.3). Unit III consists of ca. 4 m thick aggrading flat sub-horizontal travertine layers showing a lateral extension over tens of metres. This unit is highly weathered (Fig. 4.4 F) and is associated with contemporaneous red to brown soil.

4.4.2 Fabric types

A great variety of travertine fabric types characterizes the Pianetti travertine (Appendix 1). The wide range of travertine fabrics can be essentially distinguished into three categories: **1)** *travertine boundstone/cementstone s.l*, in which the original components, showing evidence of being lithified during deposition, are directly precipitated by the flowing or stagnant hydrothermal water. These fabrics include: a) dendritic boundstone; b) crystalline crust cementstone; c) laminated boundstone; d) raft boundstone/rudstone; e) coated bubble boundstone; f) micrite mudstone/microsparitic. **2)** *Encrusting travertine tobundstone s.l.,* in which the original components (acting as substrate) are directly encrusted by carbonate precipitated by hydrothermal water; this category includes substantially the coated reed boundstone/grainstone/rudstone. ***3)*** *Carbonate grains packstone/grainstone to*

floatstone/rudstone formed by intraclasts of already lithified travertine precipitates eventually associated with skeletal fragments such as ostracodes and gastropods.

Fabric type description and the proposed travertine classification are developed using the terminology of the classical classifications of carbonate textures by Dunham (1962) and Embry and Klovan (1971). The description of the porosity types is based on Choquette and Pray (1970) classification. The classical carbonate terminology is here combined with the currently travertine fabric nomenclature (cf. Chafetz and Folk,1984; Jones and Renaut, 1995; Guo and Riding, 1996).

4.4.2.1 Mineralogy, petrography, nano-scale features and characterization of the basic components of the travertine fabrics

The studied travertines are composed of almost pure $CaCO_3$ that occurs as 90% calcite and 9% aragonite (Fig. 4.5). EDS- and WDS- microanalyses reveal that sulphur, fluorite, barites, gypsum, quartz, clay minerals comprise the rests. Aragonite consists mainly of needle-like crystals (Fig. 4.5E, F and K) ca. 100 nm up to 4 μm in diameters and from ca. 5 up to 150 μm in lengths that in cross-polarized light microscopy show a characteristic sweeping extinction. These often form isopachous crusts growing normal to micrite/microspar structures (Fig. 4.5F). SEM observations show that aragonite crystals form also spherical- to ovoidal-like structures (50 to 200 μm in diameter) diverging from micrite/microspar or organic nucleus (Fig. 4.5L). Moreover, the travertine deposits are essentially made up by a mixture of micrite (anhedral crystals < 4 μm sensu Folk, 1959), microspar (subhedral to euhedral calcite crystals from 20 to 62 μm) and spar calcite (euhedral crystals > 62 μm) crystals (Fig. 4.3A-D, G-J). These carbonate crystals alone or combined form two key constituent units of the studied travertines, such as “cloudy-crystals” (Fig. 4.5 B-C, G-I) and “micrite” (Fig. 4.5A, D and J) “Micrite”, from dense to clotted peloidal (Fig. 4.5A) to peloidal (Fig. 4.5D) including often microspar, can be considered as the first basic constituent of the travertine fabrics. The aggregate arrangement of “micrite” can form elongate, tabular, laminated and dendritic structures. However, isolated masses of predominantly clotted peloidal micrite and often dense micrite of different size and shape are also observed into the studied travertine. Micrite appears frequently embedded within rhombic to bladed calcite crystals to form the “cloudy-crystals” (Fig. 4.5A-C,G-I), which show a crystalline appearance when observed at crossed polarized light, while under parallel polarized light crystals display a micrite texture (Fig. 4.5 B-C). The “turbid-crystals”, stacked or linked together, form complex branching

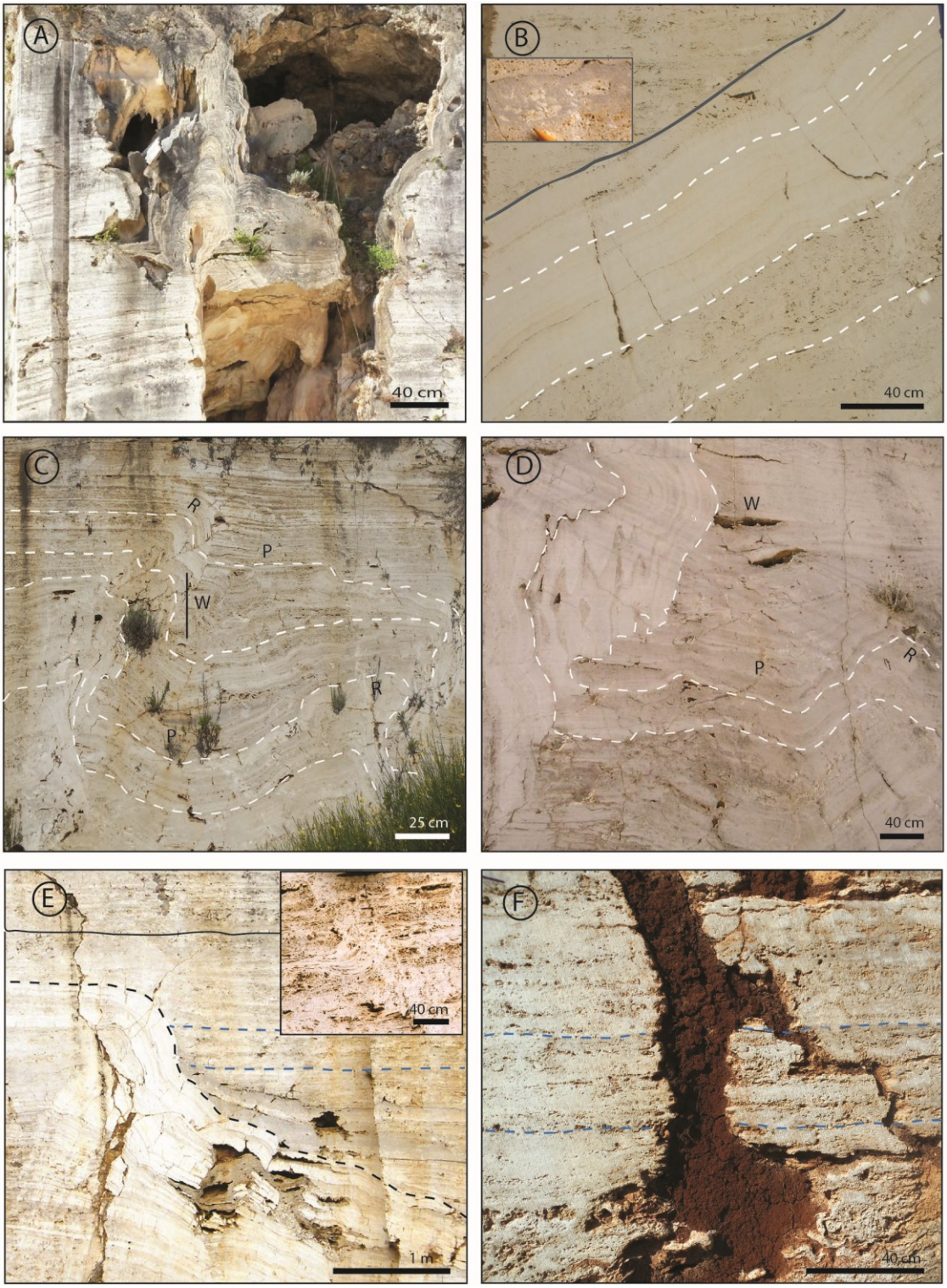

Fig. 4.4 Field images showing the different architecture patterns that characterized each travertine unit. A) Metre-scale columnar convex shaped structure localized in the thickest part (towards the SW) of Unit I. Note the highly karstified features producing caves. B) High-angle smooth slope of Unit II passing up-ward into sub-horizontal travertine topography. A brecciated discontinuity surface (grey line) with a lithoclastic rudstone/floatstone (enlarged view) dividing the clinoform deposits from the sub-horizontal one above in onlap. C) and D) Metre scale stepped topography in Unit I showing different strata orientations. W indicates layers convex outward and the upper face consists of downward thinning wedges; the lower face is usually overhanging. These sub-vertical layers bend of 90° to pass into horizontal to concave layers (P). The P layers pass laterally into raised and also convex morphologies (R). E) Clinoformal strata evolving laterally in stepped topography in Unit IIa. Note the sub-horizontal strata of Unit IIb onlapping the clinoformal/stepped layers of Unit IIb. Enlarged view of sub-horizontal strata of Unit IIb characterized by a meso-scale stepped morphology. F) Flat sub-horizontal layers of highly weathered Unit III. Note the *terra rossa* soil infilling dissolution cavitie.

structures that exhibit different architectures varying from irregular to fan-shaped to geometric dendrites. Often, the distribution of these cloudy-crystals aligned along a flat surface gives rise to continuous levels of juxtaposed basic elements that grow perpendicular to the surface.
At the nano-scale observation both "micrite" and the "turbid-crystals" seem to be composed by the assemblage of nano-globules (10 to 100 nm) (Fig. 4.5I) often associated with organic matter remains. The assemblage of these nanostructures seems to form irregular masses, 200 nm to 800 nm in diameter, that gradually organise into micron-size well developed crystals. The arrangement of the described key constituents give rise to the different fabric types.

4.4.3 Fabric description

Dendritic Boundstone

Dendritic boundstone (Figs. 4.6) consists of dendritic-like architectures exhibiting irregular to regular central region from which branches, with different morphologies, size and orientations, diverge. Mainly two different types of dendritic boundstone can be distinguished on the basis of their meso-scale morphologies. These are: 1) **shrub-like dendritic boundstone** (Fig. 4.6A-B) and 2) **radiating dendritic boundstone** (Fig. 4.6J).

1) shrub-like dendritic boundstone consists of three-dimensional structures characterized by an upward expanding, arborescent morphology (Fig. 4.6A-B). Shrub-like dendrites nucleate mainly on horizontal to gently undulated surfaces represented by laminated boundstone and brittle millimetre carbonate layers defined raft boundstone/rudstone. Bioclasts and bubbles locally represent a particular substrate for the shrub-like dendrite growth (Fig 4.6B).Microscopic analyses reveal that the shrub-like dendrite layers are essentially characterized by two principal end-members: A) *clotted peloidal dendritic boundstone* (Fig. 4.6C) composed of micrite (generally clotted peloidal micrite) arranged into dendrites whose morphology is irregular; and B) *rhomb-composed dendritic boundstone* (Fig. 4.6D-F) consisting of bush-like structures formed by cloudy-calcite crystals. Unlike the clotted peloidal end-member, the rhomb-composed dendrites display a strong geometric morphology with better defined outlines of the branches. In addition, the branches exhibit a regular morphology with systematic repeating habits. The micrite of the clotted peloidal dendrites and the turbid-calcite crystals that form the rhomb-composed dendrites give, respectively, high and low to medium response in auto-fluorescence.

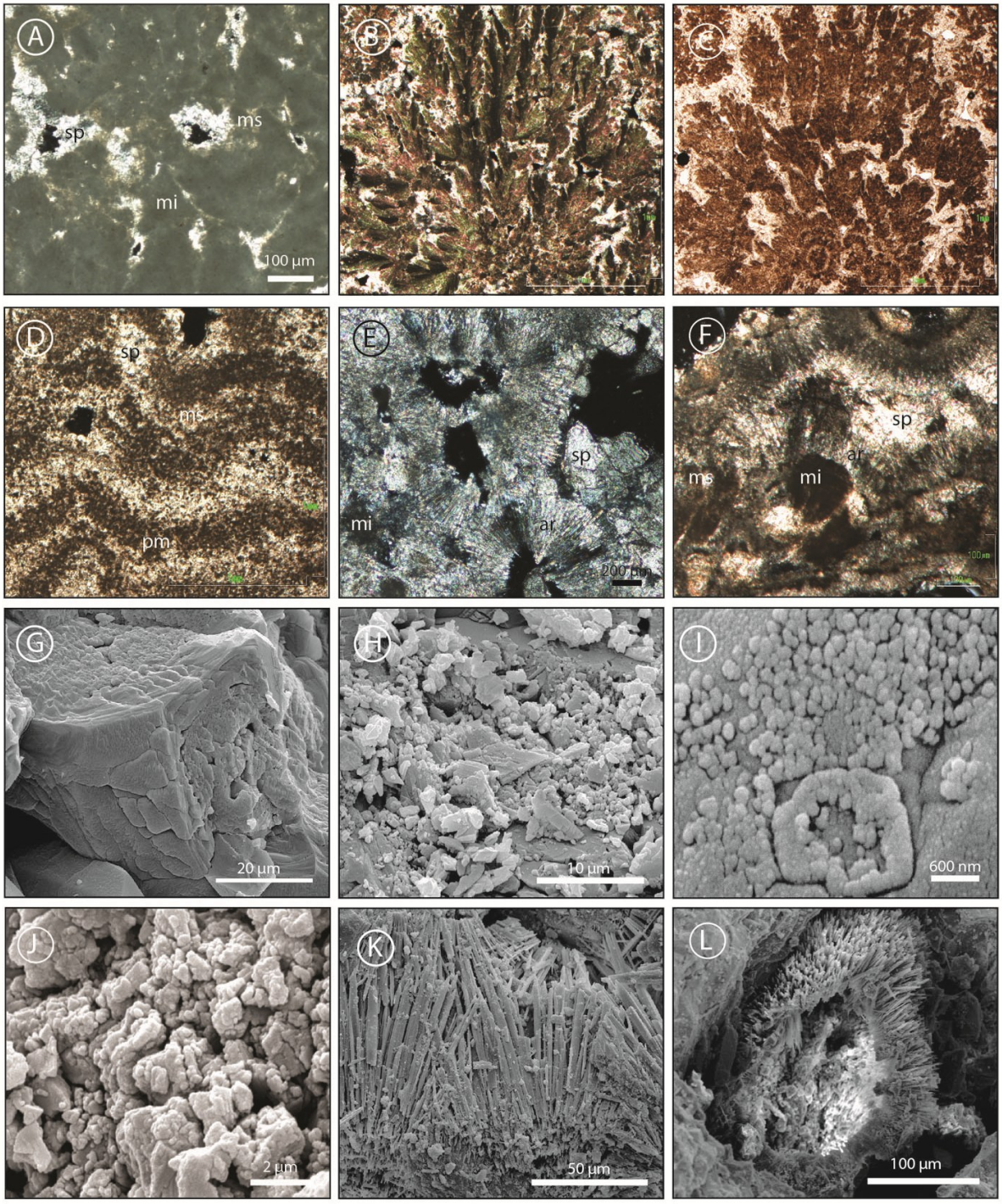

Fig. 4.5 Photomicrographs display the principal petrographic features of the Pianetti travertine. A) Close-up view of clotted peloidal dendritic boundstone characterized by dense to clotted peloidal micrite (mi) and microsparite (ms) within spar cement (sp). Pore space appears in black. B) Thin section photomicrographs of turbid-crystals organized into a dentritic morphology showing a crystalline appearance. Crossed polarized light. C) Close-up view of turbid crystals in C showing a micritic texture in plane polarized light. D) Peloidal micrite (pm) forms continuous wavy laminae alternating with calcite microspar (mp)/spar (sp) cement. Crossed polarized light. E) Cloudy acicular aragonite (ar) crystals with clumps of micrite (mi) and microspar remains in travertine sample. Coarse blocky calcite (sp) cement filling the remaining pore spaces (in black). Crossed polarized light. F) Acicular crystals forming an isopachous cement rim (ar) on dense micrite (mi) and microspar (ms) clumps. Calcite cement grows (sp) on the acicular crystals. Crossed polarized light. G) SEM image showing a section of turbid crystal characterized by the coalescence of nano-structures. H) Close-up view of a central area of the turbid-crystal in G. Nano-globules form irregular masses and partially to totally developed crystals. I) Close-up view of spherical to rod-shaped nano-globules. SEM image. J) SEM image showing mainly micrite crystals formed by the assemblage of nano-structures that gives rise to grainy-like morphology of the calcite crystals. K) SEM image of needle-like aragonite crystals. L) SEM image displaying aragonite needle crystals arranged into spherulite-like disposition around an hallow centre.

The occurrence of biogenic features is confirmed by SEM analyses (Fig. 4.6G-I). Organic matter consists mainly of mucous-like planar sheets (Fig. 4.6G-H), possible relicts of extracellular polymeric substances (EPS) and bacteria-like structures *ca.* 100 nm in size ranging from ellipsoidal/rod to spherical in shape (Fig. 4.6I). In addition, nano-globules, ranging from 20 to 100 nm, are widespread (Fig. 4.6G-I). They appear progressively to substitute EPS and gradually to coalesce to form irregular masses (200 nm to 800 nm in diameter), that organise themeselves into micrite, microspar and cloudy-spar calcite.

2) Radial dendritic boundstone occurs as typically white spherical structures showing a dendritic-like overgrowth (Fig. 4.6J). They nucleated mainly on horizontal to gently undulated surfaces represented by laminated boundstone. These dendrites are also largely lateral transitional into the shrub-like dendritic boundstone. Microscopic observation reveals that this boundstone consists mainly of dense and clotted peloidal micrite (Fig.4.6K). Often, branches made by rhombic to bladed cloudy-calcite crystals occur. Under fluorescence-light, the radiating dendritic structure shows weakly to high luminescence. It was observed that the luminescence is higher if the radiating dendritic boundstone is composed by clotted peloidal micrite. SEM analysis confirms that the radiating dendritic boundstone is composed by an association of calcite precipitates with organic matter remains (Fig. 4.6L) mostly represented by 10 nm wide filamentous-like structures and EPS. Detailed observations highlight also the diffuse presence of nano-globules (range mainly from 21 to 100 nm) within the radiating dendritic boundstone. These nano-structures replace/substitute the organic matter and coalesce to form irregular masses that progressively assume sharp crystal faces (Fig. 4.6L).

Crystalline crust cementstone

Macroscopically this cementstone consists of generally white crystalline crusts, which are subdivided on the basis of their field appearance into: 1) **Thick crystalline crust cementstone** (*ca*. 3 cm up to 20 cm in thickness; Fig. 4.7A) and 2) **Thin crystalline crust cementstone** (a few millimetres to *ca*. 3 cm thick; Fig.4.7B**).** The crystalline crusts commonly nucleate on laminated boundstone layers and micrite mudstone/microsparstone layers**.** In correspondence of a change of the topographic gradient, the crystalline crust layers pinch-out laterally into other fabric types, such as the laminated boundstone and shrub-like dendrites.

1) Thick crystalline crust cementstone consists of laterally adjacent calcite crystals showing a range of dendritic-like morphologies varying largely from those with a mostly fibrous

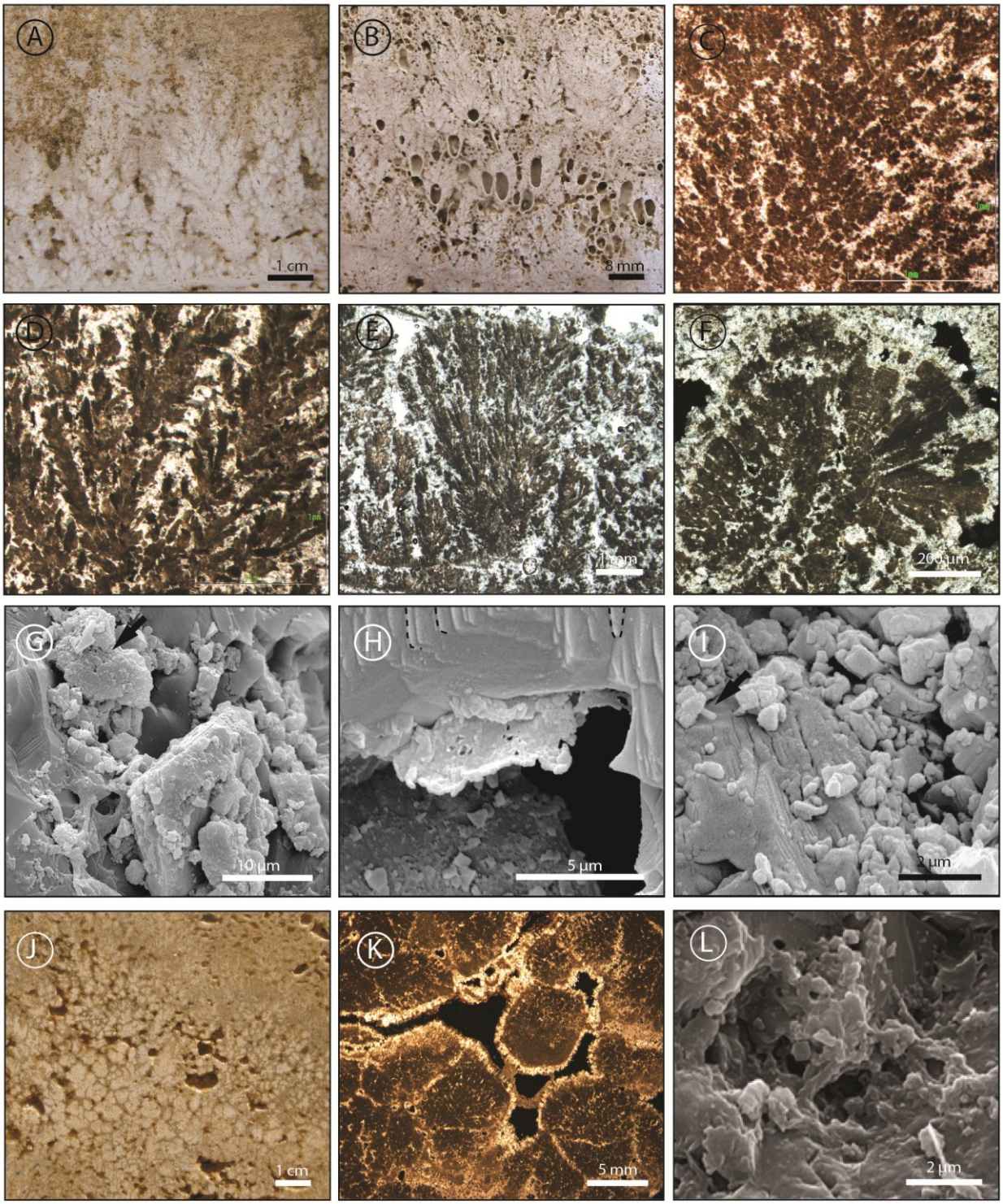

and elongate appearance to those that present a pinnate form. The calcite crystals are oriented with their long axis perpendicular to the growing surface. Locally, crystals display a slight lateral bending of their axes in the downslope (or downdip) direction. In some cases, a gravitational orientation of these crystals is also observed. Micron size to millimetre thick laminae may cross the calcite crystals. At the micro-scale observation, the thick crystalline crust cementstone is constituted by the cloudy-crystals displaying crystal habits ranging from poorly to well-

developed rational crystal faces. The cloudy-crystals form branched structures by crystal splitting exhibiting a variability of morphologies (Appendix 1). Petrographic observation shows the presence of possible filaments of organic origin embedded within the crystalline dendrites (Fig. 4.7E). Biogenic features represented by gently folded sheets, less than 100 nm up to 700 nm thick and several micrometres long structures (Fig. 4.7G) and bacterial-like forms (Fig. 4.7H) are observed under SEM. Nano-scale observations also reveal that cloudy-crystals are built-up by the aggregation of nano-globules ranging mainly from 10 to 130 nm (Fig. 4.7I). Nano-globules are often associated with organic matter.

2) Thin crystalline crust cementstone varies from white unstructured crystalline crusts to those crusts displaying calcite crystals in fan arrangement (Fig. 4.7B). Millimetre, thick and parallel to each other laminae, cross and often delimit the calcite crystals. Microscopic analysis reveals that the thin crystalline crust cementstone consists of cloudy crystals and it is essentially characterized by two end-members: A) *Crystalline fan–dendritic cementstone* (Fig. 4.7J and K) formed by finely laminated dendritic architectures exhibiting in general well-developed fan-shaped morphologies (See Appendix 1); and B) *Crystalline laminated cementstone* consisting of densely laminated crusts characterized by the juxtaposition of moderately to strongly raised structures resembling mammillate cones or fan (Fig. 4.7L). The crystalline laminated cementstone represents often the vertical evolution of the crystalline fan dendritic cementstone.

Fig.4.6 (previous page**)** Photomicrographs of dendritic boundstone. A) Field appearance of shrub-like dendritic boundstone consisting of bush-like morphologies surrounded mainly by cream coloured and often light grey matrix. Note the variation of dendrite size nucleated on brittle millimetre carbonate layers (raft boundstone/rudstone). B) Shrub-like dendrite associated with coated gas bubbles. Locally dendrites grow radially with respect to the bubble surface. Unit I. C) Densely packed clotted peloidal dendrite boundstone of Unit II. D) Rhomb-composed dendritic boundstone of Unit I characterized by well-developed dendritic morphologies. Each branch is formed by the association of several turbid-crystals. E) Rhomb-composed dendritic boundstone starting at the base with regular branched morphologies that evolve into mostly straight morphology. F) Rhomb-composed dendritic boundstone showing the turbid-crystals organized to form a well-developed fan-shaped dendrite. G) Images showing organic matter remains associated with clotted peloidal boundstone. Note the gently folded sheets of mineralized organic matter connected to calcite crystals. Sub-spherical, nanometre in size, structures combined and organized to form irregular and lumpy masses that progressively assume crystal faces (black arrow). H) Gently folded organic matter sheet within crystals extending across them. The surface of the organic matter remains is characterized by the presence of nano-spheres that appear to replace it. Note that also the surface of the large crystals shows an irregular granular appearance consisting of sub-nanometre size spherical to ovoid bodies arranged in rods that assumed a triangular-like morphologies. Clotted peloidal dendritic boundstone. I) SEM images of rhomb- composed dendritic boundstone characterized by an association of anhedral to partially developed calcite crystals varying from nanometre to micron in size. Nano-globules are mostly spherical. Bacterial-like structure are also present (black arrow). J) Field image showing from sub-rounded to sub-angular weakly compacted radial dendritic boundstone along a quarry wall of Unit I. These architectures constitute the central area of circumscribed bioherm-like structures. Note the high microporosity. K) Photomicrographs of radiating dendritic boundstone cropping out along the quarry walls of Unit I. Densely packed radiating dendrites formed by clotted peloidal micrite and microspar. The single dendrites are layered by isopachous cements. Ostracodes are also observed. In black, inter dendrite porosity. The framework porosity in between branches is partially or totally occluded by cement (white arrows). L) Scanning electron microscope (SEM) photomicrographs of radiating dendritic boundstone showing an intimate mixture between calcite precipitates and organic matter of possible mineralized EPS. Nano-structures and irregular masses are also present. These masses appear formed by the coalescence of nano-globules that gradually give rise to calcite crystals. Note the microporosity.

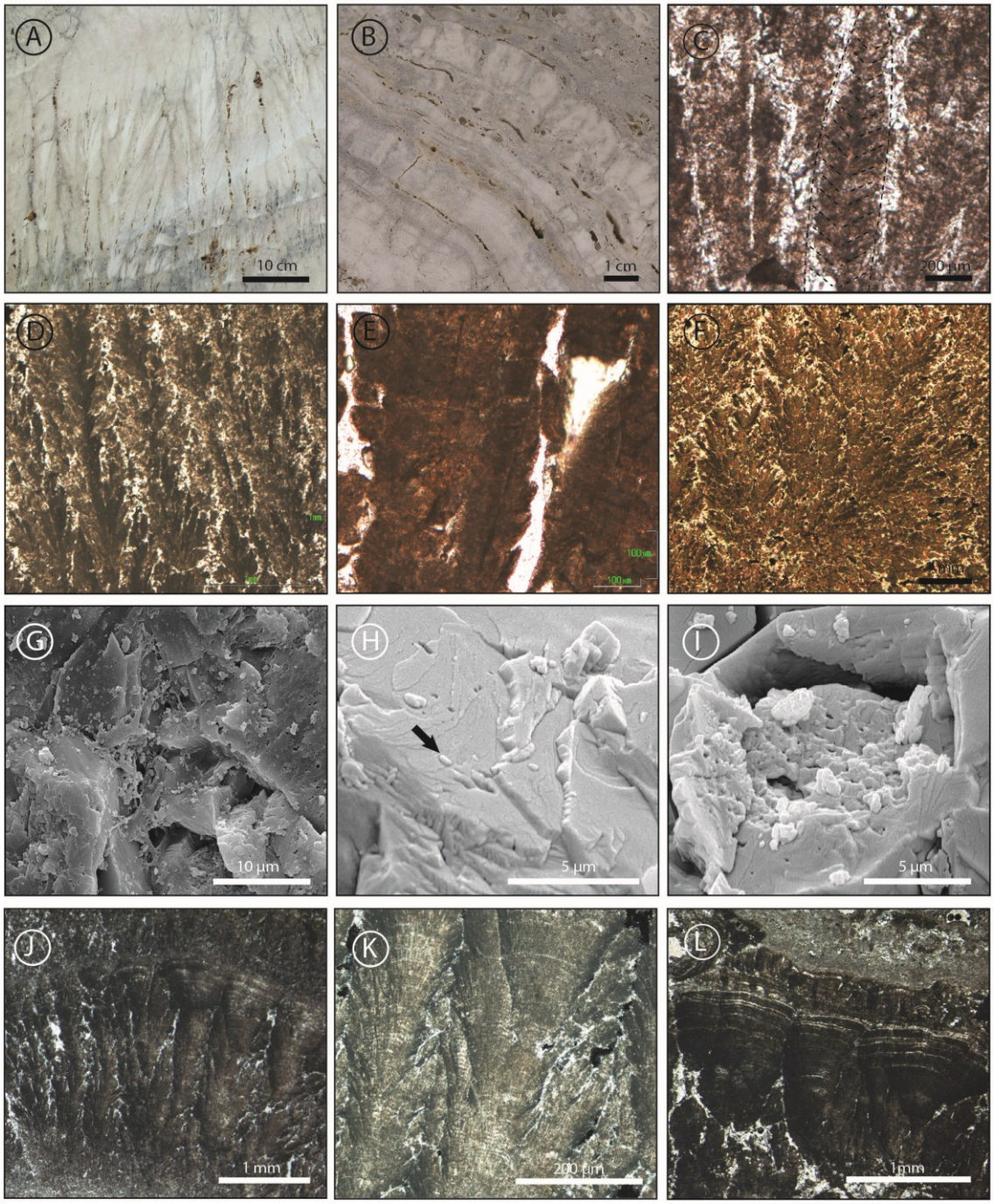

In fact, it may occur that the base of the raised cones display poorly defined dendritic-like structures. Transitions between the two end-members are observed.

Laminated boundstone

Laminated boundstone consists of millimetre-centimetre scale sub-horizontal to inclined (from ca. 5 to 90°) layers characterized by laminated structures. The laminated structures exhibit

almost entirely horizontal to wavy laminated and irregular arrangements (Fig. 4.8A-B) and also display a continuous range of meso-scale morphologies varying essentially from 1) **dense** (with porosity less than 5% per volume) to 2) **porous** (porosity >50%) **laminated boundstone**. The laminated boundstone is vertically alternated with other travertine fabrics such as crystalline dendrite cementstone, coated bubble boundstone, shrub-like dendritic boundstone (Fig. 4.8A), radiating dendritic boundstone, raft boundstone/rudstone and micrite mudstone/microsparstone. Finally, laminated boundstone layers may represent the lateral evolution of the continuous crystalline crust layers. Petrographic observation reveals that laminated boundstone types are formed by an alternation of micrite and microspar bands, often aggregated into packages with sub-spherical/lenticular discontinuous pores (Fig 4.8C-E). Micron-size filamentous structures are diffuse within the micritic/microsparitic laminae (Fig.4.8F). Micrite and microsparite show marked differences in autofluorescence: the micrite shows a strong autofluorescence, whereas microsparite is weak luminescent or black. SEM analyses show that organic matter is pervasive and generally well preserved (Fig. 4.8 G-H). Organic matter is mainly represented by C-enriched planar sheet membranes (several nanometres thick) that often show a honeycomb to filamentous-like morphology. Organic moulds of possible bacteria-like structures are associated with the mucus-like substances (Fig. 4.8G). Spheroidal bodies, ca. 1-2-μm in diameter, are widespread within the laminated boundstone (Fig. 4.8I). The walls of the spheroidal forms have a fine granular texture formed of nano-globules (ca. 30 to 100 nm in size).

Fig. 4.7 (previous page**)**. Crystalline crust cementstone. A) Thick crystalline crust cementstone mostly consisting of dense packages of bladed calcite crystals. Note the high porosity in between the elongated crystals. Pores seem to be organized into a vertical channel-like disposition. B) Slightly undulated, parallel to each other gently dipping crystalline crusts formed by fan-like to dendritic fibrous morphology. C) Photomicrographs of crystalline dendritic cementstone formed by the lateral juxtaposition of single bladed calcite crystals characterized by symmetrically branched smaller crystals with respect to a central stalk. Unit II. D) Densely packed crystalline dendrites displaying a mostly regular repetition of the branches with respect to a central area. Note the second generation of branches. E) Crossed polarized light photomicrograph of crystalline dendrite cementstone at Unit II showing the presence of possible filaments. F) Crossed polarized light photomicrograph of crystalline dendrite cementstone of Unit I. The densely packed dendrites exhibit a strong crystalline habit and fan-shaped morphology. G) SEM image showing network of EPS (extracellular polymeric substances) remains connected with calcite crystals of crystalline dendritic cementstone. H) Turbid crystals of crystalline dendrites showing intra-crystal pores, from rounded to rod-shaped . Black arrow points to possible bacterial like-bodies. These pores may be related to the decay of bacteria bodies (cf. Chafetz and Guidry 1999). I) Cross section through the calcite crystals showing the presence of a looser central area enveloped by a denser rim. The central area of the calcite crystal is formed mainly by micron size, lumpy masses formed by the coalescence of the nano-crystal units. J) Photomicrograph of crystalline fan dendritic boundstone starting as dendritic structures with a fan morphology that evolve into raised and stronger fan structures. Porosity in white. K) Crossed polarized light image showing the densely packed micron size laminae that cross perpendicularly the dendritic structures of the crystalline fan dendritic cementstone micro-fabrics. Note the pore spaces are mainly located between laterally subsequent dendrites. L) Strongly raised conic like-structures forming the crystalline laminated cementstone. These structures are oriented perpendicular to the depositional surface and are formed by the vertical and lateral juxtaposition of fan-like turbid-crystals. Micron-size laminae cross the cone-like structures and often represent the upper and basal limits of each turbid-crystals. Note the inter-laminae and inter-dendrite porosity.

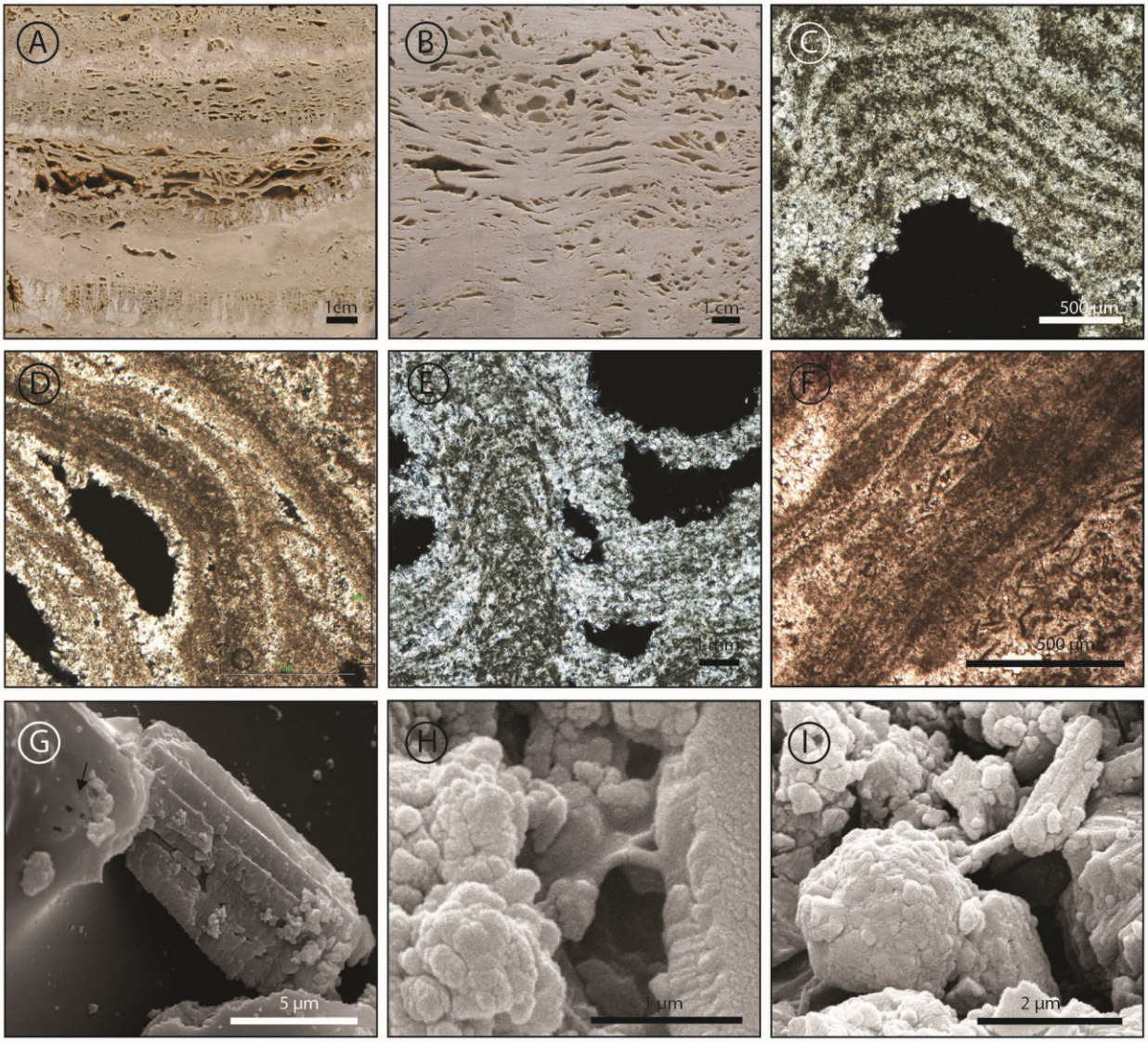

Fig.4.8 Laminated boundstone. A) Field appearance of laminated structures displaying a continuous range of meso-scale morphologies varying essentially from dense to porous. Shrub-like dendrites nucleated on the laminated boundstone. B) Outcrop image of porous laminated boundstone formed by sub-spherical to lens-shaped elongated cavities trapped between dense and wavy laminae. C) Crossed polarized light photomicrograph showing laminated boundstone with micrite/microspar laminae parallel to the underlying pore morphology. Note the scalenohedral calcite cement that lines the pores. D) Inclined and slightly convex micritic laminae aggregated into packages with sub-spherical/lenticular discontinuous pores. Porosity is in black in image with crossed polarizers. E) Micro-columnar structures formed by vertical repetition of the laminae formed by convex upward morphology. The laminae create a porous framework. Crossed polarized light photomicrograph. F) Laminated boundstone displaying filament-like structures within the laminae. Parallel polarized light photomicrograph. G) SEM photomicrograph showing the association of organic matter with the calcite precipitate. Black arrow points to organic moulds of possible bacteria-like structures associated with the mucus-like membrane. H) SEM photomicrograph of nano-globules associated with organic matter remains. These nano-crystals appear to substitute progressively the EPS and to coalesce together to form calcite crystals. I) SEM photomicrograph showing the presence of micron size spheroidal forms characterized by lumpy texture of nano-crystal aggregates.

Raft boundstone/rudstone/grainstone

Macroscopically, rafts (Kitano, 1963; Folk et al., 1985, Chafetz et al., 1991b, Guo and Riding, 1998; Özkul et al., 2002) consist of white to cream coloured, flat horizontal carbonate structures

forming boundstone (Fig. 4.9A); rarely gravitational deformations give rise to slightly convex/wavy disposition of the sheet-like forms. Frequently rafts appear fragmented (predominantly from 5 mm up to 5 cm long sub-horizontal to sub-vertical fragments) forming cemented raft grainstone to rudstone (Fig. 4.9A). Raft deposits are generally interlayered with laminated and shrub-like dendritic boundstone and are often observed in association with the coated bubble boundstone fabric. At microscopy and SEM observations, rafts are generally characterized by micrite/microspar films from which calcite/aragonite extend away to create a symmetric to asymmetric fringe (Fig. 4.9 B-I). Spherulite-like structures (*sensu* Guo and Riding, 1992) showing an hollow centre and external radial crusts of aragonite needle crystals are widespread (Fig. 4.5L and 4.9J). The micrite that constitutes the rafts gives a response in auto-fluorescence and SEM analyses confirm the presence of organic matter remains (Fig. 4.9G, K-L). These latter consist of micron-size fungi-like structures (Fig. 4.9G), mucous-like organic matter remains (Fig. 4.9K), well-preserved spheroidal bodies (1-7 μm in diameter; Fig. 4.9L), bacteria-like structures (ca. 100 nm in size) ranging from ellipsoidal/rod to spherical in shape. Nano-globules (20-100 nm in size) form the majority of the calcite crystals (mostly micrite and microspar) and are often associated with organic matter remains (Fig. 4.9G, K-L).

Coated bubble boundstone

Macroscopically, coated bubble (Kitano, 1963; Chafetz and Folk, 1984; Chafetz et al., 1991; Guo and Riding, 1998; Fouke et al., 2000; Özkul et al., 2002) boundstone consists of cream coloured to white calcite spherical precipitate enclosing a hollow space (Fig. 4.10A). The coated gas bubble boundstone displays vertical and/or lateral transitions with shrub-like dendrites, laminated boundstone, crystalline crust and raft boundstone/rudstone layers. Petrographic observation reveals that coated bubble boundstone consists of sub-spherical to circular or elongated micritic/microsparitic coatings around porous structures (Fig. 4.10 B-D). The micrite that constitutes the coated bubbles gives response to fluorescence. SEM analysis confirms the presence of organic matter remains consisting of mucous-like planar sheets representing possible relicts of EPS (Fig. 4.10E-F). The presence of nano-globules (15-100 nm in diameter) is diffuse associated mainly with possible EPS and calcite crystal.

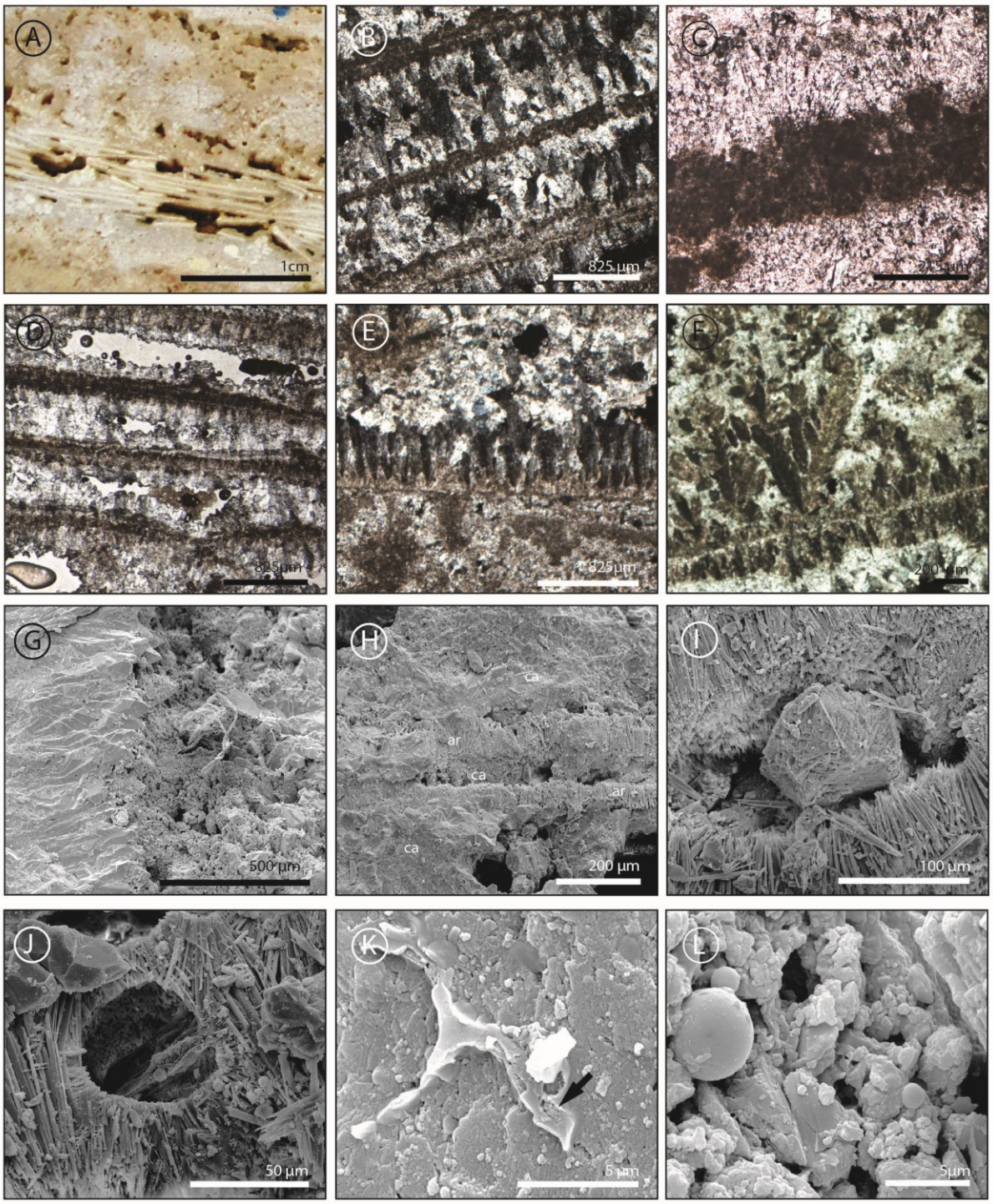

Micrite mudstone/microsparstone

Macroscopically, micrite mudstone/microsparstone consists of homogeneous, cream coloured to light grey, carbonate precipitate (Fig. 4.10G). This fabric vertically alternates with other travertine fabrics such as crystalline dendrite cementstone, coated bubble, shrub-like dendritic

boundstone, radiating dendritic boundstone, and raft rudstone. Microscopic analysis reveals that the micrite mudstone/microsparstone macro-fabric is essentially characterized by two end-members, described below: a) micrite mudstone constituted by non-laminated clotted peloidal/peloidal micrite (Fig. 4.10H) and b) microsparstone formed by dense non laminated microspar, with sub-rounded to elongate peloids observed within the microspar (Fig. 4.10I). Both the micro-fabrics show sub-spherical/lenticular to irregular pores (generally less than 60 μm up to 5 mm wide). Ostracodes are also widespread (Fig. 4.10H). SEM observations highlight the presence of organic matter remains within the micrite mudstone/microsparstone (Fig. 10J-K). Organic matter is mainly represented by C-enriched planar sheet, several nanometre in thickness, membranes that often show honeycomb to filamentous-like morphologies. On the surface of the EPS remains, nano-globules are observed (Fig.4.10J-L).

Coated reed boundstone/grainstone/rudstone

Macroscopically, the coated reeds consist of cream coloured carbonate precipitates around degraded phytoclastic reeds (Fig. 4.11A). Coated reeds are normally isolated, but rarely reed moulds are also observed forming laterally extended continuous layers. Reed fragments form rudstone and grainstone in pockets up to 15 cm in diameter. Coated reeds are commonly associated with laminated, coated bubble boundstone, dendritic cementstone, raft and carbonate

Fig. 4.9 (previous page). Raft boundstone/rudstone. A) Field appearance of raft fabric type consisting of fragmented thin carbonate layers stacked vertically and laterally whose thickness is increased by the precipitation of cement, which partially fills the pore spaces. Note also evidence of dissolution probably related to meteoric diagenesis. B) Crossed polarized light photomicrograph showing micritic (mostly clotted peloidal) to microsparitic straight elongate films. Sometimes an inner microsparitic horizontal structure divides into two parts the micrite band. Note the multiple generations of acicular/fibrous to bladed isopachous cement extending from the rafts into the elongate primary pore spaces localized between the individual rafts. C) Close-up view of B showing multiple generations of cement growing perpendicular to the micrite films that form the raft structures. Ghosts of acicular crystals grow perpendicular to the clotted peloidal micrite film. These acicular crystals seem to be incorporated within a second generation of prismatic crystals growing in optical continuity with the acicular precursor. Parallel polarized light photomicrograph. D) Flat, horizontal to wavy, mostly microsparitic and micrite rafts, which show inner microsparitic elongate structures and are laminated. E) Rafts formed by micrite/microspar layers overlain by diverging bladed crystals. Multiple generations of cement grow in optical continuity with the bladed crystals and fill the pores. Prismatic crystals occur in optical continuity with the fibrous precursor. Prismatic crystals are followed by blocky calcite. F) Crossed polarized light photomicrograph of raft boundstone characterized by the coalescence of the bladed turbid-crystals, which diverge perpendicularly oriented from the inner micrite and elongate structure. Some bladed crystals evolve into rhomb-composed dendritic boundstone. G) SEM image showing micritic layer comprised between microsparitic/sparitic layers formed by partially developed calcite rhombohedra. The micrite layer consists of anhedral to subhedral calcite crystals. Micron-size fungi-like structures occur in the micritic layer. H) SEM image showing the alternation of aragonite (ar)/calcite (ca) crystals that give rise to raft structures. I) Close-up view of H showing calcite film (characterized by the coalescence of nanoglobules) between the aragonite rims. J) SEM image displaying aragonite needle-shaped crystals arranged into spherical-like disposition around a hollow centre. K) Close-up view of mineralized mucus-like planar sheet connected to calcite crystals; black arrow points to incipient mineralization phase of EPS. Calcite and EPS remains display a lumpy texture. L) Spherical bodies within porous micrite/microspar layers. These may represent spores or possible bacterial bodies. The walls of the spheroidal forms exhibit a fine granular texture formed by nano-crystal aggregates. Note the presence of nano-globules that coalesce to form irregular masses that gradually organise into a more crystalline morphology showing incipient crystal face development.

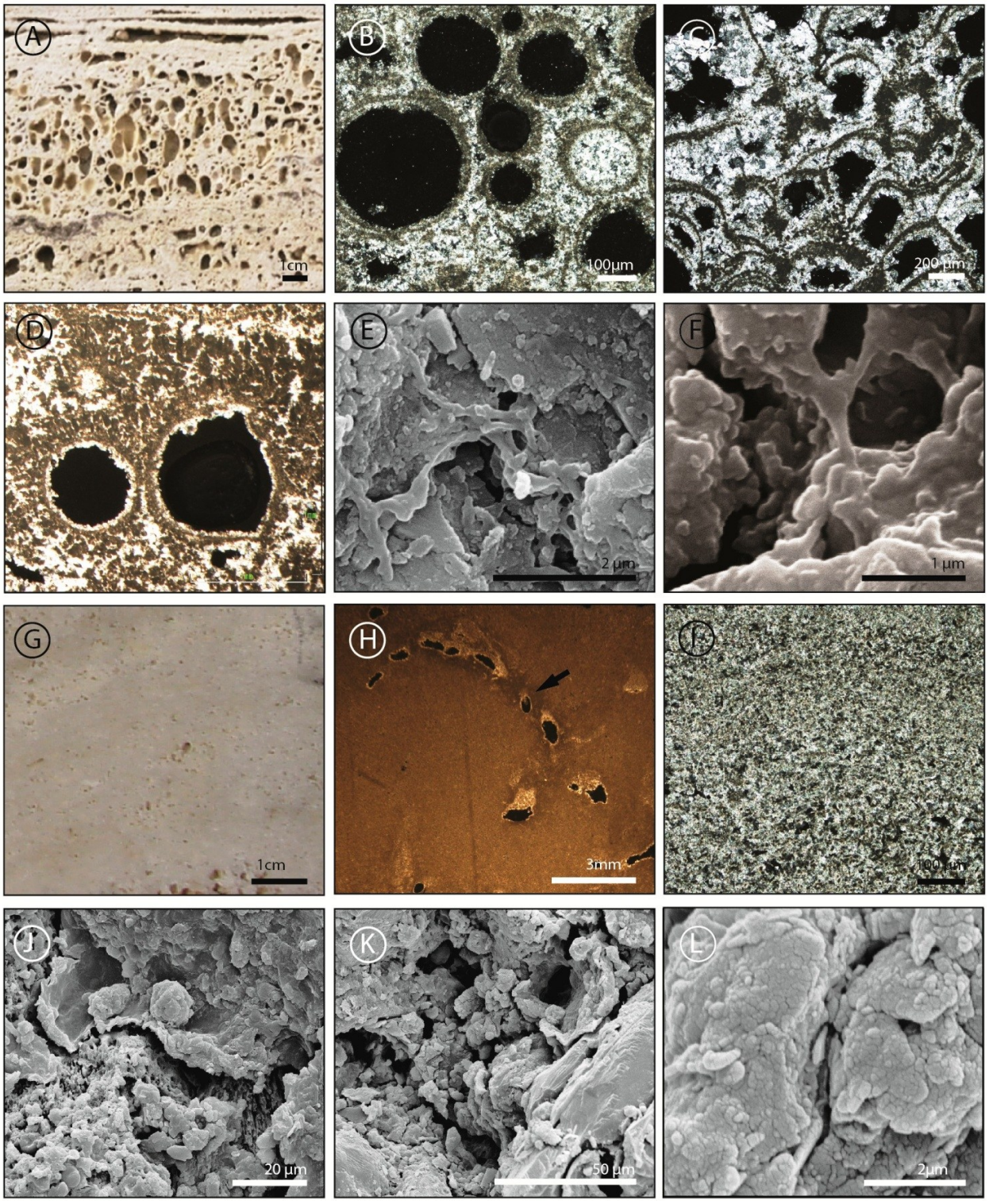

grains grainstone/rudstone layers. Frequently shrub-like dendrites grow radially from the circular. reed cross section (Fig. 4.11A). On the basis of petrographic observation, the coated reed boundstone is a highly porous microfabric, characterized by a framework of carbonate precipitate organised around sub-spherical/lenticular and elongate pores (100 µm to 7 mm in

diameter; Fig. 4.11 B-D). Petrographic observation reveals the presence of a micrite layer that isolates the internal reed porosity. SEM analysis reveals that calcite crystals that form this fabric type consist mainly of anhedral (mostly raised structures ranging from ca. 30 to 100 nm in size to a few microns in size lumpy masses) to subhedral micrite and euhedral microspar and rarely spar cloudy-crystals with rhombohedral shapes (Fig. 4.1E-F). However, scalenohedral calcite crystals are also observed. EPS remains, even less extent, are also observed

Carbonate grains packstone/grainstone to floatstone/rudstone

This fabric type consists by carbonate grains (intraclasts, extraclasts, and bioclasts) cemented together to form grainstone/rudstone and floatstone/rudstone, surrounded by a cream coloured carbonate precipitate or a light grey mixed carbonate-clay matrix (Fig. 4.11G). The travertine intraclasts are sub-rounded to sub-angular and include mainly fragments of clotted peloidal to rhomb-composed dendrites (Fig. 4.11H), crystalline dendrites, raft boundstone/grainstone and coated reeds. Petrographic observations reveal that carbonate precipitates around grains consist of microsparite and sparite (Fig.4.11H-I). Ostracod grainstone is widespread (Fig. 4.11I).

4.4.4 Porosity and permeability

Pore space is an important component of travertine fabrics (Fig. 4.12). The Pianetti travertine samples were examined for reservoir properties.

Fig. 4.10 (previous page).Coated bubble boundstone and micrite mudstone/microsparstone. A) Field appearance image showing densely packed coated bubble boundstone organized into lateral extended sub-horizontal layers. B) Crossed polarized light photomicrograph showing bubble boundstone consisting of sub-spherical to circular porous structures made of micrite layers overlain by columnar cement followed by blocky sparite. C) Honeycomb like-structure resulting from a framework of coated gas bubbles. Note the bladed crystals growing on the bubble micrite layer, followed by blocky calcite. Crossed polarized light photomicrograph. D) Isolated coated gas bubbles overlain by rhomb composed dendritic boundstone. Crossed polarized light photomicrograph. E) SEM images showing organic matter remains associated with coated bubbles. Gently folded sheets of mineralized organic matter are connected to calcite crystals. Note the lumpy texture that characterizes the calcite crystals. F) Close-up view showing the organic matter remains and the diffuse presence of ellipsoidal/rod to spherical in shape nano-crystals. The mucus-like substance seems to be progressively substituted by calcite crystals. The initial stage of precipitation is represented by isolated sub-spherical nanometre scale structures in EPS. Gradually these structures coalesce and organize to form irregular masses that progressively assume incipient crystal faces. G) Field appearance of micrite/microsparitic mudstone consisting of cream coloured to light grey layers. Note the lenticular to irregular pores that often occur. H) Photomicrograph showing the mudstone microfabric. Black arrow points to ostracode shells. Note the primary and secondary lenticular to irregular pores. I) Crossed polarized light photomicrograph showing microsparstone exhibiting the presence of sub-rounded peloids. Each peloid is included within a calcite crystal. J) and K) SEM photomicrographs showing the association of mineralized mucus-like planar sheet connected to calcite crystals. Note the presence of nano-globules associated with organic matter remains. These nano-crystals appear to substitute progressively the EPS and to coalesce together to form calcite crystals. L) Sub-spherical to globular, raised structures organized to form irregular micrite masses. The nanometre-scale nano-globules are assembled together to form irregular masses that gradually organize into more crystalline micron-size morphology showing incipient crystal face development.

4.4.4.1 Porosity type

Pianetti travertine shows a wide range of depositional and secondary porosity types (Fig. 4.12). Primary pore (or depositional pore) types include: 1) inter-dendrite porosity related to all the dendritic structures such as dendritic boundstone and crystalline crust cementstone (Fig. 4.12A-B); 2) inter-laminae porosity especially observed within the laminated boundstone (Fig. 4.12C) and crystalline laminated cementstone (Fig. 4.7 L); 3) fenestral pores formed mainly by gas bubbles trapped within the laminated boundstone and raft boundstone/rudstone (4.12 D); 4) the bubble porosity specific of the coated bubble boundstone (Fig. 4.12 E); 5) inter-particle porosity observed within the radiating dendritic boundstone (Fig.4.6K), raft boundstone/rudstone (4.12D), micrite mudstone/microsparstone (4.12 F) and in the carbonate grains grainstone/rudstone (Fig. 4.12H); 6) intra-particle pores within particles such as ostracodes and gastropods mostly in bioclastic grainstone.

Secondary porosity consists of pores that form as a result of post-depositional (manly meteoric) dissolution and tectonic fractures. Secondary porosity is also related to the stability of the primary mineralogy. Such pore types include: 1) mouldic porosity (Fig. 4.12G, I, J) including bio-mouldic of reed boundstone/grainstone/rudstone, skeletal grains and mouldic porosity related to dissolution of crystals; 2) vugs (Fig. 4.12K) such as large pores that cross fabric types, because dissolution was not fabric-selective; 3) large scale fractures and caves (Fig. 4.12L). SEM analysis reveals a significant micro-porosity varying from primary inter-crystalline to secondary intra-crystalline porosity (Fig. 4.12E and J). Micro-pores range from less than 10 nm up to 400 microns and are characterized by squared to rounded to irregular outlines.

Inter-crystalline porosity occurs between the micrite and microsparite crystals and organic matter (Fig. 4.12 D and F). The intra-crystalline porosity consists mainly of: 1) square-shaped pores within the calcite crystals (Fig. 4.12J), and rounded to rod-shape pores within crystals (Fig. 4.7H, 4.8G). Micro-porosity is high in clotted peloidal dendritic boundstone (Fig. 4.6 G-H), laminated boundstone (Fig. 4.8 G-I), raft boundstone/rudstone (Fig. 4.9 J and L) and micritic areas of coated bubble boundstone (Fig. 4.10E-F). Micrite mudstone/microsparstone reveals also a good micro-porosity network (Fig. 4.10J-K and 4.12 F).

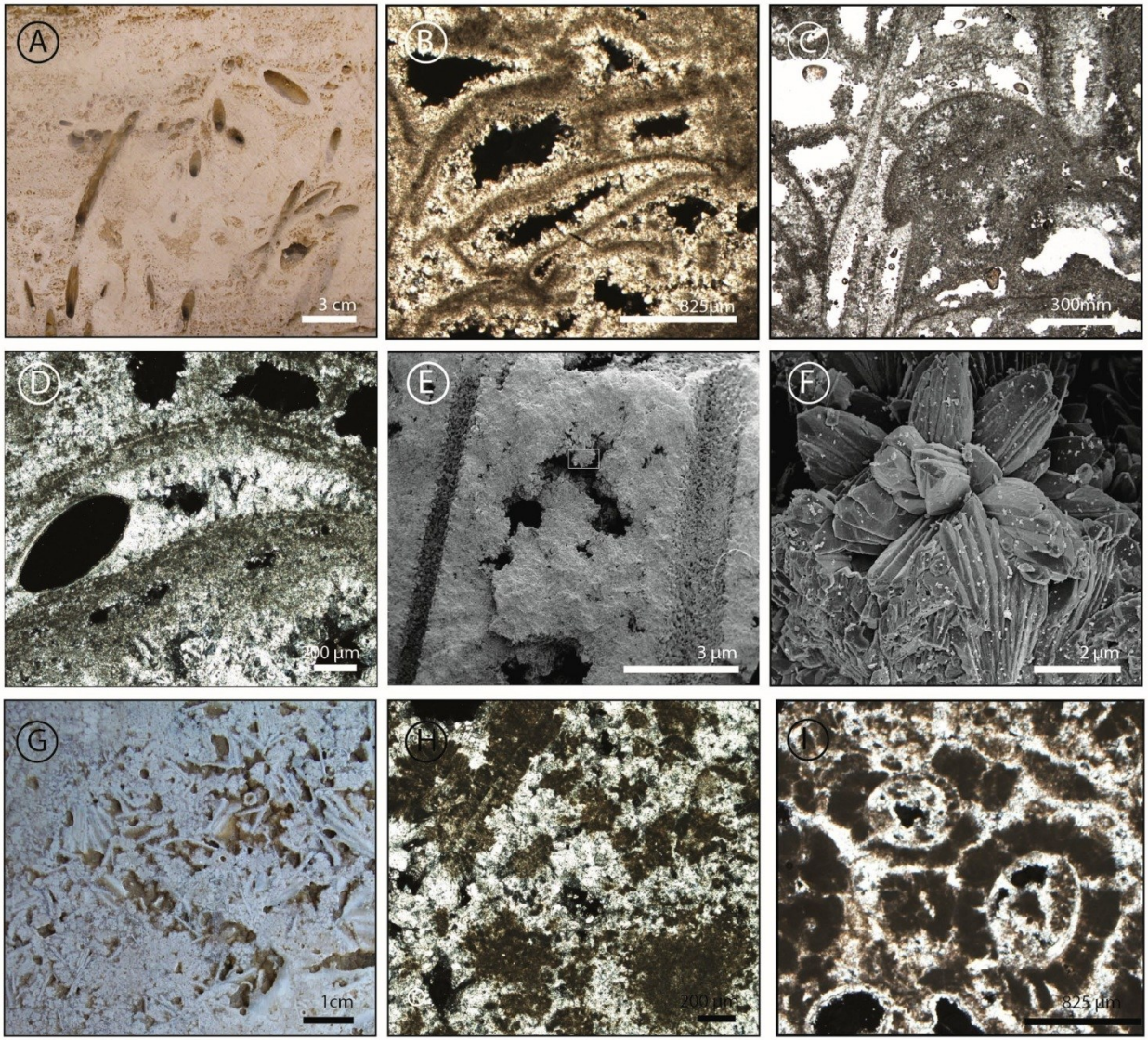

Fig. 4.11 Coated reed boundstone/grainstone/rudstone and carbonate grains grainstone/rudstone/floatstone. A) Field appearance of coated reeds consisting of carbonate coated vegetation leaving an elongated porous area in Unit I. Shrub-like dendrites grow radially with respect to the reed coating. B), C) and D) Crossed polarized (B and D) and parallel polarized light (C) photomicrographs showing the coated reed microfabric of Unit III. Micrite coatings around the reeds form sub-spherical/lenticular and elongated pores. Note the bladed cements lining and partially filling the pores. E) SEM image of coated reed boundstone highlights the presence of micrite, microspar and spar calcite. Biomoldic porosity is filled by microscpar/spar. F) Close-up view of E showing calcite crystals lining the pores. G) Field appearance of millimetre- to centimetre-size intraclasts filling pockets in sub-horizonthal layer of Unit I. H) Crossed polarized light photomicrograph of poorly sorted grainstone formed by fragments of clotted peloidal dendrites and rafts cemented by microsparite and sparite. I) Crossed polarized light (right image) showing ostracode grainstone .

4.4.4.2 Helium porosity and permeability, micro-CT scanning and Avizo Fire software

The Helium porosity and permeability measurements show that travertines display a wide range of porosity values, from 1 to 29%, and permeability, from 0.006 up to 50000 mD (Fig. 4.13A). Samples of Unit III and II present higher permeability values than sample of Unit I (4.13 B). It was observed that horizontally drilled plugs have consistently higher permeability values than

the vertically drilled plugs (Fig. 4.13C). Hydrothermal travertines show high fabric variability; for this reason, 8 fabric category associations, responsible for the wide range of porosity and permeability, were identified (Fig. 4.13D). Each category was recognized on the basis of the predominant fabric type that characterizes the analysed plugs (e.g. Fig. 4.14A). Great porosity values (from 14 to 30%) were measured in the samples with raft boundstone/rudstone (Fig. 4.15A-B), coated bubble boundstone (Fig. 4.13D) and coated reed boundstone (Fig. 4.15 C-F), while laminated boundstone (Fig. 4.16A-D), crystalline crust cementstone (Fig. 4.17), shrub-like dendritic boundstone (Fig. 4.14) and carbonate grains (Fig. 4.13D) have low to medium porosity (from 5 to 13%) (Fig. 4.13D). The permeability is different between the various categories and varies also in function of the fabric type associations. The non-cemented raft boundstone/rudstone (Fig. 4.15A), coated reed boundstone/grainstone/rudstone (Fig. 4.15C), laminated boundstone (Fig. 4.16A) categories have high permeability values (from 79 up to 50000 mD). There is not always a positive correlation between permeability and porosity. The coated bubbles, despite the high porosity, have very low values of permeability (0.056 mD) (Fig. 4.13D). Shrub-like dendritic boundstone (Fig. 4.14A) associated to raft boundstone/rudstone, laminated boundstone and also crystalline crust boundstone show medium to high permeability values (60 to 47598 mD). Crystalline crust cementstone with channelized porosity has higher permeability value (55 mD) than crystalline crust dendritic cementstone with predominant inter-dendrite porosity (less than 1 mD) (Fig. 4.17).

Pore structures of selected samples were quantify using CT scanning at a resolution of 7, 14, 34μm. Morphometric parameters (Fig. 4.18) were calculated by CT-analyser in direct 3D based on surface-rendered volume model and in 2D from individual binarised cross-section images. The most important and distinguishable pore-structure parameters related to the petro-physical properties of the heterogeneous travertine samples were identified and include:

1) Perimeter over area (PoA) 2D specific surface corresponding in 3D model to Perimeter over Volume (PoV) is the ratio between the total perimeter that encloses the pore space and the total pore space (Weger et al., 2004). Largely, a small number represents a simple geometry and a large number an intricate pore system (Verwer et al., 2011). This parameter captures the overall complexity of the pore system of values and range from less than 10 mm^{-1} to more than 50 mm^{-1}.

2) Dominant pore size (DOMsize) (2D and 3D parametes) taken at 50% cut off on the cumulative area curve, in other words 50% of the pore space area is composed of pore equal or smaller than the DOMsize (Weger et al., 2004). Subsequently, the 50% threshold on the

cumulative area curve is taken as a measure for the maximum size of pores needed to occupy half of the pore space on a given half of the pore space area is composed of pores as small or smaller than the DOMsize (Verweret al., 2011). This parameter provides an indication of the pore-size range that dominates the sample. Dome size range from less than 10 up to 1400 up to μm.

Analyses suggest that is better to use the 3D analysis with respect to 2D, because of high fabric variability at the micron scale (Fig. 4.18D).

Samples with large pores and a simple pore structure (such us laminated boundstone, raft boundstone/rudstone and coated reed boundstone/grainstone/rudstone) characterized by high DomSize and low values of PoV appear to have high permeability contrary to samples with an intricate pore network (inter-dendrite porosity). Complex pore network corresponds to large PoV numbers and low DomSize, which appear to have lower permeability (rhomb-composed dendritic boundstone, crystalline crust boundstone) (Fig. 4.18E).

4.4.5 Diagenesis

Various diagenetic processes have affected the Pianetti travertines. In particular, dissolution, neomorphism and cementation are identified as the main processes that produced modifications on the fabrics and the associated porosity (Fig. 4.19).

4.4.5.1 Cementation

Cementation is considered one of the major diagenetic processes within the Pianetti travertine. This process takes place when pore-fluids are supersaturated with respect to the carbonate mineral phase and there are no kinetic factors inhibiting the precipitation (Tucker and Wright, 1990). Several groups of cements, varying from microspar to spar, have been identified within the studied travertine. The depositional porosity space is filled by mostly equant cement (Fig. 4.19A). Multiple generations of fibrous to bladed to scalenohedral isopachous cement followed by blocky calcite extend from the microfabric architectures into the pores and gradually fill them (Fig. 4.19 B-H). Often ghosts of acicular to fibrous crystals grow perpendicular to the micro-structures (Fig. 4.19D); these crystals seem to be incorporated into a second generation of

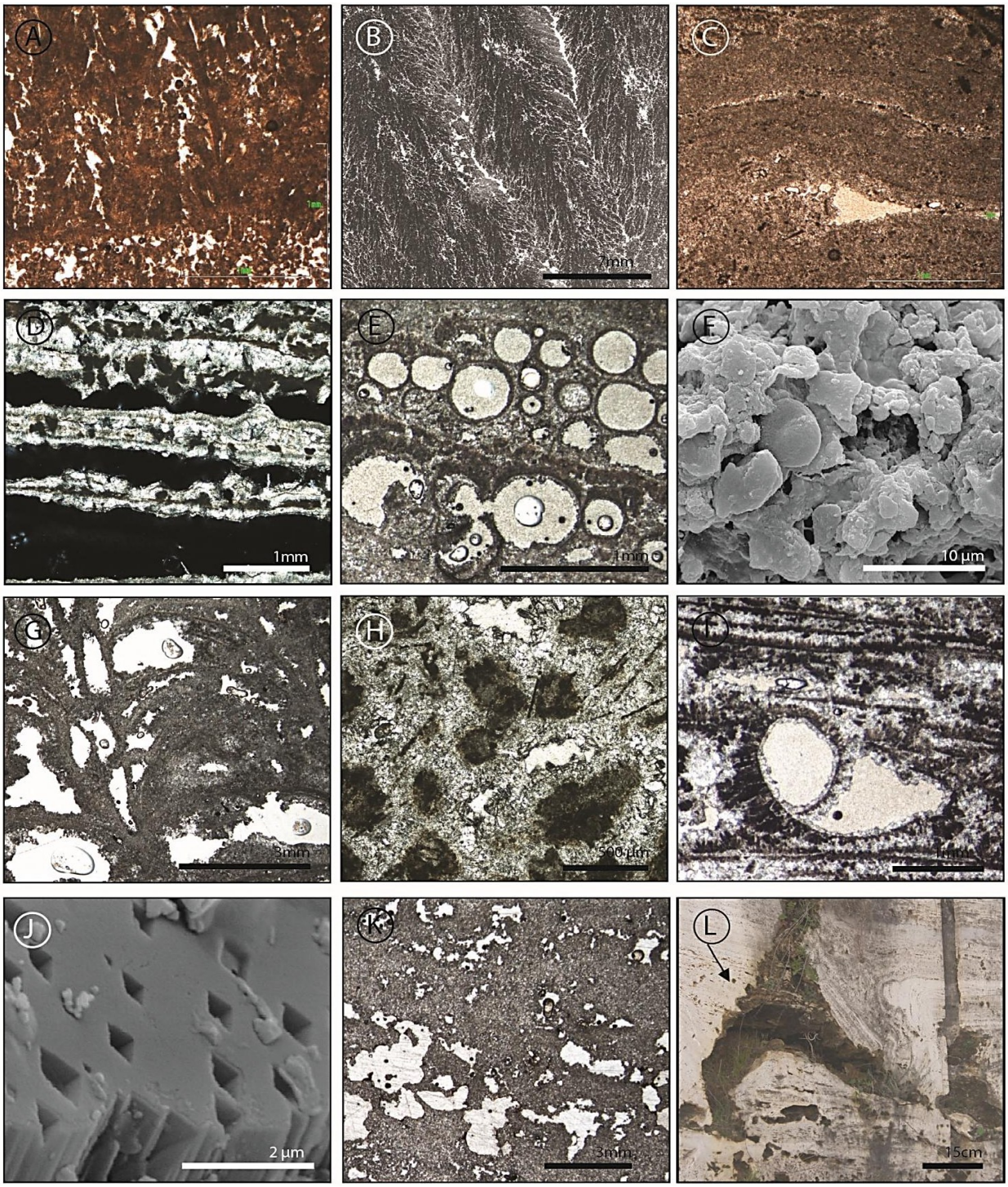

Fig. 4.12 Photomicrographs of depositional and secondary porosity characterizing the travertine fabrics. A) Framework inter-dendrite porosity in rhomb composed dendritic boundstone. B) Thin section scan showing crystalline dendritic cementstone with mostly inter-dentrite porosity; secondary porosity related to dissolution is also observed. C) Inter-laminae porosity in laminated boundstone. The pore space is almost totally filled by calcite cement. D) Secondary porosity related to dissolution processes associated with primary inter-particle raft porosity. Elongate vugs interrupting the vertical stacking of the rafts. Primary porosity if filled by fibrous and bladed cement followed by blocky sparite partially affected by dissolution. E) Bubble porosity. F) SEM photomicrograph of primary framework micro-porosity of micrite mudstone/microsparstone. G) Bio-moldic porosity related to degradation of plant stems in reed boundstone. H) Inter-particle porosity between coated grains filled by calcite cement. Dissolution pores are also observed. I) Photomicrograph of millimetre bio-mouldic porosity related to gastropod. J) Secondary intra-crystalline porosity showing square-shaped morphology. This may represents moulds of dissolved aragonite crystals. K) Photomicrograph showing micron to millimetre size irregular voids related to dissolution processes. L) Field image showing fractures and dissolution cavities (black arrow). Fractures improve permeability and make it possible for hydrothermal and meteoric fluids to circulate across the travertine deposits.

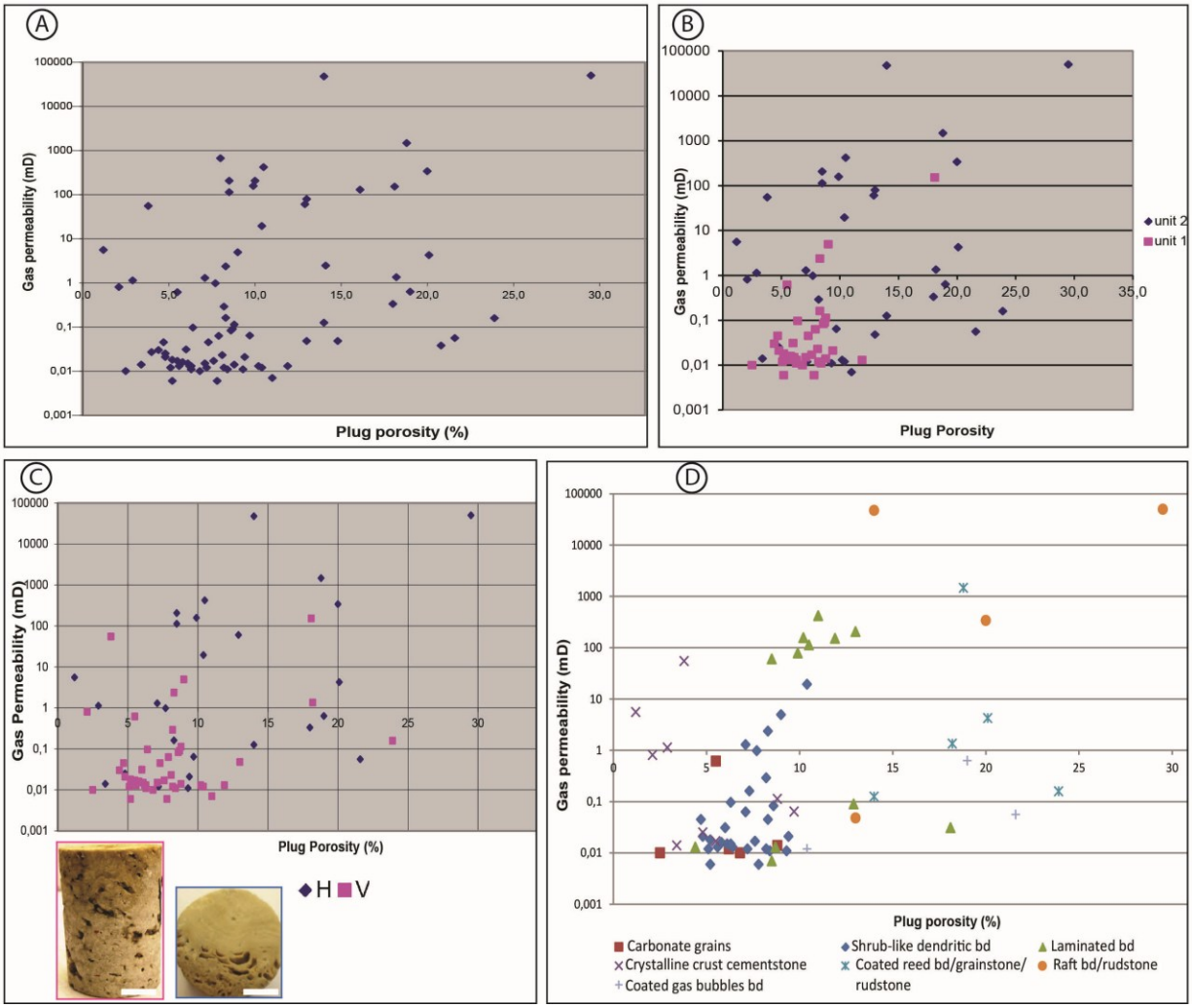

Fig. 4.13 A) Travertine porosity and permeability values based on Helium measurements. B) Travertine Units versus porosity and permeability values. Samples of Unit II present higher permeability values than samples of Unit II. C) Horizontal (H) vs. vertical (V) drilled plugs porosity and permeability value. Vertically drilled plugs in general present higher permeability value than samples horizontally drilled. The image with the pink box shows vertical drilled plug while the blue one shows the horizontal one. Scale bar 1 cm. D) Porosity and permeability values subdivided in fabric categories.

columnar-like crystals that occur in optical continuity with the possible previous acicular crystals (Fig. 4.19E). The columnar calcite crystals exhibit a pattern of sub-crystals that diverge away from substrate. Cathodoluminescence (CL) petrography (Fig. 4.19I-L) shows non-luminescent to dull luminescent to brightly luminescent to response. The CL has not proved a really valuable tool in the study of Pianetti travertines because only rarely CL allows differentiating the growth stages of the cement crystals (Fig. 4.19 J and L).

Cementation in Pianetti travertine appears inversely proportional to the age of the travertine. In facts, cementation is more abundant in travertine samples of Unit I, followed by Unit II rather than in Unit III.

4.4.5.2 Dissolution

Dissolution occurs when pore-fluids are under-saturated with respect to the carbonate mineralogy (Tucker and Wright, 1990). Large scale and micro-scale dissolution features have been extensively documented in the Pianetti travertine (Fig. 4.20 A-G). The products of large-scale dissolution are represented by karstic features (Figs. 4.4 A, 4.4F, 4.12L and 4.20A-B) consisting of fissures (up to 10 cm thick and several metres in length) and caves (up to a few metres in diameter). These features are often associated with red-coloured silty and argillaceous soil-derived sediment of the *terra rossa* type (Fig.4.4F and 4.20A). Dissolution vugs, decimetre to micron-size scale, are widespread (Fig. 4.20C-D) and often are, partially or totally, filled by red sediment (Fig. 4.20F). Dissolution processes attack indiscriminately the Pianetti travertine and their components, including the cements that occlude partially or entirely the primary porosity (Fig. 4.20D-E). Dissolution causes the leaching (Fig. 4.20G) of the different fabric types in all the distinguished travertine units.

4.4.5.3 Neomorphism

Neomorphism is widespread within the Pianetti travertine (Fig. 4.20 H-K). This includes processes related to transformations of minerals, which take place in the presence of water, such as inversion (the replacement of mineral by its polymorph) and recrystallization (change in crystal size, shape and crystal lattice without a change in mineralogy). In particular, petrographic analysis suggests that originally part of the calcite cements was probably aragonite that subsequently was transformed in calcite. The replacement of aragonite into calcite is proposed by the presence of ghosts of acicular to fibrous crystals (Figs. 4.5F, 4.9E, 4.12D and E). These crystals are often embedded into a second generation of prismatic calcite (Fig. 4.19D and E). The hypothesis of inversion may be also confirmed by observations conducted by SEM that show micron-size pores characterized by a roughly squared rim within well-developed calcite crystals (Fig. 4.20H). These pores may be related to dissolution of possible previous acicular crystals. The inversion aragonite/calcite process is common within the travertine fabrics of Unit I and II; it is not observed within the travertine of Unit III. However, the presence of aragonite crystals (especially in raft rudstone of Unit II, Fig. 4.9H-J) has been individuated not only through petrographic observations but also identified by XRD investigations. Aggrading neomorphism (Fig. 4.20J-K), a recrystallization process in which the crystals size increases and finer crystals

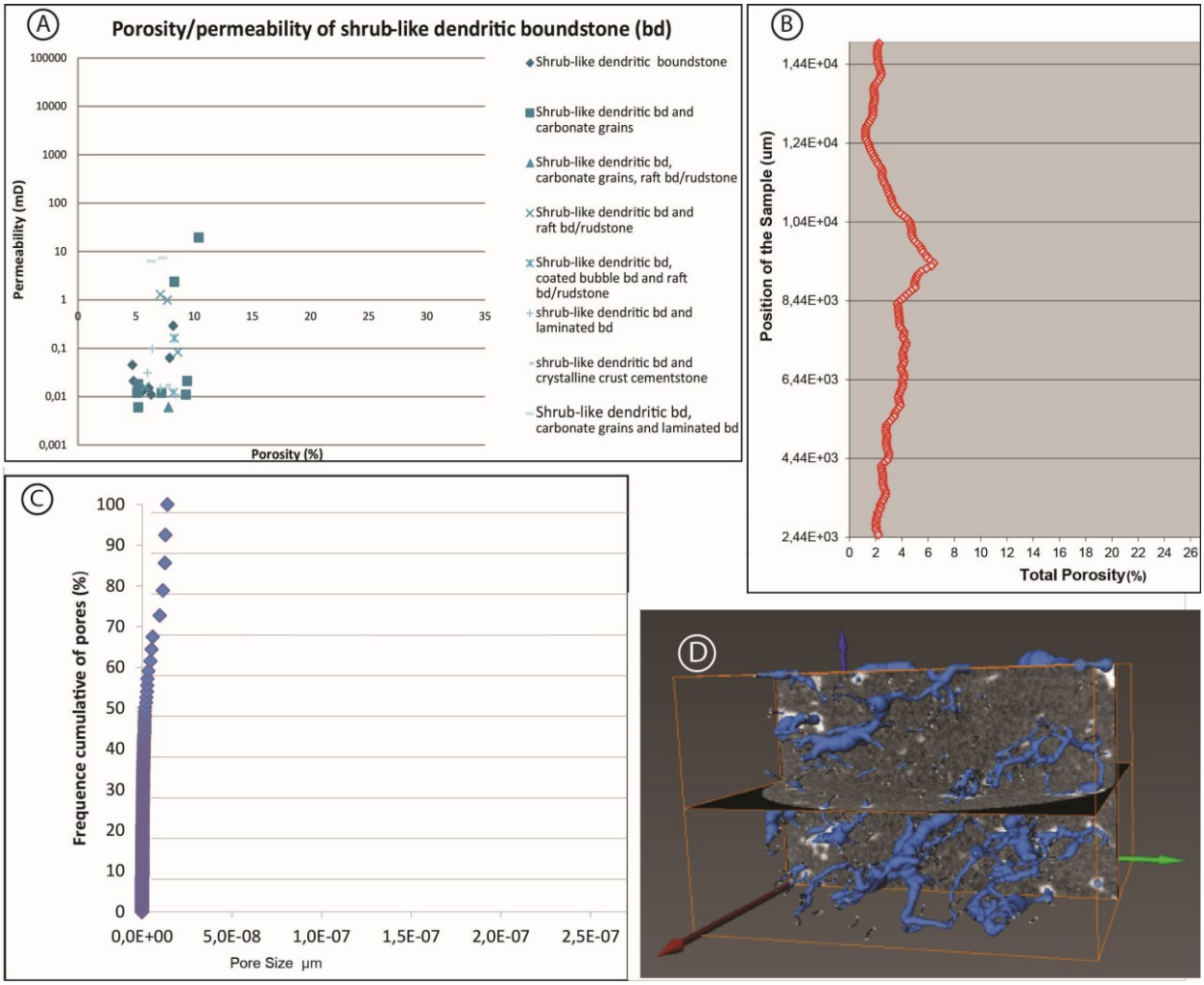

Fig. 4.14 Porosity and permeability values of shrub-like dendritic boundstone fabric category. A) Fabric associations that characterized the helium porosity and permeability values of the shrub-like dendritic boundstone category. B) Porosity variability in 2D Model. Each data point corresponds to a measurement value on 2D total Porosity. C) Frequency cumulative Pores, 3D analysis; D) Avizo image shows shrub-like dendritic boundstone porosity.

mosaic (micrite) are replaced by coarser crystals mosaic (mostly microspar and often spar), affects all different fabric types. The aggrading neomorphism can, gradually, destroy partially to totally the distinctive features of the fabrics. At the end, neomorphic microsparitic and often sparitic fabrics occur, which exhibit irregular crystals with curved and embayed boundaries and variable crystal sizes with remnants of micrite. The aggrading process concerns especially the fabric types in which the micrite component is abundant such as the clotted peloidal dendritic boundstone, laminated boundstone, micrite/microsparitic mudstone, the micritic layers of raft and coated bubble boundstone. Moreover, it was observed that the aggrading neomorphism process is more intense in travertine samples of Unit I and II (although less intensive than those of Unit I) rather than those of the Unit III.

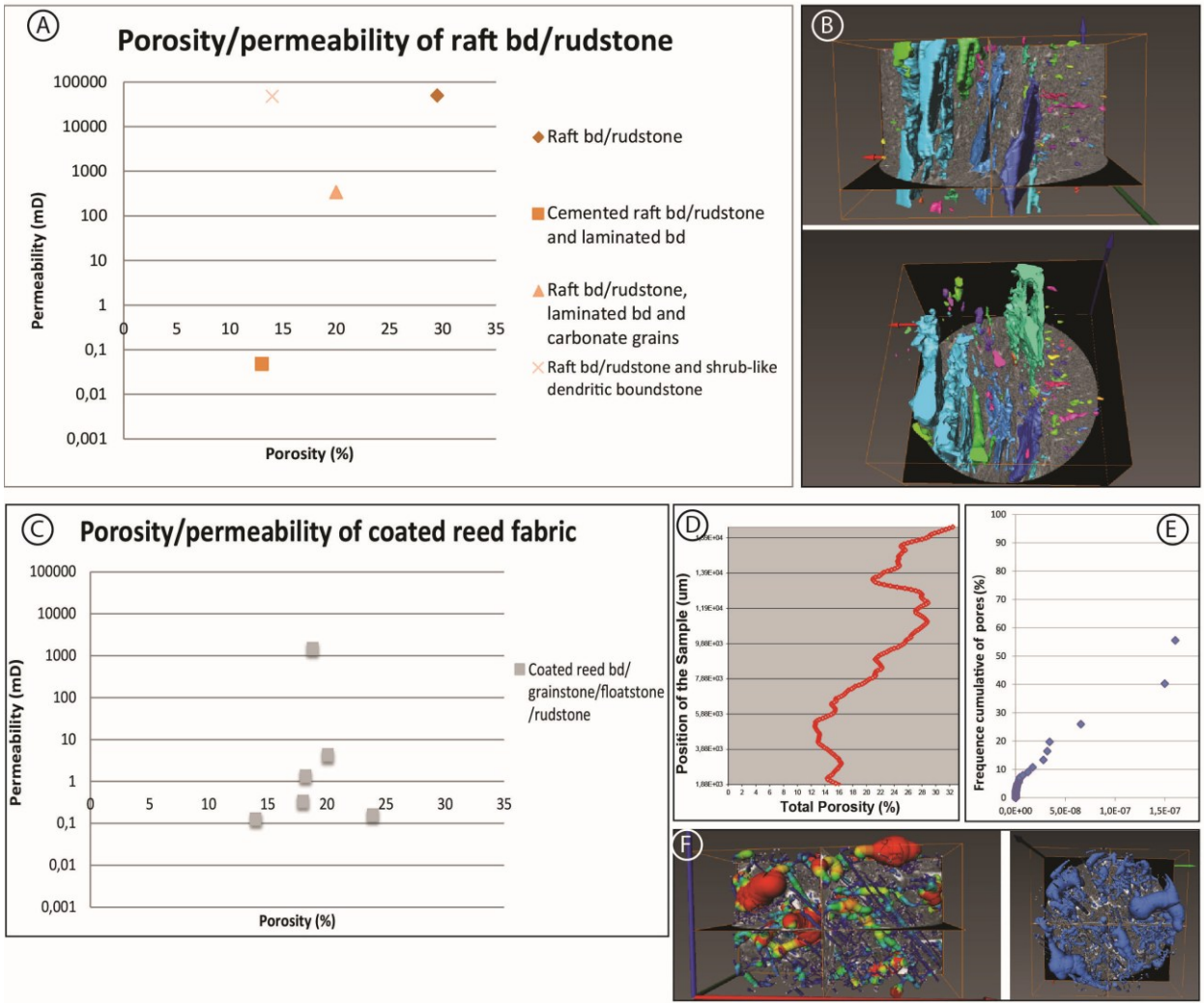

Fig. 4.15 Porosity and permeability of raft boundstone/rudststone fabric category. A) Fabric associations that characterized the Helium porosity and permeability values of the raft boundstone/rudststone category. B) Raft boundstone/rudstone porosity reconstructed with Avizo software. C) Fabric associations that characterized the Helium porosity and permeability values of coated reed boundstone/grainstone/rudstone category. D) Porosity variability in 2D Model. Each data point corresponds to a measurement value on 2D total Porosity. E) Frequency cumulative pores, 3D analysis. F) Avizo images showing the reconstructed reed porosity.

4.4.5.4 Sparmicritization

Sparmicritization (Fig. 4.20L) is present but not abundant in the studied travertine samples. This process involves the transformation of calcite spar crystals into micrite. Without careful examination, the micrite produced by sparmicritization could easily be confused with primary micrite (Fig. 4.20L). Sparmicritization affects mainly the dendritic forms that exhibit a crystalline appearance such as the rhomb-composed dendritic boundstone, radiating dendritic boundstone, crystalline dendrites and fan dendrite cementstone. Micritization is more intense within the travertine fabrics of Unit I and II rather than those of Unit III.

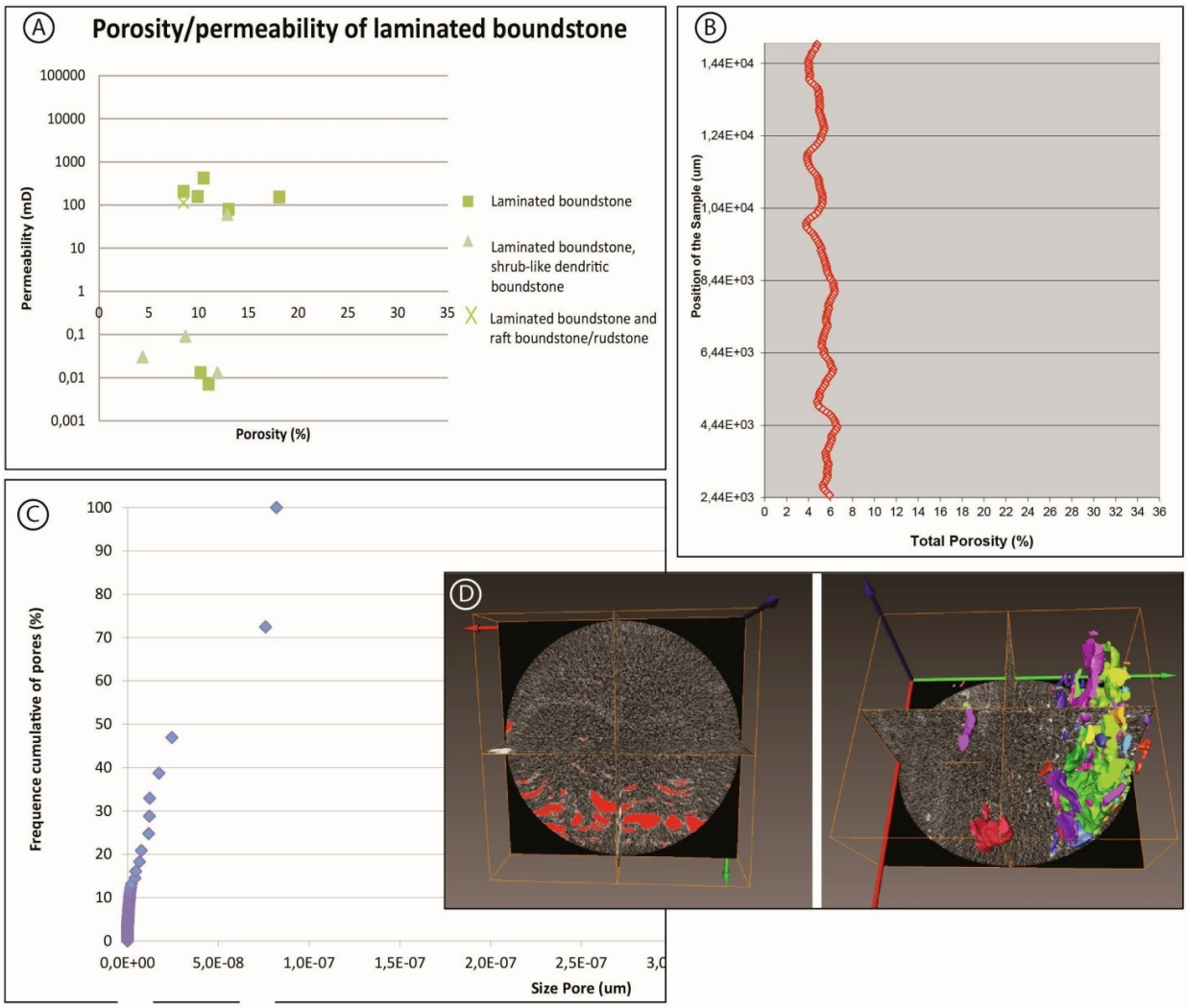

Fig. 4.16 Porosity and permeability of laminated boundstone fabric category. A) Fabric associations that characterized the Helium porosity and permeability values of the laminated boundstone category. B) Porosity variability in 2D Model. Each data point corresponds to a measurement value on 2D total Porosity. C) Frequency cumulative of pores on 3D analysis. D) Avizo images showing the laminated boundstone porosity.

4.4.6 Geochemistry and stable isotopic measurements

ICP analyses reveal that Ca range from 338840 to 373401 mg/kg, Mg from 1880 to ca 3000, Sr from 2657 to 880 mg/kg, Mn from 18080 to 83 mg/kg, Fe range 617 to 68 mg/kg and Ba from 34 to 70 mg/kg. Stable isotopic data obtained from calcite and aragonite samples of Pianetti travertine bodies show a positive field of distribution of $\delta^{13}C$ values that range from 1.14 to 7,69 ‰ PDB. The $\delta^{18}O$ range from -8.74 to -5.67 ‰. Data record a general increase of $\delta^{18}O$ and also $\delta^{13}C$ that seems to be directly proportional to the age of travertine units. In particular, $\delta^{18}O$vary from -8.74 to -6.57 ‰ in Unit I compared to -8.00 to -5.67 ‰ values of Unit II while $\delta^{13}C$ from

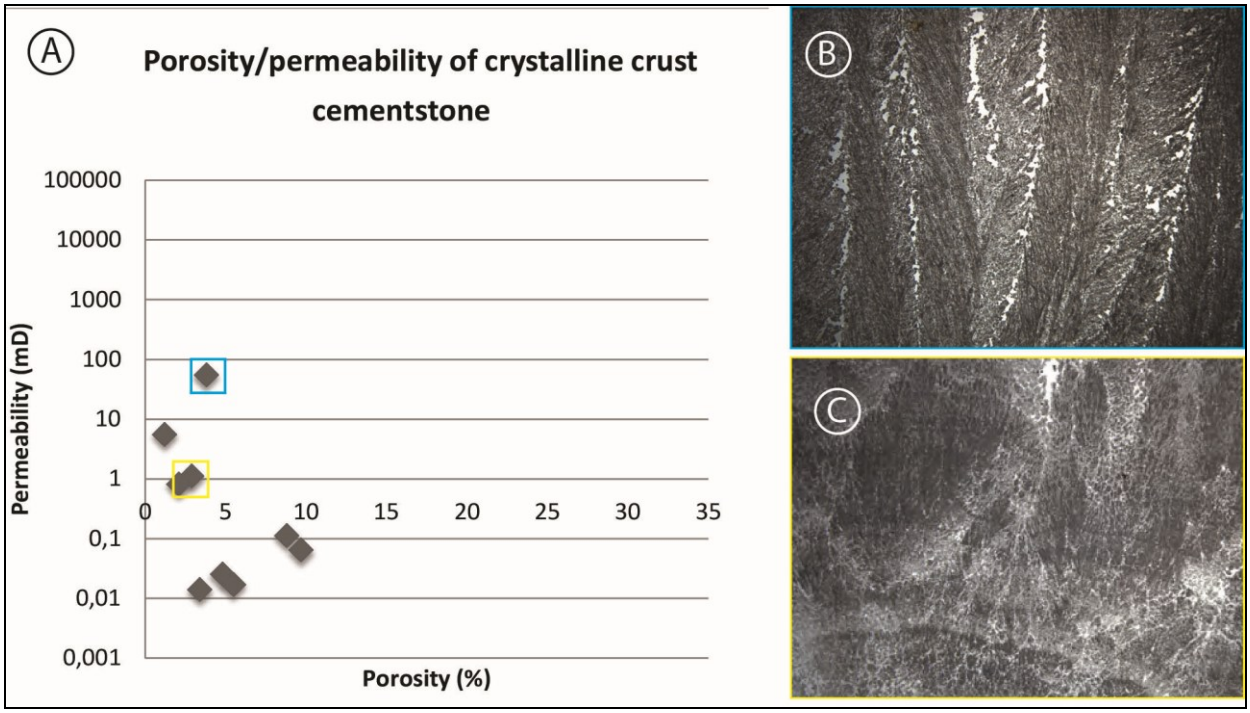

Fig. 4.17 Crystalline crust cemetstone fabric category. A) Porosity and permeability values of crystalline crust cementstone category. B) Crystalline dendrites characterized by predominant channelized porosity (blue square in A) have higher permeability value than crystalline dendrite with inter-dendrite porosity.C) crystalline dendrite cementstone with typically inter-dendrite porosity (yellow square in A). Field of view of images is 3.5 mm.

4.43 to 6.12 ‰ in Unit I and from 1.14 to 7.69 ‰ in Unit II. The same trend is observed in travertine at increasing distance from the vent, from travertine precipitated in the proximal to those formed in distal area. Instead, the stable isotopic data of travertine formed in Unit III is unclear and shows intermediate values between those of Unit I and those of Unit II with $\delta^{13}C$ comprised between 3.29 and 6.79 ‰ and $\delta^{18}O$ from -8.23 a -6.64 ‰. Isotopic data of sub-horizontal to concave layers of stepped topography reveal a slight depletion when compared with sub-vertical to raised and inclined strata of terraced and clinoformal morphology.

Mineralogical change seems to affect the travertine isotopic values. It was observed that the lowest values of $\delta^{13}C$ are related to raft boundstone/rudstone that are aragonitic in composition. In this circumstance $\delta^{13}C$ varies from 1.14 to 1.21 ‰, instead the $\delta^{18}O$ values are from -7.25 a 6.93 ‰ contrary to raft boundstone/rudstone composed of calcite that record 6.79 ‰ $\delta^{13}C$ and -6.65 ‰ of $\delta^{18}O$. Dendritic boundstone reveals a range of $\delta^{13}C$ values varying from 5.26 to 7.16 ‰ (with the higher value recorded in travertine samples of Unit II collected from large flat sub-horizontal strata) and δ^{18} O -7.58 to -6.29 ‰. Most of the dendritic boundstone isotopic data varying from $\delta^{18}O$ -7.54 to -6.92 ‰ with $\delta^{13}C$ 5.26 to 5.95 ‰ are congruent with those results observed in the sub-horizontal to concave topography. Dendritic boundstone precipitated along

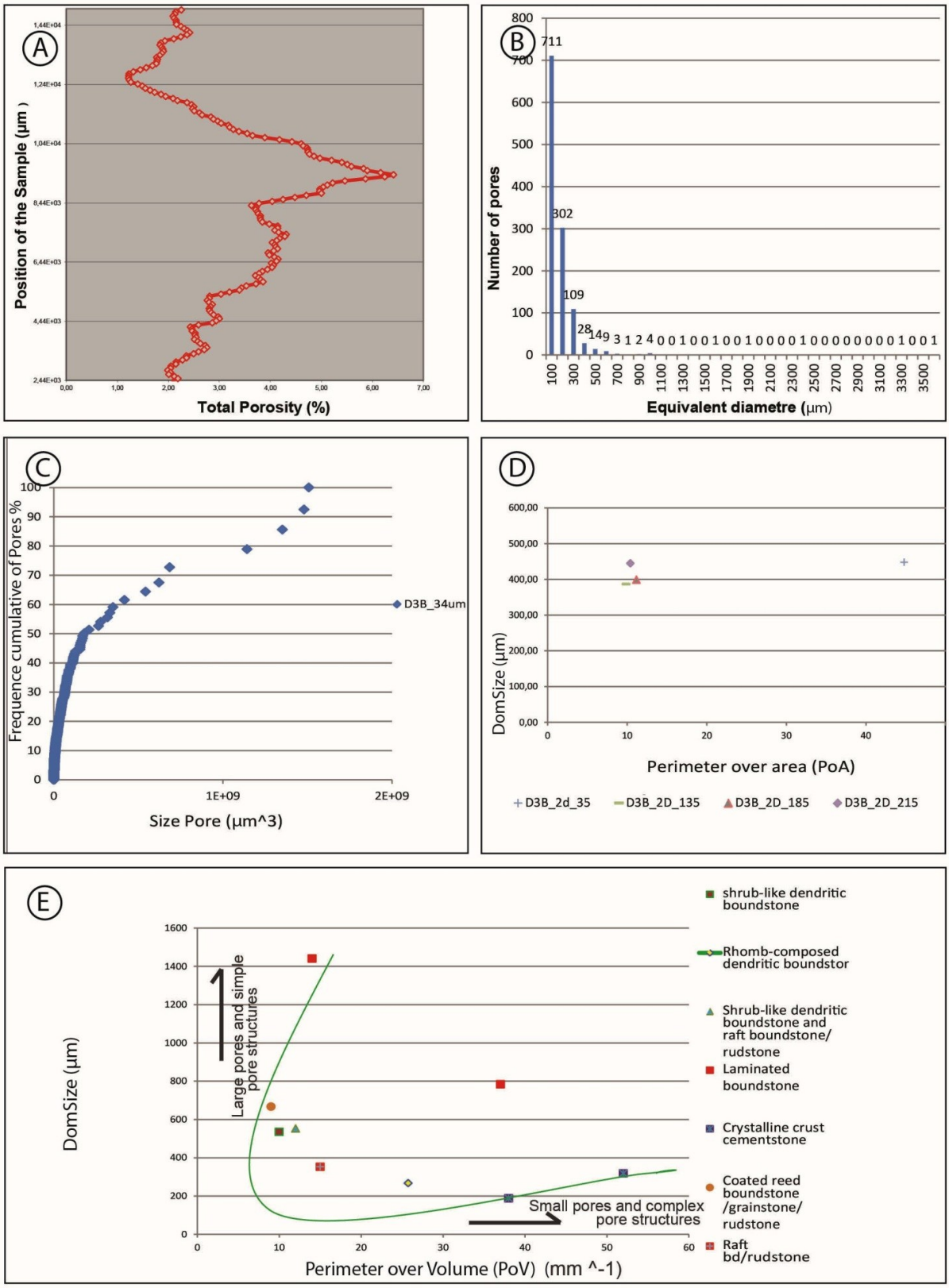

Fig. 4.18 A) Cross-plot showing porosity variability in 2D model. Each data point corresponds to a measurement value on 2D total porosity. Note the heterogeneous vertical distribution of the total porosity in carbonate grains plugs. B) Pore Size Frequency of the sample, 3D analyses. Carbonate grains formed by intraclasts of shrub-like dendritic boundstone. C) Cross-plot showing the frequency cumulative of pores in carbonate grains plugs. D) Cross-plot of PoA versus DomSIZE 2D analysis showing the high variability of travertine samples. Perimeter over area is the ratio between the pore volume and the pore surfaces. Dominant pore size is determined as the upper boundary of the pore size with 50% of the porosity. Note the high variation of PoA in different slides of the same area of drilled plugs. E) Cross-plots of perimeter over area (PoA) versus dominant pore size (DOMsize).

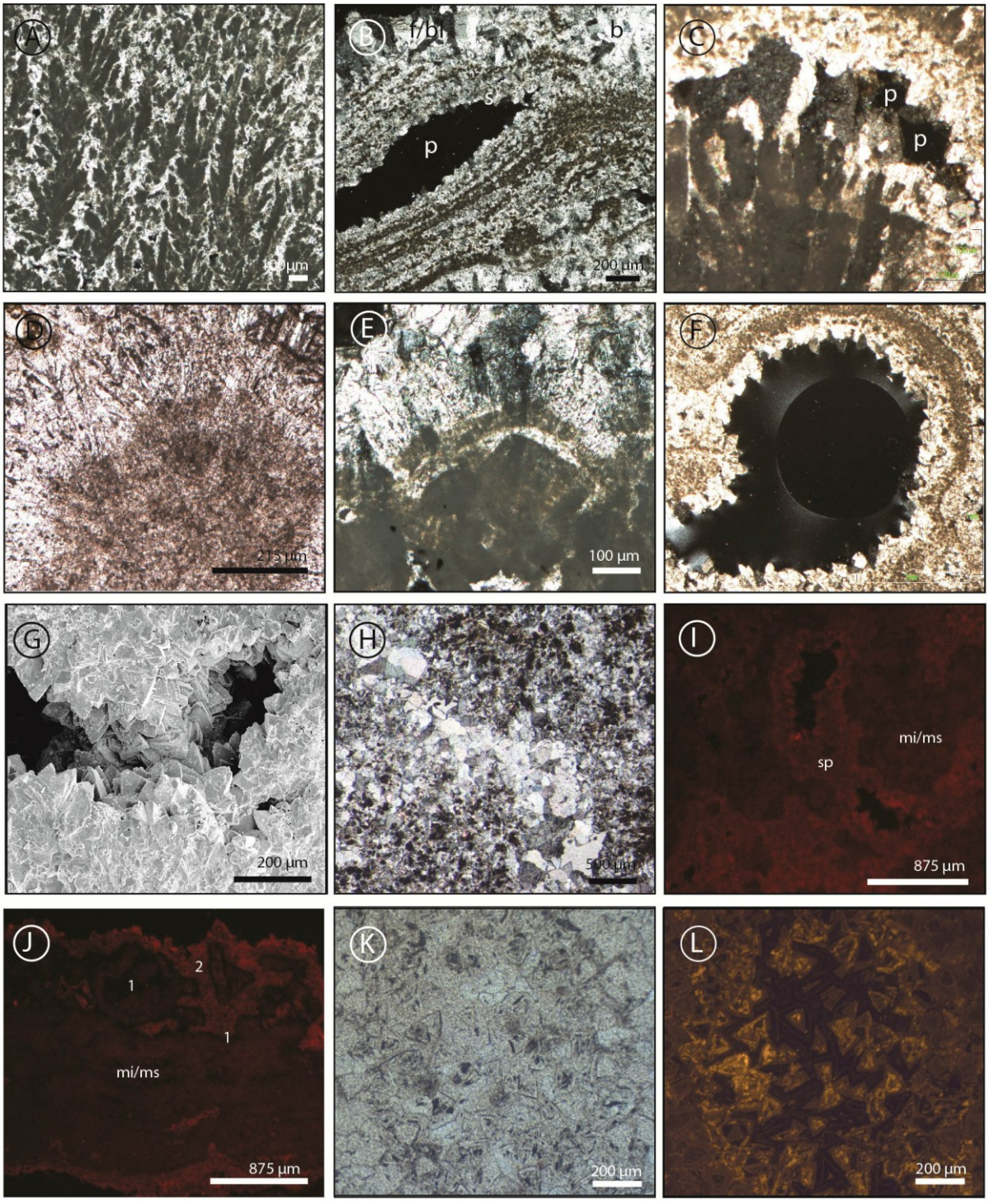

the raised and also convex morphologies of the stepped slope topography shows an increasing $\delta^{18}O$. In fact, δ^{18} O value is in general -6.57 ‰ in the case of dendritic boundstone observed along these depositional architectures. Crystalline crust cementstone (presenting value of $\delta^{18}O$ from -7.02 to -5.67 ‰ and $\delta^{13}C$ from 6.07 to 7.69 ‰) appears to be slightly enriched in heavier isotopes when compared with dendritic boundstone. Values calculated for laminated boundstone range from -7.25 to -6.56 ‰ $\delta^{18}O$, while $\delta^{13}C$ records measurements varying from 6.38 to 5.27

‰; concerning the $\delta^{18}O$ isotopic data, only one sample reaches the value of -8.05 ‰. Laminated boundstone samples of Unit I show low values of $\delta^{13}C$ compared with those of Unit II and III that reveal also a general increase of the $\delta^{18}O$ isotopic values. A general increase of $\delta^{18}O$ and $\delta^{13}C$ from Unit I to Unit III is observed (Fig. 4.21B). Coated bubble boundstone of Unit I related to stepped slope topography presents $\delta^{18}O$ between -7.81 to -7.38 ‰ and $\delta^{13}C$ 5.14 to 5.63 ‰ contrary to -7.34 ‰ for $\delta^{18}O$ and 6.09 ‰ $\delta^{13}C$ values of Unit II mainly in clinoform morphology. Instead, coated bubble boundstone of Unit III shows a lighter $\delta^{18}O$ value that reaches -8.22 ‰. Micrite mudstone/microsparstone fabric type shows -7. 25 ‰ for $\delta^{18}O$ and 5.21 ‰ for $\delta^{13}C$ isotopic composition. Stable isotopic analyses were also conducted on the different types of cements that fill the primary and secondary Pianetti travertine porosity (Fig. 4.22). The measurements interested also the calcite precipitates occurring in the dissolution caves. In this case the isotopic values, consisting of -3.78 ‰ for $\delta^{18}O$ and -8.71 ‰ for $\delta^{13}C$ occupy the negative field of distribution. Equant to fibrous calcite filling the depositional porosity falls in the positive field of $\delta^{13}C$ as the primary growth fabrics (Fig. 4.22). The same trend is shown from the carbonate precipitate sampled within a large sub-vertical fracture that crosses the travertine body in Unit I. This precipitate shows a $\delta^{18}O$ of -7.45 ‰ and $\delta^{13}C$ of 5.49 ‰. Instead the bladed to scalenohedral to blocky cements that gradually fill the porosity varies from δ^{18} O -6.32 to -5.38 ‰ and $\delta^{13}C$ from -3.36 to -4.30 ‰.

Fig. 4.19 (previous page). Photomicrographs showing some examples of the different cement types that were precipitated in the Pianetti travertine fabric types. A) Equant cement, mostly microspar and spar, fills the primary inter-dendrite porosity. B) Pores (p) of laminated boundstone partially or totally filled by fibrous to bladed (fb/bl) to scalenohedral (s) and blocky (b) calcite cement. The micritic laminae are partially affected by aggrading neomorphism. C) Crossed polarized light photomicrograph showing bladed calcite cement extending from the upper end of the rhomb composed dendritic boundstone into the pore. This cement shows optical continuity with the rhomb-composed dendritic boundstone and is followed by blocky calcite crystals. D) Fibrous calcite isopachous cement extending from the clotted peloidal micrite into the pores. E) Multiple generations of cement growing perpendicular to the dendritic structures. Fibrous to bladed calcite isopachous cement followed by blocky calcite extending into the pores. Ghosts of fibrous crystals growing perpendicular to the dendritic structures seem to be incorporated into a second generation of columnar-like crystals that occur in optical continuity with the possible previous acicular crystals. F) Bubble porosity overlain by schalenoedral cement. G) Schalenoedral crystals diverging away from the microsparitic equant rhombohedral crystals evolving inward the pore space. H) Blocky cement that completely occludes the depositional pores. I) CL petrography of travertine samples characterized by non luminescent micrite/microsparite (mi/ms) and dull luminescent sparite cement (sp) into clotted peloidal dendritic boundstone partially transformed by aggrading neomorphism. Non-luminescent response of clotted peloidal micrite may suggests that its precipitation occurs under oxidizing environments. Another explanation of these different signals may suggest that the meteoric water are characterized by higher content of CL-exciting ion than hydrothermal water. J) CL-image showing a no luminescent micrite/microspar in laminated boundstone. The calcite cement shows two stages of cementations: 1) no luminescent cement related to oxidizing environments in which the reduced forms of both Mn2+ and Fe2+ cannot be incorporated into the crystal lattices of the calcite; and 2) luminescent cement suggesting reducing conditions. K) Photomicrograph showing void filling cement. L) CL of zoned calcite cement in K showing a transition from non-luminescent to brightly luminescent to dull luminescent response. This is generally interpreted as a transition from oxidizing conditions (non-luminescence) to reducing conditions (dull luminescent to brightly luminescent) in the phreatic zone.

4.5 Interpretation

4.5.1 Travertine Units

An intermittent accretion of the Pianetti travertine body is suggested. The three travertine Units (I, II and II) record different travertine depositional events while exposure surfaces marking halt of hydrothermal activity are represented by the claystone layers (clay layer 1 and 2) and the brecciated level (Fig. 4.23). The Pleistocene Pianetti travertine deposits are interpreted as precipitated by hydrothermal water issuing from laterally shifting hydrothermal vents on a slope (Unit I and II) flowing into distal areas with reduced topographic relief; Unit III represents a distal area at the top of the previously deposited units where mixing of hydrothermal water with meteoric water occurred.

Unit I

Punctual hydrothermal vent, preserved as metre-scale columnar convex shaped structure (Fig. 4.4A), localized in the SW was individuated Unit I (Fig. 4.23). The morphology of the spring suggests an instantaneous precipitation from the emergence point with water issuing with high hydrostatic pressure and high water supply. From the higher relief of the emergence point the water flew towards areas of lower topographic relief in the NE (Fig. 4.23). As suggested by Guo and Riding (1998) in comparable travertine systems of Rapolano Terme (Tuscany, Central Italy) also the prograding and aggrading carbonate layers that characterize the Unit I are interpreted as related to high precipitation rates. During the deposition of Unit I, time intervals characterized by fluctuations of the water supply and subaerial exposure are represented by discontinuities. The deposition of Unit I was stopped by the interruption of flow of hydrothermal water out of the vent and followed by erosion and karstic dissolution of the previously deposited travertine and the accumulation of the claystone layer 1 (Fig. 4.3). Unit I travertines were buried below a cover of continental clay deriving from the reworking of the Pliocene marine clay (Argille Azzurre

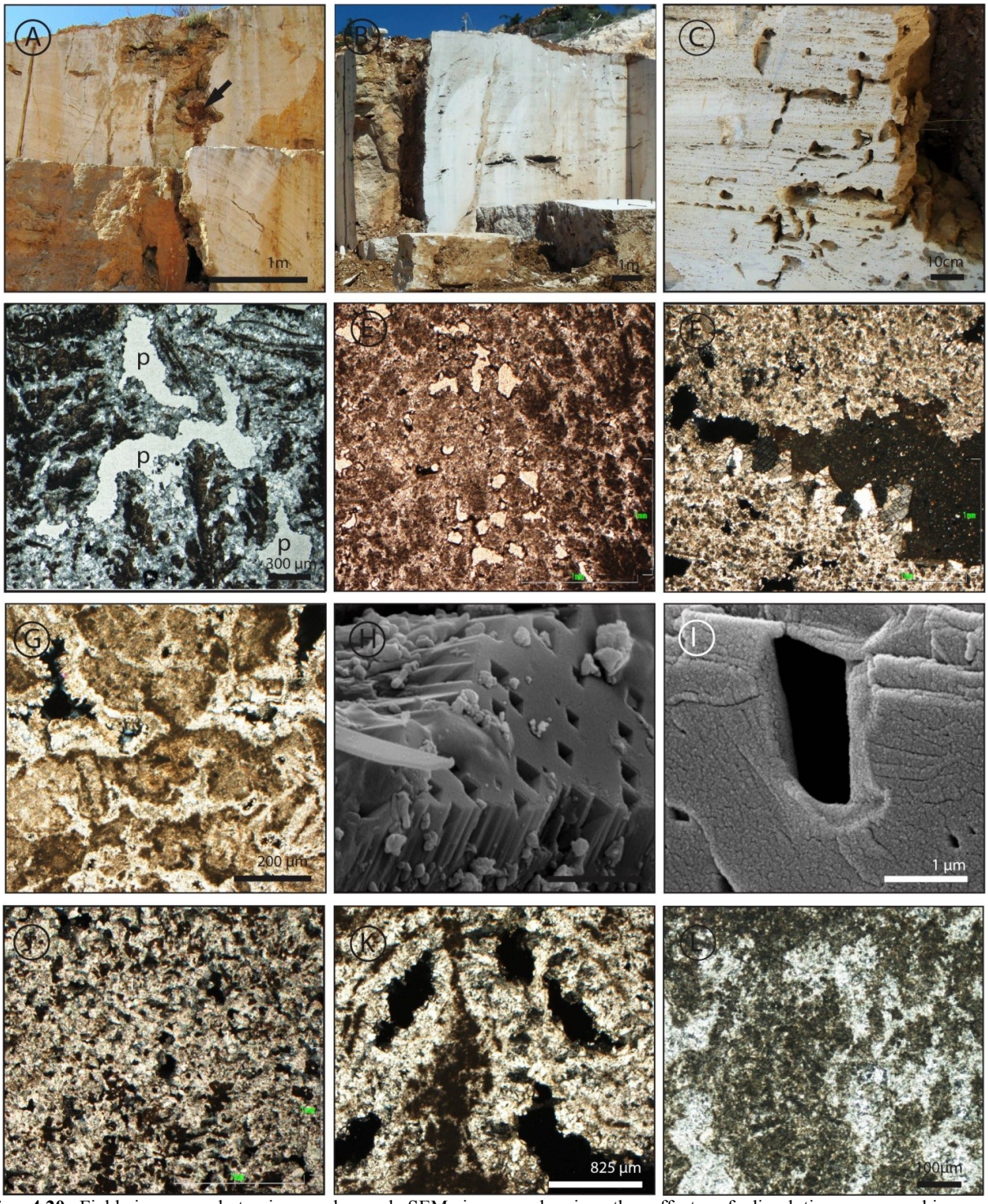

Fig. 4.20 Field images, photomicrographs and SEM images showing the effects of dissolution, neomorphism and sparmicritization on the Pianetti travertine. A) Field image showing metre-scale elongate fractures crossing the quarry wall in Unit II. Note the presence of the dark brown/red-coloured soil-derived sediment filling the fractures. B) Field image of caves within Unit II. C) Non fabric selective dissolution creates millimetre to several centimetre size vugs. D) Dissolution affects the rhomb-composed dendritic boundstone and the associated cement. Unit I. E) Photomicrograph showing micron-size irregular voids caused by dissolution processes in clotted peloidal dendritic boundstone. F) Photomicrograph showing the occurrence of micron- to millimetre-size vugs (in black) some of which are totally filled by soil-derived sediment. G) Leaching related to dissolution processes observed in Unit III just below the present-day soil cover. Cementation also occurs. H) Square-shaped pores within the calcite crystals related to dissolution of possible acicular aragonite crystals. SEM image. I) SEM image showing intra-crystalline micro-pores within the calcite crystals suggesting alteration of previous mineral. J) Aggrading neomorphism on dendritic boundstone. K) Aggrading neomorphism affecting laminated boundstone. The micritic laminae are partially recrystallized into microspar/calcite. L) Photomicrograph of crystalline dendritic cementstone affected by sparmicritization, which obliterates the crystalline dendrities in clotted peloidal dendritic boundstone.

Formation) mixed with meteorically altered volcanic deposits. This appears consistent with the claystone composition and with the regional published literature (Tozzi and Zanchi, 1987; Martelli et al., 1989). The interruption of the flow was probably due to tectonic activity and/or climate change (amount of precipitation).

Unit II

Precipitation started again with the depositions of Unit IIa that is interpreted as produced by hydrothermal water issuing from a punctual vent in the SW with water flowing towards the NE (Fig. 4.23). The hydrothermal vent was not individuated but it is supposed that it migrated backward with respect to Unit I vent. The deposition of NE prograding carbonate layers of Unit IIa implies high rates of precipitation and abundant hydrothermal water supplies as suggested in comparable systems by Guo and Riding (1998). An important interruption of water flow and travertine deposition is suggested by the inclined brecciated surface representing an unconformity (Fig. 4.4B and E, 4.23). The brecciated lithoclastic level is produced by erosion of the slope travertine following a phase of stasis in the travertine precipitation. A new depositional event led to the precipitation of the sub-horizontal Unit IIb (Fig. 4.3B and E 4.23). The hydrothermal spring was not individuated within the exposed saw-cut quarry walls; however, lateral and downward migration of the vent with respect to the vent location of Unit IIa is demonstrated by the onlap geometric relationship. The travertine Unit IIb forms an aggradational wedge suggesting high precipitation rates under intermittent water supply (as suggested by micro-scale stepped morphology individuated within the Unit IIb sub-horizontal trend). The activity of the vent gradually decreased and successively stopped as marked by the deposition of claystone layer 2 (Fig. 4.C). The claystone layer 2 is interpreted as a paleosol resulting from the exposure of the travertine system to subaerial conditions and meteoric diagenesis following an interruption of the hydrothermal water flow, or due to decrease in water supply or diversion in flow direction.

Unit III

A new travertine deposition event occurred above claystone layer 2 with Unit III (Fig. 4.23). Unit III represents the distal part of a travertine depositional system produced by the far-away

migration of the hydrothermal vent or alternatively the hydrothermal water out-flow gradually decreased and a pond/marsh with mixed hydrothermal and meteoric water established. According to Guo and Riding (1999), dilution by rainwater can lower precipitation rates. The presence of intercalated grey layers indicates intermittent water flow and periodic exposure. The hydrothermal activity of this vent stopped again and no precipitation occurred within the Pianetti travertine body. In fact, travertine unit III is highly weathered and is associated with present-day red to brown soils.

4.5.2 Internal architectures of travertine Units

The hydrodynamic of the flowing hydrothermal water, controlled by the location and the activity of the vent, the roughness of pre-existing surface and topography, influences the development of different depositional architectures such as clinoforms, stepped slopes and sub-horizontal layers corresponding, respectively, to smooth slope (cf. Chafetz and Folk 1984; Folk et al., 1985; Guo and Riding, 1998; Özkul et al., 2002), terraced slope (cf. Bargar, 1978; Chafetz and Folk, 1984; Folk et al., 1985; Guo and Riding, 1998, 1999; Pentecost, 1990; Özkul et al., 2002; Fouke, 2011) and pond (Folk et al., 1985; Guo and Riding, 1998; Özkul et al., 2002) depositional environments (Fig. 4.4 and 4.23). Smooth slopes and terrace rims and walls are considered areas of fast flowing water, while terrace pools and ponds are areas of standing to slow flowing.

Smooth slope

The smooth slope topography is widespread in Unit I and Unit IIa (Fig. 4.4 and 4.23), where smooth slopes are dominant. They are defined as non-terraced high-energy, low to high angle deposits, which show dips of 10°-40°(Guo and Riding, 1998; Özkul et al., 2002). The smooth slope formation requires an antecedent gently inclined substrate characterized by limited roughness of the surface. The development of smooth slope often occurs by rapid deposition by flowing water characterized by continuous flow/supply.

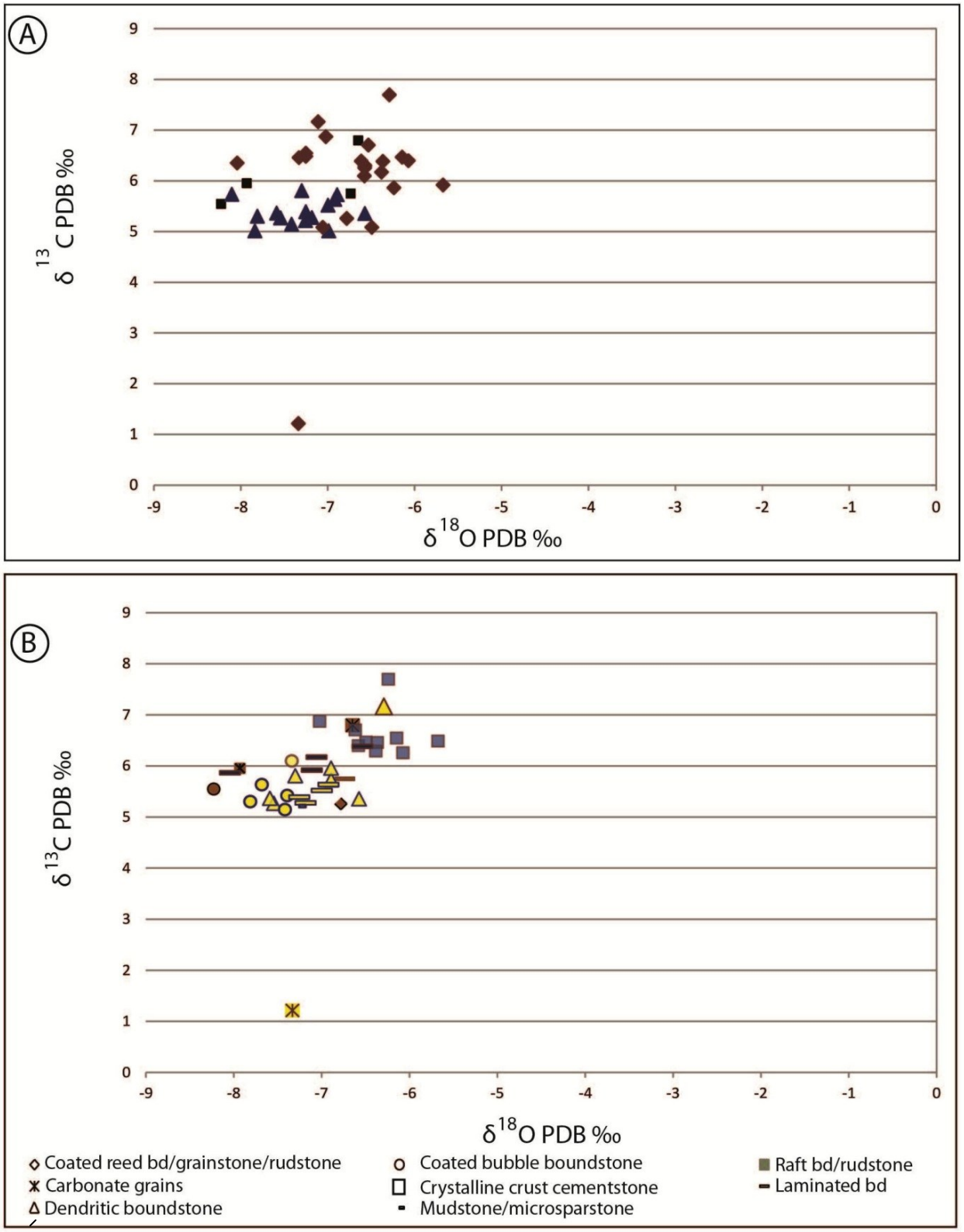

Fig. 4.21 Stable isotopic analyses of Pianetti travertine body. A) Isotopic values of $\delta^{18}O$ and $\delta^{13}C$ Pianetti travertine samples versus travertine Units. B) $\delta^{18}O$ and $\delta^{13}C$ values versus fabric types (see legend), depositional architectures and travertine Units. Yellow colour filling each symbol present in the legend indicates terraced morphology while the blue one represents fabric type derived from the clinoformal-strata. The brown colour denotes travertine fabrics deposited along the sub-horizontal topography. In addition each fabric shows a rim that indicates the provenience of the travertine sample. The black rim indicate that travertine sample was collected in Unit III while the red one in Unit II and finally the blue one in Unit I. Note the lowest value of $\delta^{13}C$ recorded from aragonite raft boundstone.

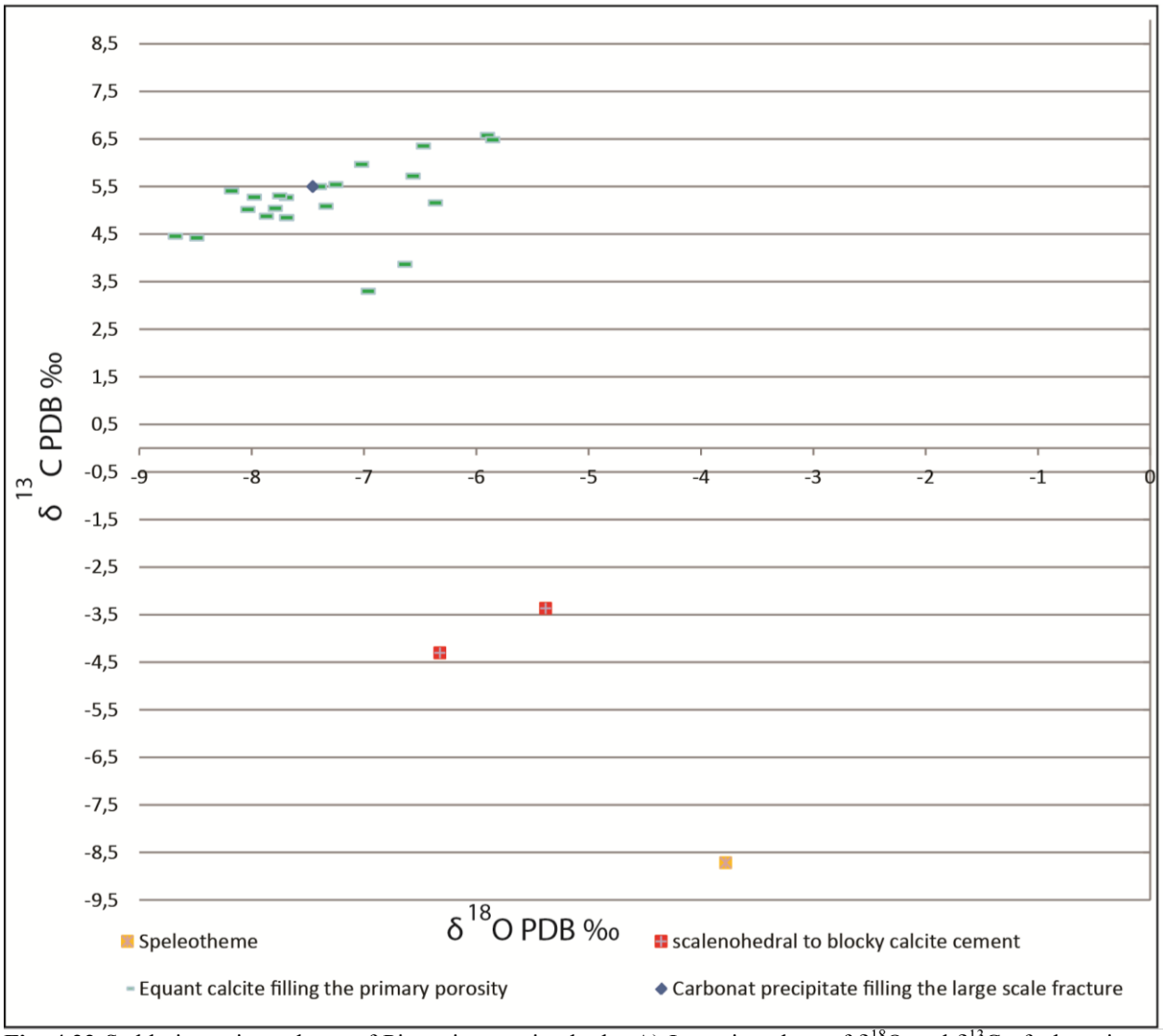

Fig. 4.22 Stable isotopic analyses of Pianetti travertine body. A) Isotopic values of $\delta^{18}O$ and $\delta^{13}C$ of the primary growth fabric. The red squares define the aragonite samples. B) $\delta^{18}O$ and $\delta^{13}C$ isotopic values of the syn-depositional and early/post depositional cements individuate in each fabric type versus carbonate precipitate that fills the large fractures and those that characterized speleotems in Pianetti travertine sample.

Terraced slope

The terraced slope depositional system characterized by a stepped geometry mostly builds Unit I but it is also observed in Unit IIb (Fig. 4.4C-E and 4.23). The terrace slope morphology is interpreted as developed from horizontal or gently dipping slope. Guo and Riding (1998) argue that terraced slope morphology does not require a steep pre-existing topography (Guo and Riding, 1998). The different stratal orientations of the stepped topography individuate vertical to overhanging drop walls, sub-horizontal pools bordered by raised and also convex morphologies interpreted as terrace rims (Fig. 4.4C-D and 4.23). The height of the break in slope of the wall

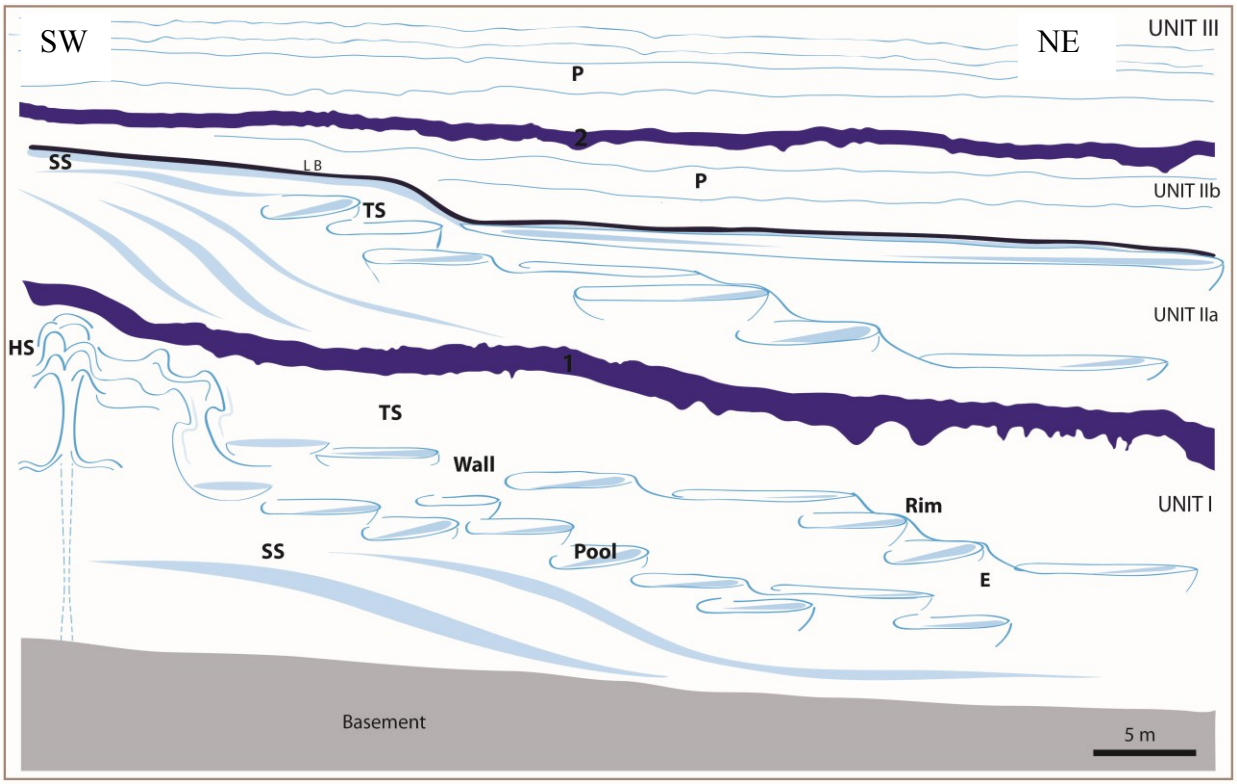

Fig. 4.23 Interpretative diagram of Pianetti travertine body showing the relationships between travertine Units (I, II a and b, III) and depositional environments. Unit boundaries are marked by the two claystone layers (1-2) and a brecciated surface (LB) representing a halt of hydrothermal activity. Depositional architectures such as clinoforms, stepped slopes and sub-horizontal layers correspond, respectively, to smooth slope (SS), terraced slope (TS) and pond (P) depositional environments. The different stratal orientations of the stepped topography individuate vertical to overhanging drop walls, sub-horizontal pools bordered by raised and also convex morphologies interpreted as terrace rims. Punctual hydrothermal vent is localized in the SW of Unit I. Lateral and vertical transitions between smooth slope (SS), terraced slope (TS) and pond (P) depositional environments that characterized each travertine Units are observed

allows distinguishing a waterfall (up to 2 m high wall) (Fig. 4.4D) from the pool wall (few millimetres to less than 2 m high; Fig. 4.4C) in a terraced slope system. The formation of terraced morphology appears mainly influenced by the hydrodynamic of the water flow and surface roughness (Folk et al. 1985; Guo and Riding, 1998, 1999; Özkul et al., 2002). The water flux varies along the terraced slope profiles: a) the lowest energy water occurs just behind the rim, with a laminar flow; b) water then runs along the rim and falls along the surface of the wall into the inner and deepest part of the subsequent pool; c) from the high turbulence at the toe of the pool wall, the energy decreases while flowing across the pool floor; d) Towards the pool rim the pool depth decreases following the rising of the pool floor. Guo and Riding (1998) proposed a model for terraced slope formation related to an alternation between laminar and turbulent flows. Under laminar flow, water shears horizontally, parallel to the direction of flow, leading to

the formation of horizontal layers. If this is disrupted by turbulent flow eddies, it can produce locally high velocities, resulting in locally rapid precipitation, which also increases the roughness of the surfaces and stepped morphology occurs.

Pond depositional system

Sub-horizontal layers corresponding to a distal slope zone or decametre-size large ponds are the only strata morphology of Unit IIb and Unit III. Ponds are interpreted as deposited by the precipitation from hydrothermal water characterized by slow flowing to standing water (low flow regime) in close to horizontal areas. However, in Unit IIb the decimetre to centimetre scale stepped morphology within the pond strata suggests events of turbulence that might be due to intermittent water flow.

4.5.2.1 Smooth slope-terraced slope depositional system evolution within the travertine Units

The travertine deposits in Unit I and II show cyclicity in the upward evolution of the smooth slope into the terraced slope system (Fig. 4.23). This change in system morphology is probably related to the activity of the spring. Reduced fluctuations in volumes and rates of water flow and supply characterized the first period of vent activity reflected by the deposition of a smooth slope system. This time was followed by an intermittent activity that created events of high turbulence alternated with time lapses of laminar flow. Also the pulsing activity of the water flow favoured irregularities in the substrate. This increase in roughness of the surface, associated with high turbulence, should have favoured the development of terraced slope morphology. Following the terraced slope deposition the hydrothermal vent activity stopped. Transitions from smooth slopes to terraced systems are observed also laterally with a smooth slope evolving in the distal portions (toe of clinoforms) into a terraced slope system. This is especially observed in Unit II (Fig. 4.23). It is suggested that the pre-existent topography has an additional role in the lateral transition from smooth slope to terraced slope systems. If during its pathway the water flow encounters obstacles (or break-in-slope that gives rise to a waterfall) the flow passes from laminar to turbulent, inducing the lateral evolution of the smooth slope into a terraced slope. Changes in travertine system geometry and depositional architecture from smooth to terraced slope have been observed in other travertine deposits. Özkul et al. (2002) suggest that recent smooth slope

sub-environments at Pamukkale (Turkey) are transitional with terraced slope both in vertical and lateral direction. Guo and Riding (1998) reported for Rapolano Terme (Tuscany) travertine, the evolution from smooth slope to terraced slope related to increased water flow.

4.5.3 Fabric types

A large variety of growth fabric types reflect the processes of precipitation, the depositional environment and subsequent diagenesis (Appendix 1). A relationship between fabric types and velocity/turbulence and discharged volumes of the flowing water is suggested (Fig. 4.24 and Appendix 2). The travertine fabrics can be differentiated into those typical of "fast flowing water areas" (such as thick crystalline crust and thin crystalline crust cementstone) and those precipitating in "stagnant to slow flowing water areas" (such as dendritic boundstone, laminated boundstone; raft rudstone; coated gas bubble boundstone; micrite mudstone) (Fig. 4.24). Several mechanisms of precipitation have been proposed to explain travertine fabric types, and these vary from abiotic to biogenic processes. Observations suggest that travertine formation is not only the result of mechanical CO_2 degassing but that interplaying abiotic and biotic processes (biologically induced by microbial metabolic process or simply influenced by nucleation on microbial biofilm substrate) are involved in the precipitation of the Pianetti travertine.

Dendritic boundstone

Shrub-like dendritic boundstone layers (Fig. 4.6A-I) are interpreted as directly precipitated by standing to slow flowing water. Carbonate precipitates similar to the shrub-like dendritic boundstone are ubiquitous in hot-spring travertines around the world (Chafetz and Meredith, 1983; Chafetz and Folk, 1984; Guo and Riding, 1998; Chafetz and Guidry, 1999). These consist of bush-like morphology defined shrubs that typically grow in terrace pools and large ponds (Chafetz and Folk, 1984; Guo and Riding, 1998), according to what is observed for the Pianetti travertine body (Fig. 4.24). Regular flat surfaces and static conditions of the hydrothermal water, flowing under low regime, promote the precipitation of clotted peloidal dendritic boundstone. However, shrub-like dendrites can also nucleate on inclined surfaces of the terrace pools characterized by relative slow flowing water with laminar to turbulent conditions. In this case the precipitation of rhomb-composed dendritic boundstone takes place (Fig. 4.6D-F).,

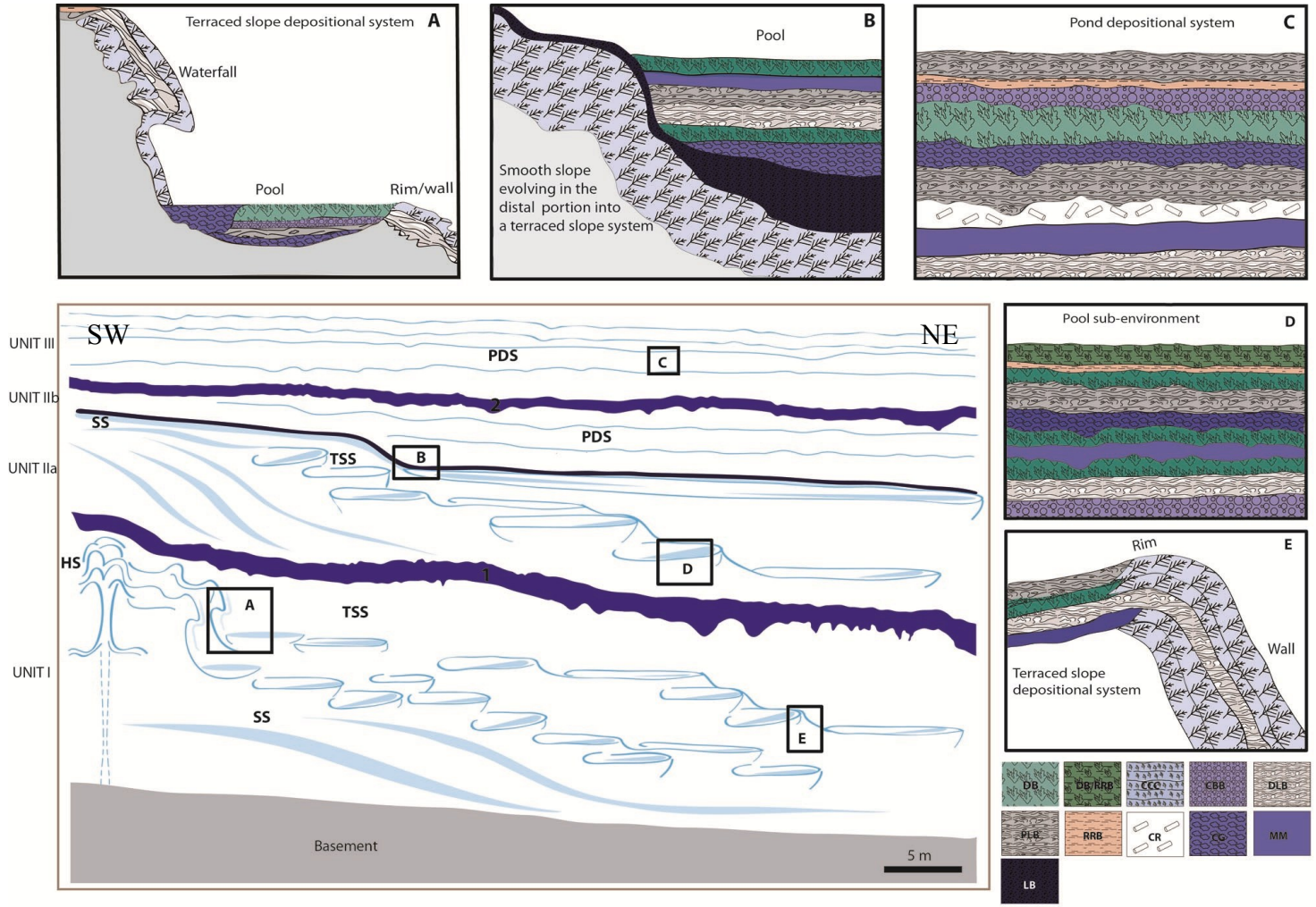

Fig. 4.24 Interpretative diagram of Pianetti travertine body showing the relationships between travertine Units (I, IIa and b, III), depositional environments and the relative fabric type occurrence (insets A, B, C, D, E). Lateral and vertical transitions between smooth slope (SS), terraced slope (TSS) and pond (PDS) depositional environments that characterized each travertine units are observed. Unit boundaries are marked by the two claystone layers (1-2) and a brecciated surface (yellow star). Scale refers to unit I, II, III size. Drawings of depositional sub-environments within units and the insets are not to scale. Hydrothermal spring (HS) at Unit I is indicated. Legend: DB) Dendritic boundstone (bd); DB/RR) Shrub-like dendritic bd on raft; CCC) Crystalline crust cementstone; CBB) Coated bubble boundstone; DSB) Dense laminated boundstone; PSB) Porous laminated boundstone; RR) Raft boundstone/rudstone; CR) Coated reed boundstone/grainstone/rudstone; CG) Carbonate grains intraclast grainstone/rudstone/floatstone; MM) Micrite mudstone/microsparstone LB) Lithoclastic breccia.

The clotted peloidal dendritic boundstone is interpreted as the product of predominantly microbially mediated processes. Microbial biofilms might exert an important influence on the formation of clotted peloidal dendritic boundstone because of the abundant presence of organic matter remains. An abiogenic control on the precipitation of the rhomb-composed dendrites is inferred because their crystalline morphology and the location of nucleation (Fig. 4.6C-H). However, fluorescence response and organic matter remains observed under SEM are arguments in favour of biogenic origins of these rhomb-composed end-member (Fig. 4.6I). All these observations reveal the interplay between abiotic and biotic processes with biofilms, which may have initiated/or influenced the initial stage of precipitation, successively overtaken by abiotic precipitation (due to the faster water for the rhomb-composed dendrites rather those forming the clotted peloidal dendrites).

Radiating dendritic boundstone (Fig. 4.6J-L) is interpreted as directly precipitated from hydrothermal water in intermittently agitated terrace pools (Fig. 4.24). Guo and Riding (1998) described in present-day travertine at Terme San Giovanni (Tuscany Italy) "radial shrub pisoids" that show similitudes with the radiating dendritic boundstone. These pisoids are formed in intermittently agitated microterrace pools where they are closely associated with abundant bacteria, cyanobacteria and diatoms (Guo and Riding, 1994, 1998). Relative slow water-flow conditions alternating with turbulent events are suggested for the formations of these peculiar dendrites. The precipitation process started with a dominantly biotic influence (as suggested by the presence of micrite, organic matter remains and nano-globules; Fig. 4.6L) and under turbulent water passed to prevalently abiotic. When the water flow was low a prevalently biotic precipitation and micritic radiating dendritic boundstone occurred; biofilms could have acted as templates for nucleation as suggested by the presence of nano-globules associated with organic matter remains. The turbulent events may correlate to an increase of the water supply that encourages the mechanical precipitation of calcium carbonate. In this circumstance, cloudy-crystals that split out from a clotted peloidal nucleus form. According to Guo and Riding (1994), fabrics comparable with the radiating dendritic boundstone are attributed to the interplay of processes ranging from microbially mediated and abiotic processes. In some cases, the spherulitic dendrites could be the results of the reworking of shrub dendrites (Guo and Riding, 1998).

Crystalline crust cementstone

Crystalline crust cementstone (Fig. 4.7; 4.24) formed through rapid precipitation from fast flowing waters (Folk et al., 1985; Guo and Riding, 1992, 1998). Crystalline dendrites forming the **thick crystalline crusts** (Fig. 4.7A) are interpreted as precipitated in conditions of significant water supply and fast flow regime; while the deposition of **thin crystalline crust cementstone** (Fig. 4.7B) reflects events of reduced water supply in the fast flowing area. Although the precipitation may have initiated under the influence of the biotic compounds as revealed by SEM analyses, all the observations lead to hypothesize that in conditions of high supersaturation with respect to calcium carbonate, abiogenic precipitation is the dominant influence on the shape, components and development of the different architectures that form the crystalline crust cementstone. The micro-fabric variety observed might be related to microscopic dynamics operating at the water body. The growth of dendrites/fan or mammillate cones occurs in stages, marked by the growth laminae.

Laminated boundstone

Laminated boundstone (Fig. 4.8) is interpreted as directly precipitated from hydrothermal water with the influence of microbially mediated processes. Slow-flowing sheets of water, mildly turbulent, are supposed necessary for the deposition of these stromatolitic-like structures. The laminated boundstone are typical of low energy areas such as ponds and pools of the terraced slope (Fig. 4.24); however, in agreement with what observed by Rainey and Jones (2009) within the Fairmont Hot Springs deposit, reduced volumes of flowing water from the hydrothermal water vent can promote the precipitation of these stromatolite-like structures in fast-flowing smooth slope areas. This could explain the alternation of laminated boundstone with crystalline crust cementstone along the fast flowing area of the terraced (Fig. 4.28) and smooth slope and marks a cyclic variation in the hydrodynamic conditions of the flowing water. It is, in fact, suggested that when the water supply decreases, low to medium flow regime may promote the precipitation of laminated boundstone in generally high-energy areas (Rainey and Jones, 2009). Variation from dense to porous texture (Fig. 4.8A-B) may be attributed to pulsating activity of the vent. Constant flow of water may favour the precipitation of the porous type encouraging more the microbial activity. While, when jets of water (related to pulsating activity of the spring) disturb the constant flow, CO_2 degassing is favoured. However, petrographic and SEM

observations (Fig. 4.8C-I) suggest that even for the dense laminated boundstone the biogenic precipitation is the major control on the overall morphology of this stromatolitic-like boundstone. In addition, the amount of microspar laminae rather than micritic laminae is interpreted as the result of the degree of lithification and diagenetic processes such as aggrading neomorphism.

Raft boundstone/rudstone

Raft boundstone interpreted as formed in slow flowing area, such as static water of pools or large horizontal ponds (Fig. 4.24), at the air–water interface (Kitano, 1963; Folk et al., 1985, Chafetz et al., 1991; Guo and Riding, 1998; Özkul et al., 2002). When these floating structures (Fig. 4.9A) are disturbed and fragmented they sink on the pool floor and give rise to rudstone/floatstone deposits (Folk et al., 1985; Guo and Riding, 1998). An interaction between abiotic and biotic processes is proposed for the formation of the raft structures. CO_2 degassing at water surface may initiate nucleation of calcite crystals on particulate matter suspended by surface tension and/or floating biofilms and may indicate high rates of evaporation, intense heating of the water surface or bio-mediated precipitation (Folk et al., 1985; Jones, 1989; Chafetz et al., 1991; Guo and Riding, 1998). Nano-globules (Fig. 4.9L), present within the micrite layers, suggest that precipitation started in association with organic compounds. The nano-globules replace the organic matter and gradually aggregated and coalesced to form crystals (Fig. 4.9K). Then, abiotic precipitation takes place represented by aragonite or calcite crystal fringes. The inner microsparite film (Fig. 4.9B and D), surrounded by micrite layers, may represent the first abiotic precipitate on the water surface due to evaporation (Jones, 1989). This microsparite film acts as a substrate on which the organic compound can nucleate. According to Guo and Riding (1992) the hollow centre aragonite spherulites is interpreted as an originally organic nucleus (Fig. 4.9J, 4.5L). Kitano (1963) observed that the surface of stationary Japanese hot-spring water was covered with a deposits resembling plate glass, consisting of fine particles of calcium carbonate. He suggested that on the surface of these hot spring waters, fine particles float causing a “Brownian” motion, and then solidify.

Coated bubble boundstone

Slow-flowing sheets of water and continually water-fed pools and ponds represent the best condition for the precipitation of coated bubble boundstone. Sub-horizontal layers of bubble boundstone are common in pools and laterally extensive equivalents in ponds deposits of the Pianetti travertine body (Fig. 4.24). Coated bubble boundstone (Fig. 4.10A-D) is consistent in travertine deposits (Kitano, 1963; Chafetz and Folk, 1984; Chafetz et al., 1991; Guo and Riding, 1998; Özkul et al., 2002; Fouke et al., 2000). Stagnant conditions are the most favourable for coated bubble formation (Folk et al., 1985; Ozkul et al., 2002). This travertine fabric is interpreted as trapped and rapidly mineralized bubbles of oxygen, methane and or/carbon dioxide (Chafetz and Folk, 1984; Chafetz et al., 1991; Guo and Riding, 1998; Bonny and Jones, 2008). A microbial activity in underlying sediment is suggested as the main gas source (Folk et al., 1985; Guo and Riding, 1998). Folk et al. (1985) suggested that 'fine drapes' of micrite enveloping coated bubbles may represent microbial EPS remains. A dominant influence of biogenic factor in the formation of Pianetti travertine coated bubble boundstone is revealed by the presence of mucous-like planar sheets (Fig. 4.10E-F), interpreted as possible relicts of EPS. Initial precipitation of calcite probably takes place along EPS through the formation of isolated nano-globules in EPS. These nano-globules gradually coalesce and organize to form irregular masses that progressively assume incipient crystal faces; these mineral masses progressively form well-developed calcite crystals. Guo and Riding (1998) suggested that surface tension facilitates chain formation by creating sufficient time for incipient lithification. This implies that coated bubbles form in standing water bodies. Peculiar bubble structures may also be preserved in fast flowing water principally if the gas bubble is protected by a ductile microbial EPS (Takashima and Kano, 2005). The occurrence of bubble boundstone in areas of fast-flowing water marks a cyclic variation in the hydrodynamic conditions of the flowing water: when the water supply increases a low to medium flow regime may promote the precipitation of coated bubble boundstone in fast flowing area. Gas bubbles due to abiotic degassing (mainly in fast flowing water) and rapidly lithified due to the supersaturation of the water are preserved as centimetre-size pockets and isolated structures. Kitano (1963) suggested that carbon dioxide gas is formed at the surface of the pool and small particles of calcium carbonate, floating and suspended on the surface and in the water cause a "Brownian" motion on the surface of the bubble and then solidify. The inner surface of the bubble coating is smooth and polished, whereas the outside surface is coarse and rough.

Micrite mudstone/microspartsone

Micrite mudstone (Fig. 4.10G) might be directly precipitated from the hydrothermal flowing water (low flow regime; Fig. 4.24) under predominant microbially mediated processes. This assumption is suggested also by SEM observations that highlight the presence of organic matter remains (Fig. 4.10J-K) within the micrite mudstone. As observed for other fabric types, on the surface of the EPS remains, nano-globules are widespread and seem to replace the organic matter (Fig. 4.10J-L). Petrographic observations suggest that microsparstone fabric type (Fig. 4.10I) may be interpreted as the result of diagenetic alteration of the micrite mudstone microfabric.

Reed boundstone/rudstone/grainstone

Reed boundstone (Fig. 4.11) is interpreted as a typical fabric type developed in ponds of distal deposits (Fig. 4.28), such as those of Unit III, where dilution with meteoric water is hypothesized (Guo and Riding, 1998). Plants form a barrier for the water flow and act as a substrate for the precipitation of calcium carbonate; in this way, plant stems and twigs become encrusted (Rainey and Jones, 2009). The deposition of calcium carbonate around stems is interpreted as a physical process. The coated reeds influence the morphology of these carbonate structures but they do not govern the precipitation of calcium carbonate. Different is the interpretation for reed boundstone observed in terraced slope and smooth slope of Unit I and II. In those cases, reeds are interpreted as evidence of interruption in the flow of hydrothermal water. When the spring activity stops, the plants colonize the dry surface. When the hydrothermal water flow starts again, the flowing water encrusts the reeds. Reed structures are interpreted as phytoclastic fragments encrusted by calcite forming rudstone/grainstone in pockets. The micrite layer that isolates the internal reed porosity (Fig. 4.11A-D) may suggest that also microbes colonizing the surface of the reed can favour the precipitation of calcium carbonate.

Carbonate grains

Carbonate grains (Fig. 4.11G-I) (similar to "lithoclastic travertine*" sensu* Guo and Riding, 1998) are interpreted as generated by erosion of already lithified travertine and are eventually transported by the flowing water towards lower topographic areas. Carbonate grains occur mainly in pools, just behind the pool rim or pond deposits (Fig. 4.28). Guo and Riding (1998)

argued that time-equivalent erosion of slope travertines contributes volumes of lithoclastic material, particularly to the toe of slopes and depressions, where eroded grains mix with *in situ* precipitates.

4.5.4 Porosity and permeability

Microfabric types, pore structures and diagenetic processes control the porosity and permeability values. The wide range of porosity and permeability (Fig. 4.13) values is interpreted as direct function of: 1) primary fabric orientation; 2) amount of cementation; 3) travertine fabric type; 4) micro-porosity.

The higher permeability values of the samples from Unit II and III rather than those from Unit I is related to diagenetic processes. Cementation and aggradational neomorphism are inverse proportional to the age of the travertine deposits, while dissolution vugs are higher in Unit II and III. The lowest porosity and permeability values are associated with well-cemented deposits. Calcite cementation partially or completely occludes the primary porosity and reduces permeability.

The consistently higher permeability values of the horizontally drilled plugs (Fig. 4.13C) rather than the vertically drilled ones reflects the vertical alternation of porous and tight layers at the millimetre to centimetre-scale. In horizontal direction the pore network is well connected within the specific millimetre to centimetre thick fabric type layer.

Pore structures (Fig. 4.18E) have a strong control on permeability. Simple pore structures, with large pores (3-20 mm wide and 3-8 mm high) such as those of raft boundstone/rudstone, coated reed fabric and laminated boundstone show high permeability values. This assumption is confirmed by observations made by Verwer et al. (2011) on a petro-physical research conducted on carbonates from five different areas and ages. According to Verwer et al. (2011), the simple pore structure with large pores provides an easy flow path for fluids, whereas the intricate pore structures have narrower pore throats and a higher capillary pressure impeding fluid flow. However, there is not always a positive correlation between permeability and porosity within the travertine samples: coated bubble boundstone displays high porosity and large pores but has low permeability as the pores are not connected (Fig. 4.13D).

CTAN low resolution acquisition might not capture the high micro-porosity that characterizes the Pianetti travertine. For this reason, mismatches between CTAN and Helium gas porosity are

observed. Another possible explanation could be related to the systematic error introduced by the visual estimate of the threshold.

This study provides the first comprehensive evaluation of the reservoir properties of hot-spring travertine carbonates and suggests that travertines may represent good reservoir quality rocks (Fig. 4.25) if the degree of cementation is intermediate or low.

4.5.5 Diagenetic environment and paragenetic sequences

The described diagenetic features can be explained by superimposed early and meteoric diagenetic processes. Two paragenetic sequences, which created textural and porosity modifications, have been individuated on the basis of the primary mineralogy: 1) aragonite deposits (first diagenetic sequence, green arrow in Figure 4.26), and 2) calcite deposits (second diagenetic sequence, orange arrow in Figure 4.26). . The space between the primary textural elements is filled by mostly equant cement (varying from microsparite to sparite) related to post depositional water flowing through the primary fabric after these had formed; thus this cement could be regarded as a syn-depositional. This hypothesis is also confirmed by isotopic analyses (Fig. 4.22). Petrographic observation and also SEM analyses show the presence of ghosts of acicular crystals and their possible moulds growing perpendicular to dendritic boundstone and cementstone, laminated boundstone, raft boundstone/rudstone. These acicular crystals seem to be embedded into a second generation of prismatic crystals growing in optical continuity with the acicular precursor (Fig. D-E). This suggests that, originally, part of the calcite cement was probably aragonite that subsequently was transformed into calcite. The inversion of aragonite into calcite might have occurred during early diagenesis. Although a poorly understood process, the time required for the aragonite to calcite inversion is highly variable. Aragonite in Bagni San Filippo in Italy inverts to calcite in less than 15 days (Malesani and Vannucchi, 1975), whereas it can be totally dissolved in the Pleistocene Rapolano Terme deposits (Guo and Riding, 1992), but it is still preserved in the Miocene Stuttgart travertine (Gregor, 1982). Meteoric diagenesis leads dominant transformations of the fabrics and the associated porosity. Isopachous cements, indicative of precipitation in the meteoric phreatic zone, occur especially in the travertine Unit I and II (Fig. 4.19F, I-J). Iron oxides often coat the travertine cements especially in Unit III, which is overlain by the present-day soil. Recrystallization of micrite to microsparite and sparite commonly is accompanied by a reduction of porosity facilitated by the precipitation

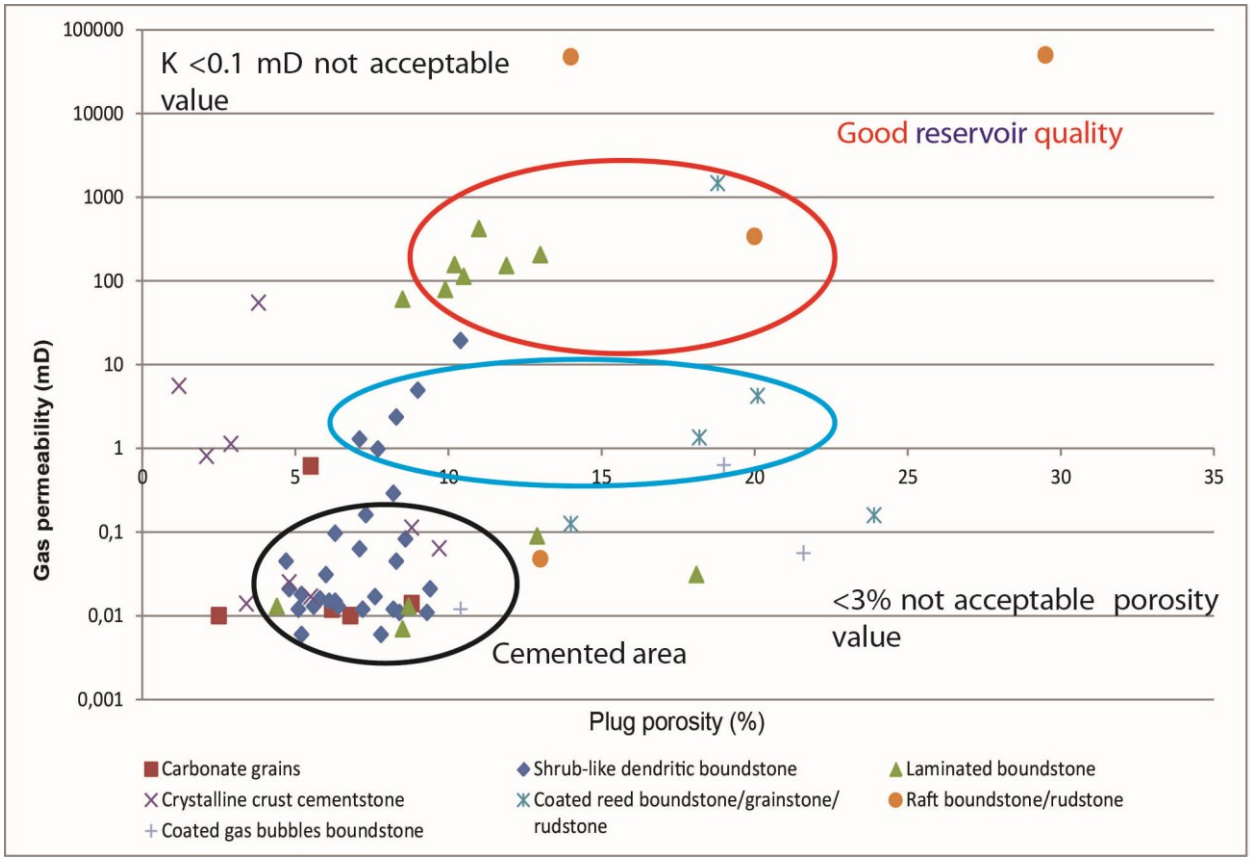

Fig. 4.25 Cross-plots of porosity versus permeability. Three large groups of interpretative reservoir travertine qualities are suggested

of additional carbonate from the circulating pore fluids (Fig. 4.20F-K). The processes of recrystallization, sparmicritization and cement deposition are probably contemporaneous. Travertine meteoric alteration has also been documented by the enrichment of Mg, depletion of Sr and Ba through ICP analyses and also by isotopic data that give value of δ^{18} O from -6.32 to -5.38 ‰ and δ^{13}C from -3.36 to -4.30 ‰ (Fig.4.22). Outcrop observation shows typical features of meteoric diagenesis such as karstic dissolution, caves and *terra rossa* sediment related to soils (Fig. 4.20A); millimetre to centimetre meteoric dissolution features are also observed (Fig. 4.20C-F). The cement present in the caves show isotopic value consisting into -3.78 ‰ δ^{18}O and -8.71 ‰ δ^{13}C , representative of cool temperature and meteoric water.

4.5.6 Stable isotope of travertine fabric growth

The change in travertine isotopic geochemistry (Fig. 4.21) observed across the Pianetti travertine system seems to be controlled by an interplay of a complex suite of physical and chemical

processes (e.g. CO_2 outgassing and consequent cooling, evaporation, temperature and saturation state of the precipitant water), hydrology of the water flows and biotic activities (e.g., photosynthesis and respiration). All these factors are strongly dependent with the depositional environments.

The negative $\delta^{18}O$ values appear to be influenced by high temperatures and supersaturation levels of the outflowing waters (Friedman, 1970; Guo et al., 1996; Fouke et al., 2000). An isotopically heavy CO_2 such as that derived from the decomposition of the substrate marine carbonates may explain the $\delta^{13}C$ values (Manfra et al., 1976). The $\delta^{13}C$ range is interpreted to reflect the contamination of the isotopic composition of groundwater by the Mesozoic bedrock marine limestones or juvenile/magmatic waters (Gonfiantini et al., 1968; Friedman, 1970; Turi,1986; Guo et al., 1996; Gandin and Capezzuoli, 2008).

Stable isotope analyses of the Pianetti travertine samples confirm the previously presented interpretations of the different depositional environments, fabric types and help to elucidate the processes involved during travertine precipitation. Continuous CO_2 degassing and temperature change of the thermal water flowing from proximal (mostly represented by travertine samples collected along Unit I) to distal areas (largely represented by samples of Unit II) of the Pianetti system, caused a general increasing trend towards heavier values for both $\delta^{18}O$ and $\delta^{13}C$. Samples collected in fast-flowing areas of the Pianetti system (such as the clinoformal strata of smooth slopes, raised to sub-vertical rims and walls of terraced slope) are characterized by higher $\delta^{18}O$ and $\delta^{13}C$ values with respect to samples typical of slow flowing area (e.g pool of terraced slope). In areas with high energy and turbulent hydrothermal water flow conditions, mechanical CO_2 outgassing is enhanced so that the correlative crystalline crust cementsone reflects slightly heavier $\delta^{13}C$ values compared to dendritic boundstone, laminated boundstone, micrite and microsparite boundstone precipitated in areas with slower water flows. In addition the $\delta^{18}O$ values in crystalline crust cementstone present also higher values compared with the other fabric types collected in slow flowing area. As suggested by Fouke et al. (2000) for Mammoth Hot Spring travertines, the shift of $\delta^{18}O$ value may be caused by evaporation of ^{16}O-enriched water vapour and cooling of the water (Gonfiantini et al., 1968; Usdowski et al., 1979; Turi, 1986; Chafetz and Lawrence, 1994; Gandin and Capezzuoli, 2008). Biogenic activity may also influence stable isotope compositions. Photosynthesis preferentially removes $^{12}C^{16}O_2$ from the water, which would increase the values of $\delta^{13}C$ and $\delta^{18}O$ in the remaining spring water and any carbonates precipitated from this isotopically heavier water (McConnaughy, 1989; Spiro and Pentecost 1991, Fouke et al., 2011). Guo et al. (1996) suggest that the abundance of

photosynthetic microbes increases downstream so a downstream increase in $\delta^{13}C$ and $\delta^{18}O$ occurs. This observation may give another explanation for the precipitation processes of the crystalline crust cementstone and is congruent with the presence of possible cyanobacteria filaments observed in the cloudy crystal (Fig. 4.7D). However, considering the depositional environment (Fig. 4.23) and consequent hydrology condition of the hydrothermal water under which crystalline crust cementstone forms, it is suggested that $\delta^{13}C$ and $\delta^{18}O$ are mainly controlled by rapid degassing of ^{12}C-enriched CO_2 rather than microbial activity.

The other fabric types, such as dendritic boundstone, laminated boundstone, mudstone/microsparstone, coated bubble boundstone show in general lighter $\delta^{13}C$ and $\delta^{18}O$ values compared with crystalline crust cementstone. If biogenic activity occurs, the $\delta^{13}C$ and $\delta^{18}O$ of slow flowing area fabric type may reflect different microbial processes compared with those of crystalline crust cementstone. Aerobic respiration, which produces progressively lower $\delta^{13}C$ and $\delta^{18}O$ as more CO_2 is released during oxidation of organic matter (Flanagan et al. 1992; Hinga et al. 1994), is consistent with the abundant presence of EPS and bacterial-like bodies observed through SEM analyses within the slow-flowing fabric types (Fig. 4.6, 4.8G-H, 4.9K, 4.10J-K).

It was observed that sample deriving from large pools and ponds compared with small pools of Pianetti terraced slope record an enrichment of $\delta^{18}O$ and $\delta^{13}C$. This reflects the hydrologically closed condition of the large pool and records the effect of evaporation, as a result of increased residence time of the water, in association with consumption of $^{12}CO_2$ through photosynthesis and equilibration with atmospheric CO_2.

Mineralogical changes across the spring system seems to affect the travertine isotope values. The lowest $\delta^{13}C$ values were recorded for the aragonite fabrics (Fig. 4.21). Fouke et al. (2000) show low $\delta^{13}C$ in association with vent deposits. However, no evidence of thermal spring has been observed in the field where the samples were collected. Kele et al. (2008) observed for the travertine in Hungary that in correspondence of lower temperature hydrothermal water, away from the spring orifice, various amounts of aragonite (5–35%) with higher Sr concentrations precipitate from solution. This aragonite precipitation is explained by fast carbonate precipitation (Kele et al., 2008).

In addition the lower $\delta^{18}O$ of Unit I compared with those of Unit II can suggest a change in hydrothermal water temperature or a seasonal climate change. The lower values may record warmer intervals/hotter water while the highest $\delta^{18}O$ values of Unit II may record a colder season/colder water.

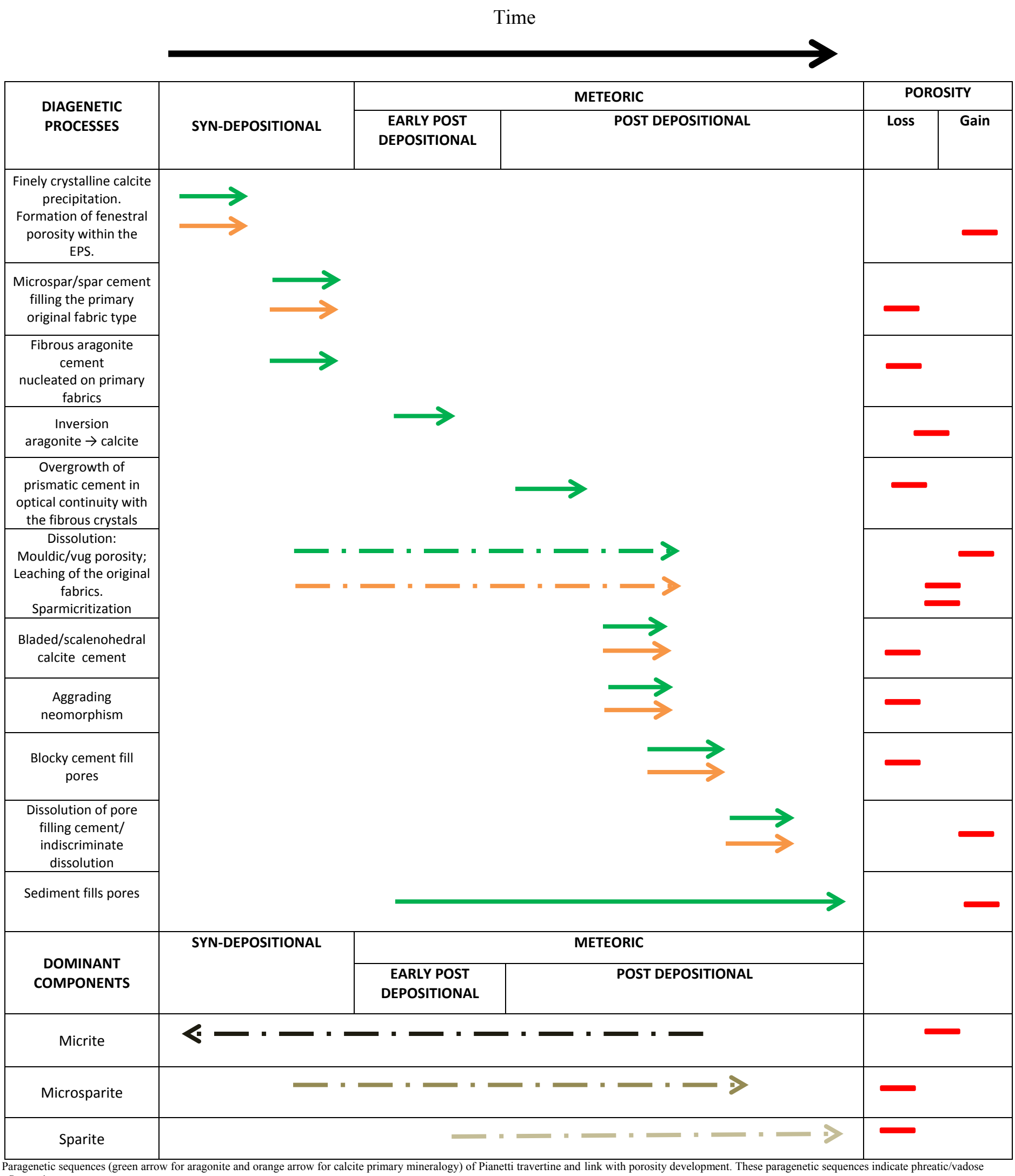

Fig. 4. 26 Paragenetic sequences (green arrow for aragonite and orange arrow for calcite primary mineralogy) of Pianetti travertine and link with porosity development. These paragenetic sequences indicate phreatic/vadose water table fluctuations.

4.6 Discussion

4.6.1 Travertine Units

The areal distribution of the travertine Units (I, II and II) within the Pianetti Travertine system and the presence of the laterally continuous exposure surfaces (claystone layers 1, 2 and brecciated horizons) provide information about the evolution of the depositional system and environments during the travertine accumulation and suggest an intermittent accretion of the Pianetti travertine system. Similar surfaces associated with palaeosols and lithoclastic-breccia intervals have been reported from different types of hydrothermal travertine systems (Guo and Riding, 1999; Özkul et al., 2002; Faccenna et al., 2008, Brogi and Capezzuoli, 2009), where these surfaces mark different travertine depositional events reflecting intermittent travertine accumulation. Lithoclastic layers have been identified and reported as "lithoclast travertine" by Guo and Riding (1999) within the Upper Pleistocene travertines of Rapolano Terme, Tuscany. These authors suggested that lithoclast travertine formed dark grey or brown layers (tens of centimetres in thickness) dominated by silt-sand grade detritus derived from break-up of adjacent light-coloured travertine slope deposits (such as crystalline crust and shrub travertine) and also contained a high proportion of plant fragments and, locally, gastropods, ostracodes and quartz silt matrix. Özkul et al. (2002) described four different brown-coloured palaeosols representing sequence boundaries between the travertine benches in the Denizli travertines and suggested that palaeosols thickness was related to the length of time of subaerial exposure. Paleosols are related to the ephemeral fluctuating character of the hot spring flow, resulting in rapid exposure of travertines to rain water, subaerial desiccation, terrestrial biological activities and soil formation (Guo and Riding, 1999; Özkul et al., 2002). Faccenna et al. (2008) individuated late Pleistocene depositional cycles in the *Lapis Tiburtinus* travertine (Tivoli, Central Italy) possibly influenced by climate and fault activity. These authors suggested that the occurrence of alternating depositional benches and erosional surfaces, which are associated with palaeosols, conglomerates, and karstic features, shows that the cyclical evolution of the travertine deposits was controlled by fluctuations of the water table in the Acquae Albule basin (Central Italy).

4.6.2 Depositional systems

The location and typology of the vents, the antecedent topography along which the water was flowing, the hydrodynamic of the hydrothermal water and mixing with meteoric water controlled the Pianetti travertine Units and their depositional geometry. These factors affected also the development of the different depositional systems. Guo and Riding (1998; 1999) suggested that the spring position is an important factor determining the travertine depositional morphotypes. Where the hydrothermal spring issues directly onto antecedent slopes or elevations, then terraced and smooth slope deposits form and pass downslope to pond depositional environments (Guo and Riding, 1998; 1999; Özkul et al., 2002). Modern travertine terrace slopes are well known from Mammoth Hot Spring in Yellowstone National Park, Wyoming (Chafetz & Folk, 1984; Pentecost, 1990; Renaut and Jones, 2000; Pentecost, 2005; Fouke, 2011), and Pamukkale in western Turkey (Antunel and Hancock, 1993; Özkul et al., 2002; Kele et al., 2011). In the Rapolano area, small terraces are periodically active at the western end of the fissure ridge at Terme San Giovanni (Guo and Riding, 1998). However, similar geometries of terraced system are also characteristic of cool water tufa deposits (Pedley, 1990; Ford and Pedley, 1996; Carthew et al., 2003; Pentecost, 2005; Pedley, 2009; Vazquez-Urbez, 2009; Arenas-Abad et al., 2010; Manzo et al., 2012;). Present-day smooth slopes, which often are laterally transitional into terraced slope systems, are identify in different travertine systems of Central Italy (Guo and Riding, 1999), Turkey (Özkul et al., 2002; Pentecost, 2005) and U.S.A (Pentecost, 2005; Fouke, 2011). Guo and Riding (1998) described smooth slopes, up to 20 m thick and 150 m long, in Cava La Chiusa (Rapolano Terme, central Italy). In contrast, the Pianetti smooth slope deposits are 2-8 m thick and can be laterally continuous for tens to hundreds of metres. Concerning the ponds deposits, sub-horizontal layers are very common in travertine deposits (Folk et al., 1985; Guo and Riding, 1998, 1999; Özkul et al., 2002). The pond depositional system occurring within the Pianetti travertine quarry, for its morphology, shows some analogies with the depression depositional system described by Guo and Riding (1998, 1999) in the Rapolano Terme travertines and by Özkul et al. (2002) in Pamukkale. Guo and Riding (1998) suggested that depression depositional environments are located in front of the slopes and consist of flats and hollows in areas of relatively low topography. The depression depositional environments were divided into two types a) Shrub flat and b) Marsh-pool (Guo and Riding, 1998; Özkul et al., 2002). The shrub flat (cf. Guo and Riding, 1998) consists of thin-bedded laterally extensive shrub lithofacies (here defined shrub dendritic boundstone). The shrub flats were previously

described by Chafetz and Folk (1984) as shallow lake-fill deposits. The marsh pool sub-environments are described as horizontal, grey, brown-coloured travertines that are rich in reed lithofacies (here defined reed boundstone/grainstone/rudstone) (Guo and Riding, 1998; Özkul et al., 2002). Guo and Riding (1998) and Özkul et al. (2002)both report that marsh-pool deposits are inter-bedded with light-coloured travertines of the shrub flat sub-environments and transitional in lateral direction; they comprise lithoclastic interlayers and common pedogenic features.

4.6.3 Fabric types

Certain precipitated fabric types distinguished in the Pianetti travertines are ubiquitous in hydrothermal travertines around the world.

Shrub-like dendritic boundstone layers are most abundant in Unit I and relatively less common in Unit II relative to other fabric types. At the meso-scale observation, shrub dendrites seem to be apparently absent in Unit III strata but petrographic investigation reveals their presence. This could be due to the high meteoric alteration/dissolution that affects the topmost travertine Unit III. Shrub-like dendritic boundstone for some aspects shows similarities with shrubs described in literature (Chaftez and Folk, 1984; Guo and Riding, 1998; Chafetz and Guidry, 1999). The similar features can be synthesized as follow: 1) shrubs grow mainly perpendicularly away from the substrate, 2) they occur densely packed to widely spaced, 3) they can be so densely packed such that individual shrub morphology is not distinguishable; 4) shrubs form laterally extended centimetre-thick layers. Chafetz and Folk (1984) indicated that shrubs probably precipitate in water as deep as the relief between their tops and bases. Both microbially mediated (Chafetz & Folk, 1984; Guo and Riding, 1994, 1998; Chafetz and Guidry, 1999) and purely abiotic (Pentecost, 1990) origins have been proposed for the “shrub” fabric type. Pentecost (1990) suggested that high rates of precipitation in waters supersaturated with respect to $CaCO_3$ and the preferential growth of crystals on sharp protuberances caused the dendritic form of shrubs at Mammoth Hot Spring (Yellowstone Park, USA). Chafetz and Guidry (1999) distinguished three kinds of shrub: bacterial, crystal and ray crystal shrubs. The bacterial shrubs were considered to be bacterially mediated, while the latter were thought to be formed by a combination of bacterial and abiotic processes. Crystal and ray crystal shrubs (Chafetz and Guidry, 1999) belong to crystallographic and non-crystallographic dendrites described by Jones and Renaut (1995), in this study defined as crystalline crust cementstone. The clotted peloidal micrite and rhomb-

composed dendritic boundstone types largely resemble the wide range of bacterial shrubs described by Chafetz and Guidry (1999). However,the rhomb-composed dendritic boundstone may show similarities with the crystal shrubs and the variety of transitional forms between bacterial and crystal shrubs (Chafetz and Guidry, 1999) in which the mineral habit only exerts a relatively minor amount of influence on the shrub morphology. Guo and Riding (1994) suggested that shrubs are built by two components: 1) micrite and 2) spar-rhomb. Micrite aggregates contain bacteria that promoted $CaCO_3$ precipitation either during life or shortly after death (Chaftez and Folk, 1984; Guo and Riding, 1994; Chafetz and Guidry, 1999). The associated spar-rhombs (‘‘leaves’’) could be controlled biogenically (by diatoms that trap particles with adhesive mucus) or abiogenically (Guo and Riding, 1994). Petrographic (Guo & Riding, 1994) and stable isotope studies (Guo et al., 1996) support the view that shrubs formed mainly under microbial influence, but with a component of inorganic precipitation. The presence of bacterial micropores and fossils within the micritic aggregates of carbonate shrubs and the association of diatom frustrules with the spar-rhombs of carbonate shrubs suggest that organisms are necessary for the formation of carbonate shrubs (Guo and Riding, 1994; Chafetz and Guidry, 1999). Chafetz and Guidry (1999) stated that the fluorescence of the leaves indicates the presence of hydrocarbons within the shrubs and the importance of bacteria for their formation. Folk (1993) described structures similar in size and shape to those termed here as nano-globules and interpreted them as calcified cells of alleged nanno-bacteria. Fouke (2011) suggests that shrubs precipitate in association with a large variety of microbial mats characterized by a high diversity assemblage of authotrophs and heterotrophs.

Structures comparable to the *radiating dendritic boundstone* have been addressed as pisoids (Chafetz and Meredith, 1983; Folk and Chafetz, 1984; Guo and Riding, 1994; 1998). Chafetz and Meredith (1983) observed similar features in warm spring travertine deposits in Idaho, ranging from 0.5 to 16 mm, and defined they as “bacterial pisolites”. Folk and Chafetz (1984) recognized within the Italian and U.S travertine deposits a particular type of pisoids composed of radially arranged bacterial shrubs around a nucleus. These “bacterial pisoids” are mostly intercalated with more arborescent dendritic layers and are abiotically influenced. Guo and Riding (1994) suggested an interplay between microbial and abiotic processes in the formation of these peculiar dendrites. In contrast with what observed by the above authors, the radiating dendritic boundstone of the Pianetti travertine lacks a well-defined nucleus.

Crystalline crust cementstone layers are abundant along the Pianetti travertine quarry walls of both Unit I and II; apparently the crystalline crusts are absent within the analysed and preserved

outcrops of Unit III. Field and petrographic studies of the Central Italian travertines by Chafetz and Folk (1984) and Folk et al. (1985) reported crystalline crusts as widespread in Italian travertine deposits. Folk et al. (1985) described: 1) thick crusts of radial fibrous calcite crystals up to 1 metre long, which show probable daily lamination due to the diurnal activity of photosynthetic bacteria and have depositional rates of as much as one metre per year; 2) Fine ray-crystal fans only 1 mm thick, made of helically-twisting radial ribbons of calcite and also show daily growth bands. Folk et al. (1985) showed that under SEM the fans are composed of strings of diamond-shaped plates about 3 μm long and 1 μm wide showing a high inter-crystalline porosity. At Rapolano Terme, Guo and Riding (1992) individuated dendrites defined as 'feather crystals' which they equated with the 'ray crystals' of Folk et al. (1985). These crystals formed well-defined layers separated by laminae of aragonite (Guo and Riding, 1992). Although the Pianetti crystalline crusts (especially *crystalline fan dendritic cementstone*) are comparable with those described by Folk et al. (1985), the large ray-crystal crusts and the fine ray-crystal fans do not cover all the range of morphologies of the *thick* and *thin crystalline crust cementstone* here described. Jones and Renaut (1995) defined a dendrite as a single, tree-like crystal that commonly has multiple levels of branching. These authors indicated that crystallographic dendrites have branches with definite crystallographic orientations, whereas non-crystallographic dendrites do not. Two types of non-crystallographic dendrites were described in the Kenyan hot-spring deposits (Jones and Renaut, 1995): 1) feather dendrites, characterized by complex branches (commonly curved) and accessory branches that give them a pinnate form; and 2) scandulitic dendrites with branches formed of plate-like crystals that are stacked *en echelon* (Jones and Renaut, 1995). In the same study Jones and Renaut (1995) also explained that the terminology "fan spherulitic" refers to spherulitic fibers radiating form a point in a fan-shaped array. Jones and Renaut (1995) made a correlation of crystal form with the disequilibrium factor that controls crystal precipitation; the disequilibrium factor depends on various parameters, including the $CaCO_3$ saturation level. In addition, crystal form may be intimately tied to the spatial relationship between the fluid and the growth surface (Jones and Renaut, 1995). Morphologies similar to non-crystallographic and crystallographic dendrites were described by Chafetz and Guidry (1999) who distinguished "crystal shrubs" and "ray-crystal shrubs" that represent primarily abiogenic carbonate shrub-forms. They suggested that these range from 1.0 to 3.0 cm in height and 1.0 to 3.0 mm in width (Chafetz and Guidry, 1999) and that the morphologies of their crystals are controlled by the abiotic precipitation of the calcite. The bacteria in the crystal shrub structures and large ray-crystal crusts probably influenced the

precipitation of the carbonate, however, abiogenic precipitation is the major control on the overall morphology of these forms (Chafetz and Guidry, 1999). *The feather-like crystalline and crystalline fan dendritic cementstone* individuated in the Pianetti travertine bear a close resemblance to some of the crystallographic, non-crystallographic dendrites and fan spherulite described by Jones and Renaut, (1995) and consequently with the crystal shrubs and the ray crystal fans of Chafetz and Guidry (1999). However, the high variability of morphology does not allow a precise comparison between the different types of crystalline dendrites identified in this study and those distinguished in previous studies. Concerning the *laminated cementstone*, it seems that this cementstone was not previously described among the travertine fabrics and no evident similitudes are observed with the fabric type described in the literature in travertine deposits.

The *laminated boundstone* is abundant in all the individuated travertine units. Compared with the other fabric types, the laminated boundstone shows a greater extent along the quarry walls of Unit IIb and Unit III. This fabric type was not described by Guo and Riding (1998), Folk and Chafetz (1984), Folk et al. (1985), and Özkul et al. (2002). Rainey and Jones (2009) reported the occurrence of "stromatolitic facies" within the Fairmont Hot Springs deposits. They suggested that this facies is present in accumulations that are up to 2 m thick and laterally continuous for tens of metres and it is formed on both horizontal and inclined surfaces. Depositional environments with slow flowing, weakly agitated water or reduced water volume discharges lead to stromatolite formation (Rainey and Jones, 2009). In agreement with the Pianetti laminated boundstone, Rainey and Jones (2009) suggested that reduced volumes of flowing water from the hydrothermal vent can promote the precipitation of stromatolites in fast flowing areas. The same authors report that the stromatolite facies is composed of thin sheets (100 μm to 2 mm) of calcite crystals separated by fenestral cavities that represent moulds of microbial mats that were encrusted by calcite sheets. These stromatolite fabric formed under conditions where microbial growth rates were higher than calcite precipitation rate.

At the meso-scale observation, *raft boundstone/rudstone* lenses and layers are mostly abundant in Unit I and III and relatively less common in Unit II. Raft boundstone/rudstone shows analogies with "plate glass" (Kitano, 1963), "calcite raft" defined by Folk et al. (1985), "raft" defined by Chafetz et al. (1991), "paper-thin raft travertine" described by Guo and Riding (1998) and Özkul et al. (2002). They are composed of calcite and/or aragonite crystals (Folk et al., 1985; Chafetz et al., 1991; Guo and Riding, 1998) and their lateral extent is quite limited, but up to metre scale (Özkul et al., 2002). Folk et al. (1985) suggested that initial precipitation of

micrite takes place at the air-water interface and is followed by the growth of small calcite spar crystals downwards. Growth of the spar layer causes the raft to sink slightly, allowing fluid to come into contact with the topside of the raft, permitting growth of upward trending calcite spar (Folk et al., 1985). Asymmetry of spar cements can be preserved and/or enhanced by continued crystal growth after rafts settle to the sediment-water interface (Pentecost, 2005). Folk et al. (1985) suggested that most of the pore spaces and vugs are partially filled with early diagenetic crystals that are variants on the basic rhombohedra; finally, palisade calcite cement is the last pore-filling in large cavities. Cementation at the sediment-water interface promotes their preservation in travertines (Folk et al., 1985).

Coated bubble boundstone deposits are copious along all the identified travertine units but they are more abundant in Unit I and II compared with those of the Unit III. Coated bubble boundstone fabric type was described by Kitano (1963), Chafetz and Folk (1984), Chafetz et al. (1991), Guo and Riding (1998; 1999), Özkul et al.(2002), Fouke et al. (2000), and Rodríguez-Berriguete et al. (2012) as hollow, spherical accumulations of calcite and aragonite, generally a few millimetres in diameter that form around gas bubbles due to biogenic and abiogenic sources. In contrast with the coated bubble boundstone, observed in the Pianetti quarry, Chafetz et al. (1991) suggested that bubbles are composed of three layers: 1) a very thin inner layer of stellate clusters of aragonite crystals, 2) a thin middle layer of hemispherical spherulites of aragonite, and 3) an outer layer of equidimensional to slightly elongate calcite crystals. Calcite is, however, the predominant constituent of the bubble crusts (Chafetz et al., 1991). Porous laminated boundstone is characterized by porosity up to 50%, while porosity within the coated bubble boundstone is up to 70%. *Micrite mudstone/microsparstone* was not described in previous studies about travertine deposits. The micrite mudstone/microsparstone layers are abundant in all the identified travertine units but mostly within Unit I and II. Diffuse is the presence of ostracods within this fabric type. Blanchard (1903) noted ostracods living up to 51°C in the water of Hamman Meskoutine, Algeria. In the 'pulpit basins' of Pamukkale, Turkey, *Heterocypris incongruens* was found in abundance at temperatures of 20–30°C (Pentecost et al., 1997).

Coated reed boundstone/grainstone/rudstone is more common in Unit III and IIb. This fabric type was previously described by Guo and Riding (1998) and subsequently by Özkul et al. (2002) as reed travertine, while Rainey and Jones (2009) defined them as macrophyte facies. Reeds and coarse grasses can grow in rain influenced diluted and cooled waters from hot springs (Guo and Riding, 1998), as well as in cool rivers or lake waters (Pedley, 1987). Guo and Riding (1998) and Özkul et al. (2002) suggested that reeds, grasses and similar water plants are ordinary

components of both marsh-like shallow depressions, temporarily drying out, and reed mounds. Rainey and Jones (2009) suggested that the "macrophyte facies" is most common at the base of the deposit where local vegetation was inundated by spring water and encrusted with calcite. The plant clusters obstruct the water flow and the roots stabilize the sediment (Özkul et al., 2002). Some small lenses and beds of detrital macrophyte facies (<10 cm thick) are observed where leaves or trees fall or are washed onto the bedding surface (Rainey and Jones, 2009). Rainey and Jones (2009) suggested that plants were encrusted by trigonal, gothic arch and biterminal calcite crystals, like those observed in the stromatolite (here described laminated boundstone) and bubble fabric type.

According to several authors (Folk et al., 1985; Guo and Riding, 1998; Özkul et al., 2002; Rainey and Jones, 2009), a relationship between fabric types and velocity/turbulence and discharged volumes of the flowing water exists. *Crystalline crust cementsone* is typical of fast flowing areas such as smooth slope, walls and pool rims of terraced slope depositional systems (Folk et al., 1985; Guo and Riding, 1998; Özkul et al., 2002). The thickness of these crystalline cementstone is dependent on water supply and flow regime (Folk et al., 1985; Guo and Riding, 1998; Özkul et al., 2002). *Carbonate grains grainstone/rudstone/floatstone* with intraclasts of already lithified travertine fabrics are present also on the pool floor next to the wall drop where turbulent water regime occurs. The above observations are congruent with those suggested from Chafetz and Folk (1984), Folk et al., (1985), Guo and Riding (1998) for different travertine systems of Central Italy, Turkey described by Özkul et al., (2002) and Fairmont Hot Springs deposit reported by Rainey and Jones (2009). According to Guo and Riding (1998), periodic exposures are marked by the deposition of lithoclastic breccia followed by *coated reed boundstone/grainstone/rudstone* when the growing vegetation is encrusted by carbonate precipitated by the re-establishment of hydrothermal water flow. *Coated reed boundstone* indicates events of exposure and mixing with rain water (Özkul et al., 2002).

4.6.4 Biogenic versus abiogenic precipitation

One of the most controversial issue in the study of hydrothermal travertine deposits is the mechanisms of precipitation involved in the formation of these continental carbonates. Different modes of mineral precipitation have been claimed to explain travertine formation (Chafetz and Folk, 1984; Folk, 1994; Guo and Riding, 1996; Chafetz and Guidry, 1999; Tekin et al., 2000; Fouke, 2011). These range from abiotic to biotic processes to intermediate mechanisms

attributed tothe interaction between abiotic and biotic processes. $CaCO_3$ precipitation at hydrothermal springs has been considered as related to inorganic–physicochemical processes due to CO_2 degassing and increased supersaturation with respect to carbonate minerals (Kitano, 1963; Pentecost, 1990; Farmer, 2000; Fouke et al., 2000;). Carbon dioxide outgassing is favoured in agitated waters, such as areas of high current velocity and turbulence (e.g. waterfalls, walls of terraced slope, smooth slopes). Evaporation is induced by high temperature of the water at the air-water interface and it can be an important process in CO_2 transfer (Pentecost, 2005; Jones and Renaut, 2010). Microbial communities are widespread within travertine deposits. Although Weed already in 1889 suggested that micro-organisms should promote $CaCO_3$ precipitation, yet it is difficult to determine the degree to which micro-organisms influence the calcium carbonate precipitation in hydrothermal travertines. Hydrothermal springs nurture photosynthetic cyanobacteria and chemolithotrophic thermophiles, some of which can grow in total darkness (Allen et al., 2000). Pentecost (1996) showed that phototrophic and chemolithotrophic thermotrophilic microbes such as *Synechococcus*, *Chloroflexus*, *Oscillatoria*, *Calothrix*, *Thermothrix*, can mediate carbonate mineral precipitation. Other possible reactions involve denitrifying bacteria producing ammonia or the oxidation of S or H; many thermophilic bacteria and archea utilise oxidised S-compounds as electron acceptors (Renaut and Jones, 2000). At Mammoth Hot Springs, Fouke (2011) reported that microbial mat communities in the vent facies, apron and channel facies are dominated by chemoautotrophic metabolisms, including S oxidation and anoxygenic photosynthesis; conversely, microbial communities in the pond, proximal-slope and distal-slope facies contain a diverse mixture of photoautotrophic and heterotrophic metabolic activities. Diverse species exist in close proximity and, in some cases, coexist with mineral deposits in endolithic communities (Allen et al., 2000). Endolithic cyanobacteria and diatoms are ubiquitous up to 10 mm below the travertine surface (Pentecost et al., 1997). There is a clear case for arguing for biotic precipitation and active mediation when metabolic processes (e.g., photosynthetic removal of CO_2) not only induce nucleation but maintain the level of mineral supersaturation needed for continued precipitation (Renaut and Jones, 2000). Pentecost et al. (1997) suggested that cyanobacteria locally influenced the travertine microfabrics by providing sites for the trapping and nucleation of calcite at the cell surface, but the bulk of the travertine did not appear to be influenced by the presence of these microbes. Folk at al. (1985) suggested photosynthetic bacteria induced calcite precipitation in the daytime, while heterotrophic bacteria continued to develop a micritic band at night. The process of forming the daily lamination in travertine in Shionoha hot-spring (China) is closely related to

daily metabolism of cyanobacteria and does not confirm the role of heterotrophic bacteria in the formation of micritic bands as suggested by Folk (1993), according to(Jones and Peng (2012). Guo and Riding (1992) suggested that the aragonite was precipitated in the daytime under higher calcite supersaturation induced by microbial photosynthesis. Chafetz and Guidry (1999) suggested that prokaryotic organisms (other than cyanobacteria) in the shrub fabrics act as catalyst, facilitating the precipitation of minerals in the microenvironment immediately surrounding the clumps of the micro-organisms. Fouke (2011) suggested that the suite of microbial metabolic processes potentially capable of affecting these carbonate reactions include: 1) the consumption or production of CO_2 during oxidation–reduction coupled metabolic reactions and photosynthesis; 2) the consumption or production of organic and inorganic acids; and 3) the biosynthesis of membrane bound biomolecules and enzymes on outer cell walls that affect $CaCO_3$ nucleation kinetics. Arp et al. (1999) proposed that if bacteria play any role in travertine formation, they may serve as low-energy surface sites for nucleation. Petrographic analysis and SEM observation reveal the presence of the organic matter remains within the Pianetti travertine. Also, fluorescence microscopy, showing fluorescence of the micrite, indicates the diffuse organic matter within the travertine fabrics. The organic matter remains consist mainly of extracellular polymeric substances (EPS), filaments and bacteria-like structures. Many microbes adapted to carbonate hydrothermal springs produce EPS and form extensive biofilms (Allen et al, 2000). EPS of biofilm generally plays an important role in trapping detrital particles (Riding, 2000). Cyanobacteria secrete EPS by photosynthetic dark reaction, which lasts longer in a light-deficient condition. EPS can induce calcite nucleation and precipitation by binding calcium ions to their negatively charged sites (Pentecost, 1985). SEM observations of travertine highlight the presence of nanometre-size, sub-spherical to globular, structures (10-150 nm in size) on EPS or often associated with bacteria-like remains. Following studies from marine and non-marine microbialites and reproduced in laboratory experiments (Merz-Preiβ and Riding, 1999; Sprachta et al., 2001; van Lith et al., 2003; Dupraz et al., 2004, 2005; Pedley et al., 2009; Spadafora et al., 2010; Manzo et al., 2012; Perri and Tucker, 2007; Perri et al., 2012) it was observed that these nano-globules coalesce and gradually organize into a more crystalline morphology showing incipient rational crystal face development. These mineral masses appear to progressively substitute and eventually replace the mucus-like substance until they form well-developed calcite crystals. These observations suggest that travertine formation is not only the result of mechanical CO_2 degassing but that both abiotic and biotic processes (biologically induced by microbial metabolic process or simply influenced by nucleation on microbial biofilm

substrate) are involved in the precipitation of the Pianetti travertine. The nano-globules show morphology similar to the nanobateria individuated by Folk (1993). Allen et al. (2000) individuated biologically mediated submicrometre mineralized spheres composed of calcium fluoride or silica and suggested that the spheres themselves are apparently not fossils or microbes. Recently, features similar to nano-globules where observed by Jones and Peng (2012) on travertine in the Shionoha hot-spring. These authors assume that formation of these nano-particles may be related to physicochemical conditions that develop in micro-domains existing within the EPS. Pedley et al. (2009) recognized nano-globules as the first product of mineralization, successively developing clusters composed of micro-peloids in laboratory produced tufa. The processes of EPS degradation are significant particularly in modern microbial mats because they commonly lead to carbonate precipitation, whereas the bacterial bodies themselves are less involved (Dupraz et al., 2005). Carbonate precipitation processes associated with the EPS degradation progressively infill the space left by the degraded EPS structure (Spadafora et al., 2010). It has been shown that nano-spheres with a high organic matter content replace both the EPS structure (Dupraz et al., 2004) and bacterial bodies (Sprachta et al., 2001; van Lith et al., 2003). Moreover, nano-globules, in a more advanced stage of mineralization, coalesce to form larger (20 to 50 μm) peloids (Pedley et al., 2009; Spadafora et al., 2010). Pedley et al. (2009) suggested that the precipitation of calcite appears to occur freely within the freshwater biofilm experiments. Reid et al. (2000) suggested for present-day Bahamian marine stromatolites a biomediated precipitation model in which heterotrophic bacteria (and invertebrate grazers) digest the EPS and release the chelated calcium ions from the EPS polymer chains for calcite precipitation.

Many Pianetti travertine fabrics represent transitional forms of a continuum between the two end-members of purely abiogenic and microbially mediated precipitation. This is also confirmed by isotopic values (Fig. 4.21 B). Fabrics that occur in low energy areas might be more biologically influenced than fabrics occurring in fast-flowing, dipping surfaces for which the abiotic processes of physical degassing might prevail. In addition, in slow flowing areas, micrite represents the main carbonate precipitate, while well-developed crystals are the main fabric precipitated in fast flowing environments where abiotic degassing is predominant. This is congruent with the observation derived from microbial carbonates from marine and non-marine settings, which are dominated by micritic precipitates as leiolitic or clotted peloidal micrite (Riding, 2000). Clotted peloidal micrite appears to be precipitate within EPS membrane or to represent calcified bacteria aggregates (Riding, 2002). Concerning the spar and microspar

precipitation, Riding (2000) suggested that the extent of their microbial origin is uncertain. The origin of spar and microspar crystals in travertine systems is generally considered mainly abiotic (Guo and Riding, 1998; Chafetz and Guidry, 1999); however an interplay between abiotic and biotic processes is here suggested. The biologically influenced carbonate precipitation process (*sensu* Dupraz et al., 2009) might be the predominant one that affected the Pianetti fabric types accumulated in low energy ponds and pools and that revealed high content of embedded EPS. These are the clotted peloidal dendritic boundstone, laminated boundstone, coated bubble boundstone and micrite mudstone. Regarding the predominantly inorganic fabric types (crystalline crust cementstone), although carbonate precipitation results mainly from an abiotic process of degassing promoted by water turbulence, it might likely be that precipitation initiated on organic substrates.

This study demonstrated that during the formation of hydrothermal travertine deposits there might be the interaction between abiotic and microbially mediated and influenced processes.

4.7 Conclusions

The Pianetti travertine body, well exposed within an active quarry, exhibits a wedge-shape differentiated into three decametre scale travertine units. Exposure surfaces represented by claystone layers constitute the travertine sequence boundaries and suggest an intermittent accretion of the travertine system.

Different architectural patterns including clinoforms, stepped and sub-horizontal layers corresponding to smooth slope, terraced slope and pond depositional environments, respectively, were individuated within the travertine units. The smooth slope system consists of extensive and laterally continuous, planar to convex, clinoformal layers dipping ca. 4° to 45°. The terraced slope system consists of a stepped morphology differentiated into flat sub-horizontal pools, raised and convex pool rims, and vertical/overhanging strata of pool walls and waterfalls. Laterally continuous and vertically alternated sub-horizontal layers identify the pond deposits. The hydrodynamic of the flowing hydrothermal water, controlled by the location and the activity of the vent, the roughness of pre-existing surface and topography, influences the development of the terraced slope system. Smooth slopes and terrace rims and walls are considered areas of fast flowing water, while terrace pools and ponds are areas of standing to slow flowing. A

classification of the several travertine fabrics identified at the centimetre-scale is proposed. Fabric type description and the proposed travertine classification are developed using some terms of classical classifications of carbonate textures by Dunham (1962) and Embry and Klovan (1971). The classical carbonate terminology is here combined with the published travertine fabric nomenclature (Chafetz and Folk, 1984; Jones and Renaut, 1995; Guo and Riding, 1996). Travertine fabrics can be essentially distinguished into three categories: 1) travertine boundstone and cementstone s.l. in which the original components are directly precipitated from hydrothermal thermal water that include: a) shrub-like dendritic boundstone; b) thick crystalline crust cementstone; c) thin crystalline crust cementstone; d) laminated boundstone; e) coated gas bubble boundstone; f) raft boundstone/rudstone; g) micrite mudstone/microsparstone; 2) encrusted travertine coated reed boundstones/grainstone/rudstone in which original components (acting as substrate) are directly encrusted by carbonate precipitated by flowing hydrothermal water; 3) carbonate grains packstone/grainstone to floatstone/rudstone formed by fragments of already lithified travertine precipitates (intraclasts) and other lithoclasts. The individuated fabric types reflect the precipitation processes due to an interplay of abiotic and biotic processes (biologically induced by microbial metabolic process or simply influenced by nucleation on microbial biofilm substrate) and subsequent diagenesis. Pore space is an important component of travertine fabrics, which show a wide range of depositional porosity and secondary porosity. SEM analysis reveals a significant micro-porosity. The description of the porosity types is based on Choquette and Pray (1970) classification. This study provides also the first comprehensive evaluation of the reservoir properties of hot-spring carbonates and suggests that travertines may represent good quality reservoir rocks. The Helium porosity and permeability measurements show that travertines display a wide range of porosity, from 1 to 29%, and permeability, from 0.006 up to 50000 mD. The pore structure of ten samples was quantified using microCT scanning and AVIZO, which has proved to be an excellent visualization tool in the travertine sample. The diagenetic features can be explained by superimposed early hydrothermal and meteoric diagenetic processes. Dissolution, neomorphism and spar-micritization combined with cementation are the main diagenetic processes that can alter the fabric appearance.

Petrographic and XRD diffraction analyses confirm that the studied travertines are composed predominantly of calcite with minor amounts of aragonite. Fibrous morphology of a significant amount of the calcite suggests that transformation of aragonite into calcite might have occurred.

Organic matter remains and organomineral nano-globules within the Pianetti travertine suggest that for some precipitates the biologic influence is fundamental. However, even for the

biologically induced mineralization, abiotic processes and physical-chemical characteristic of the precipitating thermal water are necessary for travertine formation.

A relationship between fabric types and velocity/turbulence and discharged volumes of the flowing water is suggested. In addition, fabrics occurring in low energy areas might be more biologically influenced than fabrics occurring in fast flowing dipping surface for which the abiotic processes of physical degassing might prevail. However, many fabrics represent transitional forms of a continuum between the two end-members of purely abiotic and microbially mediated (biologically influenced/induced mineralization).

All the observations above suggest that the Pianetti travertine deposits can have implications for comparable carbonate reservoirs in the subsurface.

Chapter 5

The present as a key to the past: present-day travertine precipitation at Bagni di Saturnia, Albegna Valley, southern Tuscany, Italy.

Abstract

Actively forming travertines occurring today at Bagni di Saturnia (Bagni di Saturnia, Tuscany, Central Italy) have been investigated with the purpose of understanding the biological, chemical and physical processes that interact together to produce hydrothermal travertine deposits.

Thermal water discharges at Bagni di Saturnia reach a rate of 800 litres per second at a maximum temperature of 37.5 °C and a pH of ca. 6.4. The spring expels water enriched in H2S-CO2-SO42- and HCO3- and divalent cations (Ca > Mg). The total dissolved solids in the water amount to 2.94 g/l.

Four depositional environments encompass the present-day Bagni of Saturnia depositional system and can be differentiated into: 1) hydrothermal vent, 2) self-built channel, 3) waterfall, and 4) terraced slope. The self-built channel depositional environment extends for a length of ca. 900 m and consists of a channel and associated pond sub-environments. Channel sub-environments occur as sinuous to sub-horizontal conduits. It varies in width between 80 cm to more than 1.80 m. The channel is usually characterized by high-energy laminar to turbulent water flow. In the central part of the channel, characterized by gentle topographic gradient, some hemispherical ponds are associated with the channel. These ponds, up to 50 cm in width, form in marginal zones of the channel and correspond to slow flowing, low-energy areas. The flowing of the water across a sharp break in slope gives rise to two sub-vertical waterfalls about 4 m high. Velocity and the energy of the spring-water increase in the waterfall environment. Down-current the waterfalls, the gradient reduces to 20-25° and the water splashes into the pools of the adjacent terraced slope system. Travertine deposits belonging to the terraced slope consist of

vertical to overhanging walls (ranging between several centimetres to 2 m in height), sub-horizontal pools (width between 30 cm and up to 5 m) and raised rims confining the margin of the pools. Water flow varies along the terraced slope. The water is generally fast flowing but pools represent a relative slow-moving portion of the terraced slope system. However, pulsating sheet flows produce periodic rim and wall exposures. At lower altitude the thermal waters mix with the cold water of the river Stellata.

Prokaryotes, diatoms, green algae and ostracods mainly populate the travertine deposits and influence their fabrics. Five macro-fabric groups characterize the Bagni di Saturnia deposit including: 1) layered travertine boundstone/cementstone, 2) coated bubble boundstone travertine, 3) encrusted travertine, 4) coated grain travertine, 5) carbonate and non-carbonate intraclasts and extraclasts. Micro-scale observations reveal a large variety of micro-fabric types. These include: a) dendritic boundstone, b) laminated boundstone, c) crystalline crust cementstone, d) micrite mudstone, e) coated bubble boundstone, f) coated reed boundstone/grainstone/rudstone, and g) grainstone/rudstone/packstone/floatstone.

Bagni di Saturnia travertine shows a wide range of macro- and micro-porosity. In terms of depositional porosity, nanometre to centimetre size framework porosity ranges from tight to high. The depositional porosity can be differentiated mainly into: 1) inter-branching porosity, 2) inter-laminae porosity, 3) inter-particle porosity, and 4) coated bubble porosity. Secondary porosity is firstly related to bio-mouldic porosity. Meteoric dissolution produces millimetre to centimetre size vugs.

A relationship between microfabric types and velocity/turbulence of the flowing water and probably also volumes of water discharged is suggested. Fabric types consisting mostly of micrite suggest that precipitation occurs under slow flow regime of the hydrothermal water, while those fabric types essentially formed by cloudy spar are typical of fast flowing water. Fabrics that occur in low energy areas might be more biologically influenced than fabrics occurring in fast flowing dipping surface for which the abiotic processes of physical degassing might prevail.

SEM analysis shows the common presence of the organic extracellular polymeric substances (EPS) and filaments that appear located where the calcite minerals nucleate and grow. Diatoms, cyanobacteria filaments and other bacteria are associated with the EPS and often appear totally or partially entombed in it. Detailed observations of Bagni di Saturnia travertine highlight the presence of nanometre-size, from sub-spherical to globular, structures (mainly from 10 to 150 nm) on EPS. These nano-structures gradually coalesce to form rhombic calcite crystals. Gypsum

crystals were mainly individuated in the upper zone of microbial mats; filamentous organic structures connected to the crystals are observed. A biologically induced process is claimed for the precipitation of framboidal pyrite associated with organic matter remains related to possible sulphate reducing bacteria. These observations suggest that travertine formation is not only the result of mechanical CO2 degassing. Travertine precipitates are mainly strongly influenced and, in some circumstances, induced by the microbial biofilms. Nevertheless, also in the case of biologically-induced mineralization some abiotic processes and physical-chemical characteristic of the precipitating thermal water exert an important control on the carbonate precipitation.

5.1 Introduction

Calcium carbonate precipitation around hydrothermal springs produces diversified deposit-related fabric types, which are mainly calcite and aragonite in mineralogy (Kitano, 1963; Chafetz and Folk, 1984; Folk et al., 1985; Jones and Renaut, 1995; Guo and Riding, 1998; Chafetz and Guidry, 1999). Crystal fabrics and composition of the travertine deposits are inferred as sensitive environmental record of water chemistry, hydrologic transport, climate and microbial populations (Fouke et al., 2000). $CaCO_3$ precipitation at hydrothermal springs has been considered as an inorganic–physicochemical process (Kitano, 1963; Pentecost, 1990; Farmer, 2000; Fouke et al., 2000; Pentecost, 2005). Nevertheless, biomediation of calcium carbonate is now recognized to be equally important especially in slow flowing and standing water sites (Pedley, 2009). Microbes serve as initial sites of calcium carbonate nucleation in hydrothermal spring and can become both encrusted and replaced; once stable nuclei have formed, crystal growth may continue in already supersaturated fluids (Renaut and Jones, 2000). Detailed studies on micro-fabric and nano-scale physical and biological structures description lack in travertine deposits. This appears essential to gain a more complete understanding of the mechanisms and the conditions that lead to the precipitation of these continental carbonates. Thus, with the main purpose to define the relationship existing between depositional environments and fabric types and with the aim to understand in which way the biological, chemical and physical processes interact together to produce the hydrothermal “Bagni di Saturnia" travertine deposits, a multi-scale study is here presented. This chapter reports a detailed description of Bagni di Saturnia depositional systems, microbial biofilms, main components of carbonate fabrics, porosity and nanostructures. A model for calcium carbonate precipitation based on the interplay of abiotic and

biotic processes is also suggested. These findings can help to better understand broader questions for the ancient hydrothermal travertine deposits.

5.2 Material and methods

In order to understand the relationship between water physical and chemical parameters and the interplay between abiotic and biotic processes inducing the formation of travertine, carbonate precipitates and water samples were collected during field work.

Travertine samples and adherent biofilms were sampled and returned to the Milan University laboratory facilities. Samples were air dried, embedded in a resin and thin sectioned. To investigate the travertine modern precipitates formed in association with organic components traditional petrographic methods were associated with SEM-EDS analysis, XRD, cathodoluminescence, and epifluorescence analysis. Traditional petrographic investigation and the microphotography documentation were carried out on the thin sections using a Zeiss microscope. SEM analyses were conducted using a Cambridge Stereoscan 360 equipped with an energy-dispersive X-ray spectrometer (EDS). SEM analyses were carried out on representative etched and non-etched fresh broken surfaces and polished thin sections. These were previously carbon coated or gold coated, depending on whether they were prepared for micro-analysis or textural study, respectively. The mineralogical composition was determined using X-ray powdered diffraction (XRD). The travertine specimens were grinded into a very fine powder using a mortar and pestle and after analysed using a X-RAY Powder Diffractometer Phillips X'Pert MPD with a high temperature chamber.

Geochemical parameters of the thermal water where measured in part in the field and in part in a laboratory Redox potential, pH, temperature of water samples were measured immediately in the field using a portable multi-parameter data logger (DeltaOHM Instruments). Standardization of pH-measurements was made using buffers solutions at 4 and 7. The total alkalinity was analysed in the field using a hand-held HCl titration according to Gran's method (Gran, 1952) using methyl-orange as indicator. Pressure-filtered (acetate membrane filter; pore size: 0.45 μm) splits were taken in acid-washed polyethylene bottles and acidified to pH < 2 using ultrapure nitric acid. In the laboratory (IGG-CNR of Pisa) major cations were analysed by atomic absorption and metals were quantified on Inductively Coupled Plasma Optical Emission Spectrometry (ICP-OES; Perkin Elmer Optima 2000DV). Water samples for sulphide analysis were stored into 100

ml glass bottles containing 0.5 ml of NaOH 8N solution and zinc acetate saturated solution immediately added upon collection. Unfiltered splits were taken in a dark-glass bottle for Major Anions and Ammonia (N-NH3) and analysed within 48 h. All the water samples have been kept cool at +4°C immediately after collection. Sulphide determination was done by iodometric titration using starch as an indicator (Kolthoff et al., 1969). The concentrations of anions were determined by ion chromatography with conductivity detection using a DX-100 instrument (Dionex Co.). Ammonia values were measured by an Ion Selective Electrode (Thermo Scientific Orion) according to the methods of Kolthoff et al. (1969). The oxygen isotopic composition of the water was determined by the water-CO_2 equilibration method at 25°C with mass spectrometry using a Finnigan MAT 252. For hydrogen isotope analysis, water samples were reduced to H2 at 450°C using Mg and analysed with using Europa Scientific GEO 20-20 mass spectrometry. Water isotopic data are reported with respect to V-SMOW. Stable isotopes (Oxygen and Carbon) analyses were performed using a MAT253 mass spectrometer with automated carbonate preparation device (Gas bench II) at the University of Bochum, Institute for Geology, Mineralogy und Geophysics stable isotope facility. Stable isotope results were calibrated to the PDB scale by the international standards CO-1 and CO-8. The analytical precision is better than 0.07 ‰ for $\delta^{13}C$ and 0.13 ‰ for $\delta^{18}O$.

5.3 Hydrogeological setting of Bagni di Saturnia

Bagni di Saturnia system is placed in the Albegna Valley Basin (southern Tuscany, central Italy) a broad tectonic depression oriented NNE–SSW, which is located East of the Middle-Tuscan Ridge with its southern extension reaching the M. Argentario (Fig. 5.1A). Before emerging at the surface, the hydrothermal water that gives rise to the Bagni di Saturnia travertine complex, crosses a long underground transect from north-east to the southwest. The water flow starts away from a “catchment area” located on the slope of Monte Amiata (located about 30 km from the Bagni di Saturnia hydrothermal vent; Fig. 5.1B) crossing the “Calcare Cavernoso Formation” (Triassic Formation of the non-metamorphic Tuscan Nappe) that extends through the foothills of southern Tuscany. Mt. Amiata is a Pleistocene volcano (0.1-0.4 Ma) characterized by slightly alkaline (K) affinity that produced three lava flows. Its elevation is 1,713 m a.s.l. and several thermal springs are located at the periphery of the volcano (Duchi et al., 1987; Minissale et al., 1997). On its pathway the water, supercharged with CO_2, dissolves a high quantity of minerals

from the Mesozoic formations that it crosses through. A fault that interrupts the continuity of the Pliocene claystone cover allows the rising of the thermal water from the ground through an orifice located below the local spa of Saturnia (Fig. 5.1C). After having served for the many spa activities, hydrothermal water is discharged forming a wide range of flowing-water depositional systems. The discharged spring water flows rapidly through a gently inclined conduit or channel called "the Gorgello creek" (Fig. 5.1 C). The water flows for hundreds of metres before forming a steep waterfall and subsequently a terraced slope system (Fig. 5.1C). Then the spring water continues to flow down into a gently dipping area intercepting the River Stellata (Fig. 5.1C).

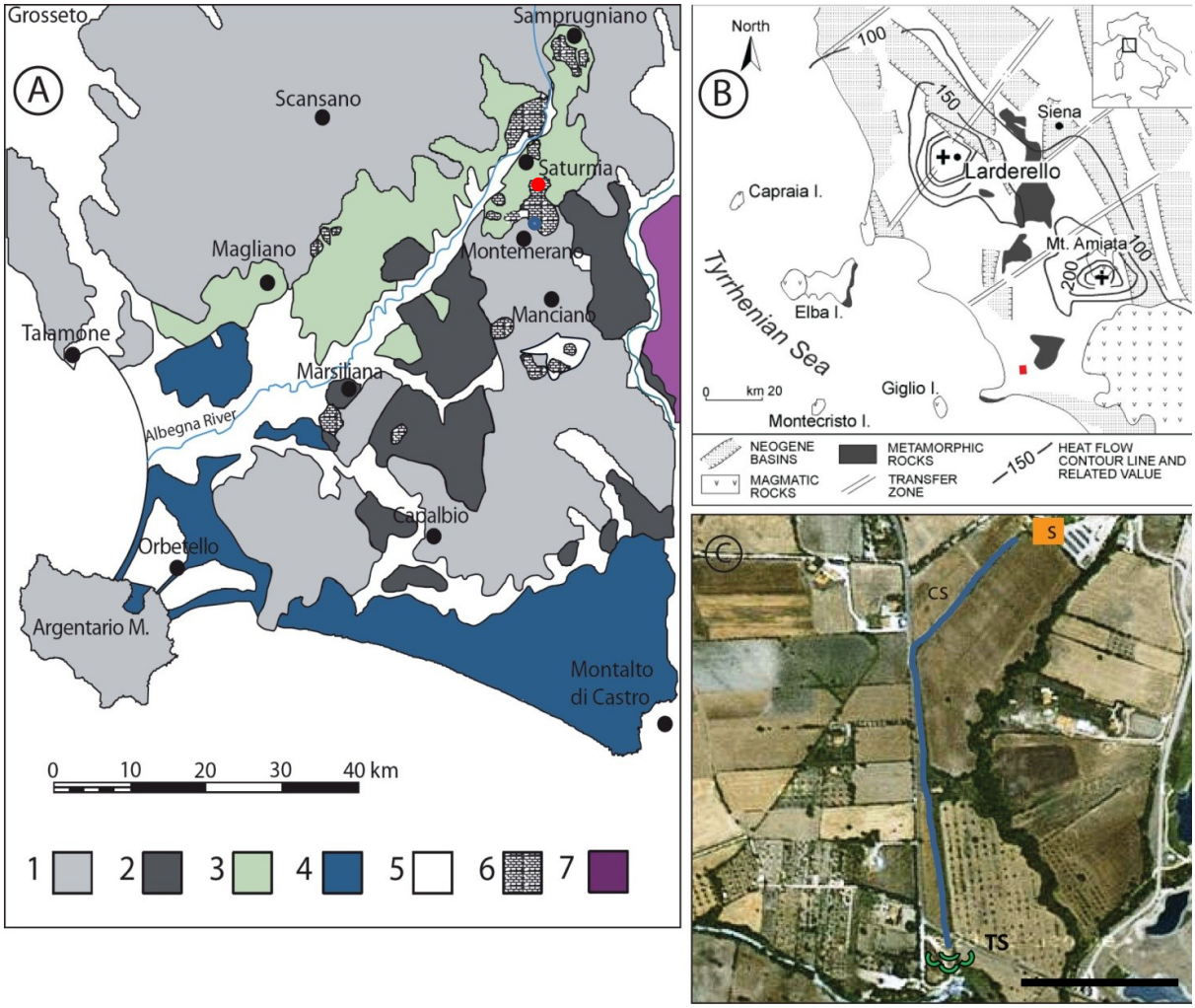

Fig. 5.1 Geological setting of the study area. A) Simplified geological map of the Albegna Valley. The red point marks the localization of Bagni di Saturnia while the blue point indicates the Pianetti travertine body (See Chapter IV). Legend: 1) Tuscan Nappe and allochthonous units; 2) Messinian continental, brackish and marine deposits; 3) Pliocene marine deposits; 4) Pleistocene marine and coastal deposits; 5) alluvial-colluvial sediment; 6) Miocene to Holocene Travertines; 7) Volcanic deposits of Vulsini Mountains (map modified after Bosi et al., 1996). B) Structural sketch map of southern Tuscany with the regional heat flow contour lines (heat flow contour line spacing: 50 mW/m2). The Larderello-Travale and Mt. Amiata geothermal fields are located in areas where heat flow reaches 1 W/m2 and 0.6 W/m2, respectively. The Albegna Valley is indicated with the red symbol (map modified after Baldi et al., 1995). C) Thermal water emerges from the orifice located below the local spa (S). The discharged spring water flows rapidly through a gentle slope conduit called "the Gorgello creek" (CS). In correspondence of a sharp break in slope, waterfalls form and after building a terraced slope, thermal water continues to flow down into a gently inclined area intercepting the Stellata River. Image from Google map. Scale bar 300 m.

5.4 Bagni di Saturnia travertines: results

Discharge and flow of the hydrothermal water from the spring to the lower morphology areas give rise to a series of shallow-water environments (Fig. 5.2). The different depositional environments differ in morphology, topographic gradient, hydrology and chemistry of the water flow and occurrence of distinctive microbial mat. Microbial biofilms, ranging in thickness from 0.4 mm to 1.5 cm, cap the underlying lithified travertine or sediment.

5.4.1 Hydrothermal water geochemistry

The Saturnia spring water was previously investigated from a geochemical (Minissale, 2004) and medical (Benedetti et al., 2010; analyses made by Saturnia Spa) point of views. These investigations attest that the spring expels water enriched in H_2S-CO_2-SO_4^{2-} and HCO_3^- and divalent cations (Ca > Mg) at temperature of nearly 37°C. Thermal water discharges at Bagni di Saturnia reach a rate of 800 litres per second.

In situ and in laboratory geochemistry investigations were made in order to characterize the thermal water and establish a variation in the measured parameters. A first set of measurements was performed to evaluate the variation of temperature and pH along the water flow paths from the channel depositional system to the final part of the terraced slope. The *in situ* pH and temperature values measured are presented in Table 5.1. The temperature decreases gradually from 35.5°C to 33.8°C along the water outflow from the channel system to the terminal part of the terraced slope system, before mixing with the cold water of the Stellata river. The water pH increases along the flow path, ranging from 6.67 to 7.1. The increase of the water pH and the decreasing of the water temperature were confirmed by a subsequent and more complete geochemical water investigation. Additional analyses such as element and isotopic composition analyses are listed in Table 5.2. $\delta^{18}O$ values range from -6.27 to -6.20 ‰ (SMOW). Na^+, K^+ and Cl^- ions are present in low concentrations, while S^- is represented in minor quantities (Table 5.2). Water is also enriched in H_2S-CO_2 and minerals dissolved in water amount to 2.94 g/l (Minissale et al., 2004). The δ_2H (‰SMOW) values show variations from –37.789 to -44.836 ‰.

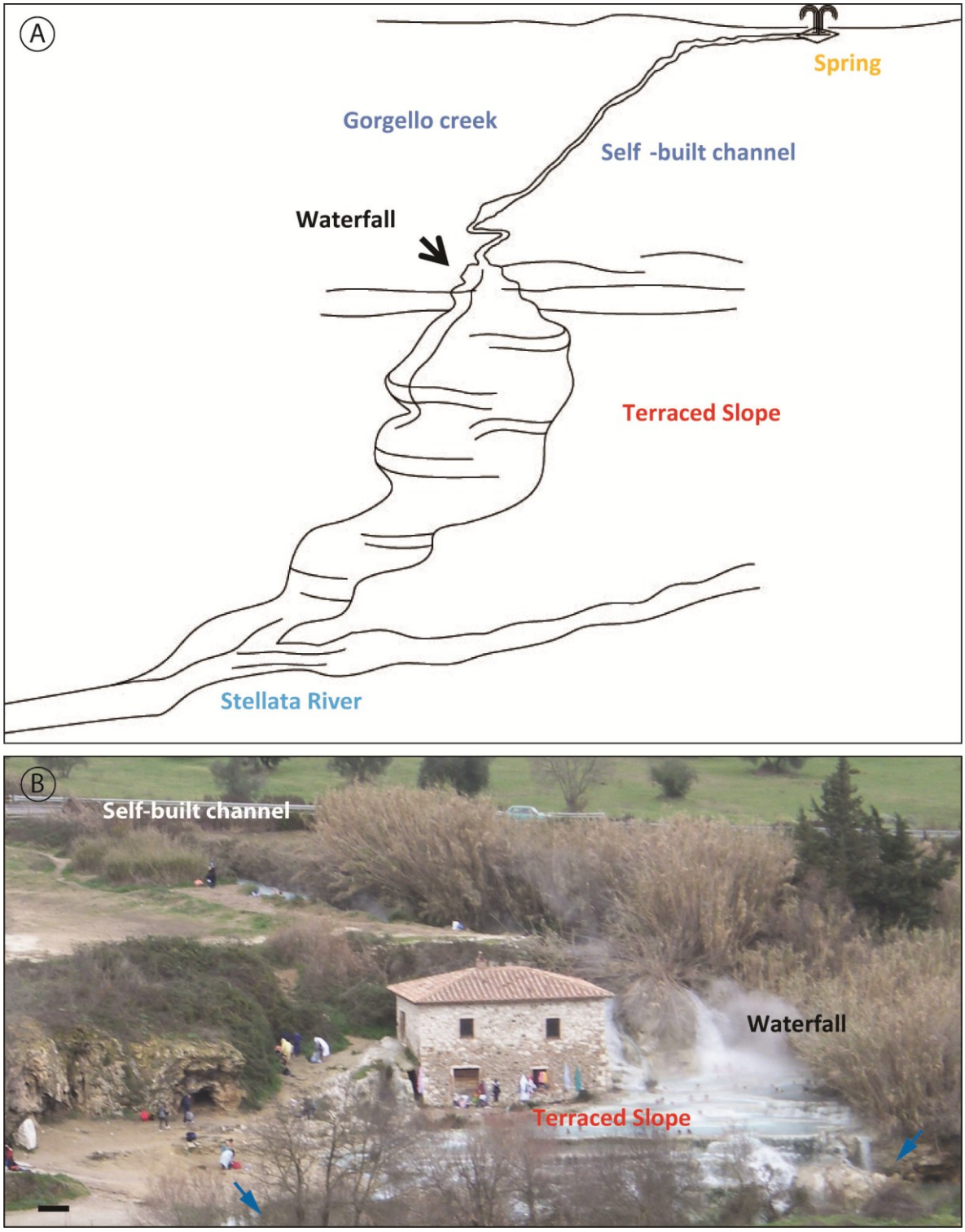

Fig 5.2 A) Not to sale schematic diagram of the anthropogenic Bagni di Saturnia travertine system. Thermal water emerges from the orifice located below the local spa. The discharged spring water flows rapidly through a gentle slope conduit called "the Gorgello creek". Here the deposition of travertine occurs as a self-build channel. In correspondence of a sharp break in slope the self-built channel passes into the waterfall system. After the waterfall, the gradient reduces to 20-25° and the water splashes into the following terraced slope systems. Then the spring water continues to flow down into a gently inclined area intercepting the Stellata river. B) Field image of Bagni of Saturnia complex and the relative depositional environments ranging from self-built channel, waterfall and terraced slope systems. Blue arrows indicate the Stellata river. Along the left side of the final part of the terraced slope depositional system, the hydrothermal water directly falls from the drop wall of the pools (blue arrow on the right). On the right side of the terraced slope system the hydrothermal water intercepts the Stellata river water flowing through a 4 m long irregular water conduit with less intense terraced morphology (blue arrow on the left). Scale bar 2 m.

GPS location	T°C	pH	Depositional setting
N 42° 39' 25.2'' E 11° 30' 52.3''	35.5	6.79	CS
N 42° 39' 24.3'' E 11° 30' 51.1''	35.1	6.84	CS
N 42° 39' 23.8'' E 11° 30' 50.3''	35.2°	6.84	CS
N 42° 39' 23.5'' E 11° 30' 50.0''	35.2	6.84	CS
N 42° 39' 22.6'' E 11° 30' 48.8''	35.1	6.86	CS
N 42° 39' 22.3'' E 11° 30' 48.6''	35.2	6.86	CS
N 42° 39' 21.9'' E 11° 30' 47.9''	35.3	6.87	CS
N 42° 39' 21.2'' E 11° 30' 47.1''	35.4	6.88	CS
N 42° 39' 20.5'' E 11° 30' 46.3''	34.9	6.89	CS
N 42° 39' 19.4'' E 11° 30' 45.2''	35.3	6.90	CS
N 42° 39' 19.0'' E 11° 30' 44.7''	35.1	6.90	CS
N 42° 39' 18.6'' E 11° 30' 44.2''	35.3	6.91	CS
N 42° 39' 17.9'' E 11° 30' 43.5''	35.2	6.91	CS
N 42° 39' 17.7'' E 11° 30' 43.5''	35.3	6.91	CS
N 42° 39' 16.3'' E 11° 30' 41.7''	35.3	6.92	CS
N 42° 39' 16.2'' E 11° 30' 41.7''	34.9	6.93	CS
N 42° 39' 15.8'' E 11° 30' 41.8''	34.9	6.93	TS
N 42° 39' 06.6'' E 11° 30' 42.8''	34.7	6.99	TS
N 42° 38' 53.7'' E 11° 30' 46.0''	33.9	7.72	TS
N 42° 38' 53.6'' E 11° 30' 45.6''	33.9	7.72	TS
N 42° 38' 53.6'' E 11° 30' 45.6''	33.8	7.76	TS
N 42° 38' 53.4'' E 11° 30' 44.9''	33.8	7.81	TS

Table 5.1 *In situ* pH and temperature measurements of thermal water collected along the self-built channel depositional system (CS) and the terraced slope system (TS) moving from more proximal to more distal areas following the water flow direction.

5.4.2 Depositional systems

Four depositional systems encompass the present-day Bagni of Saturnia travertine deposit and can be differentiate into: 1) hydrothermal vent, 2) self-built channel; 3) waterfall; and 4) terraced slope (Fig. 5.2).

5.4.2.1 Self-built channel

The discharged spring water flows rapidly through a gently inclined conduit that individuates the self-built channel depositional system (Fig. 5.2). This system extends for a length of ca. 900 m and consists of a channel and associated ponds (Figs. 5.3 A-C). Channel sub-environments occur as sinuous to sub-horizontal conduits (Fig. 5.3 A-B). The channel varies in width between 80 cm to more than 1.80 m and it is restricted from both sides by vertical margins (Fig. 5.3A-B) that generally are bent in arches downward. These are constituted by subaqueous to raised, sometimes bulging rims, varying in height from ca. 20 cm to 150 cm. The fresh, actively precipitating, uppermost travertine surface of the vertical margins is interwoven with thin, cream coloured to green living microbial mats (Fig. 5.3 D).

High water flow with laminar to turbulent activity usually typifies the channel environment (Fig. 5.3A-B). As a consequence of the topography, the morphology of the channel system and the water flux vary along the length of the pathway.

In the central to final part of the channel system, characterized by gentle topographic gradient, hemispherical ponds with external irregular margins are observed (Fig. 5.3 C). These ponds, up to 50 cm in width, form in lateral zones of the channel and correspond to low energy areas. Subaqueous and mostly elongated barriers, ca. 10 to 40 cm high, divide, in general, the channel from the hemispherical ponds (Fig. 5.3C). Thus, the warm water of the channel enters laterally into the ponds and mixes with their cooler slow-flow/stagnant water. The dividing barriers show a typical translucent to cream coloured mucilaginous surfaces with greenish-brown patches mats (Fig. 5.3 D-E). The hemispherical ponds contain a wide variety of microbial mat morphologies and pigmentations. The protected areas of the marginal sides of the pond sub-environment, exhibit light to dark green in colour microbial mat that form small domed structures extending from a cream-coloured smooth mats (Fig. 5.3F). These peculiar mats assume pink to reddish colours when are located more downstream. Both the down-stream and the upper surfaces of the pond irregular margins exhibit patches of green and more gelatinous biofilm (Fig. 5.3 G-H). In

addition, at the air-water interface two millimetre thick light green to cream coloured mucilage covers the muddy sediments of the marginal area of the pond sub-environments (Fig. 5.3I).
In the terminal part (the last ca. 30 m) of the channel system, where the topographic gradient increases, a series of natural steps are created (Fig. 5.3 J); these range from 30 to 80 cm in height. In this area, convex to tongue-shaped rims and walls dominated by translucent and white hardened mats with carbonate precipitation are individuated. The final section of the channel system displays a high-energy and turbulent water flow (Fig. 5.3J). Splashed water is constant along the banks of the steps. Flat protected zones with slow flowing water develop on the raised large barrages. These are dominated by green microbial biofilms mixed with yellow mats. Few millimetre long filaments branch from the mats (Fig. 5.3K) and resemble flat dendritic morphology. Exposed areas of high-flow water of the channel sub-environment show orange pigmented mats mixed with millimetre thick yellow domed structures and green mucilage (Fig. 5.3L). Patches of carbonate precipitates are also observed.

5.4.2.2 Waterfall depositional environment

After a wide depression (180 cm), channel depositional system passes into the waterfall system (Figs. 5.2 and 5.4 A-C). The transition between these two different depositional environments corresponds to a sharp break in slope, where two sub-vertical waterfalls develop.

Sample	T (°C)	pH	Alkalinity	mg/l Ca	mg/l Mg	mg/l Na	mg/l K	mg/l SO4	mg/l Cl	mg/l S	$\delta^{18}O$ (‰SMOW)	$\delta^{2}H$ (‰SMOW)
Bs 107 (CS)	35.1	6.7	10.15	534.85	117.436	22.684	2.799	1228.014	20.358	2.208	-6.27	-39.700
Bs 100 (CS)	33	7.16	10.2	540.68	125.230	50.799	5.761	1352.846	52.945	Nd	-6.24	-39.556
Bs 101 (CS)	33	7.25	9.6	544.49	125.832	67.093	7.573	1459.053	60.708	0.928	-6.22	-44.836
Bs 102 (W)	32,5	7.67	9.6	490.19	117.436	49.201	5.566	1243.847	44.264	0.416	-6.27	-39.115
Bs 103 (TS)			9.6	538.43	125.102	43.770	2.457	1289.356	38.875	1.184	-6.21	-37.789
Bs 104 (TS)	32,3	7.68	9.8	543.77	124.104	27.414	3.823	1254.580	43.460	0.832	-6.23	-39.602
Bs 105 (TS)	32,2	7.67	10	549.12	124.749	30.990	4.027	1191.368	39.653	0.336	-6.15	-39.504
Bs 106 (TS)	33,2	7.68	9.85	538.90	125.102	43.770	2.184	1253.500	39.496	0.816	-6.20	-39.371

Table 5.2 Physical parameters, elemental and isotopic composition of Bagni di Saturnia water related to the depositional environment. CS: self-built channel depositional system; W: waterfall system; TS: terraced slope system.

The two distinct waterfalls (about 4 m high) show different progradational profiles. One waterfall exhibits a stepped section due to a series of small dam-like structures (Fig. 5.4 B). The walls of the steep dams vary from 10 up to 60 cm. The second one presents a non-stepped section with a stronger water drop wall (Fig. 5.4A-B).

The velocity and the energy of the spring-water increase in the waterfall system and high CO_2 degassing occurs in correspondence of the drop wall of the waterfalls.

White to yellow and hardened microbial mats with the greenish to brown patches characterize the waterfall surfaces interested by the flowing of the water (Fig. 5.4 A). Nevertheless, the zones of the waterfall domain, where the water no longer flows and it is affected only by water splashes exhibit orange to yellow pigments alternating with areas formed by more translucent and white hardened mats (Fig. 5.4B).

5.4.2.3 Terraced slope system

After the waterfalls the gradient reduces to 20-25° and the water splashes into the pools of the following terraced slope system (Figs. 5.2 and 5.4), in which vertical to overhanging walls, sub-horizontal pools and raised rims confine the margin of the pools (Fig. 5.4 C).

Pools, rims and walls occur in series along the water flow and are characterized by a variety of microbial mat morphologies and filaments (Fig. 5.4C-H). Terraced pools appear as a concave upward morphology regularly interrupted by barriers situated in their frontal area (Fig. 5.4C). The pool floor is inclined and the area just behind the previous rim corresponds to the deeper and internal part of the pool varying from 30 cm to 1 m. From the inner pool zone the angle of dip increases towards the next rim. Pool size varies in width between 30 cm and up to 5 m. Pools are in general interconnected but in some cases the connection is discontinuous. The pool floor is occupied by a) elongated to rounded pisoids and oncoids (5 mm up to several centimetres in diameter), showing an external grey surface varying from smooth to nodular (Fig. 5.4C), b) by clay and c) mostly by fine detrital grains and plant debris (Fig. 5.4D). Dark in colour sediment occurs especially 2 cm below the pool floor.

The pool rims occur as raised sinuous to irregular barriers characterized by white-grey to yellow and generally hardened mats exhibiting green colours (Fig. 5.4C and 5.4D-E). These mucilaginous mats vary in morphology from cauliflowers to domed networks. White and elongated filaments, less of 0.3 mm in diameter, are diffuse near the rim of the pools. Locally

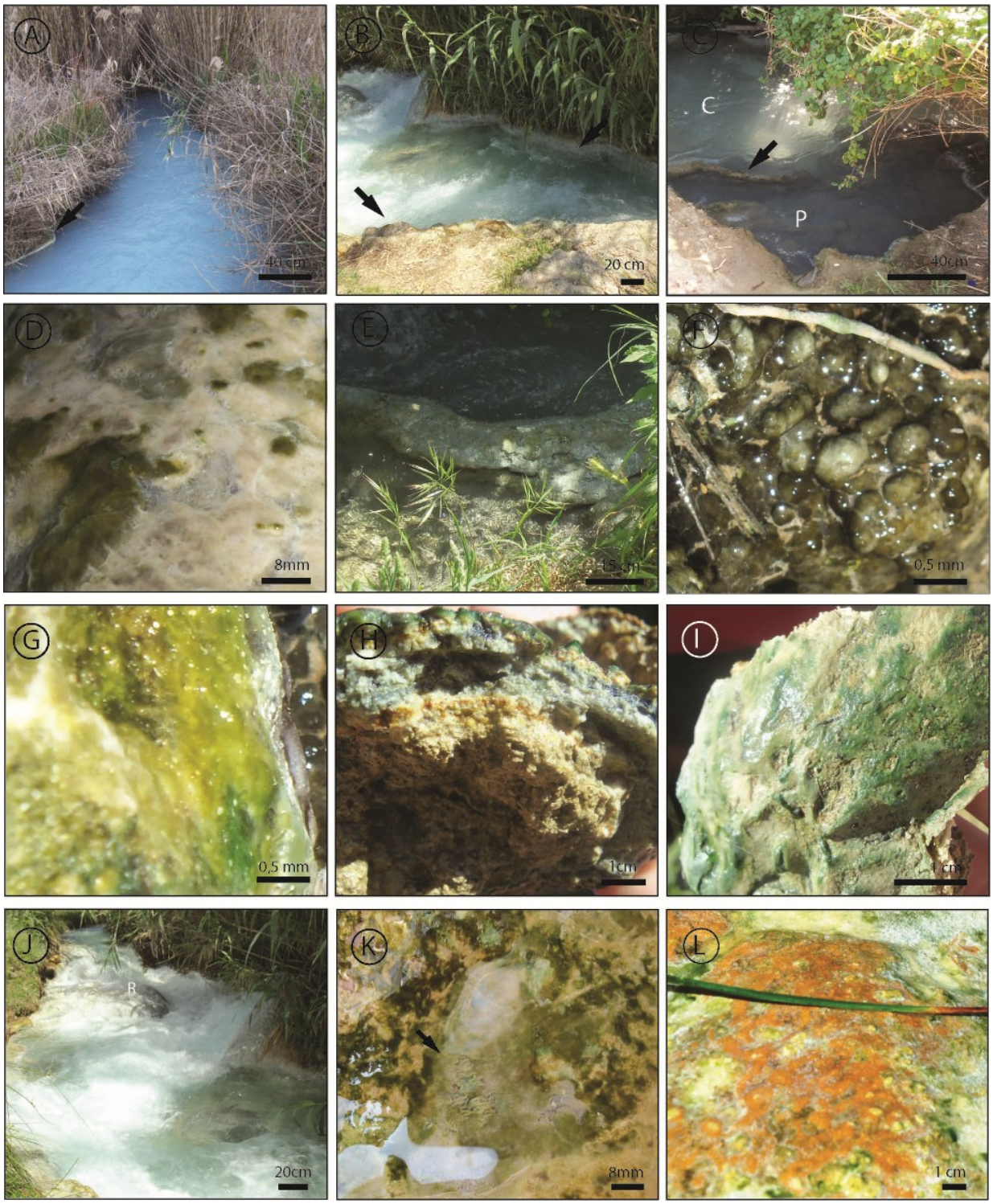

reeds are present on the sides of the rim where there has been temporally no thermal water flow. If the water flow direction changes, reeds are flooded by the thermal water and encrusted by calcium carbonate precipitation. In the zone where the water no longer flows dark green to black microbial biofilms are associated with white to orange to cream colour areas (Fig. 5.4E)

Walls are identified from the external area of the rim to a height nearly equal to the base of the pool (Fig. 5.4C). The walls vary from vertical to overhanging, convex-outward structures. The height of the walls ranges between several centimetres to 2 m extending vertically from the outside area of the rim to the base of the pool. The wall surface exhibits filamentous microbial mat community with dark to light green colours associated with hardened cream coloured to grey microbial mat (Fig. 5.4F-G). These mats show a cauliflower morphology resembling dendritic textures. Walls exhibiting often an irregular surface formed by the coalescence of small vertical cones (Fig. 5.4H).

The marginal part of the terraced slope system is characterized by thin sheets of flowing water or by some areas where the water no longer flows. In the first region, black filament-like structures attached on the substrate of terraced travertine are present. These are disposed hanging down and are moving away from the water flow.

Water flow varies along the terraced slope. The water is generally fast flowing but pools represent a relative slow-moving portion of the terraced slope system. The lower energy of the water flow happens in the pool just behind the rims with a laminar flow. Along the wall drop of the rims, the water runs and falls to the inner part of the subsequent pool that represents a zone of major turbulence. After this zone of major turbulence, the energy of the flow decreases until the next rim. However, pulsating sheet flows affect sometimes the rim and wall areas and create periodic rim and wall exposures (Fig. 5.4I).

Along the left side of the final part of the terraced slope depositional system, the hydrothermal water directly falls from the drop wall of the pools; on the right side of the terraced slope system the hydrothermal water intercepts the Stellata River water flowing through a 4 m long irregular water conduit with less intense terraced morphology (Fig. 5.2B).

Fig. 5.3 (previous page). Self-built channel depositional system and the associated microbial mats and biofilms. A) Channel environment characterized by a sub-horizontal conduit and low flowing water. The black arrow points to the vertical margin. B) Channel sub-environment exhibiting a sinuous conduit and turbulent water flow. The channel is restricted from both sides by vertical margins (black arrows). C) Hemispherical pond (P) juxtaposed to the channel depositional system (C). The elongate barrier (black arrow) divides the pond from the channel. D) Close-up view of mucilaginous thin cream coloured to more gelatinous green living microbial mats that characterize the channel vertical margins. E) Elongated barrier that divides the channel sub-environment from the hemispherical ponds. The barrier shows translucent to cream coloured mucilaginous surfaces with greenish-brown patches mats. F) Domed, light to dark green in colour microbial mat. G) Green and more gelatinous biofilm. H) Cross section of pond sub-environment travertine sample. Millimetre thick green gelatinous mats cover the carbonate precipitates alternated and often mixed with black horizons. The lithified internal structures beneath the soft microbial mats are cream colour. I) Two millimetre thick light green mucilage covering the muddy sediments on the marginal area of the pond sub-environment in the channel system. J) Final part of the channel environment shows a high turbulent water flow and the presence of stepped morphology. K) A few millimetres thick dendritic filaments (black arrows) branch from the green microbial mats associated with slow flowing area. L) Orange pigmented mats mixed with millimetre yellow domed structures and green mucilage associated with fast water flow and splash area. Patches of carbonate precipitates (in white) are also observed.

Fig. 5.4 (next page). Waterfall and terraced slope depositional systems. A) Waterfall depositional system occurring along a sharp break in slope. An exposed domed cliff area divides two waterfalls with different profiles. The black arrow indicates a waterfall with a parabolic section. Note that the water falls into a subsequent terraced slope. B) Waterfalls showing different progradational profiles. On the left side a waterfall showing a stepped profile (STW) due to a series of dam-like structures with a wall ranging from 30 cm to 1 m. White to yellow and hardened microbial mats with the greenish to brown patches are observed (black arrow). On the right side, waterfall with a non-stepped profile (PaW). Note the dome shaped area that marks a boundary between the two waterfalls. This dome-like zone, affected only by the splash of the water that falls from the waterfall, exhibits orange to dark yellow pigments (blue arrow) alternating with areas formed by more translucent and white hardened mats. C) Terraced slope system at Bagni di Saturnia consisting of vertical to overhanging walls, sub-horizontal pools and raised rims confining the margin of the pools. Terraced pools occur as hollow-like morphologies regularly interrupted by barriers situated in their frontal area. Black arrow indicates the green to cream in colour microbial mat extending on the terraced walls. Note the coated grains collected by the terraced pool. D) Terraced pool bordered by regular to irregular centimetre-thick raised rims. Note the base of the pools characterized by the diffuse presence of coated centimetre-size grains and dark fine sediment. Fine detrital material and plant debris are also present. E) The pool rims showing mostly mucilaginous mats exhibiting different colours. F) Microbial mat and biofilm that characterize the wall. G) Cross section through the present-day travertine samples collected along the wall. Stratified white carbonate layers alternating with organic-rich layers occur in the upper part of the sample. Gelatinous green biofilm covers the carbonate precipitate. Black layers are observed and suggest that anoxic conditions are present in microenvironments during degradation of the organic matter. This dark layer is followed by a well-lithified zone characterized by porous and un-laminated structures. H) Wall located at marginal area of terraced slope where water no longer flows. Dark green to black microbial mat associated with white carbonate precipitation and grey hardened mats. Calcium carbonated precipitation occurs also around reeds giving an irregular surface formed by the coalescence of small vertical cones. I) Image testifying the periodic rim and wall exposure related to a pulsating activity of the water supply. Note the presence of reeds at the side of the rim.

5.4.3 Microbial community and biota colonizing the different depositional environments

Biota ranging from microbes to macrophytes (higher plants) occur in the Bagni di Saturnia travertine deposits. The present-day precipitates are typically laminated (Figs. 5.3H and 5.4G); however, porous and un-laminated structures are also observed (Fig. 5.4G). Although the composition and gross morphology of the studied travertine may be different, they show common features. Cross-sections through the travertines show well-lithified internal areas exhibiting different structures beneath stratified inner and differently coloured organic-rich layers alternating and/or mixed with layers of carbonate precipitate (Fig. 5.3H and 5.4G). Conspicuous living microbial mats and biofilms constitute the top cover layer.

Studies conducted based on light microscopic and scanning electron microscope observations joint with literature research allowed the identification of the microorganisms and of the other biota that populate the Bagni di Saturnia. Morphological analyses suggest that prokaryotes are well represented and with diatoms populate the distinctive microbial mats (Fig. 5.5A-K

The cyanobacteria are oxygenic, photosynthetic prokaryotes. Different cyanobacteria varying from filamentous to coccoid in shape and exhibiting different sizes and morphologies have been distinguished. At least two filamentous morphotypes have been distinguished. A first morphotype consists of organisms typically organized in upright colonies (Fig. 5.5 A) exhibiting

a tubular-like bodies (ca. 4 µm thick) with a mostly uniform external surface of the sheath (Fig. 5.5B). In thin sections, these cyanobacteria appear as opaque dark to grey un-branching or slightly falsely branched filaments within micrite and microsparite and often they appear totally or partially encapsulated by spar (Fig. 5.5C). The filamentous cyanobacteria orientation is

variable from vertical to sub-horizontal. In addition, filaments are sometimes contained within a brownish/reddish organic rich cloud of micrite (Fig. 5.5C). The second morphotype is distinguishable by organism with elongate trichome characterized by isodiametric cells (Fig. 5.5 D). The cells are cylindrical in shape, range from long ca. 3.5 μm long and 3 μm wide. The cyanobacteria belonging to the second morphotype are often distributed within a 1μm thick, uniform EPS membrane (Fig. 5.5D). Even if two cyanobacteria morphotypes have been distinguished, a precise assignment of cyanobacteria species is problematic. The classification of cyanobacteria is difficult and controversial and ambiguities arise depending on whether the botanical or bacteriological code in used (Castennholz, 1992). On the basis of described morphological features the filamentous cyanobacteria may belonging to the *Oscillatoriales*. Morphotype 1 may be assigned to the genus *Schizothrix* (characterized by brownish pigmented mats) while the morphotypes 2 may belong to *Phormidium* (light to dark green from continuous to domed microbial mats).

Although less common when compared with the filamentous organisms, spheroidal structures and empty moulds nearly 250 μm in diameter (Fig. 5.5E) are also present. These structures are interpreted as coccoid cyanobacteria forming "colonial" association and are commonly observed as spherical bodies in EPS or like circular–subcircular hollows within micrite/microsparite precipitate. These coccoid cyanobacteria might belong to the Chroococcales, *Gloeocapsa* genus (Fig. 5.5E; cf. Figure .8F in Dupraz et al., 2004) and show an orange-pigmented mat.

Filamentous-like structures, ca, 300 to 600 nm in diameter with branches and some regular septation occur (Fig. 5.5F). Some of the apparent branching may be due to fusion between overlying hyphae (Wilkinson, 2003). These fine filamentous structures are often attached to EPS to the other organic tissue. These show similitudes with *Streptomycetaceae*, actinobacteria characterized by long and well-developed filaments (Wilkinson, 2003). These filaments are widespread in the cream coloured microbial mats.

Organisms characterized by a chain of subsequent ovoidal to cilindric cells are also observed (Fig. 5.5G). The cells are less than 500 nm in diameter and less than 400 nm to 1μm long. Contrary to the previous filamentous morphotypes observed, these organisms show an intricate and non-linear morphology. These organisms are morphologically similar to the sulphur-oxidizing bacterium *Beggiatoa* (Fig. 5.5G; cf. figure 2 in Zhang et al, 2005). These filaments occur mainly within orange mats.

Bacteria with a more simple morphology ranging from bacilli to cocci (Fig. 5.5H-J) colonizing any organic substrates are widespread. These bacteria are characterized by uniform or rugose

surfaces and range mainly from 200 nm to less than 1 μm in diameter and occur mainly into dark to grey and cream coloured horizons of the microbial mats.

Eukaryotic algae are also an important element of the travertine community. In particular, diatoms, 2 μm to 11 μm wide and between 8 μm to 30 μm long, are the main component of the eukaryotic algae in Bagni di Saturnia travertine (Fig. 5.5K). Diatoms are photosynthesizing phytoplankton consisting of Chrysophyta unicellular algae that house themselves within frustule of amorphous silica . Most species observed in the studied travertine belong both the group of raphid and araphid pennate diatoms. Diatoms are found associated with and often entombed in EPS, mainly in the upper surface of the microbial mats characterized by green colours.

Charophytes macrophytic green algae are also present in the travertine deposit (Fig. 5.5L). Cross and oblique sections of charophyte stems have been seen in thin sections (Fig. 5.5L). Although rarely, ostracode shells were observed (Fig. 5.5L).

Higher plant communities (Fig 5.4A-C, I) grow when the thermal water no longer flows in certain areas. When the course of the water changes or the water supply is higher these are flooded by the flowing water and encrusted by calcium carbonate (Fig. 5.4H).

5.4.4 Fabric types

Large scale observations, combined with characterization and identification of the travertine components that together form the different fabric types are fundamental for the understanding of the processes that lead travertine precipitation. Macroscopically, Bagni di Saturnia travertines are essentially distinguishable by their structures in four groups: 1) layered travertine boundstone/cementstone (Fig. 5.6A); 2) coated bubble boundstone travertine (Fig. 5.6B); 3) encrusted travertine (Fig. 5.6 C); 4) coated grain travertine (Fig. 5.4 C); 5) carbonate and non-carbonate intraclasts and extraclasts. Micro-scale observations reveal that a large variety of micro-fabric types characterizes the Bagni di Saturnia systems. These include: a) dendritic boundstone; b) laminated boundstone; c) crystalline crust cementstone; d) micrite mudstone, e) coated bubble boundstone; f) coated reed boundstone/grainstone/rudstone; g) grainstone/rudstone/packstone/floatstone. The different fabric types (Table 5.3) show a wide range porosity (Fig.5.7). Petrographic and SEM analyses indicate micrite, microsparite, and spar calcite, associated with biota and pore spaces, as the major constituents of the identified fabrics (Fig. 5.D-H). However, through optical microscope

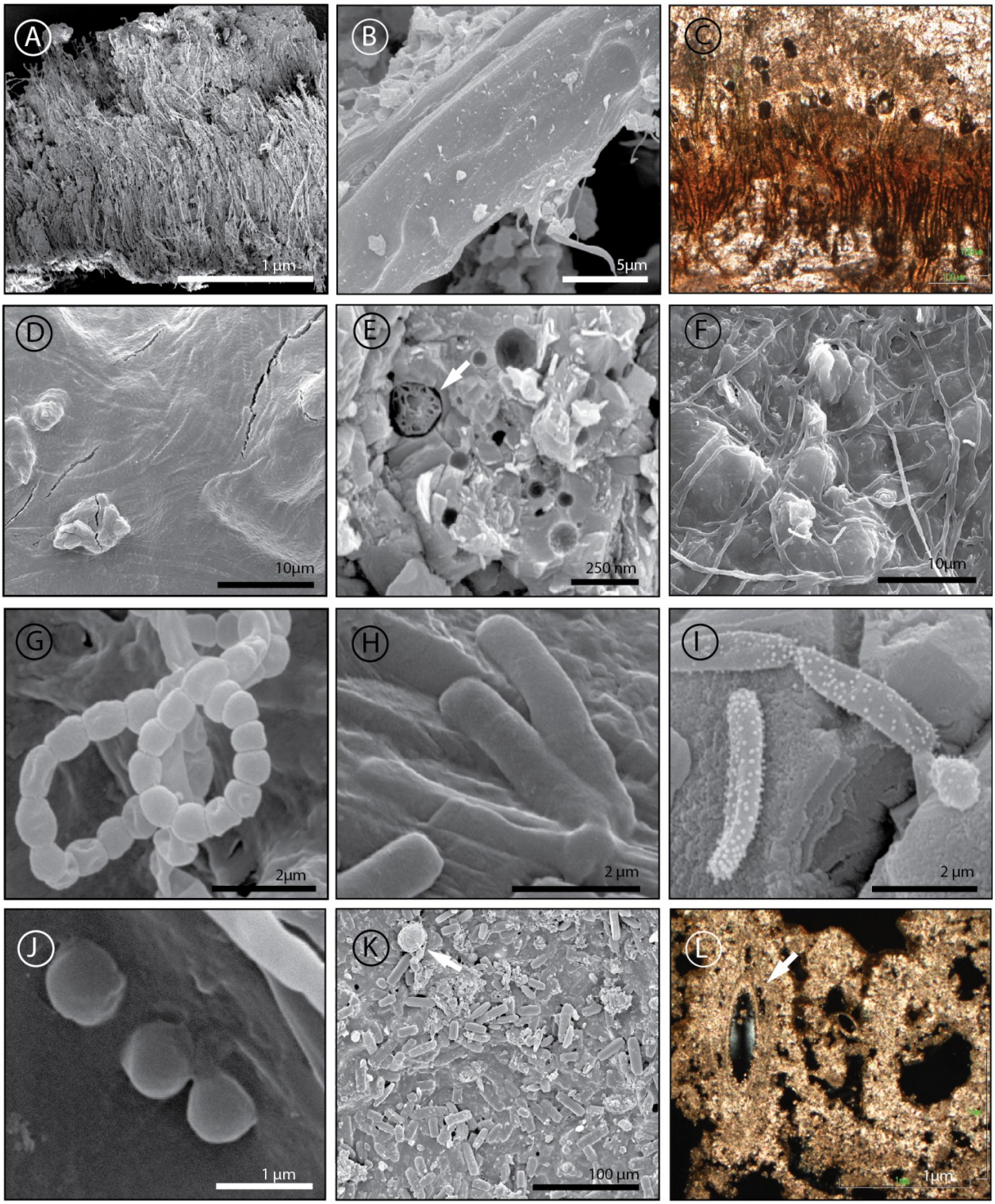

Fig. 5.5 Biota populating the Bagni di Saturnia travertine deposits. A) Colony of filamentous cyanobacteria. SEM image. B) Close-up view of A. Note the mostly uniform external surface of the sheath. C) Thin section image showing filamentous cyanobacteria within a brownish/reddish cloud. Micrite, microspar and spar are also observed. D) EPS membrane with cyanobacteria showing an elongate trichome characterized by isodiametric cells. SEM image. E) SEM image of coccoid cyanobacteria (cf. figure 8F in Dupraz et al. 2004). F) Filamentous-like branches and some regular septation occur. SEM image. G) Ovoidal to cilindric cells with different dimension organized to form a non-linear and intricate body (cf. with figure 2 in Zhang et al., 2005). H) SEM image showing bacilli. I) Bacteria exhibiting rugose surfaces. J) Small cocci associated with EPS. K) Diatoms often entombed in EPS. L) Oblique section through a charophyte (white arrow). Ostracode shell is also observed. Note the presence of dissolution vugs.

and nano-scale investigations it was also possible to observe the presence of other crystalline phases (Fig. 5.6I-L). The fabric type description and the travertine classification use some terms of classification of carbonate textures (Dunham, 1962; Embry and Klovan, 1971) combined with the currently travertine fabric nomenclature (Chafetz and Folk, 1984; Jones and Renaut, 1995; Guo and Riding, 1996). The description of the porosity types is based on Choquette and Pray (1970) classification. In the proposed travertine fabric description the term "boundstone" is used to indicate travertine showing signs of being lithified during deposition because they are directly precipitated by the flowing or stagnant water. Different from the definition of Dunham, travertine boundstones are not bound by organisms with a carbonate skeleton such as corals or algae.

5.4.5 Petrographic components of Saturnia travertine

Petrographic observations suggest that the studied travertines are composed of almost pure $CaCO_3$ that occurs mainly as calcite showing micrite (anhedral crystals < 4 μm; Folk, 1959), microspar (subhedral to euhedral calcite crystals from 20 to 62 μm) and spar calcite (euhedral crystals > 62 μm) crystal habits (Fig. 5.6D-H). Micrite is organized in continuous and non-continuous horizons to irregular masses, ranging from dense to peloidal to clotted peloidal (Fig.5.6D-E). Dense micrite appears as a brownish and opaque mass andit is often organized in continuous or non-continuous layers or in irregular clumps (generally from 60 to 200 μm in size). Peloidal micrite, formed by abundant peloids of irregular shape and size, is characterized by rounded to sub-angular to elongate in shape micritic grains. These range mainly from a few microns to *ca.* 50 μm in diameters and vary from densely spaced to sparse. The micrite peloids commonly show no differentiated internal structures and are surrounded by clear rims of microspar. The clotted peloidal micrite is formed by dense spaced peloids forming amalgamated clots. Peloids scattered within dense micrite range mainly from sub-rounded to rounded to oval shape. The clotted peloidal micrite is principally arranged into laminated and dendritic masses.
Microsparite (Fig. 5.6F) is characterized by calcite crystals ranging from 20 to 62 μm in diameters with partially or totally developed crystal faces. It is important to notice that different authors use different size categories for the microsparite: 5-15 μm (Tucker, 1981), 4-30 μm (Folk, 1959, 1965); and 5-50 μm (Bathurst, 1975). At Bagni di Saturnia microsparite is characterized mainly by a mosaic micro-texture and sometimes shows a patchy distribution

within the micrite. Organic structures are observed within the micrite or microsparite crystals (Fig. 5.6G).

Sparite (Fig. 5.6H) consists of euhedral crystals larger than 62 μm in size. These crystals are in general cloudy and range from equant to columnar crystals. The contacts of the crystals vary from sharp to irregular boundaries. Often microorganisms such us cyanobacteria are entombed within the sparite. In addition, remains of micrite apparently float within the sparite.

5.4.6 Fabric types description and characterization

5.4.6.1 Layered travertine boundstone

This macro-fabric group consists of almost entirely horizontal to wavy laminated precipitates. The micron to millimetre in size laminae are often rich of organic matter and display different colour (Figs 5.3H, 5.4G, 5.6A). Microscopic analyses reveal that the alternation of several microfabric types characterizes the layered travertine boundstone and includes: 1) shrub-like dendritic boundstone; 2) crystalline fan dendritic cementstone; 3) crystalline laminated cementstone; 4) laminated boundstone.

Dendritic boundstone (Fig. 5.7A-C) consists of dendritic structures exhibiting irregular to regular central region from which branches, with different morphologies, size and orientations, diverge. Mainly two different types of dendritic boundstone can be distinguished on the basis of their morphologies. These are:

1) *Clotted peloidal dendritic boundstone* (Fig. 5.7 A-B) composed primarily of micrite arranged into upward expanding three-dimensional structures arranged into continuous layers (Fig. 5.7A). These layers range from less than 100 μm up to 1 mm thick. The dendrites are composed primarily by clotted peloidal micrite; however, dense micrite, and rarely microsparite, constitutes the other components of the clotted peloidal dendritic boundstone. In general, sub-angular to spherical peloids together with micrite are structured into poorly developed dendritic morphology. The bush-like structures exhibit a poorly defined “stalk” from which branches diverge. The branches exhibit an irregular morphology lacking a systematic repeating habit (Fig. 5.7 A-B). Isolated clumps of clotted peloidal micrite (less than 30 μm to 200 μm) arranged into

MACRO-FABRIC Main category based on cross-section observation	**MICRO-FABRIC** Sub-category based on petrographic observation	
LAYERED TRAVERTINE BOUNDSTONE	**Dendritic boundstone**	*Clotted peloidal dendritic boundstone*
		Radiating dendritic boundstone
	Laminated boundstone	
	Crystalline crust cementstone	
	Micrite mudstone/peloidal micrite	
COATED BUBBLE BOUNDSTONE TRAVERTINE;	**Coated bubble boundstone**	
ENCRUSTED TRAVERTINE	**Coated reed boundstone/ grainstone/rudstone**	
CARBONATE AND NON CARBONATE INTRACLAST AND EXTRACLAST	**Grainstone/rudstone/packstone/floatstone**	
COATED GRAIN TRAVERTINE **Pisoid to oncoidal grains**	**Laminated boundstone**	
	Crystalline crust cementstone	
	Grainstone/rudstone/packstone/floatstone	

Table 5.3 Classification of Bagni di Saturnia travertine fabric types

an arborescent-like disposition (Fig. 5.7B) often form the clotted peloidal dendrites. The space between the micritic arborescent structures is filled by microspar. Frequently, the clotted peloidal dendrites evolve upward and laterally into fan-shaped branched morphology.

2) *Radiating dendritic boundstone* (Fig. 5.7C) occurs as a single and compound spherical structure showing a dendritic-like overgrowth. These dendrites are commonly composed of micrite occurring largely as clotted peloidal. The radiating dendrites are composed by irregular to regular branches that radiate from a central area to form spherical to sub-spherical dendrites (ca. 20 up to 400 μm). Branches often show a fan-like pattern.

Laminated boundstone (Fig. 5.7 D-G) are formed mainly by an alternation of organic rich micrite and microspar bands often aggregated into packages with sub-spherical/lenticular discontinuous pores (nanometre to centimetre in size). A continuous range of meso-scale morphologies varying from dense (with porosity less than 5% per volume) to porous (porosity >50%) characterizes the laminated boundstone.

The micrite laminae are generally made by clotted peloidal micrite to dense micrite. The laminae, growing parallel to each other and parallel to the substrate on which they nucleate,

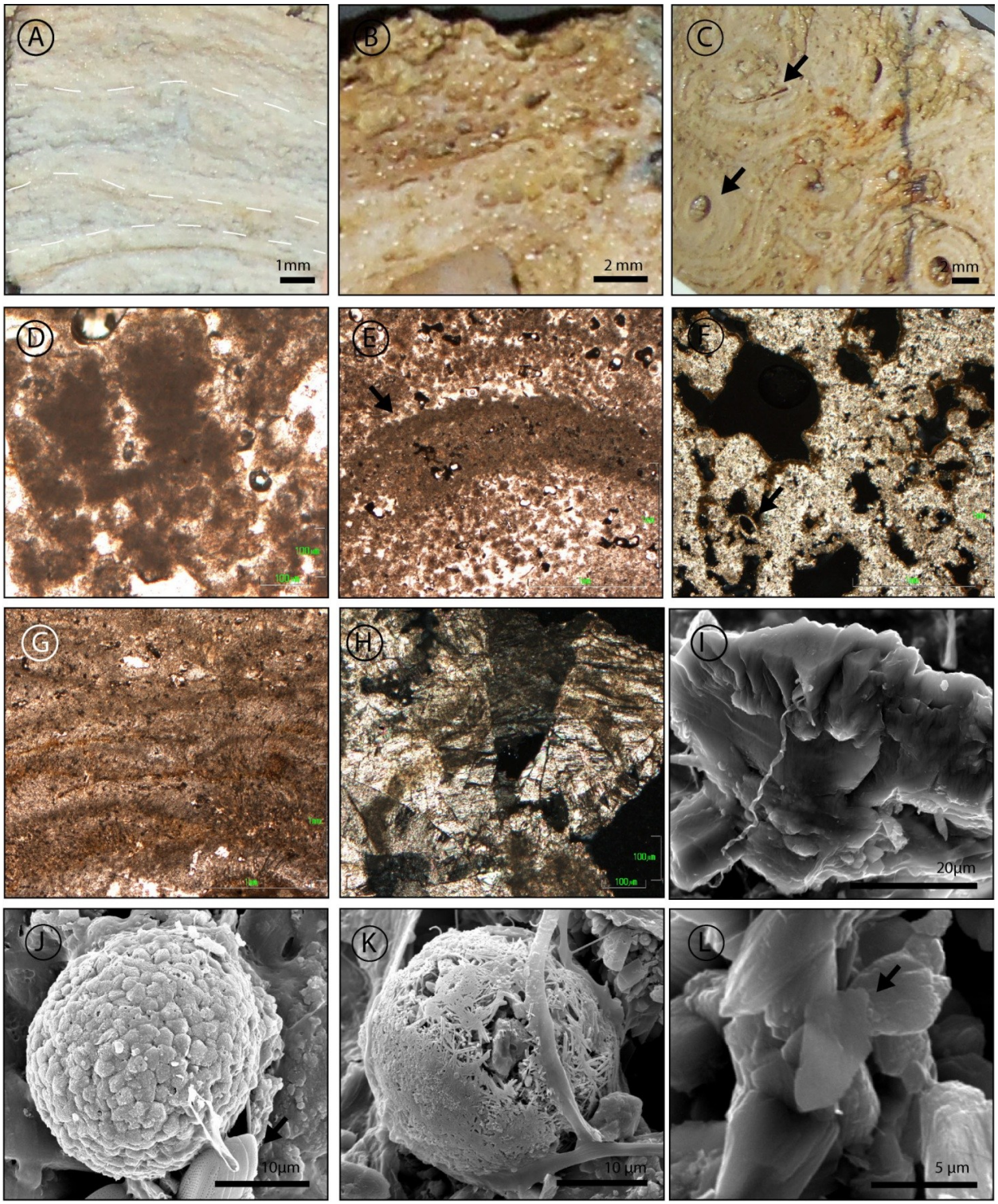

Fig. 5.6 Bagni di Saturnia structures and petrographic components. A) Layered travertine boundstone formed by the alternation of micrite, microspar and organic-rich laminae. B) Densely packed coated bubble boundstone. C) Encrusted travertine consisting of carbonate coated vegetation leaving porous areas. D) Thin section photomicrograph of dense to clotted peloidal micrite organized into a dentritic morphology. Pore space appears in white. Plane polarized light. E) Peloidal micrite alternates with a micritic lamina (black arrow). Pore space appears in white. Plane polarized light. F) Crossed polarized light thin section photomicrograph of microsparitic fabric associated with ostracod (black arrow). G) Photomicrograph showing cyanobacteria filaments within microspar. Micrite and organic-rich layer are also present. Pore space appears in white. Plane polarized light. H) Cloudy sparite crystals. I) Gypsum. Note the filamentous structures associated with the crystals. J) SEM image of isolated framboidal aggregates of pirite associated with EPS and diatom (black arrow). Calcite crystals are also present. K) Trapped spherical aggregate of SiO_2 fibrous minerals. Note the micron size EPS sheet. L) Clay mineral (black arrow) and calcite crystals.

range from loosely packed to densely packed. These exhibit dense to wavy and less commonly horizontal arrangement (Fig 5.7D-E). Vertical to prostrate cyanobacteria filaments constitute an important component of the dense micrite/microsparite laminated boundstone (Fig. 5.7 F). Often a vertical repetition of mainly dense laminae characterized by convex morphology creates micro-columnar structures (Fig. 5.7 D). The columnar structures are mainly oriented perpendicular to the substrate and often display a porous framework . Convex to spider web-like microsparitic laminated boundstone is also frequent due tosubspherical/lenticular discontinuous cavities bulged up by large and elongate gas bubbles or degradation of organic matter (Fig. 5.7G) .

Crystalline crust cementstone consists of laterally adjacent cloudy calcite crystals growing dominantly perpendicular to the surface (Fig. 5.7 H-I). The calcite crystals vary from microspar to spar and show often a course columnar appearance with poorly defined terminations. Fan-shaped arrangement of cloudy crystals is widespread. The calcite crystals are arranged to form ub-horizontal crystalline crusts, slightly undulated and parallel to each other, ranging from ca. 20 up to 500 μm. Regular to irregular concentric and radially arranged crystalline layers constitute also the cortex of coated grains.

Micritic laminae are often associated with the crystalline crust cementstone. These laminae often constitute the basal and upper boundary of a series of laterally adjacent and vertically alternated cloudy-crystals. In addition, cyanobacteria filaments are often observed within the crystalline crust cementstone.

Micrite mudstone consists of homogeneous regions constituted by non-laminated clotted peloidal/peloidal micrite in which sub-spherical/lenticular to irregular discontinuous pores (less than 10 μm up to 300 μm wide) frequently occur (Fig. 5.7J). Microspar and rarely spar line the pores and often fill them completely.

5.4.6.2 Coated bubble boundstone

Macroscopically, coated bubble boundstone (Fig. 5.6B) consists of cream coloured to white calcite spherical precipitate enclosing a hollow space (porosity up to 80 %) varying mainly from a few microns to less than 5 mm in diameter. Rarely, bubbles reach centimetre size diameters. Coated gas bubbles can be widely or densely spaced and rarely occur isolated.

Coated bubble boundstone consists of sub-circular to elongated carbonate structures consisting of micritic thin layer (5-100 μm thick) isolating a porous region (Fig. 5.7K). The micritic layer

displays a clotted peloidal or structureless texture. The space in between the adjacent bubbles is porosity or rarely microspar is observed within.

5.4.6.3 Encrusted travertine boundstone

Macroscopically, the encrusted boundstone consists of elongated, sub-circular to tabular vegetation (plant stems) encrusted by precipitated carbonates and preserved as porous areas following the degradation of the organic material (Fig. 5.6C). The coated reeds vary from a few microns to 1 cm in diameter. On the basis of petrographic observation, the coated reed boundstone is a highly porous microfabric, characterized by a framework of carbonate precipitates organised around sub-spherical/lenticular and elongate pores (Fig. 5.7L). Carbonate precipitates are micrite and microsparite. Micrite displays a structureless to clotted peloidal texture. Ostracods may occur in this fabric type. Phytoclastic reed fragments form rudstone and grainstone.

5.4.6.4 Carbonate grains packstone/grainstone to floatstone/rudstone

Carbonate grains such as travertine intraclasts, extraclast and bioclasts (ostracodes, gastropods) form packstone/grainstone and floatstone/rudstone surrounded by a cream coloured carbonate precipitate or a light grey mixed carbonate-clay matrix (Fig. 5.7I). Grain size varies from a few microns to several centimetres in diameter.
Inter-particle porosity ranges from a few microns to several centimetres in diameter. Packstone/grainstone to floatstone/rudstone layers constitute in general the nuclei of coated grains or the base from which the layered travertines nucleate (Fig. 5.7I).

5.4.6.5 Coated grains

The coated grain travertine consists of loose and poorly sorted variously shaped (often spheroidal) pisoids to oncoids (Fig. 5.4C). Cross-sections of these grains (Fig. 5.7I) show that they consist of a nucleus surrounded by regular to irregular concentric, radially arranged, layers that create a cortex varying from 2 mm to 1 cm in thickness. However, the coalescence of different coated grains is common and produces “popcorn-shaped” aggregate grains.

At the microscopic scale observation, the nucleus of the coated grains (Fig. 5.7I) includes detrital packstone/grainstone to oncoidal floatstone composed mainly by plant debris and biota. These biota are combined with lithoclasts (allochthonous and autochthonous) and clotted peloidal micrite. The cortex of the coated grains often consists of crystalline crust cementstone with fan-morphology alternating with laminated micrite and also microsparite boundstone.

5.4.7 Three-dimensional structures of present-day precipitate

High magnification analysis suggests that precipitation at Bagni di Saturnia occurs in association with widespread organic matter (Fig. 5.8). Minerals and organic matter give rise essentially two types of stratified structures with up-ward dome-shaped or flat morphologies (Fig. 5.8 A and B).
Organic extracellular polymeric substances appear the location where the calcite minerals nucleate and grow (Fig. 5.8 C-G). The organic matrix is less than 1 μm in thickness and shows a diversity of forms such as continuous films (Fig. 5.8 B) or honeycomb structures (Fig. 5.8C). The breakage of the EPS is expressed mainly through the presence of circular holes or irregular cuts in the film (Fig. 5.8A). When observed at very high magnification the EPS membrane appears both smooth and commonly irregular granular. Diatoms, cyanobacteria filaments and other bacteria (Fig. 5.5 A-K) are then associated with the EPS and often appear totally or partially entombed in it (Fig. 5.5K).
Detailed observations of the extracellular polymeric substance surface highlight the presence of nanometre-size, from sub-spherical to globular-like, raised structures (mainly from 5 to 150 nm) (Fig. 5.8 G). The nano-globules organize in rods (Fig. 5.8 G, I) that subsequently assemble together to form lumps with a granular appearance (Fig. 5.8 G). The lumpy bodies gradually organize into a more crystalline morphology showing incipient crystal face development. The rods of nano-globules coalesce (Fig. 5.8 I) and form triangular-like morphology (Fig. 5.8 G-I) and calcite crystals (Fig. 5.8 H) that are typically rhombic with a rounded shape.
Calcite precipitates around filamentous-like EPS alternating with porous areas create a dendritic network, whereas, calcite precipitation occurring in association with smooth EPS forms laminated boundstone .
Calcite precipitation is also associated with typically 1 μm wide filaments (Fig. 5.8J). In this circumstance, the precipitation occurs around the filaments that are often entombed in calcite crystals (Fig. 5.8J). Holes from which filaments protrude are often observed in the centre of the crystals that grow around the filaments.

Fig. 5.7 (next page**).** Photomicrographs displaying the principal micro-fabric of the Bagni di Saturnia travertine. A) Thin section photomicrograph of clotted peloidal dendritic boundstone characterized by dense to clotted peloidal micrite. Pore space appears in white. B) Thin section photomicrograph of clotted peloidal dendritic boundstone within microspar. Dendrites showing a stubby morphology. Pore space appears in black. Crossed polarized light. C) Thin section photomicrograph of radiating dendritic boundstone. Pore space appears in white. D) Wavy laminated boundstone composed mainly by an alternation of organic-rich micritic and microsparitic layers. Trapping of detrital grains is also observed (black arrow). Fenestrae and framework porosity appears in black. E) Close-up view of D showing a regular alternation of micrite and microspar laminae. The micritic laminae range from dense to clotted peloidal micrite, often observed within the microspar layers. F) Black arrow points on massive micrite layer, rich of organic matter in which sub-angular to rounded trapped detrital grains occur. Micrite/microsparite laminated boundstone is characterized by the presence of filaments of cyanobacteria. Crossed polarized light photomicrograph. G) High porous laminated boundstone showing a spider-web morphology. Laminae are made by micrite (mostly peloidal) within microspar. H) Crossed polarized light photomicrograph of crystalline cementstone with fan morphology. Note the cloudy appearance of the calcite crystals. I) Cross section of a coated grain. The nucleus consists of detrital grainstone to rudstone while the cortex is made by an alternation of laminated boundstone and laminated cementstone. J) Plane polarized light of peloidal fabric. F) Plane polarized light of coated bubble boundstone withbubble porosity in white. L) Reed boundstone/ rudstone fabric type.

Other crystalline phases, different from calcium carbonate, are observed in association with organic substrates (Fig. 5.8 K-L). Gypsum crystals occur in the upper surface of the present-day travertine. It precipitates in association of EPS (Fig. 5.8 K) and filamentous organisms (Fig. 5.6 I). Isolated framboidal aggregates of pyrite crystals are 15 μm in diameter, partially entombed by EPS are observed in present-day travertines (Figs. 5.27 C and D). The framboidal pyrite occurs in general in levels characterized by the presence of cocci and bacilli bacteria and diatoms. It was observed that the organic compounds trap other minerals such us spherical aggregate of SiO_2 fibrous minerals (Fig. 5.6K). In addition, clay minerals are also observed (Fig. 5.6L).

5.4.8 Porosity types of present-day precipitates

Bagni di Saturnia travertine shows a wide range of macro and micro-porosity. In terms of depositional porosity, nanometre to centimetre size framework porosity ranges from tight to high (Fig. 5.8). The depositional porosity can be differentiated into: 1) inter-branching porosity related to all the dendritic structures (Fig. 5.9A) to the adjacent crystals of the crystalline crust (Fig. 5.9C); 2) inter-laminae porosity especially observed within the laminated boundstone (Fig. 5.9B); 3) inter-particle porosity (Fig. 5.9D) especially within the radiating dendritic boundstone (Fig. 5.7C) and in the carbonate grain grainstone/rudstone (Fig. 5.9F); 4) the bubble porosity specific of the coated bubble boundstone (Fig. 5.9E); 5) intra-particle pores within particles such as ostracodes (Fig. 5.6 E).

Secondary porosity is related to bio-mouldic porosity observed in coated reed (Fig. 5.7L). Meteoric dissolution forming from millimetre to centimetre size vugs is possible (Fig. 5.5L).

SEM analysis reveals a significant micro-porosity varying from primary inter-crystalline to secondary intra-crystalline porosity (Fig. 5.8 G-I). Micro-pores range from a few nanometres up to 600 microns. Framework porosity is in general associated to EPS (Fig.5.8G). The intra-crystalline porosity consists mainly of rounded to rod-shaped pores within crystals (Fig. 5.8I).

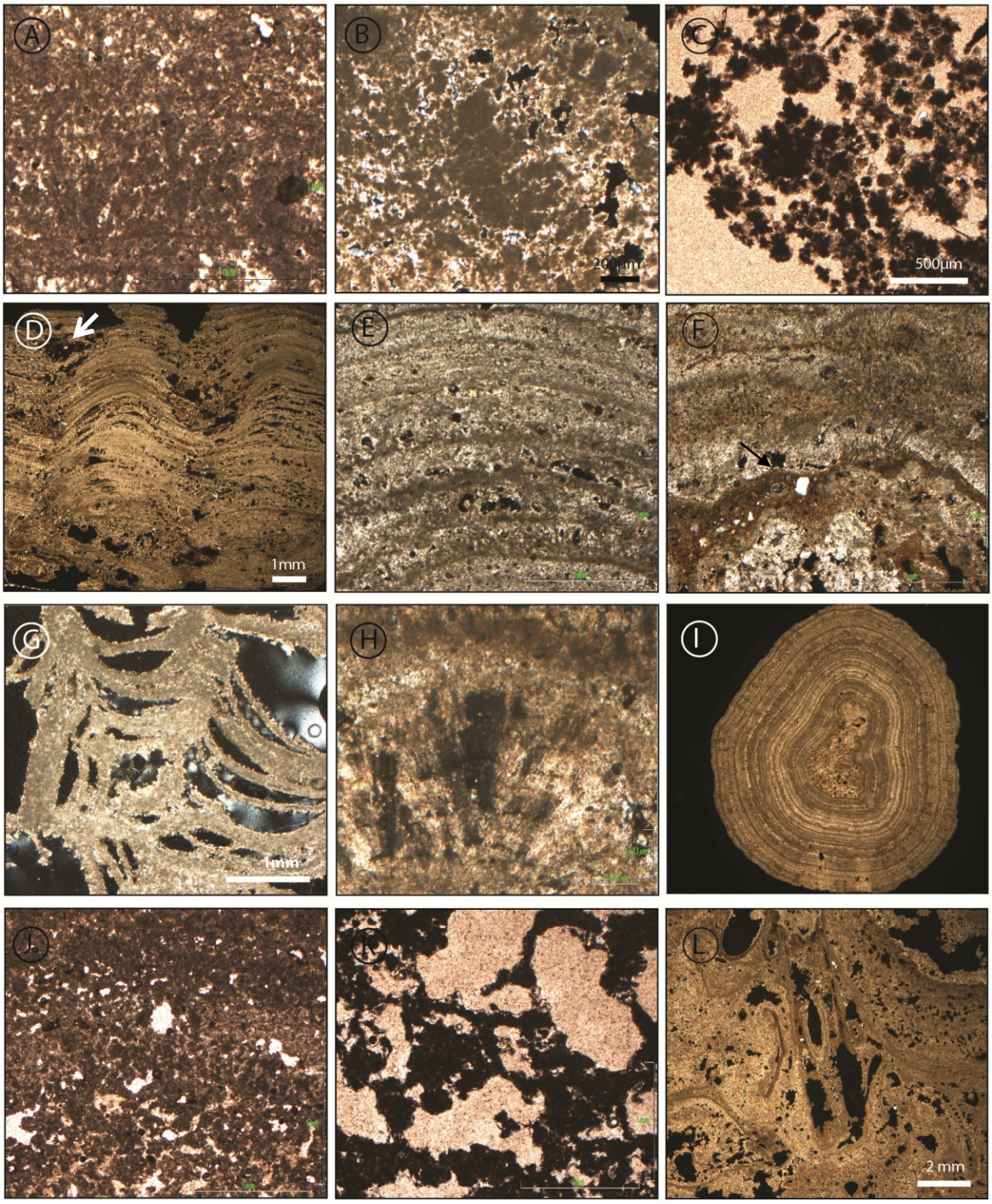

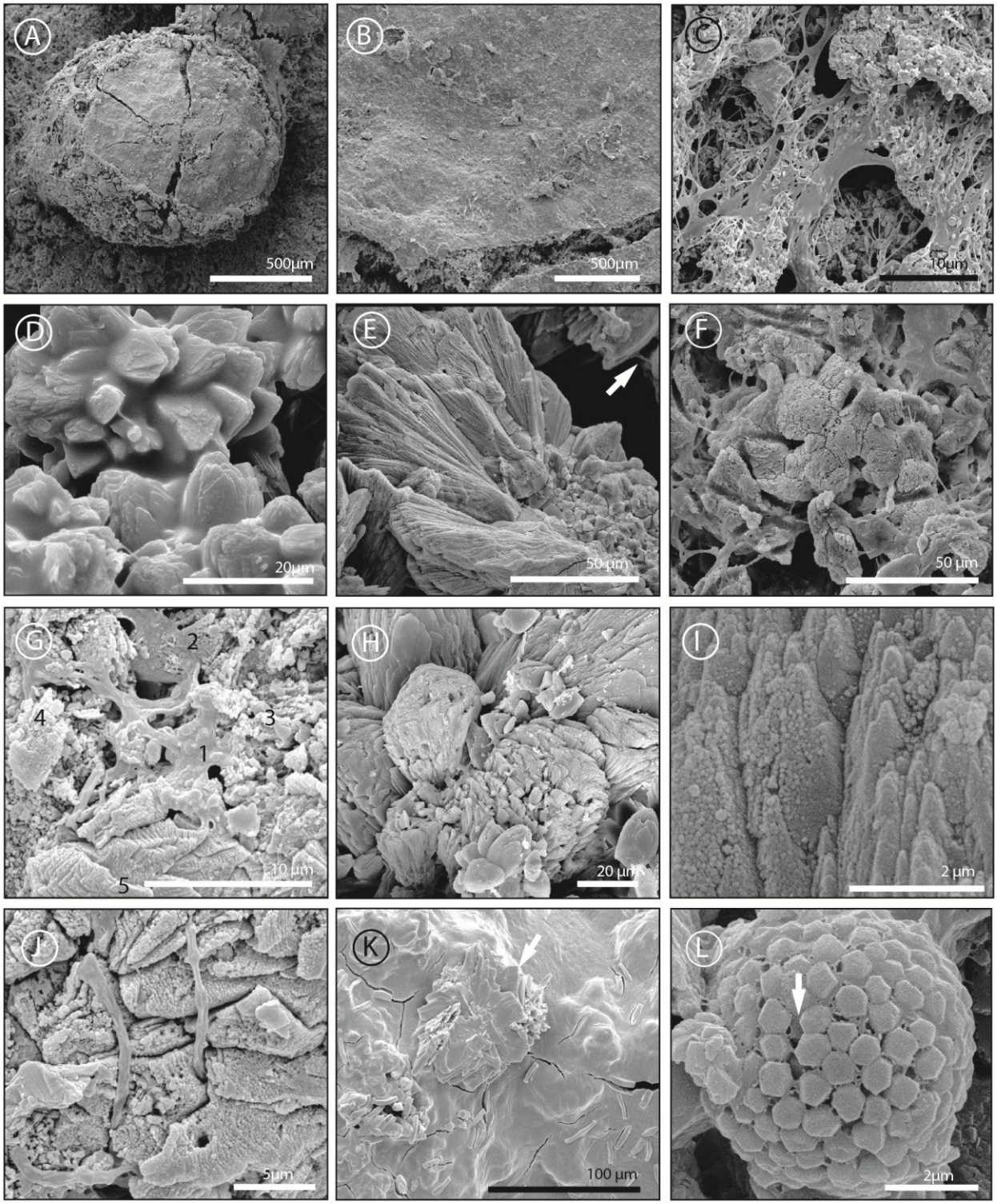

The lowest porosity is in general associated with crystalline cementstone (Fig. 5.9 C). The highest porosity is observed in the coated bubble boundstone (Fig. 5.9E), in the coated reed boundstone/rudstone (Figs 5.9L and 5.9F), and in the porous laminated boundstone (Fig. 5.9B), while dendritic boundstone (Fig. 5.9A), dense laminated boundstone (Fig. 5.7E) and coated grains (Fig. 5.7I) have in general medium to low porosity.

Fig. 5.8 (previous page). SEM photomicrograph showing the three-dimensional appearance of present-day Bagni di Saturnia travertine precipitates. A) Up-ward micro-column. The inner surface is covered by continuous EPS. B) Smooth surface of present-day precipitate. Note the presence of irregular cracks in the continuous gently film. C) Calcite precipitation in association with EPS. Calcite crystals progressively substitute the EPS. D) Micrite and microspar crystals associated with organic matter into laminated boundstone. D) Well-developed crystals with fan-morphology of crystalline crust cementstone. White arrow point on organic matter remains. F) Calcite crystals and EPS. Calcite crystals show stratified morphologies made of the overlap of parallel plates with triangular termination. Each plate is formed by denser packing of nano-globules. G) The initial stage of precipitation is represented by isolated sub-spherical nanometre size structures (1) in EPS. These structures became pervasive (2) and gradually coalesced and organized to form irregular and lumpy masses (3) that gradually assumed incipient crystal faces (4). These mineral masses progressively formed well-developed calcite crystals (5). The surface of the crystals is formed by nano-globules arranged in rods that assume triangular-like morphology. H) Neo-formed minerals. The surfaces of the crystals show triangular terminations originated by I) the aggregation of nano-globules into rod-morphology. J) Calcite crystal precipitation associated with non-dendritic filaments. Crystals grown around the filaments. The crystal surface is formed by nano-globules aligned in rods and organized to form crystalline faces. K) Gypsum growing on continuous and smooth EPS masses associated with diatoms. Diatoms are often entombed into EPS. Globose and raised masses formed by nano-globules are present. Note the irregular cracks in the film. L) Framboidal aggregates of pyrite associated with EPS (white arrow).

5.4.9 Geochemistry of present-day precipitates

X-ray diffraction analyses on seven bulk samples collected along the different depositional systems confirm that calcite is the dominant mineral phase forming nearly the 80-90% of the rock-volume, with detrital quartz accounting for the rest (Fig. 5.10). ICP analyses reveal that Ca is around 309392 mg/kg, Mg 5144.5 mg/kg, Sr 5609.53 mg/kg, Mn 176.51mg/kg and Ba 134.89 mg/kg.

Stable isotopic data obtained from Bagni di Saturnia sample show a positive field of distribution of $\delta^{13}C$ values that range from 2.23 to 5.94 ‰ PDB. The $\delta^{18}O$ values range from -9.22 to -7.39 ‰. The highest value of $\delta^{13}C$ is related to the layered travertine deposited in slow flowing areas such as the ponds of the self-built channel ($\delta^{13}C$ 4.28‰ PDB) and the pools of the terraced slope ($\delta^{13}C$ 5.95‰ PDB), while the lower values are related to samples collected along the pool rims ($\delta^{13}C$ 2.23 ‰ PDB) and barriers of the channel ($\delta^{13}C$ 2.67‰ PDB). The $\delta^{18}O$ values show a general decrease at increasing distance from the channel (-7.39 ‰ PDB) to the terraced slope (-9.22‰ PDB). Isotopic data of sub-horizontal to concave pools ($\delta^{13}C$ 5.95 ‰ and $\delta^{18}O$ -7.38 ‰) of stepped topography are heavier than those of sub-vertical rims ($\delta^{13}C$ 3.58 ‰ and $\delta 1^{8}O$ -8.26 ‰) and walls ($\delta^{13}C$ 2.23 ‰ and $\delta^{18}O$ -8.87 ‰) of terraced morphology. In addition, the organic rich black laminae of the layered travertine have $\delta^{13}C$ value of 2.88‰ while $\delta^{18}O$ of -9.04 ‰ whereas the green uppermost layers present $\delta^{13}C$ and $\delta^{18}O$ values of 4.28 and -7.53‰, respectively.

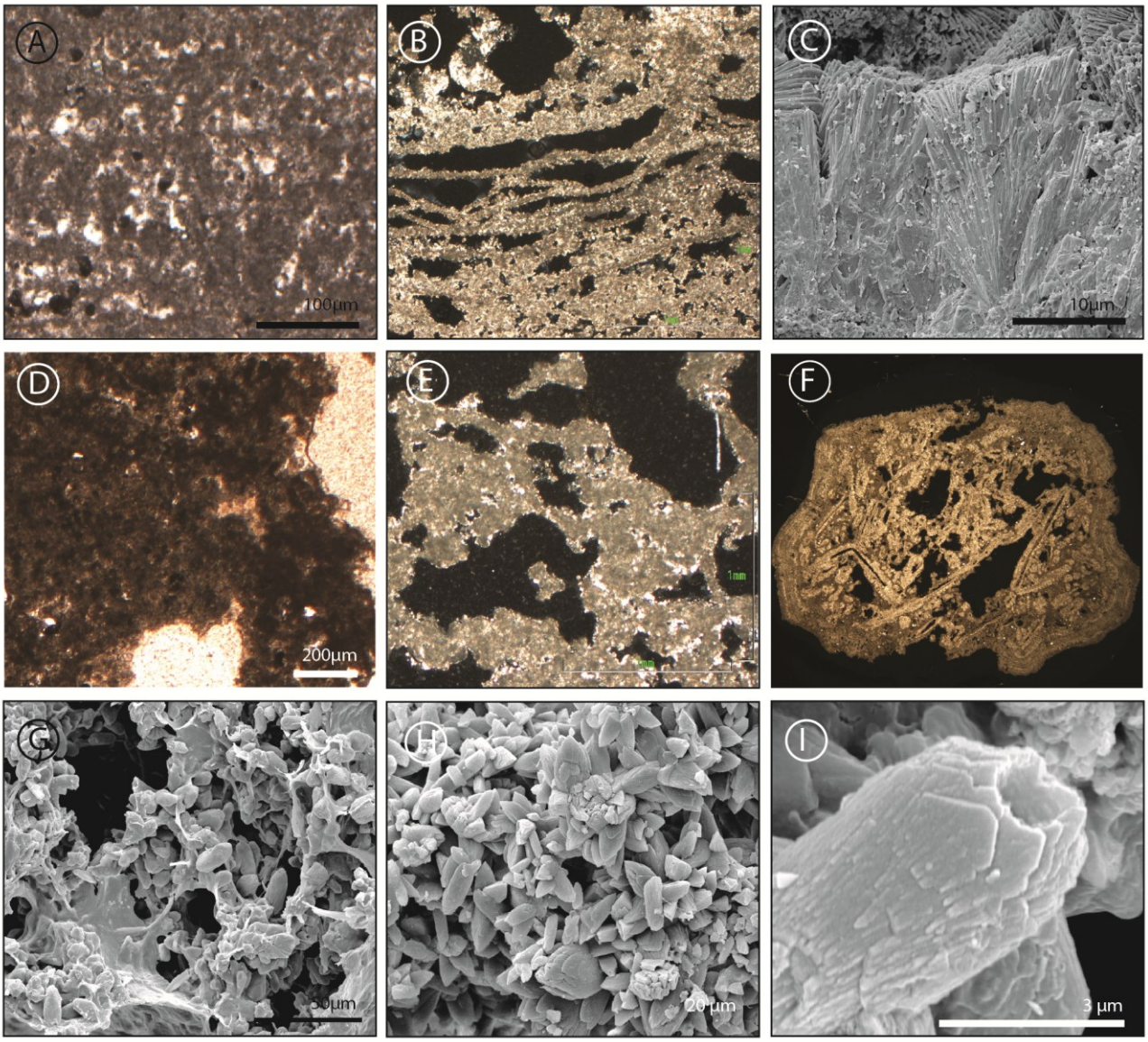

Fig. 5.9 Photomicrographs showing the different porosity types associated with present-day travertines. A) Inter-dendrite and inter clotted peloidal porosity in white. B) Inter-laminae porosity and fenestrae porosity. C) SEM image showing inter-crystalline porosity in crystalline crust cementstone. D) Porosity associated to peloidal fabric. E) Coated bubble boundstone porosity. F) Intra- and inter-particle porosity. Grainstone/rudstone. Field of view 28 mm. G) SEM image showing framework porosity related to EPS. H) Inter-crystalline micro-porosity. SEM image. I) Intra-crystalline micro-porosity. SEM image.

5.5 Fabric occurrence within depositional systems

A clear relationship between the depositional environment and the diversified travertine fabric exists. Laminated boundstone represents the main micro-fabric type constituting the Bagni di Saturnia travertine. This fabric type is typically individuated in terraced pools and ponds and

marginal areas of the self-built channel. Although, less frequently, laminated boundstone is also observed in alternation of crystalline crust cementstone that is characteristic of the cortex of the coated grains and of wall and rim deposits. Instead, the dendritic boundstone grows in terrace pools. In particular, the radiating dendritic boundstone is observed in the transitional area from the terraced pool towards the rim. Concerning the micrite mudstone, it is directly precipitated in pond and pool deposits. The encrusted travertine is peculiar of external areas of the rims and constitutes often part of the wall deposits. Reed rudstone is also observed along the pool floor where it often constitutes also the nucleus of coated grains. The coated bubble boundstone occurs in pond and pool deposits and also in external areas of the rim toward the wall deposits. Carbonate grain packstone/grainstone to floatstone/rudstone are observed indistinctly in all the depositional environments.

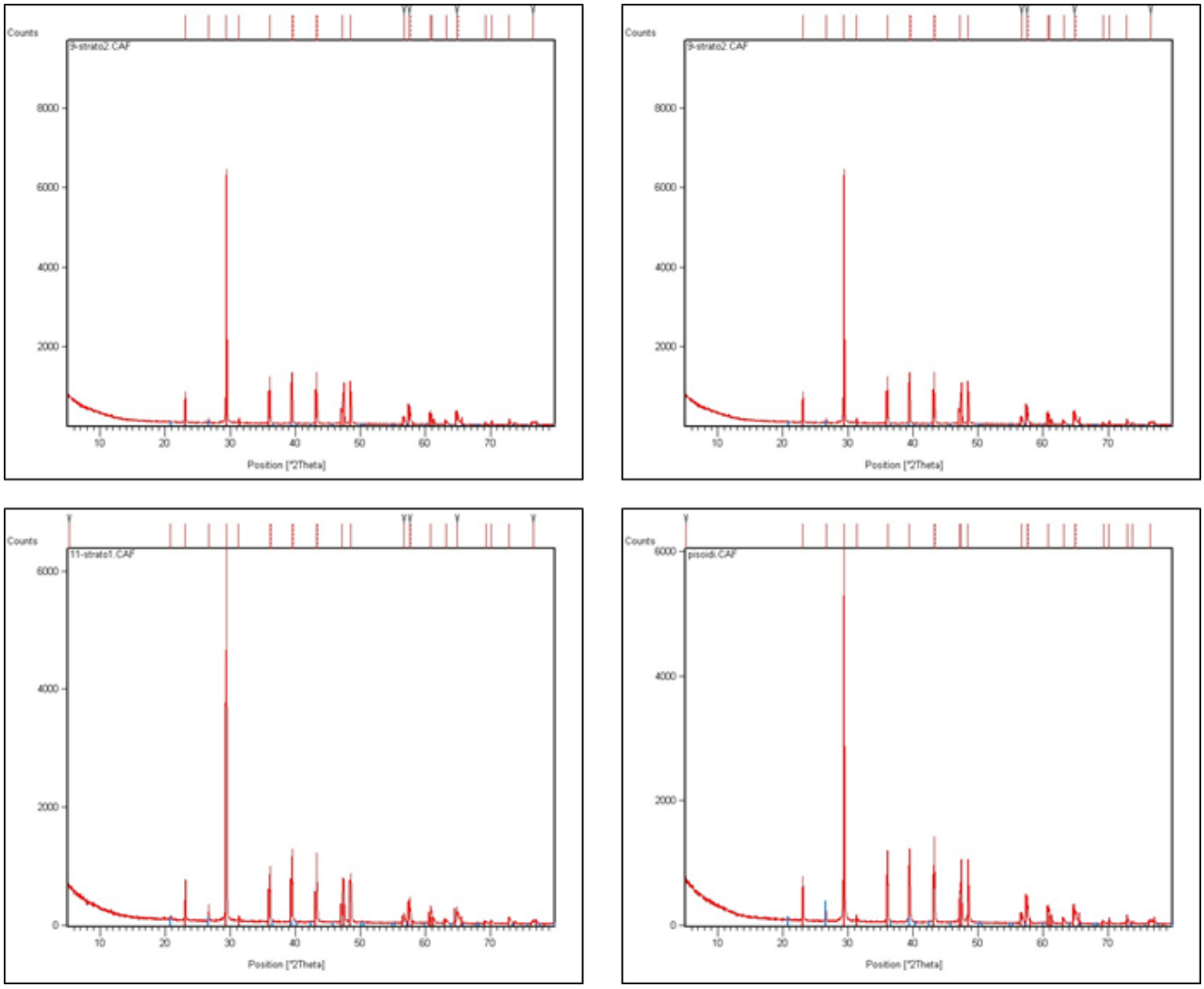

Fig. 5.10 XRD spectra of bulk analyses of present-day travertine samples at Bagni di Saturnia characterized by calcite peaks (in red) with the presence of secondary blue peaks indicating quartz.

Sample code	$\delta^{13}C_{PDB}$ [‰]	$\delta^{18}O_{PDB}$ Carbonate [‰]
BS 2_B	3.14	-8.31
BS 3_B	3.52	-8.29
BS 5	2.85	-8.75
BS 6_A	2.99	-9.22
BS 8	3.575	-8.26
BS 101_A	3.54	-8.25
BS 101_B	2.67	-8.76
BS2	4.28	-7.52
BS4_B	2.23	-8.87
BS 6_B	2.87	-9.03
BSL	5.94	-7.39
BSR 1	3.80	-8.15

Table 5.4 Isotopic values of Bagni di Saturnia travertine

5.6 Bagni di Saturnia: interpretation

5.6.1 Hydrothermal water geochemistry

Geochemical evaluation of hydrothermal water suggests that a complex suite of physical and chemical processes is the primary factor controlling the travertine precipitation at Bagni di Saturnia. Control on mineral precipitation is driven by CO_2 degassing and evaporation of the water outflowing from the spring, resulting in supersaturation with respect to calcium carbonate (Pentecost, 2005; Pentecost and Coletta, 2007; Dupraz et al., 2009). Removal of CO_2 through degassing favours the precipitation of $CaCO_3$. The pH increases along the Bagni di Saturnia flow path is interpreted as the result of CO_2 degassing and cooling of the hydrothermal waters; while the negative $\delta^{18}O$ values appears to be influenced by high temperatures and supersaturation levels of the outflowing waters.

5.6.2 Depositional systems

The development of the different depositional systems at Bagni di Saturnia appears influenced by hydrodynamic of the flowing water that is controlled by different factors such as the location and the activity of the vent, topography and roughness of the pre-existing surface. All these depositional systems developed on a pre-existent low-gradient topography except for the waterfalls forming where there is a break in slope and high topographic gradient.
Terrace rims and walls are considered areas of fast flowing water, while terrace pools and ponds are interpreted as areas of standing to slow flowing water. The channel sub-environment is characterized by low to fast flowing area. The mechanical carbon dioxide outgassing, that leads precipitation of calcium carbonate, seems to be favoured in agitated waters, such as areas of high current velocity and turbulence (e.g. final part of the self-built channel, waterfall, rims and walls of the terraced slope). However, the widespread presence of the microbial biofilms along the individuated depositional environments suggests that precipitation is not purely a consequence of physical processes .

5.6.3 Organic matter and mineral precipitation at Bagni di Saturnia

Carbonate precipitation at Bagni di Saturnia seem to take place essentially in correspondence of organic matter. However, the saturation index of the water is considered necessary for the calcium carbonate precipitation. Microbial mats are typically laminated and the upper layers correspond to diatoms and also coccoid cyanobacteria followed by filamentous cyanobacteria in which most of the oxygen photosynthesis take place. Beneath this layer a transition to anoxia takes place. Photosynthesizing cyanobacteria can create a supersaturated microenvironment in the vicinity of the filaments (Merz-Preiß, 2000). The removal of CO_2 from solution by cyanobacteria may facilitate $CaCO_3$ crystallization producing calcium carbonate precipitation on the photosynthesizing organisms (Freytet and Verrecchia, 1998, 1999; Merz-Preiß and Riding, 1999; Riding, 2000). However, high magnification SEM analysis shows that only a negligible amount of precipitation is directly associated to filamentous cyanobacteria, indicating that most of the carbonate precipitation is not associated with CO_2 uptake during photosynthesis.
It seems that exopolymeric substances (EPS) associated with diatoms, *Gloeocapsa*, filamentous cyanobacteria and heterotrophic bacteria combined with environmental conditions have a

predominant role in travertine formation, rather than photosynthesis. Degradation of organic matter appears as the fundamental factors that promotes the calcium carbonate precipitation. The decomposition of EPS, liberating HCO^{3-} and $Ca^{2+,}$ both of which activities will increase the saturation index, produces 'hotspots' of precipitation (Dupraz and Visscher, 2005).

The black organic layers within the present-day travertine may testify the hypothesis of a biological degradation of organic matter. In additions, as suggested by several authors (Dupraz et al., 2004, Pope et al., 2004; Spadafora et al., 2010) the presence of framboidal pyrite in association with bacteria at Bagni di Saturnia confirms that these bacteria are sulphate reducing bacteria.

Other precipitates, different from calcite have been observed within the Bagni di Saturnia. Gypsum occurs in general in the uppermost layers of the microbial mat. Even if, filaments are observed in association with the crystals, mineralization in that case is interpreted as the result of abiotic processes. In particular, evaporation leads the formation of these crystals.

5.6.4 *Organomineralization sl.* (*sensu* Dupraz et al., 2009) process

The mechanism of carbonate precipitation inferred in the precipitation of is the following. Initially organic matter may inhibit calcium carbonate formation by binding calcium. In order to precipitate calcium carbonate minerals, the Ca-binding capacity of the EPS matrix has to be greatly reduced (Dupraz and Visscher, 2005; Dupraz et al., 2009). This can occur through biologically-induced or biologically-influenced mineralization processes. In the initial stage the EPS appear to inhibit a spontaneous physical-chemical precipitation especially in areas of slow flow energy of the water. Degradation increases bicarbonate ion concentration providing ideal conditions for purely inorganic precipitation (Dupraz and Visscher, 2005; Dupraz et al., 2009). When all the functional groups of the polymers that inhibit the calcium carbonate are occupied with bound cations, a combination of local alkaline conditions and the presence of free Ca^{2+} ions can lead to the nucleation of calcium carbonate on the EPS matrix (Arp et al., 1999). Extrinsic factors such as environmental parameters rather than biological activity are also responsible for creating conditions for mineral precipitation Thanks to the super-saturation of the water with respect to calcium carbonate the available negatively charged groups are soon saturated with Ca^{2+}. A change of the hydrology activity (such us increasing of turbulence) that results in local supersaturation events promotes $CaCO_3$ formation. When the inhibition of precipitation is terminated, the nucleation starts.

Mineralization can also start around bacterial cells or filaments that are passively or actively entombed (Dupraz et al., 2004). Fossilization of the bacterial bodies is possible, as during entombment the bacterial cells adsorb divalent cations that then combine with bicarbonate produced during microbial respiration to precipitate crystals on the surface of the cellular membrane (Van Lith et al., 2001, 2003). However, the nano-globules appear to replace EPS and dead bacterial cell with or without the presence of degrading microorganisms. Passive entombment of bacteria occurs during rapid carbonate precipitation with bacterial growth on crystal faces (Dupraz et al., 2004).

5.6.6 Fabric types

The clotted peloidal dendritic boundstone, laminated boundstone, micrite mudstone and coated bubbles are interpreted as directly precipitated by standing to slow-flowing water with the influence of microbially mediated processes. Concerning the radiating dendritic boundstone, the precipitation process occurs with a dominantly biotic influence under intermittent water flow. Crystalline crust cementstone is interpreted as precipitated in conditions of significant water supply and fast flow regime; although the precipitation may have initiated under the influence of the biotic compounds as revealed by SEM and petrographic analyses, all the observations lead to hypothesize that in conditions of high supersaturation with respect to calcium carbonate, abiogenic precipitation is the dominant influence on the shape, components and development of the crystalline crust cementstone.

Encrusted travertine fabric type is interpreted as developed by abiotic processes. Plants form a barrier for the water flow and act as a substrate leading to the precipitation of the calcium carbonate around them. Whether the precipitation of calcium carbonate is only a physical process and the role of the reeds consist only in helping to create turbulence and thus increase CO_2 outgassing is not well understood. Another assumption is that reeds remove carbon dioxide from the water column during photosynthesis (Merz-Preiß and Riding, 1999). SEM observations show that the carbonate precipitated around the reeds is equally concentrically organized and varies from laminated to columnar calcite aggregates forming in association with EPS, filaments and diatoms. It is suggested that the biotic carbon dioxide up-take in conjunction with the mechanical CO_2 increasing calcium carbonate saturation leads the precipitation (Yoshimura et al. 2004).

Alternation of predominantly abiotic with dominantly biotic fabrics occurs in the Bagni di Saturnia. This reflects a change in the physical-chemical variables of the water related mainly to changes in the water supply and consequent energy of the flow. For example, reduced volumes of flowing water from the hydrothermal water vent can promote the precipitation of biotic fabric types also in fast flowing area. Bedding due to the alternation of the laminated boundstone and crystalline crust cementstone is commonly cyclic. This cyclicity may develop in response to changes in microbial growth (seasonal?) and/or of physico-chemical variables. Similar cyclicity is observed in the layered cortex of the coated grains. The coated grains grow on the pool floors, totally immersed within the intermittent and agitated thermal water of the pool. Their formation is related to the super-saturation level of the water but the presence of organic matter and microbes associated with the laminae suggests that these grains are also influenced by biotic processes. When the water flow is low a prevalently biotic precipitation and laminated boundstone occurs; turbulent events, correlated to an increase of the water supply that encourages the mechanical precipitation of calcium carbonate, encourage the precipitation of prevalent abiotic crystalline crust.

5.6.7 Stable isotope of travertine fabric growth

The individuated Bagni di Saturnia fabric types reflect the precipitation processes due to the interplay of biotic and abiotic processes. Fabrics occurring in low energy areas might be more biologically influenced than fabrics occurring in fast flowing dipping surface for which the abiotic processes of physical degassing might prevail. This physical-chemical and biological interaction is also registered in travertine isotopic geochemistry. The negative $\delta^{18}O$ values appear to be influenced by high temperatures and super-saturation levels of the outflowing waters (Friedman, 1970; Guo et al., 1996; Fouke et al., 2000). The $\delta^{13}C$ data range reflects the contamination of the isotopic composition of groundwater by the bedrock marine limestones or juvenile/magmatic waters (Gonfiantini et al., 1968; Friedman, 1970; Turi, 1986; Guo et al., 1996; Gandin and Capezzuoli, 2008). Continuous CO_2 degassing, evaporation and temperature change of the thermal water from the self-built channel to the terraced slope system caused a general increasing trend of $\delta^{18}O$ value. Samples collected in low flowing areas are characterized by higher $\delta^{18}O$ and $\delta^{13}C$ values with respect to samples typical of fast flowing area. These may testify not only a mechanical CO_2 outgassing but also a biogenic activity due to an increased presence of organisms in slow flowing area rather than fast flowing settings.

In addition, the lower value of $\delta^{13}C$ in black laminae characterized by white colours may reflect aerobic respiration. Thus, stable isotope analyses conducted on the Bagni di Saturnia precipitates confirm the previously presented interpretations of the different depositional environments, fabric types and help to elucidate the processes involved during travertine precipitation.

5.7 Bagni di Saturnia: discussion

Present-day travertine deposits are widespread in different geographic areas. Active and inactive examples of the self-built channel depositional systems have been described for different travertine systems from Mammoth Hot Spring in Yellowstone National Park, Wyoming (Fouke et al. 2000; Fouke, 2011), Pamukkale in western Turkey (Ozkul et al., 2002) and Egerszalók, Hungary (Kele et al., 2008). Several authors (Bean, 1971; Hancock et al., 1999; Fouke et al. 2000; Ozkul et al., 2002; Kele et al., 2008; Fouke, 2011) described these deposits as linear travertine masses built up by spring waters in the flow direction. Ozkul et al. (2002) suggested that Pamukkale channels are restricted by rims on both sides; rims developed along the points where precipitation is maximum (Ozkul et al., 2002). Self-built channels observed in Turkey are characterized by an alternation of micritic laminae and crystalline crusts (Ozkul et al., 2002). Different from the Bagni di Saturnia travertines, pisolith clumps have been observed in some hollows placed along the channel; in addition, the channels present slopes that are developed on both sides by overflowing and splashing water. Self-built channel depositional systems consist of narrow (0.5 to 3.0 m) up to 10 m high, wall-like masses of travertine and distribute carbonate-rich water to lower grounds (Bean, 1971). The wall-like perched form of these petrified channels is the result of the continuous deposition of travertine from turbulently flowing water on the channel floor and sides (Hancock et al., 1999). Fouke et al (2000) suggested that the channel deposits of Mammoth Hot Spring is floored by sinuous microbial mats composed of sulphide-oxidizing filamentous bacteria (*Aquificales* group). The same observation was made by Kele et al. (2008), for the Hungarian travertine.In addition, Fouke (2000) referred that aragonite precipitates on the surface of these bacterial filaments to form carbonate tubes. Kele et al. (2008) for refers that gently sloping artificial channel and ponds from Egerszalók is characterized by the water temperature ranging from 45–55 °C and by floating fibrous travertine and oncoidal channel deposit.

Modern travertine terrace slopes are well known from Mammoth Hot Spring in Yellowstone National Park, Wyoming (Chafetz & Folk, 1984; Pentecost, 1990; Fouke, 2011; Renaut and Jones, 2000; Pentecost, 2005), and Pamukkale in western Turkey (Özkul et al., 2002; Antunel and Hancock, 1993; Kele et al., 2011). In the Rapolano area (Southern Tuscany, Italy), small terraces are periodically active at the western end of the fissure ridge at Terme San Giovanni (Guo and Riding, 1998). These authors argued that terraced slope morphology does not require a steep pre-existing topography and they proposed a model for terraced slope formation related to an alternation between laminar and turbulent flows. Under laminar flow, water shears horizontally, parallel to the direction of flow, leading to the formation of horizontal layers. If this is disrupted by turbulent flow eddies, it can produce locally high velocities, resulting in locally rapid precipitation, which also increases the roughness of the surfaces favouring stepped morphologies. Kele et al. (2008) referred that the size of the rims of the Egerszalók travertine bodies vary between 0.1 m and 1 m and the height of the vertical terrace-walls range from centimetres to 1 m; the terrace pools range from decimetres to metres wide and are up to 30 cm deep . The pools at Egerszalók contain fewer pisoids and paper-thin rafts. At Bagni di Saturnia paper-thin rafts were not observed.

Recent and sub-recent examples of waterfall travertines have been mentioned (Chafetz and Folk, 1984; Casanova, 1986). An example of ancient waterfall was described by Guo and Riding (1998) in the Rapolano area as resembling terrace wall and low angle slope deposits. However, similar geometries are also characteristic of cool water tufa deposits (Pedley, 1990; Ford and Pedley, 1996; Pentecost, 2005; Pedley, 2009; Vazquez-Urbez, 2009).

The precipitation of calcite mineralogy at Bagni di Saturnia may be related to the water temperature. Previous studies (Friedman, 1970; Folk, 1994; Fouke et al., 2000) pointed out that aragonite usually occurs at temperature > 40-45°. Aragonite is generally associated with water that has attained very high levels of supersaturation with respect to $CaCO_3$ (Jones and Renaut, 2010).

The precipitation of Bagni di Saturnia travertines occurs in association with organic matter. Many authors have suggested that microbes contribute to the precipitation of authigenic minerals in a wide variety of sceneries including hydrothermal spring settings. Travertine formation resulting from precipitation within an organic matrix is a good example of biologically-influenced mineralization since the carbonate precipitation is not due to biological activity, but the lithified organisms are indirectly modifying the features of the resulting organomineral (Dupraz et al., 2009). Renaut and Jones (2000) suggested that biotic precipitation and active

mediation in travertine formations occurs when photosynthetic removal of CO_2 not only induced nucleation but maintain the level of mineral supersaturation needed for continued precipitation. Cyanobacteria, other bacteria and diatoms can play a role in calcite and aragonite nucleation in travertines (Chafetz and Folk, 1984; Folk et al., 1985; Guo and Riding, 1992; Chafetz and Guidry, 1999), and through photosynthesis and other biochemical processes may mediate mineral precipitations (Renaut and Jones, 2000). Microbial metabolic activity triggers a change in solution chemistry that leads to oversaturation; this alone can induce mineral precipitation (Stumm and Morga, 1996).

Winsborough (2000) suggested that microbial mat containing diatoms and the extracellular polysaccharide substances secreted by them is intimately associated with all the carbonate precipitates, even rapidly growing facies such as coated bubbles and calcite rafts. This biofilm plays a central role in the precipitation, trapping and binding carbonate crystals, and its presence in ancient carbonates provides insights into possible diagenetic pathways (Winsborough, 2000). Guo and Riding, (1994) suggested that spar-rhombs in shrub lithofacies could be controlled biogenically by diatoms that trap particles with adhesive mucus.

Calcification in cyanobacteria depends on water chemistry as well as on physiological and morphological factors such as photosynthetic bicarbonate up-take and the existence of a suitable sheath (Merz-Preiß, 2000). The sheaths are formed by polysaccharides and can absorb high amounts of divalent metal ions (Decho, 1990) rising concentrations far above those found in the ambient water (Merz-Preiß, 2000). Pentecost et al. (1997) analysed the typology, distribution and influence of phototrophic microorganisms in the Pamukkale travertine (Turkey) suggesting that this travertine was colonized by a wide range of algae, but *Oscillatoriales* were predominant; these authors suggested that cyanobacteria locally influenced the travertine microfabric by providing sites for the trapping and nucleation of calcite at the cell surface, but the bulk of the travertine did not appear to be influenced by the presence of these microbes.

Precipitation connected with dead cyanobacteria is suggested for travertine fabric type precipitation connected to cyanobacteria filaments at Bagni di Saturnia. Preferential bacterial calcification on dead rather than living cyanobacteria filaments (Chafetz and Buckzynski, 1992) is due to the production of antimicrobial substance which is widespread among cyanobacteria species (Channel et al., 1988). The bacteria produce characteristically dumbbell-shaped crystals (Chafetz and Buckzynski, 1992). Only after the death of the cyanobacteria, when production has ceased, heterotrophic bacteria can decompose the sheaths and undergo calcification (Merz-Preiß, 2000).

Formation of $CaCO_3$ particles in microbial mats and other environments might, at least in part, be due to heterotrophic bacteria, as suggested by Drew (1914), Krumbein et al. (1977), Chafetz and Buczynsky (1992). Carbonate precipitation by bacteria is apparently a by-product of physiological activities that increase carbonate alkalinity, rather than a result of a specific mechanism; bacteria can function as nucleation sites and they become embedded in growing carbonate particles, but similar particles can also form in the absence of bacteria (Knorre and Krumbein, 2000). Carbonate precipitation related to heterotrophic bacteria appears to be a response to enrichment in organic matter (Castanier et al., 2000). Actinomycetes have been reported (Pentecost, 2005) but they are not well-known in travertine deposits. In different thermal springs of USA, Europe and Turkey the heterotrophic bacteria have been observed in association with cyanobacteria that provide the energy sources (Pentecost, 2005). At Mammoth Hot Springs, Fouke (2011) individuated heterotrophic bacteria in the microbial communities in pond, proximal-slope and distal-slope facies. Sulphate-reducing bacteria, as indicated by FeS/pyrite precipitate and black horizons within the microbial mats, must be present within the Bagni di Saturnia.

Sulphate-reducing bacteria are a group of diverse anaerobes which carry out dissimilatory reduction of sulphur compounds such as sulphate, sulphite, thiosulfate and even sulphur itself to sulphide (Beech and Gaylarde, 1999). Pentecost (2005) suggested that *Beggiatoa* is found in abundance in sulphide contain waters, such as those of Saturnia. Weed (1889) argued that *Beggiatoa* form characteristic vegetation in sulphur springs. Because of the mucilaginous sheaths, *Beggiatoa* communities trap and bind other sedimentary particles, their mats constitute "potential stromatolites" (Krumbein, 1983), which develop best in low-oxygen environments (Williams, 1984).

Many fabric types of hydrothermal travertine preserve evidence of microbes (Renaut and Jones, 2000). Bacterial fossils and micropores have been observed at Bagni di Tivoli, Tivoli, Italy and in the Terraced Mountain, Yellowstone National Park, Wyoming, USA (Folk and Chafetz, 2000). These similar structures have been previously recognized by Folk (1990) and called nano-bacteria. Following studies on modern microbial mat lithification (Merz-Preisß and Riding, 1999; Sprachta et al., 2001; van Lith et al., 2003; Dupraz et al., 2004;. Dupraz et al., 2005; Perri and Tucker, 2007; Pedley et al. 2009; Spadafora et al., 2010; Manzo et al., 2012; Perri et al., 2012), in this study the nanobacteria of Folk are interpreted as nano-globules representing the first product of calcium carbonate mineralization on degrading EPS.

Several fabric types have been distinguished at Bagni di Saturnia and these are the results of an interaction between abiotic and biotic processes.

Carbonate precipitates similar to the clotted peloidal dendritic boundstone are ubiquitous in hot spring travertines around the world (Chafetz and Meredith, 1983; Chafetz and Folk, 1984; Guo and Riding, 1998; Chafetz and Guidry, 1999). These consist of bush-like morphology defined shrubs that typically grow in terrace pools and large pond (Chafetz and Folk, 1984; Guo and Riding, 1998), according to what is observed for the Bagni di Saturnia travertine. The presence of bacterial micropores, fossils and diatoms within the carbonate shrubs suggests that organisms are necessary for the formation of carbonate shrubs (Guo and Riding, 1994; Chafetz and Guidry, 1999). Folk (1993) described structures similar in size and shape to those termed here as nano-globules and interpreting them as calcified cells of nano-bacteria. Fouke (2011) suggested that shrubs precipitate in association of large variety of microbial mats characterized by a high diversity assemblage of autotrophs and heterotrophs. Guo and Riding (1998) described in present-day travertine at Terme San Giovanni (Tuscany Italy) “radial shrub pisoids” that show similitudes with the radiating dendritic boundstone. These pisoids are formed in intermittently agitated microterrace pools where they are closely associated with abundant bacteria, cyanobacteria and diatoms (Guo and Riding, 1994, 1998). Guo and Riding (1994) suggested an interplay between microbial and abiotic processes in the formation of these peculiar dendrites. In contrast with what observed by Guo and Riding (1994) for comparable travertine deposits, the micritic appearance of the clotted peloidal micrite at bagni di Saturnia is not diagenetic due to micritization processes but primary.

Structures comparable to the laminated boundstone have been reported by Rainey and Jones (2009) within the Fairmont Hot Springs deposits as “stromatolite facies”. The “stromatolite facies” forms under slow flowing, weakly agitated spring water or reduced water volume discharged (Rainey and Jones, 2009). In agreement with the Bagni di Saturnia laminated boundstone, Rainey and Jones (2009) suggested that this fabric type is microbially induced and that reduced volumes of flowing water from the hydrothermal water vent can promote the precipitation of stromatolite in fast flowing areas.

Crystalline crust cementstone is attributed to rapid precipitation from fast flowing waters (Folk et al., 1985; Guo and Riding, 1992, 1998). Guo and Riding (1992) individuated dendrites defined as ‘feather crystals’, which they equated with the ‘ray crystals’ of Folk et al. (1985) that form crystalline crusts. In present-day Bagni di Saturnia, crystalline crusts formed by the coalescence of feather-like crystals are not individuated.

Coated bubbles boundstone is quite common in travertine pools (Kitano, 1963; Chafetz and Folk, 1984; Guo and Riding, 1998; Özkul et al., 2002). Stagnant conditions are the most favourable for coated bubble formation (Folk et al., 1985; Ozkul et al., 2002). This travertine fabric is interpreted as trapped and rapidly mineralized bubbles of oxygen, methane and or/carbon dioxide (Chafetz and Folk, 1984; Chafetz et al., 1991; Guo and Riding, 1998; Bonny and Jones, 2008). A microbial activity in underlying sediment is suggested as the main gas source (Folk et al., 1985; Guo and Riding, 1998). Folk et al. (1985) suggested that 'fine drapes' of micrite enveloping coated bubbles may represent microbial EPS remains. Chafetz et al. (1991) suggested that the bubbles at the hot springs of SW Colorado formed as pure abiotic precipitation, the mineralogy and crystal habit of the carbonate precipitate being controlled by the saturation index level of the waters.

Micrite mudstone was not described in previous studies about travertine deposits.

Encrusted travertine fabric type was previously described by Guo and Riding (1998) and subsequently by Özkul et al. (2002) as reed travertine, while Rainey and Jones (2009) defined them as macrophyte facies. Plants form a barrier for the water flow and act as a substrate for the precipitation of calcium carbonate; in this way, plant stems and twigs become encrusted (Rainey and Jones, 2009). The deposition of calcium carbonate around stems is interpreted as a physical process. Rainey and Jones (2009) suggested that the "macrophyte facies" is most common at the base of the deposit where local vegetation was inundated by spring water and encrusted with calcite.

Coated grains show similitudes with "pisoids" described in other travertine systems. Pisoids are common in travertines (Chafetz and Meredith, 1983; Folk and Chafetz, 1983; Guo and Riding, 1998; Kele et al., 2008) andoccur in pools, ponds and channel depositional environments. Travertine pisoids range in shape from spherical, through irregularly rounded, to irregular (shrub-like, hemispherical), depending on water-energy and microbial involvement (Guo and Riding, 1998). Concentrically laminated pisoids form in splashing and turbulent water (Guo and Riding, 1998). They are rarely transported and show little abrasion. This type has been regarded as inorganic (Folk and Chafetz, 1983), but formation of of pisoids may be partly influenced by biotic processes.

This study suggests that travertine precipitates are mainly strongly influenced and, in some circumstances, induced by the microbial biofilms. However, it is clear that also in the case of biologically-induced mineralization some abiotic processes and physical-chemical characteristic of the precipitating thermal water can control the precipitation.

5.8 Conclusions

Actively forming travertines occurring today at Bagni di Saturnia, Tuscany, Italy have been investigated with the purpose of understanding the biological, chemical and physical processes interacting together producing hydrothermal travertine deposits

Several depositional systems have been individuate and includes: 1) hydrothermal vent, 2) self-built channel, 3) waterfall, and 4) terraced slope system.

The development of the different depositional systems individuated at Bagni di Saturnia appears influenced by hydrodynamic of the flowing water that is controlled by different factors such as the location and the activity of the vent, topography and roughness of the pre-existing surface.

Terrace rims and walls are considered areas of fast flowing water, while terrace pools and ponds are interpreted as areas of standing to slow flowing; in addition, the channel sub-environment is characterized by low to fast flowing area.

Geochemical evaluation of hydrothermal water suggests that a complex suite of physical and chemical processes is the primary factor that regulates the travertine precipitation at Bagni di Saturnia.

Carbonate precipitation at Bagni di Saturnia takes place both in alternation to and amalgamated with the living microbial mats. Prokaryotes, diatoms, green algae and ostracods mainly populate the travertine deposits and influence their fabrics.

SEM analysis reveals that the initial stage of precipitation in Bagni di Saturnia is mainly represented by random distributed nano-globules that coalesce and gradually organize into a more crystalline morphology showing incipient crystal face development. These mineral masses progressively substitute and eventually replace the mucus-like substance until they form well-developed calcite crystals. Degradation of organic matter appears as a fundamental factor that promotes the calcium carbonate precipitation and can be accomplished through different processes varying from abiotic to biotic.

Five macro-fabric groups characterized the Bagni di Saturnia deposit including: 1) layered travertine boundstone/cementstone. 2) coated bubble boundstone travertine; 3) encrusted travertine; 4) coated grain travertine; 5) carbonate and non-carbonate intraclasts and extraclasts. Micro-scale observations reveal a large variety of micro-fabric types. These include: a) dendritic boundstone; b) laminated boundstone; c) crystalline crust cementstone; d) micrite mudstone, e)

coated bubble boundstone; f) coated reed boundstone/grainstone/rudstone; g) grainstone/rudstone/packstone/floatstone.

Bagni di Saturnia travertine shows a wide range of macro and micro-porosity. In terms of depositional porosity, nanometre to centimetre size framework porosity ranges from tight to high. The depositional porosity can be differentiated mainly into: 1) inter-branching porosity; 2) inter-laminae porosity; 3) inter-particle porosity; 4) bubble porosity; 5) intra-particle pores within particles such as ostracodes. Secondary porosity is firstly related to bio-mouldic porosity. Meteoric dissolution form millimetre to centimetre size vugse.

A relationship between microfabric types and velocity/turbulence of the flowing water and probably also volumes of water is suggested. The clotted peloidal dendritic boundstone, laminated boundstone, micrite mudstone and coated bubbles are interpreted as directly precipitated by standing to slow flowing water with the influence of microbially mediated processes. Concerning the radiating dendritic boundstone, the precipitation process occurs with a dominantly biotic influence under intermittent water flow. Crystalline crust cementstone is interpreted as precipitated in conditions of significant water supply and fast flow regime; although the precipitation may have initiated under the influence of the biotic compounds Encrusted travertine fabric type is interpreted as developed by abiotic processes.

This study suggests that travertine formation is not only the result of pure mechanical CO_2 degassing. An interplay between abiotic and biotic processes occurs. Travertine precipitates are mainly strongly influenced and, in some circumstances, induced by the microbial biofilms. However, it is clear that also in the case of biologically-induced and influenced mineralization some abiotic processes and physical-chemical characteristic of the precipitating thermal water can control the precipitation. However, microbial communities are recognized for playing a potentially important role in calcite precipitation.

Chapter 6
Final remarks and conclusions

This study not only provides valid tools to clarify the problematics related to products and processes of hydrothermal carbonate precipitation but also presents some innovative results. It does not claim, however, to represent a conclusive answer to the understanding of the complexity of the hydrothermal travertines.

Investigations on travertine deposits are often deficient in fabric descriptions, especially at the micro- and nano-scale. In this research, the description and characterization of macro- and micro-fabric types and their nano-scale features have been considered a fundamental tool for the understanding of the role of microorganisms and the processes involved in travertine formation. This PhD research proposes a detailed fabric description and a relative travertine fabric classification, developed using the terminology of the classical classifications of carbonate textures by Dunham (1962) and Embry and Klovan (1971), and with the previously published travertine fabric nomenclature (cf. Chafetz and Folk,1984; Jones and Renaut, 1995; Guo and Riding, 1996). This classification gives directly information on the components and texture of the fabric types and also on the mechanisms that acted during their deposition. The proposed classification may contribute to the definition of a necessary general travertine, and possibly continental carbonate, classification.

Several fabric types observed in the Albegna travertines, such as laminated boundstone, laminated cementstone and micrite mudstone/microsparstone have been described for the first time among the travertine fabrics reported in literature, and no evident similitudes are observed with the fabric types found in other travertine deposits.

For the first time, the main diagenetic processes that produced modifications on the fabrics and the associated porosity have been described in detail. In disagreement with what suggested by some authors (e.g., Guo and Riding, 1994) this research demonstrates that the clotted appearance of some fabrics (such “shrubs” *sensu* Guo and Riding, 1994) is not diagenetic but primary.This study also suggests that even if the amount of microspar and spar increase with the age of travertine, spar calcite cement may be also a primary component precipitated by hydrothermal water.

The study of the Albegna travertine deposits clearly demonstrates the complex interplay existing between biotic and abiotic processes, the influence that these processes have on the fabric growth, and the relationship between fabric types and depositional environments. The data here presented confirm that travertine formation is not only the result of mechanical CO_2 degassing but that both abiotic and biotic processes (biologically induced by microbial metabolic processes or simply influenced by nucleation on microbial biofilm substrate) are involved in the precipitation of the studied travertine deposits. Nevertheless, it is inferred that also in the case of biologically-induced mineralization some abiotic processes and physical-chemical characteristic of the precipitating thermal water are fundamental for calcium carbonated precipitation. A model for travertine precipitation is here proposed, on the basis of published studies on modern microbial mat lithification in marine and non marine settings. SEM analysis shows that the first product of calcium carbonate mineralization on EPS or organic matter is represented by nano-globules. These findings deviate from the interpretation of Folk (1993) who described structures similar in size and shape to the here described nano-globules and interpreted them as calcified cells of putative nano-bacteria.

The study of the Pianetti travertine provides also the first comprehensive evaluation of the reservoir properties of hydrothermal-spring carbonates. This evaluation was made using classical and modern methodology for porosity and permeability determination. It is apparent that travertines may represent good quality reservoir rocks.

In addition, the Albegna Valley travertines contribute to characterize the different depositional systems observed also in comparable travertine systems worldwide and confirm a relationship between fabric types and depositional environments.

Ultimately, travertines share common characteristics with other classes of continental and marine carbonates, and therefore similar approaches of study, methodology and classifying criteria may be utilized.

In detail, from the study of Albegna Valley travertine deposits the following conclusions can be drawn:

i. **Depositional systems.**

The present-day Bagni di Saturnia complex can be subdivided into four laterally distributed depositional systems. These can be mainly distinguished as follows: 1) hydrothermal vent, 2) self-built channel system usually characterized by high water flow with laminar to turbulent activity and low flowing area, 3) waterfall where turbulent water regime occurs, and 4) terraced slope system. Travertine deposits belonging to terraced slope systems consist of vertical to

overhanging walls, sub-horizontal pools and raised rims confining the margin of the pools. Water flow varies along the terraced slope. The water is generally fast flowing but pools represent a relative slow-moving portion of the terraced slope system. However, pulsating sheet flows affect sometimes the rim and wall areas and create periodic rim and wall exposure.

Hydrothermal vent and terraced slope consisting of terrace pools, terrace rims and walls (including waterfalls) were also observed within the Pianetti travertine walls. In addition, the Pianetti travertines exhibit also smooth slope (fast flowing area) and pond (low flowing area) depositional environments.

ii. **Fabric types**

Five macro-fabric groups characterized the Bagni di Saturnia deposits including: 1) layered travertine boundstone/cementstone. 2) coated bubble boundstone travertine; 3) encrusted travertine; 4) coated grain travertine; 5) carbonate and non-carbonate intraclasts and extraclasts. Micro-scale observations reveal a large variety of micro-fabric types. These include: a) dendritic boundstone; b) laminated boundstone; c) crystalline crust cementstone; d) micrite mudstone, e) coated bubble boundstone; f) coated reed boundstone/ rudstone; g) grainstone/rudstone/packstone/floatstone.

Travertine fabrics of the Pianetti travertine deposit can be distinguished into three categories: 1) travertine boundstone and cementstone *s.l.* in which the original components are directly precipitated from hydrothermal thermal water, including: a) shrub-like dendritic boundstone; b) thick crystalline crust cementstone; c) thin crystalline crust cementstone; d) laminated boundstone; e) coated gas bubble boundstone; f) raft boundstone/rudstone; g) micrite mudstone/microsparstone; 2) encrusted travertine coated reed boundstone/grainstone/rudstone in which original components (acting as substrate) are directly encrusted by carbonate precipitated by flowing hydrothermal water; 3) carbonate grains packstone/grainstone to floatstone/rudstone formed by fragments of already lithified travertine precipitates (intraclasts) and other lithoclasts.

The individuated fabric types in the Pianetti and Bagni di Saturnia systems reflect the precipitation processes due to an interplay of abiotic and biotic processes (biologically induced by microbial metabolic process or simply influenced by nucleation on microbial biofilm substrate) and, only subsequent diagenesis (especially for the Pianetti travertines).

iii **Travertine i porosity and permeability**

Pore space is an important component of travertine fabrics, which show a wide range of depositional and secondary porosity. SEM analysis reveals a significant micro-porosity.

The description of the porosity types is based on Choquette and Pray (1970) classification. The Helium porosity and permeability measurements of Pianetti travertine system show that travertines display a wide range of porosity, from 1 to 29%, and permeability, from 0.006 up to 50000 mD. The pore structure of ten samples was quantified using microCT scanning and AVIZO, which has proved to be an excellent visualization tool in the travertine sample. The wide range of porosity and permeability values is interpreted as direct function of: 1) primary fabric orientation; 2) amount of cementation; 3) travertine fabric type; 4) micro-porosity.

iv **Travertine mineralogy**

As confirmed by X-ray diffraction analyses the majority of the investigated present-day travertines is calcite in mineralogy. However, the fossil travertines are composed predominantly of calcite with minor amounts of aragonite. Acicular to fibrous morphology of a significant amount of the calcite suggests that transformation of aragonite into calcite might have occurred. In terms of crystal size, Bagni di Saturnia and Pianetti travertines are essentially composed of a mixture of micrite, microsparite and sparite crystal size.

iv **Diagenetic processes**

Dissolution, neomorphism and spar-micritization combined with cementation are the main diagenetic processes that can alter the fabric appearance. In particular, diagenetic features can be explained by superimposed early and meteoric diagenetic processes.

v **Relationships between fabric types and velocity/turbulence and discharged volumes of the flowing water**.

The travertine fabrics can be differentiated into those typical of “fast flowing water areas” (such as thick crystalline crust and thin crystalline crust cementstone) and those precipitating in stagnant to slow flowing water areas (such as dendritic boundstone, laminated boundstone, raft rudstone, coated gas bubble boundstone, micrite mudstone).

vi **Precipitations occurs in association with organic biofilms**

Carbonate precipitation at Bagni di Saturnia takes place both in alternation to and amalgamated with the living microbial mats. SEM analysis reveals that the initial stage of precipitation in Bagni di Saturnia is mainly represented by randomly distributed nano-globules that coalesce and gradually organize into a more crystalline morphology showing incipient crystal face development. These mineral masses progressively substitute and eventually replace the mucus-like substance until they form well-developed calcite crystals. Degradation of organic matter appears as fundamental factors that promotes the calcium carbonate precipitation and can be

accomplished through different processes varying from abiotic to biotic. Prokaryotes, diatoms and green algae and ostracods mainly populate the travertine deposits and influence their fabrics. The presence of organic matter remains within the fossil Pianetti travertine is revealed by petrographic analysis and SEM observations. These organic matter remains consist mainly of extracellular polymeric substances (EPS), filaments and bacteria-like structures. Detailed observations highlight the presence of nano-globules also in the Pianetti travertine system.

vii **Geochemistry reflects the interplay between biotic and abiotic processes.**

Geochemical data of the studied travertine deposits seem to be controlled by the interplay of complex physical and chemical processes (e.g. CO_2 outgassing and consequent cooling, evaporation, temperature and saturation state of the precipitant water), hydrology of the water flows and biotic activities. All these factors are strongly dependent on the depositional environments.

The negative range of $\delta^{18}O$ values appears to be influenced by high temperature and supersaturation levels of the outflowing water. The $\delta^{13}C$ range is interpreted to reflect the contamination of the isotopic composition of groundwater by the Mesozoic bedrock marine limestones or juvenile/magmatic waters. In addition, isotopic data show that fabrics occurring in low energy areas seems to be more biologically influenced than fabrics occurring in fast flowing dipping surface for which the abiotic processes of physical degassing might prevail. All these findings highlight the importance of the conducted research and suggest that the Albegna travertine deposits can have implications for the understanding of comparable carbonate reservoirs in the subsurface.

Appendix 1

	FABRIC TYPE				Depositional environment and hydrodynamics
	MACRO-FABRIC Main category		MICRO-FABRIC Sub-category based on petrographic observation		
	Name	Description	Name	Description	
TRAVERTINE BOUNDSTONE/CEMENTSTONE *s.l*	DENDRITIC BOUNDSTONE – Shrub-like dendritic boundstone	White bush-like forms (mainly 0.2-8 cm high, a few microns to 2cm wide) surrounded by cream coloured and often light grey matrix and cement. Shrub dendrites exhibit a range of branching morphologies, from rounded or knobbly to more geometric; the branches appear oriented upward in a direction away from the substrate. Spherical to lenticular and elongated pores varying in size from a few microns to less than 1 cm characterize the shrub-like dendrite layers . Shrub-like dendrites create sub-horizontal (a few centimetres up to 10 cm) and lateral continuous (several tens of metres) layers.	Clotted peloidal micrite dendritic boundstone	**COMPONENTS**: sub-angular to spherical peloids (3- 10 µm in size) that together with micrite are arranged into bush-like structures exhibiting a poorly defined "stalk" from which branches (50 µm to a few millimetres in length, 50-400 µm wide) diverge. The branches exhibit an irregular morphology lacking a systematic repeating habit. Frequently, the clotted peloidal dendrites evolve upward and laterally into fan-shaped branched morphology formed by laterally adjacent cloudy bladed turbid-crystals (varying from 30 up to 100 µm in diameter) that often show an undulose extinction Isolated clumps of clotted peloidal micrite (less than 30 to up to 400 µm) arranged into an arborescent-like disposition (often form the clotted peloidal dendrites. The space between the micritic arborescent structures is filled by equant cement (varying from microsparite to sparite). **PROCESS**: dominantly biotic. **POROSITY**: inter-dendrite, framework, vug. **DIAGENESIS:** Aggrading neomorphism, aragonite-calcite inversion, dissolution and cementation.	Common on sub-horizontal surfaces of terraced slope (**pool**) and **pond** depositional systems. They are found also in flat area of smooth slope system. This fabric forms as a result of rapid precipitation from **standing to slow flowing water.**
			Rhomb-composed dendritic boundstone	**COMPONENTS**: turbid-crystals (20-100 µm wide, 30 µm to 1 mm long), arranged into dendrite with defined outline and a geometric and complex branching morphology. The dendritic morphology varies from: • Dendrites characterized by a mostly defined elongated central area ("stalk") from which complex branches with geometric and straight pinnate form diverge • Dendrites formed by elongate and straight branches, which split from an area located in general at the base of the dendrite rather than a central stalk. • Dendrites displaying from well to partially developed fan-morphologies. **PROCESS:** interplay between biotic and abiotic. **POROSITY:** inter-dendrite, framework, vug. **DIAGENESIS**: dissolution, spar-micritization, cementation and aragonite-calcite inversion.	Gently dipping irregular surfaces of **pools** of terraced slope system. **Relative slow flowing water with laminar to turbulent regime.** Rhomb-composed boundstone precipitates by faster water rather than those forming clotted peloidal micrite dendrite.
	DENDRITIC BOUNDSTONE – Radiating dendritic boundstone	Radiating dendritic boundstone occurs as a single and compound white spherical structure showing a dendritic-like growth (200 µm up to 1 cm in diameter). These dendrites form layers (a few millimetres to 5 cm thick) ranging from irregular and lateral discontinuous (3 cm to tens of decimetres) to regular and relatively lateral continuous (a few metres).	Radiating dendritic boundstone	**COMPONENTS**: micrite (mainly clotted peloidal micrite) with often an amount of microsparite arranged into spherical to sub-spherical dendrites. Dendrites vary from ca. 200 µm up to 5 mm in diameter and are composed by irregular to regular branching that radiates from a central area. Branches often show a fan-like pattern. The fan-like branches consist of turbid-crystals (20 up to 150 µm wide). Radiating dendrites can grade into clotted peloidal dendritic boundstone or rhombic composite dendritic boundstone. Ostracodes mainly in between two single radial dendrites occur. **PROCESS**: interplay between biotic and abiotic. **POROSITY:** Inter-dendrite, intra-particle, framework, vug. **DIAGENESIS:** Dissolution, spar-micritization.	**Pool**s of terraced slope system. Relative **low flow regime**.
	CRYSTALLINE CRUST CEMENTSTONE – Thick crystalline crust cementstone	White coarsely crystalline crusts consisting of laterally adjacent calcite crystals (a few microns up to 15 cm long and few millimetres to 2 cm wide) growing perpendicular to the surface. The calcite crystals show a range of dendritic morphologies varying from fibrous/bladed and elongate appearance to a pinnate form. Microns to millimetre-thick laminae may cross the calcite crystals. Thick crystalline crusts (3 cm up to 20 cm) form mainly medium to high angle (up 15 to ca. 90°) inclined beds (tens of metres laterally extended) organized mainly into slightly undulated and parallel to each other crusts alternating for several centimetres to more than 1 m.	Crystalline dendritic cementstone	**COMPONENTS:** Turbid calcite crystals embedding micrite. The turbid-crystals (30 µm-2 mm long, 10-700 µm wide) are arranged into dendritic structures showing a wide range of morphologies including: • Symmetric dendrites where an apparently millimetre-size single bladed crystal (from 30 to 300 µm wide) is composed of multiple smaller crystals (less than 15 µm up to 50 µm long) occurring in pairs symmetrically with respect to a central "stalk" • Asymmetric to rarely symmetric dendrites composed of turbid-crystals (mainly from 10 to 400 µm wide and 20 µm to 2mm long) arranged into a pinnate-like morphology (Branches diverge from an elongated stalk (few microns up to 100 µm in width) with an angle ranging from 10 to 85°. The branches, with a variable length and width ratio (L/W > 1 to L/W > 10), show in general straight morphology; although less abundant, curved branches are observed. Dendrites with a radial arrangement of the branches occur. • Laminae (50 µm to 600 µm thick) formed by turbid-crystals (ca. 10 µm up to 40 µm in width and from 50 µm up to 300 µm) occur perpendicularly to the main direction of growth of the crystalline dendrites. Each lamina is repeated with an average distance of 100-160 µm from the other. • fan-shaped dendrites (characterized by mostly stubby appearance (L/W ≥ 1). These consist of poorly defined branches (mainly 80 µm to 600 µm wide and 100 µm up to 1.5 mm long) diverging away from a wide central area (300-800 µm) localized at the base of the dendrites. **PROCESS:** dominantly abiotic **POROSITY:** Inter-dendrite, vug. **DIAGENESIS:** Dissolution, spar-micritization, aragonite-calcite inversion.	Lateral continuous clinoformal beds of **smooth slope**. Regarding the **terraced slope** topography, the crystalline crusts identify both the vertical to overhanging drop layers of the wall (**pool walls** and **waterfalls**) and the raised and also convex morphologies of the **rim** sub-environments. Also they are associated with columnar convex shaped layers constituting the **hydrothermal vent**. Rapid precipitation from significant hydrothermal water
	CRYSTALLINE CRUST CEMENTSTONE – Thin crystalline crust cementstone	Generally white, crystalline crusts ranging from dense to those that display laterally adjacent calcite crystals (from a few mms up to 2 cm thick). The calcite crystals display length to width ratio (L/W) ≥ 1 and show a variety of fan morphologies varying from elongate to triangular-like forms. Rarely, elongate and fibrous-like crystals are observed. Micron to millimetre-thick and parallel to each other laminae cross and often delimit the calcite crystals. It forms mainly low to medium angle (*ca.* 4-15°), continuous inclined beds organized into slightly undulated and parallel to each other crusts alternated for several centimetres to 1 m on the quarry walls. These inclined beds can be laterally found from tens of metres along the quarry walls. However, this fabric type forms convex, vertical to overhanging beds and creates also locally extended (mostly 2-3 cm thick) sub-horizontal raised layers.	Crystalline fan-dendritic cementstone	**COMPONENTS**: The turbid-crystals (less than 50 µm to 2 mm long and ca. 15 µm to more than 500 µm wide) are arranged into dendritic structures exhibiting a continuous range of morphologies varying from: • typically elongate (*ca.* 600 µm to 4 mm high and from 100 to 200 µm wide) structures showing a dendritic network characterized by an almost regular disposition of branches about a central and elongate area ("stalk"). Dendrites show incipient fan morphologies that become stronger at the terminal area of the dendrites. The branches exhibit a mostly symmetric repeating pattern along both sides of a central stalk and appear numerous at the base of the dendrites. At their terminal end, dendrites evolve into wider and raised fan morphologies.Toward the top of the dendrites, the branches become lesser in number and apparently coalesce to form wider poorly defined branches with fan morphology. The dendrites show undulose extinction. Densely vertically spaced microsparite laminae aligned across the growth direction of the dendrites are observed. • Generally dendritic structures (80-500 µm high, 100-550 µm wide) show fan morphologies These are characterized by stubby appearance (L/W ≥ 1) and consist of poorly defined branches diverging away from a supposed area localized at the base of the structures in a fan-shaped array; this gives rise to a sort of fan arrangement. Undulose extinction and thin micron-size micrite/microspar laminae characterize in general the crystalline dendrites. **PROCESS:** dominantly abiotic. **POROSITY:** Inter- dendrite, inter- laminae, vug**.** **DIAGENESIS:** Dissolution, spar-micritization, cementation.	Diffuse along clinoformal beds of **smooth slope** topography. Less widespread in **terraced slope** where they characterize the **terraced wall** and **rim** morphologies. Reduced water supply and velocity (compared with dendritic crystals of thick crystalline crust) downdip high-speed (upper flow regime). Fan-dendrite crystalline crusts pass vertically into crystalline laminated cementstone suggesting a decreasing of the water supply and of the velocity of the water flow.
			Crystalline laminated cementstone	**COMPONENTS:** fan-shaped turbid crystals. Layers are formed by the juxtaposition of raised structures resembling mammillate cones/fan. These are densely laminated and are oriented perpendicular to the depositional surface. Micrite/microspar laminae (a few microns up to 20 µm in thickness) crossing perpendicularly the cone-like architectures are observed. Sometimes these laminae constitute the basal and upper boundary of a series of lateral adjacent and vertical alternated turbid-crystals that form the mammillate-like structures. **PROCESS:** dominantly abiotic **POROSITY:** Inter- laminae, vug. **DIAGENESIS**: Dissolution; spar-micritization, cementation.	
	LAMINATED BOUNDSTONE – Dense laminated boundstone	Laminated boundstone consisting of dense (with porosity less than 5%) laminae cream to light grey in colour. Layers of laminated boundstone range mainly from 3 mm up to 6 cm in thickness and contain isolated sub-spherical to lenticular pores (1 mm to several millimetres thick and from ca. less than 1 mm up to 6 mm wide). An inner densely fine (less than 1 mm thick) lamination may be observed within the laminae. Laminated boundstone forms horizontal to concave layers, 0.3-6 cm in thickness, that can be laterally followed for tens of metres along the quarry walls.	Micrite/microsparite from well to poorly laminated boundstone	**COMPONENTS:** micron-size micritic laminae alternating with microsparitic layers and interlaminae pores (nm to cm in size). However, laminated boundstone with no or rare inter-laminae pores also occurs. The laminae are generally made by clotted peloidal micrite. The micrite laminae, growing parallel to each other and parallel to the substrate on which they nucleate, range from loosely packed to densely packed. These exhibit dense to wavy and less commonly horizontal arrangement. Often a vertical repetition of the laminae characterized by convex morphology creates micro-columnar structures. The columnar structures are mainly oriented perpendicular to the substrate and often display a porous framework. Convex to spider web-like micritic (mostly clotted peloidal)/microsparitic laminae are also frequent. Subspherical/lenticular discontinuous cavities bulged up by large and elongate gas bubbles or degradation of organic matter are observed. **PROCESS**: dominantly biotic. **POROSITY:** Inter-laminae, fenestrae, vug. **DIAGENESIS:** Aggrading neomorphism, dissolution, cementation.	This boundstone constitute the major constituent of **pond** deposits. This is also a common fabric of inclined beds dipping of **smooth slope** topography. Laminated boundstone occurs also along the **pool** and rim morphology of terraced slope. Also along the vertical to overhanging drop layers of the wall (**pool walls** and **waterfalls**). Reduced water supply (l**ower flow regime**). This boundstone is deposited by alternating with high flow fabric on the smooth slope and on rim pools of terraced slope system. This suggests a change from high to low energy of the water flow and a decrease of the water supply.
	LAMINATED BOUNDSTONE – Porous laminated boundstone	Cream to white in colour porous laminated boundstone consisting of sub-spherical to lens-shaped elongated cavities (ranging from a few microns up to 4 cm wide) trapped between dense laminae (ranging from wavy to irregular and often convolute, less than 1 mm up to 2 cm wide) and/or thin (less than 1 to 5 mm) brittle undulated sheets. Occasionally the dense laminae and the thin sheets exhibit micron- to a few millimetres in size white lamination. The porous laminae, varying mainly from sub-horizontal to wavy laminated to irregular disposition, are arranged into sub-horizontal to inclined (from ca. 5 to 90°) beds ranging mainly from 0.5 cm up to 20 cm. The porous laminated boundstone forms also micro-columnar structures.			
	RAFT BOUNDSTONE/RUDSTONE	Raft fabric consists of microns to millimetre thick, white to cream coloured, flat horizontal structures; rarely gravitational deformation gives rise to wavy morphologies of the carbonate films. The vertical repetition of widely to densely-packed, parallel raft structures preserve elongate intra-raft porosity. Raft rudstone with intra-raft porosity creates layers 2-10 cm thick. Raft fragments (5 mm-5 cm long) form cemented grainstone to rudstone/floatstone, 20 cm thick, extending laterally several metres. Dense concentrations of raft fragments, vertical to straight or inclined, create centimetre-thick lenses. Shrub-like dendritic boundstone often grows on rafts.	Calcite/aragonite raft rudstone	**COMPONENTS**: raft consists of clotted peloidal to dense micrite band (30-200 µm thick) that often contains an inner microsparitic layer (10-100 µm thick). Frequently, the micrite film is laminated, mostly along its upper side. Acicular aragonite crystals form isopachous rims around micritic layers of rafts (80-150 µm), followed by bladed calcite crystals. It may also occur that turbid calcite crystals diverge from the inner microspar horizon; these turbid-crystals are perpendicularly oriented with respect to the micritic band and can develop on both or only on one of the sides of the raft morphologies. **PROCESS:** interplay between abiotic and biotic. **POROSITY**: Inter-particle; fenestral, vug. **DIAGENESIS:** Dissolution, aggrading neomorphism, aragonite-calcite inversion, cementation.	Rafts precipitate at the water-air interface of stagnant pond systems and pools of terraced slope system. Dense accumulations of raft fragments concentrate in the area just behind the pool rim morphology. Rafts form also in ponds near the hydrothermal vent orifices.
	COATED BUBBLE BOUNDSTONE	Coated bubble boundstone consists of circular to tabular porous structures with carbonate coating (porosity up to 70 %) which are gas-filled bubbles (mainly a few microns to 5 mm in diameter; rarely, bubble structures reach centimetre size in diameter). Bubble boundstone forms sub-horizontal layers, 8 cm thick, and extend horizontally for several metres. Coated bubbles form also centimetre-size pockets.	Coated bubble boundstone	**COMPONENTS:** micrite thin layers (5-40 µm thick) forming porous structures (70 µm to a few centimetre in diameter) showing sub-spherical to elongated or droplet shape. The micrite layer is clotted peloidal or structureless. The internal wall of the micrite layers coating the gas bubble is lined by isopachous bladed to scalenohedral sparite cement. The space in between the adjacent bubbles is filled by microsparite to sparite cement. Densely packed layers of coated bubble produce a honeycomb framework. The outer surface of the coated bubble might act as the substrate for the radial growth of rhomb-composed dendritic boundstone and turbid-crystals. **PROCESS:** dominantly biotic **POROSITY:** bubble porosity **DIAGENESIS:** cementation, compaction, aggrading neomorphism.	Coated bubbles occur in sub-horizontal strata of ponds and pools of terraced slopes. Discontinuous lenses of coated bubbles occur within the smooth slope topography. This fabric forms as a result of rapid precipitation from **relative low flow and mostly laminar water.**
	MICRITE MUDSTONE/MICROSPAR-STONE	Micrite mudstone/microsparstone consists of a few millimetres to 5 cm thick layers characterized by dense, cream coloured to light grey, carbonate precipitate. Layers range from sub-horizontal to inclined (5 to 90°) and extend horizontally for several metres along the quarry walls. The micrite mudstone contains isolated sub-spherical to lenticular pores (a few microns to 6 mm wide and a few microns to several millimetres thick).	Micrite mudstone/Microsparstone	**COMPONENTS**: non laminated clotted peloidal to dense micrite and/ microspar. This fabric is often associated with rare/sparse ostracodes. **PROCESS:** dominantly biotic. **POROSITY**: framework, skeletal, vug; **DIAGENESIS:** Aggrading neomorphism and dissolution.	Typical fabric of pools of terraced slope and pond depositional systems. It is also observed along the low angle areas of smooth slope topography. Micrite/microspar mudstone/cementstone precipitates by **low flow and mostly laminar water.**
ENCRUSTING TRAVERTINE BOUNDSTONE *s.l.,*	COATED REED BOUNDSTONE/GRAIN-STONE/RUDSTONE	Reed fabric type consists of micrite coatings precipitated around plant stems and root moulds and isolating elongate to sub-circular porous areas (a few microns to 1 cm in diameter) following plant organic matter degradation. Coated reeds are locally exposed, but rarely reed moulds form laterally extended continuous layers. Reed preservation as moulds is responsible for the high porosity of these deposits.	Micrite/microspar reed boundstone/grainstone/rudstone	**COMPONENTS:** micrite and microsparite form the layers coating the reeds. This boundstone is often observed in association with ostracodes. Micrite ranges from 20 µm up to 200 µm in size and displays a structureless to clotted peloidal texture. **PROCESS**: dominantly abiotic. **POROSITY:** bio-mouldic, framework. **DIAGENESIS:** Aggrading neomorphism, dissolution and cementation.	Reeds occur extensively on **pond** environments. This porous boundstone is a common fabric of **terraced slope** domain; however, reed structures occur commonly within the **smooth slope** topography.
CARBONATE GRAINS	GRAINSTONE/RUDSTONE/ FLOATSTONE	Carbonate grains grainstone/rudstone/floatstone consists of travertine intraclasts (a few microns up to several centimetres in size) and bioclasts within a cream coloured to light grey carbonate precipitate. Carbonated grains form sub-horizontal to inclined layers (1-10 cm thick) tens of metres laterally extended layers.	Carbonate grains grainstone/rudstone/ floatstone	**COMPONENTS:** Sub-rounded to angular intraclasts consist of already lithified travertine fragments such as clotted peloidal to rhomb-composed dendrites, crystalline dendrites, raft and reed structures. Skeletal grains are represented by ostracodes in densely packed grainstone/packestone. **PROCESS:** abiotic. **POROSITY:** Inter- particle, skeletal, bio-mouldic, inter-framework, vug. **DIAGENESIS:** Aggrading neomorphism, dissolution and cementation.	Carbonate grains diffuse in sub-horizontal layers of pool and pond deposits. In particular, fragments of already lithified travertine precipitates are common after pool rim and on dipping areas of pool of terraced slope system. They are also present in smooth slope systems. Rudstones/floatstones with intraclasts represents

Table 4.1 Classification and brief description of travertine fabric types (including components, origin, porosity and diagenesis) and their occurrence with respect to the depositional environments

Appendix 2

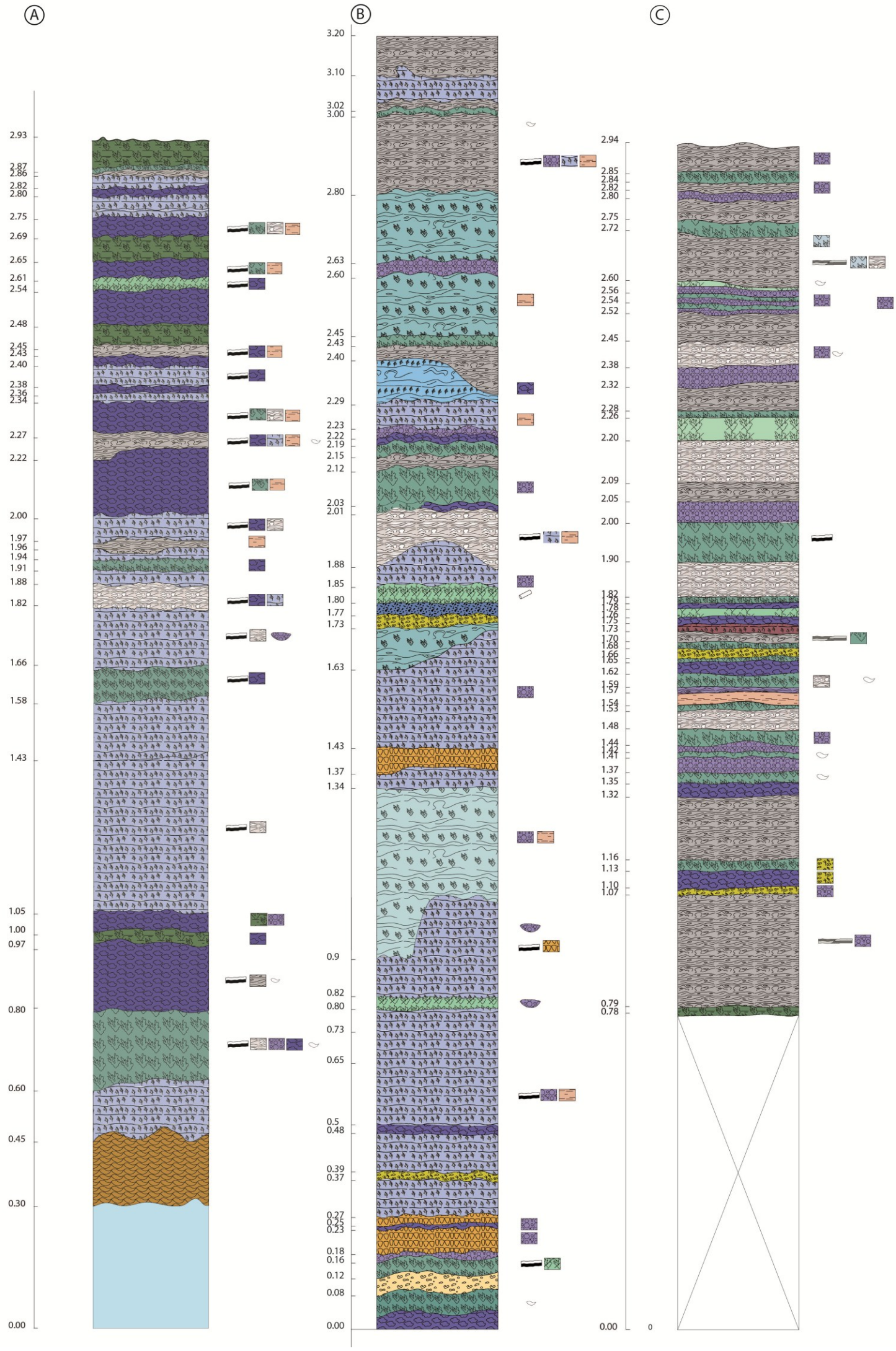

Appendix 2a. Smooth slope stratigraphic section in A and B, an d log of large pool in C . A) Low angle smooth slope (from 0 to 2 m) of Unit I passing into a pool of a terraced slope system (from 2m to 2.93m). Thick crystalline crust cementstone is the main fabric type within the smooth slope and often alternates with laminated boundstone. Rhomb-composed dendritic boundstone is also present in gently dipping low relief areas of the smooth slope. When the smooth slope evolves in a terraced slope system, this is marked by the occurrence either of a) pool sub-environments with clotted peloidal micrite dendritic boundstone, laminated boundstone, raft rudstone (on which often rhomb-composed dendritic boundstone nucleate) and carbonate grainstone/rudstone/floatstone fabric types or of b) crystalline crust cementstone of rim and wall sub-environments. B) Log showing high angle smooth slope (Unit IIa) passing upward, and laterally, into sub-horizontal pond deposits (Unit IIb), which onlap the slope system. A lithoclastic-breccia interval marks the transition from Unit IIa to IIb. Crystalline crust cementstone is the main fabric type of the smooth slope. Both thick and thin crystalline cementstone layers occur. Rhomb-composed dendritic boundstone is also present in the gently dipping areas of the smooth slope (for example at the base of the section). The terraced slope of Unit IIa is onlapped by sub-horizontal strata (IIb) that show a decimetre to centimetre scale stepped morphology. These strata are dominated by laminated and shrub-like dendritic boundstone in the sub-horizontal areas, whereas thick crystalline crust cementstone beds or isolated crystalline feather dendrite transitional to laminated boundstone are widespread in the rim morphology. C) Laminated boundstone, clotted peloidal micrite dendritic boundstone, coated bubble boundstone and raft boundstone constitute the main fabric types of the pond in Unit II. Beds with fragments of already lithified travertine are also observed. For legend see Appendix 2b

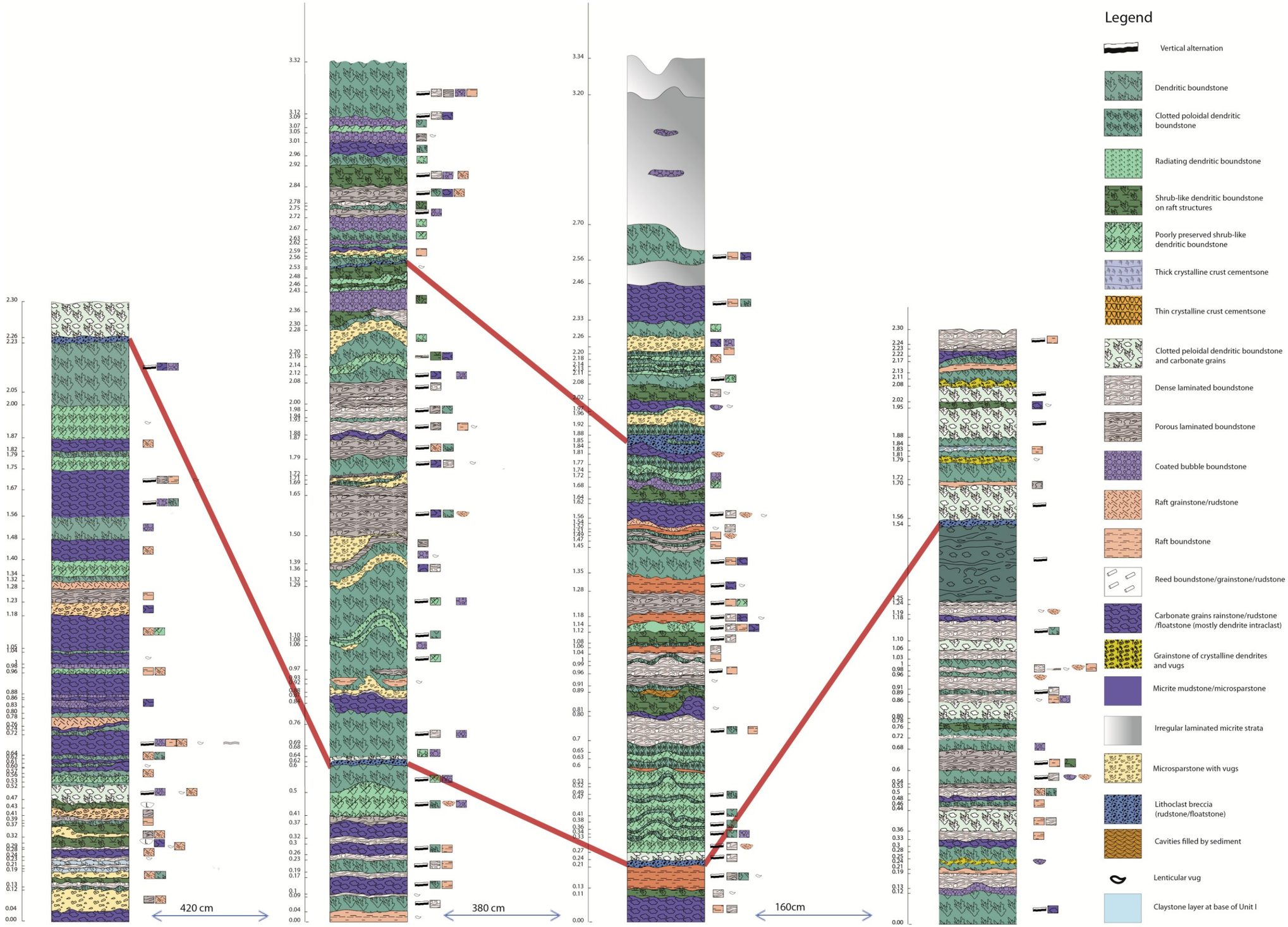

Appendix 2b) Correlation of stratigraphic logs across pool sub-environments of the terraced slope system (Unit I). The stratigraphic sections show that dendritic boundstone alternated with laminated boundstone, raft and coated bubble boundstone in the pool sub-environments. Micrite mudstone/microsparstone and intraclst grainstone/rudstone/floatstone also occur in pools. Discontinuities horizons (1-4 cm thick) are used as marked beds for the log correlation.

Acknowledgements

Foremost, I would like to express my sincere gratitude to my tutor Dr. Giovanna Della Porta who expertly guided me through this stimulating experience and for her continuous support, availability and enthusiasm. Her passion injected into me a further sense of rigor and the absolute devotion necessary to animate a research path.
I would like to express my appreciation to Prof. Elisabetta Erba for guiding the PhD students with effective organisation, understanding and sympathy.
BG Group (UK), Repsol (Brasil) and Statoil (Norway) are acknowledged and warmly thanked for funding the Ph.D. project. I am sincerely grateful to all those met during the overseas and inland meetings. In particular, I warmly thank for stimulating discussions, support and advises: Paul Wright (BG), Jeff Lukasik, Klaas Verwer, Fabio Lapponi and Josep Bernaus (Statoil), Jose Luis Algibez Alonso and Lorenzo Villallobos (Repsol).
I am grateful to Statoil and obviously to Giovanna, for the important opportunity that I had to live one of the most beautiful experience of my life: the summer internship in Bergen. I would like to thank Fabio Lapponi, Klaas Verwer, Aart- Jan van Wijngaarden, Giulio Casini and all the TNE RD EXP CARB for their support, professionality and friendship. I would like also to express my gratitude to Laurent Gindre for the interesting debate and for his kindness.
I would like to thank Dr Enrico Capezzuoli (Siena University) for the time shared in the field in Tuscany and for the stimulating discussions.
Many thanks to the Puliti family for allowing me to access and get in touch with the most concrete and visible part of my research: the “Travertine Quarry” in Saturnia.
I am also indebted to prof. Flavio Jadoul for helpful suggestions and advices. Many thanks to Dr. Alessandro Lanfranchi.
My appreciation is also directed to the Earth Sciences Department staff: Gabriele Pezzi, Giovanni Chiodi, Agostino Rizzi, Marco Foi and Curzio Malinverno are thanked for their technical assistance to my project and also for providing a positive atmosphere in for doing science. Andrea Niedermayr from Bochum University is thanked for processing the stable isotope analyses.
Dr Monica Dapiaggi, Prof. Luisa De Capitani and Dr Elena Ferrari are warmly thanked for the precious help for the XRD and geochemistry analyses.
I am grateful to Edoardo, Alessandra, Ludovica and Francesco for being a solid support in these years.
Thanks to Alessandro De Bernardo, workmate and dear friend.
I thank all my “acquario friends” for the fun that we had together, for their sensibility and affection shared with me.
Many thanks to Michela, Maria, Tizi and Ana, Peppe, Salvatore, Pamela, Alessandro, Alessia, Laetitia, Wuilmer, Kumasi, Fabio, Irene, Fabio, Cristina, Francesca and Enrico for their love and continuous presence.
But my biggest thank is addressed to my beautiful “big family”. From my deep heart my thank to my parents, to Enrico and Roberta for believing in me and supporting me during my life
A special thoughts to prof. Claudio Neri.

References

Allen, C.C., Albert, F. G., Chafetz, H. S., Combie, J., Graham, C. R, Kieft, T.L, Kivett, S. J., McKay, D.S, Taunton, A.E., Taylor, M.R, Thomas-Keprta, K.L and Westall, F., 2000. Microscopic physical biomarkers in carbonate hot springs: implications in the search of life on Mars. Icarus, 147, 49–67.

Aloisi, G, Gloter, A, Wallmann, K, Guyot, F, Zuddas, P, 2006. Nucleation of calcium carbonate on bacterial nanoglobules. Geology, 34,1017–1020.

Alonso-Zarza, A.M, and Wright, V.P (2010). Palustrine Carbonates. Developments in Sedimentology, Volume 61, 103-131. Elsevier B.V

Altunel E., and Hancock, P. L., 1993b. Morphology and structural setting of Quaternary travertines at Pamukkale, Turkey. Geological Journal, 28, 335-346.

Altunel, E. and Hancock, P.L., 1993a. Active fissuring and faulting in Quaternary travertines at Pamukkale, Western Turkey. Zschr. Geomorph. Suppl., 94, 285-302.

Altunel, E., 2005. Travertines: neotectonic indicators. In: Ozkul M, Yagiz S, Jones B (eds) Travertine, Proceedings of 1st international symposium on travertine, September 21–25, 2005, Denizli-Turkey, 120–127. Kozan Ofset, Ankara.

Amundson, R. and Kelly, E., 1987. The chemistry and mineralogy of a CO_2-rich travertine-depositing spring in the California Coast Range. Geochimica et Cosmochimica Acta, 51, 2883-2890.

Andrews , J. E., and Brasier, A. T., 2005. Seasonal records of climatic change in annually laminated tufas: short review and future prospects. Journal Of Quaternary Science 20(5) 411–421

Andrews, J. E., Riding, R., Paul, F., Dennis, P.F., 1997. The stable isotope record of environmental and climatic signals in modern terrestrial microbial carbonates from Europe Palaeogeography, Palaeoclimatology, Palaeoecology 129 171 – 189

Andrews, J.E. and Brasier, A.T., 2005. Seasonal records of climate change in annually laminated tufas: short review and future prospects. Journal of Quaternary Science, 20, 411-421.

Andrews, J.E., Pedley, H.M., Dennis, P., 2000. Palaeoenvironmental records in Holocene Spanish tufas: stable isotope approach in search of reliable climatic archives. Sedimentology 47, 9612978.

Anzalone, E., Ferreri, V., Sprovieri, M., and D'Argenio, B., 2007. Travertines as hydrologic archives: The case of the Pontecagnano deposits (southern Italy). Advances in Water Resources V., 30, 2159–2175.

Arenas, C., Auqué, L.F., Elías, M.J., Longares, L.A., Osácar, M.C., Pardo, G., Peña, J.L., Sancho, C., Vázquez, M., 2004. Depósitos tobáceos actuales y fósiles del río Piedra en el entorno del Monasterio de Piedra (provincia de Zaragoza). Geo-Guías, 1: Itinerarios Geológicos por Aragón, Sociedad Geológica de España, pp. 11–31.

Arenas-Abad, C., Va´zquez-Urbez, M., Pardo-Tirapu, G., and Sancho-Marce´ C. 2010. Fluvial and Associated Carbonate Deposits. Developments in Sedimentology, Volume 61, 133-170.

Argnani, A., Bernini, M., Di Dio, G. M., Papani, G., and Rogledi, S., 1997. Stratigraphic record of crustal scale tectonics in the Quaternary of the northern Apennines (Italy). Quaternario, 10, 595 – 602.

Arp, G, Reimer, A, Reitner, J, 2003. Microbialite formation in seawater of increased alkalinity, Satonda Crater Lake, Indonesia. Journal of Sedimentary Research 73, 105–127.

Arp, G., Thiel, V., Reimer, V., Michaelis W., Reitner, J.,1999. Biofilm exopolymers control microbialite formation at thermal springs discharging into the alkaline Pyramid Lake, Nevada, USA. Sedimentary Geology, 126, 159–176.

Atabey, E., 2002. The formation of fissure ridge type laminated travertine-tufa deposits microscopical characteristics and diagenesis, Kirşehir Central Anatolia. Mineral Res. Expl. Bul., 123-124, 59-65.

Baldi, P., Bellani, S., Ceccarelli, A., Fiordelisi, A., Squarci, P. and Taffi, L., 1995. Geothermal anomalies and structural features of southern Tuscany. World Geothermal Congress Proceedings, Florence, Italy, May 1995, 1287-1291.

Barazzuoli, P, Costantini, A, Fondi, R, Gandin, A, Ghezzo, C, Lazzarotto, A, Micheluccini, M, Salleolini, M, Salvadori, L, 1988. I travertini di Rapolano sotto il profilo geologico e geologico-tecnico. In: Coli V (ed) Il travertino di Siena. Al.Sa.Ba Grafiche, Siena, pp 26–35.

Barazzuoli, P., Costantini, A., Lazzarotto, A., Micheluccini, M., Salleolini,M., Salvadori,L. and Sandrelli, F., 1986. Ricerche strutturali ed idrogeologiche sulle aree alimentatrici del serbatoio geotermico. In: sulle risorse geotermiche a medio-bassa temperatura nella parte settentrionale

Barazzuoli P., Izzo S., Menicori, P., Micheluccini,M. & Salleolini, M. 1991. Un esempio di acquifero superficiale alimentato da acqua termale (Rapolano Terme, Siena). Boll. Soc. Geol. It. 110, 3–14.

Barberi, F., Cioni, R., Laurenzi, M.A., Sbrana, A. and Villa, I.M., 1990. Tefrostratigrafia ed evol.uzione vulcanologica della provincia comagmatica romana settentrionale. Mem. Soc. Geol. It., 45, 1001-1002.

Bargar, K.E., 1978. Geology and thermal history of Mammoth Hot Springs, Yellowstone National Park, Wyoming. U.S. Geol. Surv. Bull., 1444, 54.

Bartole, R., 1995. The North Tyrrhenian-Nothern Apennines postcollisional system-costraints for a geodynamic model. Terra Nova, 7, 7-30.

Bathurst, R.G.C., 1975. Carbonate sediments and their diagenesis. Elsevier, Amsterdam.

Bean, G.E.,1971: Turkey Beyond the Maeander, an Archaeological Guide, 262, London (Ernest Benn Ltd.)

Beech, I. B. and Gaylarde, C. C., 1999. Recent advances in the study of biocorrosion, Rev. Microbiol., 30, 177-190.

Bellani, S., Brogi, A., Lazzarotto, A., Liotta, D. and Ranalli, G., 2004. Heat flow, deep temperatures and extensional structures in the Larderello geothermal field (Italy): constraints on geothermal fluid flow. J. Vol.c. Geoth. Res., 132, 15-29.

Benedetti, S., Canino, C., Tonti, G., Medda, V., Calcaterra, P., Nappi, G., Salaffi, F., Canestrari, F., 2010. Biomarkers of oxidation, inflammation and cartilage degradation in osteoarthritis patients undergoing sulfur-based spa therapies. Clinical Biochemistry, 43, 973–978.

Benzerara, K. and Menguy, N., 2009. Looking for traces of life in minerals. C. R. Palevol., 8, 617-628.

Bertini, G., Cameli, G.M., Costantini, A., Decandia, F.A., Di Filippo, M., Dini, I., Elter, F.M., Lazzarotto, A., Liotta, D., Pandeli, E., Sandrelli, F. and Toro, B., 1991. Struttura geologica fra i Monti di Campiglia e Rapolano Terme (Toscana Meridionale). Studi Geologici Camerti, vol. speciale (1991/1), 155-178.

Billi, A. and Tiberti, M.M., 2009. Possible causes of arc development in the Apennines, central Italy. GSA Bull. (2009) http://dx.doi.org/10.1130/B26335.1.

Boccaletti, M., Elter, P. and, Guazzone, G., 1971. Plate tectonics model for the development of the Western Alps and Northern Apennines. Nature 234, 108–111.

Boch, R., Spolt, C., Reitner, J. M., and Kramers J., 2005. A lateglacial travertine deposit in Eastern Tyrol (Austria). Austrian Journal of Earth Science, 98, 78-91.

Bonazzi, U., Fazzini, P. and Gasperi, G., 1992. Note alla Carta Geologica del bacino del fiume Albegna. Boll. Soc. Geol. It., 111, 341-354.

Bonazzi, U., Fregni, P. and Gasperi, G., 1980. Il bacino neoautoctono del F. Albegna. Mem. Soc. Geol. It., 21, 260-271.

Bonny, S. M. and Jones B., 2008. Petrography and textural development of inorganic and biogenic lithotypes in a relict barite tufa deposit at Flybye Springs, NT, Canada. Sedimentology, 55, 275–303

Bortolotti, V., Sagri, M., Abbate, E.and Passerini P.,1969. Geological map of the Northern Apennines and adjoining areas. CNR.

Bose, S. and Chafetz, H.S., 2009. Topographic control on distribution of modern microbially induced sedimentary structures (MISS): A case study from Texas coast. Sedimentary Geology 213, 136–149

Bosi, C., Messina, P., Rosati, M. and Sposato, A., 1996. Età dei travertini della Toscana meridionale e relative implicazioni neotettoniche. Mem. Soc. Geol. It., 51, 293-304.

Bossio, A., Costantini, A., Lazzarotto, A., Liotta, D., Mazzanti, R., Mazzei, R., Salvatorini, G. and Sandrelli, F., 1993. Rassegna delle conoscenze sulla stratigrafia del neoautoctono toscano. Mem. Soc. Geol. Ital., 49, 17-98.

Bossio, A., Foresi, L.M., Mazzei, R., Salvatorini, G. and Sandrelli, F., 1995. Evoluzione tettonico-sedimentaria neogenica lungo una trasversale ai Bacini di Vol.terra e della Val d'Elsa. Studi Geol. Camerti, 1995/1 (volume speciale), 93-104.

Bossio, A., Foresi, L.M., Mazzei, R., Salvatorini, G., Sandrelli, F., Bilotti, M., Colli, A. and Rossetto, R., 2003-2004. Geology and Stratigraphy of the southern sector of the Neogene Albegna river basin (Grosseto, Tuscany, Italy). Geologia Romana, 37, 165-173.

Brogi, A., 2004. Faults linkage, damage rocks and hydrothermal fluid circulation: tectonic interpretation of the Rapolano Terme travertines (southern Tuscany, Italy) in the context of the Northern Apennines Neogene-Quaternary extension. Eclogae Geol. Helv., 97, 307-320.

Brogi, A., 2004. Miocene low-angle normal detachments and upper crust megaboudinage in the Mt Amiata geothermal area (Northern Apennines Italy). Geodinamica Acta 17, 375-387.

Brogi, A., 2008. The structure of the Monte Amiata volcano-geothermal area (Northern Apennines, Italy): Neogene-Quaternary compression versus extension. International Journal of Earth Sciences, 97, 677-703

Brogi, A., 2011. Variation in fracture patterns in damage zones related to strike-slip faults interfering with pre-existing fractures in sandstone (Calcione area, southern Tuscany, Italy). Journal Of Structural Geology, 33 (4),644-661. Doi: 10.1016/j.jsg.2010.12.008.

Brogi A., Capezzuoli E., Buracchi E., Branca M., 2012. Tectonic control on travertine and calcareous tufa deposition in a low-temperature geothermal system (Sarteano, Central Italy Journal of the Geological Society, London, 169, 461-476. doi: 10.1144/0016-76492011-137.

Brogi A.,and Fulignati P., 2012. Tectonic control on hydrothermal circulation and fluid evolution in the Pietratonda–Poggio Peloso (southern Tuscany, Italy) carbonate-hosted Sb-mineralization. Ore Geology Reviews, 44, 158–171.

Brogi, A. and Capezzuoli, E. 2007. Travertine deposition and faulting: the fault-related travertine fissure-ridge at Terme S. Giovanni, Rapolano Terme (Italy). International Journal of Earth Sciences (Geol Rundsch), DOI 10.1007/s00531-007-0290.

Brogi, A. and Capezzuoli, E., 2009. Travertine deposition and faulting: the fault-related travertine fissure ridge at Terme S. Giovanni , Rapolano Terme (Italy). Int. J. Earth Sci, 98, 931-947.

Brogi, A., Capezzuoli, E., Aque´, R., Branca, M., Voltaggio, M., 2010. Studying travertines for neotectonics investigations: Middle–Late Pleistocene syn-tectonic travertine deposition at Serre di Rapolano (Northern Apennines, Italy). Int J Earth Sci (Geol Rundsch) 99, 1383–1398 DOI 10.1007/s00531-009-0456-y

Brogi, A., Costantini, A. and Lazzarotto, A., 1999 . Carta geologica dell'area di Rapolano Terme. Sel. Ca, Firenze, 1999.

Brogi, A. and Fabbrini, L. 2009. Extensional and strike-slip tectonics across the Monte Amiata–Monte Cetona transect (Northern Apennines, Italy) and seismotectonic implications. tectonophysics, 476, 195–209.

Brogi, A. and Liotta, D., 2008. Highly extended terrains, lateral segmentation of the substratum, and basin development: the Middle-Late Miocene Radicondoli Basin (inner northern Apennines, Italy). Tectonics, 27, TC 5002. doi:10.1029/2007TC002188.

Brogi, A., Liotta, D., Meccheri, M., and Fabbrini, L., 2010. Transtensional shear zones controlling volcanic eruptions: the Middle Pleistocene Mt Amiata volcano (inner Northern Apennines, Italy) Terra Nova, 22, 137–146.

Brogi, A., Lazzarotto, A., Liotta, D., Ranalli, G., 2005. Crustal structures in the geothermal areas of southern Tuscany (Italy): insights from the CROP 18 deep seismic reflection lines. J. Vol.canol. Geoth. Res., 148, 60-80.

Buczynski, C. and Chafetz, H.S., 1991. Habit of bacterially induced precipitates of calcium carbonate and the influence of medium viscosity on mineralogy. J. Sediment. Petrol., 61, 226-233.

Burne, R.V., Moore, L.S, 1987. Microbialites: organo-sedimentary deposits of benthic microbial communities. Palaios 2, 241–254.

Calcagnile, G. and Panza, G.F., 1980. The main characteristics of the lithosphere-astenosphere system in Italy and surrounding regions. Pure Appl. Geophys., 199, 865-879.

Capezzuoli, E., Gandin, A. and Sandrelli, F., 2008a. Evidence of associated deposition of travertine and calcareous tufa in the Quaternary carbonates of Valdelsa Basin (Tuscany). Italian Journal of Quaternary Science, 21(1B), 113-124.

Capezzuoli, E., Gandin, A. and Sandrelli, F., 2008b. Calcareous tufa as indicators of climatic variability: a case from the Southern Tuscany (Italy). Workshop “Tufas, Speleothems and Stromatolites: Unravelling the Physical and Microbial Controls”. University of Hull (UK), 23-24 Maggio 2008, Abstract Volume, 6.

Capezzuoli, E., Gandin, A., and Pedley, H.M., 2009. Field Trip Guide Book: Travertines and calcareous tufa in Tuscany (Central Italy). 27th IAS Meeting Sedimentary of Mediterranean Island(S), Field trip 7,129-158.

Carmignani, L., Conti, P., Cornamusini, G. and Meccheri, M., 2004. The internal northern Apennines, the northern tyrrhenian sea and the Sardinia-Corsica block. Geology of Italy, spec. vol. of It. Geol. Soc. for IGC32 Florence- 2004, 59-77.

Carmignani, L., Decandia, F.A., Disperati, L. et al., 2001. Inner Northern Apennines. In “Anatomy of an Orogen: the Apennines and adjacent, Mediterranean basin” (G.B. Vai and I.P. Martini Eds.). Kluwer Academic Publishers Dordrecht, 197-214.

Carmignani, L., Decandia, F.A., Disperati, L., Fantozzi, P.L., Lazzarotto, A., Liotta, D. and Oggiano, G., 1995. Relationships between the Sardinia-Corsica-Provencal Domain and the Northern Apennines. Terra Nova, 7, 128-137.

Carmignani, L., Decandia, F.A., Fantozzi, P.L., Lazzarotto, A., Liotta, D. and Meccheri, M., 1994. Tertiary extensional tectonics in Tuscany (Northern Apennines, Italy). Tectonophysics, 238, 295-315.

Carmignani, L., Funedda, A., Oggiano, G. et al., 2004. Tectono-sedimentary evolution of southwest Sardinia in the paleogene: Pyrenaic or apenninic dynamic? Geodinamica Acta,17 (4), 275-287.

Carrara C., Ciuffarella L., Paganin G., 1998. Inquadramento geomorfologico e climatico ambientale dei travertini di Rapolano Terme (Siena). Il Quaternario 11, 319–329.

Carthew, K.D., Taylor, M.P., Drysdale, R.N., 2003. Are current models of tufa sedimentary environments applicable to tropical systems? A case study for the Gregory River. Sedimentary Geology, 162, 199-218.

Casanova, J., 1986. East African Rift stromatolites, in Frostick, L. E., Renaut, R. W., Reid, I., and Tiercelin, J. J., eds., Sedimentation in the African rifts: Oxford, Blackwell, 201–210.

Castanier, S., Le Métayer-Levrel, G., Perthuisot, J.P., 2000. Bacterial roles in the precipitation of carbonate minerals. In Microbial Sediments (eds Riding RE, Awramik SM). Springer-Verlag, Berlin, 32–39.

Castellarin, A., Cantelli, L., Fesce, A.N., Mercher, J.L., Picotti, V., Pini, G.A., Prosser, G. and Selli, L., 1992. Alpine compressional tectonics in the southern Alps. Relationships with the Northern Apennines. Annales tectonicae 6, 62–94.

Castennholz , R.W., 1994. Microbial mats research: the recent past and the new perspectives. In: Stall L,J, Caumette P (Eds) Microbial mats: structure, developments and environmental significance. Springer, Berlin Heidelberg New York, 3-18.

Chafetz, H. S. and Buczynski, C., 1992. Bacterially induced lithification of microbial mats. Palaios, 7, 277-293.

Chafetz, H. S. and Folk, R. L., 1984. Travertines: Depositional morphology and the bacterially constructed constituents. Journal of Sedimentary Petrology, 54, 289-316.

Chafetz, H.S. and Guidry, S.A., 1999. Bacterial shrubs, crystal shrubs, and ray-crystal shrubs: bacterial vs. abiotic precipitation. Sedimentary Geology, 126, 57-74.

Chafetz, H.S. and Lawrence, J.R., 1994. Stable isotopic variability within modern travertines. Géographie Physique et Quaternaire, 48, 257-273.

Chafetz, H.S. and Meredith, J.C., 1983. Recent travertine pisoliths (pisoids) from southeastern Idaho, U.S.A. In: Peryt, T.M., ed., Coated Grains, Springer-Verlag, 450-455.

Chafetz, H.S., Akdim, B., Julià, R. and Reid, A., 1998. Mn-and-Fe-rich black travertine shrubs: bacterially (and nannobacterially) induced precipitates. Journal of Sedimentary Petrology, 68, 404-412.

Chafetz, H.S., Rush, P.F.and Utech, N.M., 1991. Microenviromental controls on mineralogy and habitat of CaCO3 precipitates: an example from an active travertine system. Sedimentology, 38, 107-126.

Chafetz, H.S., Utech, N.M. and Fitzmaurice, S.P., 1991b. Differences in the δ18O and δ13C signatures of seasonal laminae comprising travertine stromatolites. Journal of Sedimentary Petrology, 61, 1015-1028.

Channel, R.J.P., Owsisnks, A.M. and Walker, J.M., 1988. Results of a large scale screening programme to detect anti-bacterial activity from fresh-water algae. Br Phylcol J, 24, 41-44.

Chen, J., Zhang, D.D., Wang, S., Xiao, T. and Huang, R., 2004. Factors controlling tufa deposition in natural waters at waterfall sites. Sedimentary Geology, 166, 353-366.

Chiodini, G., Frondini, G., Cardellini, C., Parello, F. and Peruzzi, L., 2000. Rate of diffuse carbon dioxide Earth degassing estimated from carbon balance of regional aquifers: the case of central Apennine, Italy. J. Geophys. Res., 105, 8423-8434.

Choquette, P.N. and Pray, C., 1970. Geologic nomenclature and classification of porosity in sedimentary carbonates, Bull. Am. Ass. Petrol. Geol., 54, 207–250.

Costantini, A., Lazzarotto, A. and Sandrelli, F., 1982. Conoscenze geologico strutturali in: il Graben di Siena. CNR PFE RF9,11–32. del Bacino di Siena. CNR PFE SEG SI-4, 175-189.

Costerton, J.W., Geesey, G. G. and Cheng, K.J., 1978. How bacteria stick. Scientific American, 238 (1), 86-95.

Costerton, J.W., Lewandowski, Z., Caldwell, D.E., Korber, D.R. and Lappin-Scott, H.M., 1995. Microbial biofilms. Annu. Rev. Microbiol., 49, 711-745.

Dandurand, J.L., Gout, R., Hoefs, J., Menschel, G., Schott, J. and Usdowski, E., 1982. Kinetically controlled variations of major components and carbon and oxygen isotopes in a calcite-precipitating spring. Chemical Geology, 36, 299-315.

Decandia, F.A., Lazzarotto, A., Liotta, D., Cernobori, L. and Nicolich, R., 1998. The Crop 03 Traverse: Insights On Post-Collisional Evol.ution Of Northern Apennines. Mem. Soc. Geol. It., 52, 427-439.

Decho, A.D., 1990. Microbial exopolymeric secretions in ocean environments: their role (s) in food webs and marine processes. Oceanogr. Mar. Biol. Annu. Rev., 28, 73-154.

Decho, A.D., 2000b. Exopolymer microdomains as a structuring agent for heterogeneity within microbial biofilms. In: Riding, R.E., Awramik, S.M. (Eds.), Microbial Sediments. Springer-Verlag, N.Y, 1-9.

Deer, W. A., R. A. Howie, and Z. Zussman 1992. An Introduction to the Rock-Forming Minerals. Addison–Wesley–Longman, Essex, UK.

Defarge, C., J. Trichet, A.-M. Jaunet, M. Robert, J. Tribble, and F. J. Sansone 1996. Microbial sediments revealed by cryo-scanning electron microscopy. J. Sed. Res. 66, 935–947.

Dini, A., Gianelli, G., Puxeddu, M., Ruggieri, G., 2005. Origin and evol.ution of Pliocene–Pleistocene granites from the Larderello geothermal field (Tuscan Magmatic Province, Italy). Lithos, 81, 1-31. doi:10.1016/j.lithos.2004.09.002.

Dini, A., Mazzarini, F., Musumeci, G., Rocchi, S., 2008. Multiple hydrofracturing by boron-rich fluids in the Late Miocene contact aureole of Eastern Elba Island (Tuscany, Italy). Terra Nova, 20, 318-326. doi:10.1111/j.1365-3121.2008.00823.x.

Drew, G. H., 1914, On the precipitation of calcium carbonate in the sea by marine bacteria, and on the action of denitrifying bacteria in tropical • and temperate seas: Carnegie Institution of Washington Publication ,182, 7-45.

Duchi, V., Giordano, M.V. and Martini, M., 1978. Riesame del problema della precipitazione di calcite od aragonite da soluzione naturali, Rend. Soc. Ital. Miner. Pet., 34, 605–618.

Dunham, R.J., 1962. Classification of carbonate rocks according to depositional texture. In: Ham, W.E. (Ed.), Classification of Carbonate Rocks. American Association of Petroleum Geologists Memoir, 1, 1082121.

Dupraz C, Reid, RP, Braissant, O, Decho, AW, Norman, RS, Visscher, PT,2009. Processes of carbonate precipitation in modern microbial mats. Earth Science Reviews 96, 141–162.

Dupraz, C. and Visscher, P.T., 2005. Microbial lithification in marine stromatolites and hypersaline mats. Trends in Microbiology, 13 (9), 429-438.

Dupraz, C., Visscher, P.T, Baumgartner, L.K. and Reid, R.P., 2004. Microbe–mineral interactions: early carbonate precipitation in a hypersaline lake (Eleuthera Island, Bahamas). Sedimentology, 51, 745-765.

Elter, F. M.,Elter, P., Eva, C., et al., 2011. Strike-slip geometry inferred from the seismicity of the Northern-Central Apennines (Italy). Journal Of Geodynamics, 52 (5), 379-388,Doi. 10.1016/j.jog.2011.03.003.

Embry, A.F., Klovan, E., 1971. A late Devonian reef tract on northeastern Banks Island, N.W.T. Canadian Society of Petroleum Geologists Bulletin 19, 7302781.

Evans, J.E., 1999. Recognition and implications of Eocene tufas and travertines in the Chadron Formation, White River Group, Badlands of South Dakota. Sedimetology, 46: 771-789.

Faccenna, C., Becker, T.W., Lucente, F.P., Jolivet, L. and Rossetti, R., 2001. History of subduction and back-arc extension in the Central Mediterranean. Geophys. J. Int., 145, 809–820.

Faccenna, C., Soligo, M., Billi, A., De Filippis, L., Funiciello, R., Rossetti C., Tuccimei, P., 2008. Late Pleistocene depositional cycles of the Lapis Tiburtinus travertine (Tivoli, Central Italy): Possible influence of climate and fault activity. Global and Planetary Change, 63, 299–308.

Farmer, J. D., and Des Marais, D. J., 1994. Biological versus inorganic processes in stromatolite morphogenesis: Observations from mineralizing sedimentary systems. In Microbial Mats: Structure, Development and Environmental Significance (L. J. Stal and P. Caumette, Eds.), pp. 61–68, Springer Verlag, New York.

Farmer, J.D., 2000. Hydrothermal systems: doorways to early biosphere evolution. GSA Today, 10, 1-9.

Ferrari, L., Conticelli, S., Burlamacchi, L., Manetti, P., 1996. Volcanological evolution of the Monte Amiata Southern Tuscany: new geological and petrochemical data. Acta Vulcanol., 8, 41–56.

Ferris, F.G., 2000. Microbe-Metal Interaction in sediment. In Riding R.E and Awramik S.M (Eds) (2000). Microbial sediments. Springer-Verlag Berlin Heidelberg.

Flanagan, L.B., Ehleringer, J.R., Marshall, J.D., 1992. Differential uptake of summer precipitation among co-occurring trees and shrubs in a pinyon-juniper woodland. Plant Cell and Environ, 15, 831-836.

Flügel, E., 2004 Microfacies of Carbonate Rocks: Analysis, Interpretation and Application Springer, Berlin, 976.

Folk, R.L., 1959. Practical petrographic classification of limestones, Bull. Am. Ass. Petrol. Geol., 43, 1–38.

Folk, R. L., 1962, Spectral subdivision of limestone types, in W. E.Ham, ed., Classification of Carbonate Rocks: Tulsa, OK, American. Association of Petroleum Geologists Memoir 1, p. 62-84.

Folk, R. L., 1965, Some aspects of recrystallization in ancient limestones, in L. C. Pray, and R. S. Murray, eds., Dolomitization and Limestone Diagenesis: Tulsa, OK, SEPM Special Publication No. 13, p. 14-48.

Folk, R. L., 1992. Bacteria and nannobacteria revealed in hardgrounds, calcite cements, native sulfur, sulfide minerals, and travertines. Geol. Soc. America Abs. Programs 24, 104.

Folk, R. L., 1993b. Dolomite and dwarf bacteria (nannobacteria). Geol. Soc. America Abs. Programs 25, A-397.

Folk, R.L., 1994. Interaction between bacteria, nannobacteria, and mineral precipitation in hot springs of central Italy. Géographie physique et Quaternaire, 48, 233-246.

Folk, R.L., and Chafetz, H.S. 1983. Pisoliths (pisoids) in Quaternary travertines of Tivoli, Italy. In: Coated Grains (Ed T. Peryt), 474-487. Springer.

Folk, R.L., Chafetz, S. and Tiezzi, P.A., 1985. Bizarre forms of depositional and diagenetic calcite in hot-spring travertines, central Italy. Carbonate Cements (Eds by N. Schneidermann and P. M. Harris), Spec.publs Soc. econ. Paleont. Miner., Tulsa, 36, 349-369.

Folk., R. L, 1993. SEM imaging of bacteria and nannobacteria in carbonate sediments and rocks. Journal of Sedimentary Petrology, 63, 990-999.

Ford, T.D., Pedley, H.M., 1996. A review of tufa and travertine deposits of the world. Earth-Science Reviews, 41, 117-175.

Fouke, B. W., 2011. Hot-spring Systems Geobiology: abiotic and biotic influences on travertine formation at Mammoth Hot Springs, Yellowstone National Park, USA. Sedimentology, 58, 170–219.

Fouke, B.W., Farmer, J.D., Des Marais, D.J., Pratt, L., Sturchio, N.C., Burns, P.C. and Discipulo, M.K., 2000. Depositional facies and aqueous-solid geochemistry of travertine-depositing hot springs (Angel Terrace, Mammoth Hot Springs, Yellowstone National Park, USA). J. Sediment. Res., 70, 265-285.

Francese, R., Mazzarini, F., Bistacchi, A., Morelli, G., Pasquarè, G., Praticelli, N., Robain, H., Wardell, N. and Zaja, A., 2009. A structural and geophysical approach to the study of fractured aquifers in the Scansano-Magliano in Toscana Ridge, Southern Tuscany, Italy. Hydrogeology Journal ScholarOne support: (434)817.2040 ext. 167.

Frank, N., Braum, M., Hambach, U., Mangini, A. and Wagner, G., 2000. Warm period growth of travertine during the last interglaciation in Southern Germany, Quat. Res., 54, 38–48.

Freytet, P. and Verrecchia, E., 1998. Freshwater organisms that build stromatolites: a synopsis of biocrystallization by prokaryotic and eukaryotic algae. Sedimentology, 45, 535-563.

Freytet, P. and Verrecchia, E.P., 1999. Calcitic radial palisadic fabric in freshwater stromatolites: diagenetic and recrystallized feature or physicochemical sinter crust. Sedimentary Geology, 126, 97-102.

Friedman, I., 1970. Some investigations of the deposition of travertine from hot springs – 1. The isotopic chemistry of a travertine-depositing spring, Geochim. Cosmochim. Acta, 34, 1303–1315.

Frisia, S., Borsato, A., Fairchild, I. J., and Mcdermott, F., 2000. Calcite fabrics, growth mechanisms, and environments of formation in speleothems from the Italian Alps and Southwestern Ireland. Journal of Sedimentary Research, Vol. 70, N° 5, 1183–1196.

Gandin, A. and Capezzuoli, E., 2008.Travertine versus Calcareous tufa: distinctive petrologic features and stable isotopes signatures. Italian Journal of Quaternary Science, 21(1B), 125-136.

Gernot, A.G., Thiel, V., Reimer, V., Michaelis, W. and Reitner, J.,1999. Biofilm exopolymers control microbialite formation at thermal springs discharging into the alkaline Pyramid Lake, Nevada, USA. Sedimentary Geology, 126, 159-176.

Geurts, M.A., 1976. Formation de travertins postglaciaries en Belgique. In: T. Vogt (Editor): Colloque Types de Crofltes et leur rrpartition regionale, Strasbourg 9-11 Janier 1975. Universit6 de Louis Pasteur, Strasbourg, pp. 76-79.

Gibert, R.O., Taberner, C., Saez, A., Giralt, S., Alonso Ricardo, N., Edwards, R.L. and Pueyo, J. J., 2009. Igneous origin of CO2 in ancient and recent hot-spring waters and travertines from the Northen Argentinean Andes. Journal of Sedimentary Research, 79, 554-567.

Gierlowski-Kordesch, E.H., 2010. Lacustrine carbonates, in Alonso-Zarza, A.M. and Tanner, L.H., Eds., Carbonates in Continental Settings: Processes, Facies, and Application, Developments in Sedimentology 61, Elsevier, Amsterdam, 1-101.

Given, R.K. and Wilkinson, B.H., 1985. Kinetic control of morphology, composition, and mineralogy of abiotic sedimentary carbonates. Journal of Sedimentary Petrology, 55, 109-119.

Glover, C., and Robertson, A.H.F., 2003. Origin of tufa (cool water carbonate) and related terraces in the Antalya area, SW Turkey. Geol. J., 38, 329–358.

Golubic, S., 1969. Cyclic and non-cyclic mechanisms in the formation of travertine. Verh. Int. Ver. Theor. Ungew. Limnol., 17: 956-961.

Golubic, S., 1973.The relationship between blue-green algae and carbonate deposits, 434–472, in: N.G. Carr, B.A. Whitton (eds), The Biology of Blue-green Algae, Oxford (Blackwell).

Gonfiantini, R., Panichi, C. and Tongiorgi, E., 1968. Isotopic disequilibrium in travertine deposition. Earth and Planetary Sc. Lett., 5, 55-58.

Gran, G., 1952. Determination of the equivalence point in potentiometric titrations- Part II.- The Analyst, 77, 661-671.

Gregor, H.H., 1982. Die miozane Flora aus dem Bottinger Thermalsinterkalkeine. Revision. Stuttgart Beitr. Naturkd , ser. B, 88, 1-15.

Guo, L. and Riding, R., 1992. Aragonite laminae in hot water travertine crusts, Rapolano Terme, Italy. Sedimentology, 39, 1067-1079.

Guo, L. and Riding, R., 1994. Origin and diagenesis of Quaternary travertine shrub fabrics, Rapolano Terme, Central Italy. Sedimentology, 41, 499-520.

Guo, L. and Riding, R., 1998. Hot-spring travertine facies and sequence, Late Pleistocene, Rapolano Terme, Italy. Sedimentology, 45, 163-180.

Guo, L. and Riding, R., 1999.Rapid facies changes in Holocene fissure ridge hot spring travertines, Rapolano Terme, Italy. Sedimentology, 46, 1145-1158

Guo, L., Andrews, J., Riding, R., Dennis, P. and Dresser, Q., 1996. Possible microbial effects on stable carbon isotopes in hot travertine. J. Sed. Res. 66, 468-473.

Hammer O. Dysthe D.K. and Jamtveit B., 2007.The dynamics of travertine dams. Earth and Planetary Science Letters, 256, 258-263.

Hancock, P.L., Chalmers, R.M.L., Altunel, E. and Cakir Z., 1999. Travitronics: using travertines in active fault studies. J. Struct. Geol., 21, 903-916.

Harris, A. G., E. Tuttle, and S. D. Tuttle 1990. Hot Springs National Park. In Geology of National Parks, pp. 568–576. Kendall/Hunt, Dubuque, IA.

Hartley, A., House, W., Callow, M. and Leadbetter, B., 1996. The use of microelectrodes to study the precipitation of calcite upon algal biofilms. J. Colloid. Interface Sci., 183, 498-505.

Herman, J. and Lorah, M., 1987. CO2 outgassing and calcite precipitation in Falling Spring Creek, Virginia, U.S.A. Chemical Geology, 62, 251-262.

Herman, J. and Lorah, M., 1988. Calcite-precipitation rates in the field: measurement and prediction for a travertine-depositing stream. Geochimica et Cosmochimica Acta, 52, 2347-2355.

Hinga, K.R., Arthur, M.A., Pilson, M.E.Q., Whitaker, D., 1994. Carbon isotope fractionation by marine phytoplankton in culture: the effects of CO2 concentration, pH, temperature and species. Global Biogeochemical Cycles 8, 912102.

Horvatincic, N., Calic, R., Geyh, M.A., 2000. Interglacial growth of tufa in Croatia. Quaternary Research, 53, 185-195.

Innocenti, F., Serri, G., Ferrara, G., Manetti, P. and Tonarini, S., 1992. Genesis and classification of the rocks of the Tuscan Magmatic Province: thirty years after Marinelli's model. Acta Vulcanologica, 2, 247-265.

Irion, G. and Muller, G., 1968. Mineralogy, petrology and chemical composition of some calcareous tufa from the Swabische Alb, Germany. In: G. Muller and G.M. Friedmen (Editors): Recent Developments in Carbonate Sedimentology in Central Europe. Springer-Verlag, Berlin, pp. 157-171.

Jacobson, R.L. and Usdowski, E., 1975. Geochemical controls on a calcite precipitating spring. Contributions to Mineralogy and Petrology, 51, 65-74.

Jones, B. and Renaut, R.W., 1995. Non-crystallographic calcite dendrites from hot-spring deposits at Lake Bogoria, Kenya: Journal of Sedimentary Research, A65, 154-169.

Jones, B. and Renaut, R.W., 1996a. Skeletal crystals of calcite and trona from hot-spring deposits in Kenya and New Zealand: Journal of Sedimentary Research, 66, 265-274.

Jones, B. and Renaut, R.W., 2010. Calcareous spring deposits in continental settings. In: Alonso-Zarza, A.M., Tanner, L.H. (Eds), Continental Settings: Processes, Facies and Applications. Developments in Sedimentology. Elsevier, Amsterdam, 61.

Jones, B., Peng, X., 2012. Intrinsic versus extrinsic controls on the development of calcite dendrite bushes, Shuzhishi Spring, Rehai geothermal area, Tengchong, Yunnan Province, China. Sedimentary Geology , 249–250, 1 April, 45–62.

Jones, B., Renaut, R.W. and Rosen, M.R., 1996. High-temperature (W901C) calcite precipitation at Waikite Hot Springs, North Island, New Zealand. Geological Society of London, 153, 481-496.

Jones, B., Renaut, R.W., 2010. Calcareous spring deposits in continental settings. In: Alonso-Zarza, A.M., Tanner, L.H. (Eds), Carbonates in Continental Settings: Facies, Environments, and Processes. Developments in Sedimentology, 61, Elsevier, Amsterdam, 177–223.

Julia, R., 1983. Travertines. In: Carbonate Depositional Environments (Eds P.A. Schole, D.G. Bebout and C. Moore), AAPG Mem., 33, 64–72.

Kano, A., Hagiwara, R., Kawai, T., Hori, M., Matsuoka, J., 2007. Climatic conditions and hydrological change recorded in a high-resolution stable-isotope profile of a recent laminated tufa on a subtropical island, southern Japan. Journal of Sedimentary Research 77, 59267.

Kano, A., Matsuoka, J., Kojo, T., and Fujii, H., 2003. Origin of annual laminations in tufa deposits, southwest Japan: Palaeogeography, Palaeoclimatology, Palaeoecology, v. 191, p. 243–262.

Kawaguchi, T. and Decho, A.W. 2002. Isolation and biochemical characterization of extracellular polymeric secretions (EPS) from modern soft marine stromatolites (Bahamas) and its inhibitory effect on CaCO3 precipitation. Prep. Biochem. Biotechnol., 32, 51–63.

Kazmierczak, J., Krumbein, W.E., 1983. Identification of calcified coccoid cyanobacteria forming stromatoporoid stromatolites. Lethaia 16, 2072213.

Kele, S., Demény, A., Siklòsy, Z., Németh, T., Tòth, M.B. and Kovàcs M., 2008. Chemical and stable isotope composition of recent hot-water travertines and associated thermal waters, from Egerszalók, Hungary: Depositional facies and non-equilibrium fractionation. Sediment. Geol. 2008, 211, 53.

Kele, S., Özkul, M ., Fórizs, I., Gökgöz, A., Baykara, M.O., Alçiçek, M. C., Németh, T., 2011. Stable isotope geochemical study of Pamukkale travertines: New evidences of low-temperature non-equilibrium calcite-water fractionation. Sediment. Geol. (2011), doi:10.1016/j.sedgeo.2011.04.015

Kelts, K. and Hsu, K.J., 1978. Freshwater carbonate sedimentation. In: Lerman, A. (Ed.), Lakes: Chemistry, Geology, Physics. Springer, Berlin, 295-323.

Kitano, Y., 1963. Geochemistry of calcareous deposits found in hot springs. J. Earth Sci., 2, 68-100.

Knorre, H.V. and Krumbein, W.E., 2000. Bacterial calcification. In Microbial Sediments (eds Riding RA, Awramik SM). Springer- Verlag, Berlin, 25–31.

Koşun, E., Sarigül, A. and Varol, B., 2005. Sedimentological investigation of Antalya tufas. In: Özkul, M., Yagiz, S., Jones, B. (Eds), Proceedings of the 1st International Symposium on Travertine. Kozan Ofset Matbaacilik San. ve Tic. Ltd. Sti. Ankara, 50-61.

Koşun, E., Sarıgül, A., Varol, B., 2005. Lithofacies characteristics of Antalya Tufa. Min Res Explor Bull (Ankara) 130, 57–70.

Krumbein, W.E., 1983. Stromatolites – the challenge of a term in space and time. Precambrian Res., 20, 493–531.

Krumbein, W.E., Cohen, Y., Shilo, M., 1977. Solar Lake (Sinai). 4.Stromatolitic cyanobacterial mats. Limnology and Oceanography 22, 635–656.

Larsen, D., and Crossey L.J , 1996. Depositional environments and paleolimnology of an ancient caldera lake: Oligocene Creede Formation, Colorado. Geological Society of America Bulletin 108, 526-544.

Last, F. M., Last W.M., and Halden N.M., 2010. Carbonate microbialites and hardgrounds from Manito Lake, an alkaline, hypersaline lake in the northern Great Plains of Canada. Sedimentary Geology 225, 34–49.

Lazzarotto A., 1973. Caratteri strutturali dei nuclei mesozoici di Montalceto, Trequanda e Piazza di Siena (Prov. di Siena). Atti Soc. Tosc. Sc. Nat. Mem. Serie A 79, 251–266.

Liotta D., Pandeli E., Sandrelli F., and Toro B., 1991. Struttura geologica fra i monti di Campiglia e Rapolano Terme (Toscana meridionale): stato attuale delle conoscenze e problematiche. Studi Geol. Camerti 1, 155–178.

Liotta, D., 1994. La tettonica distensiva post-collisionale nell'Area Geotermica di Larderello (Toscana meridionale), Studi Geol. Camerti, vol. spec. 1, 183-193.

Liotta, D., Cernobori, L. and Nicolich, R., 1998. Restricted rifting and its coexistence with compressional structures: results from the CROP03 traverse (Northern Apennines, Italy). Terra Nova, 10, 16-20.

Lippmann F. (1973) - Sedimentary carbonate minerals. Springer-Verlag, Berlin, 228 pp

Locardi, E. and Nicolich, R., 1988. Geodinamica del Tirreno e dell'Appennino centromeridionale: la nuova carta della Moho. Mem. Soc. Geol. Ital., 41, 121-140.

Locardi, E. and Nicolich, R., 1992. Geodinamica del Tirreno e dell'Appennino centromeridionale: la nuova carta della Moho. Mem. Soc. Geol. It. 41, 121–140.

Love, K.M. and Chafetz, H.S.,1988. Diagenesis of laminated travertine crust , Arbukle Mountains, Oklahoma. Journal of Sedimentary Petrology, 58 (no 3), 441-445.

Malesani, P. and Vannucchi, S., 1975. Precipitazione di calcite o di aragonite dalle acque termominerale in relazione alla genesi e all'evoluzione dei travertini. Atti della R. Accademia d'Italia, 58, 761-776.

Manfra, L., Masi, U. and Turi, B., 1976. La composizione isotopica dei travertini del Lazio. Geol. Rom., 15, 127-174.

Manzo, E., Perri, E. and Tucker, M.E., 2012. Carbonate deposition in a fluvial tufa system: processes and products (Corvino Valley - southern Italy). Sedimentology, 59, 553-577.

Marinelli, C., Barberi, F. and Cioni, R., 1993. Sollevamenti neogenici ed intrusioni acide della Toscana e del Lazio settentrionale. Mem. Soc. Geol. It., 49, 279-288.

Martelli, L., Moratti, G. and Sani, F., 1989. Analisi strutturale dei travertini della Toscana meridionale (Valle dell'Albegna). Boll. Soc. Geol. Ital., 108, 197-205.

Martini, I.P. and Sagri, M., 1993. Tectonosedimentary characteristics of Late Miocene-Quaternary extensional basins of the Nothern Apennines. Earth-Sci. Rev., 34, 197-233.

Martini, I.P., Sagri, M., 1993. Tectono-sedimentary characteristics and the genesis of the recent magmatism of Southern Tuscany and Northern Latium. Per. Mineral. 56, 157–172.

Mauffret, A., Contrucci, I. and Brunet, C., 1999. Structural evolution of Nothern Tyrrhenian Sea from new seismic data. Mar. Petrol. Geol., 16, 381-407.

McConnaughey, T., 1989. 13C and 18O isotopic disequilibrium in biological carbonates II: In vitro simulation of kinetic isotope effects, Geochim. Cosmochim. Acta, 53, 163–171.

Melezhik, V.A. and Fallick A.E., 2001. Palaeoproterozoic travertines of volcanic affiliation from a 13C-rich rift lake environment. Chemical Geology, 173, 293–312.

Melezhik, V.A., Fallick, A.E. and Grillo, S.M., 2004. Subaerial exposure surfaces in a Palaeoproterozoic 13C-rich dolostone sequence from the Pechenga Greenstone Belt: Palaeoenvironmental and isotopic implications for the 2330-2060 Ma global isotope excursion of 13C/12C. Precambrian Research, 133(1-2), 75-103.

Merla G., 1951. Geologia dell'Appennino Settentrionale. Boll. Soc. Geol. It., 70, 95-382.

Merz-PreiB, M., 2000. Calcification in cyanobacteria In Riding R.E and Awramik S.M (Eds) (2000). Microbial sediments. Springer-Verlag Berlin Heidelberg.

Merz-Preiβ, M. and Riding, R., 1999. Cyanobacterial tufa calcification in two freshwater streams: ambient environment, chemical thresholds and biological processes. Sedimentary Geology, 126, 103-124.

Minissale , A., Magro G., Vaselli, O., Verrucchi, C., Perticone, I., 1997: Geochemistry of water and gas discharges from the Mt. Amiata silicic complex and surrounding areas (central Italy). Journal of Volcanology and Geothermal Research, 79, 223 -251.

Minissale A, Kerrick, D.M, Magro, G, Murrell MT, Paladini, M, Rihs, S, Sturchio, NC, Tassi, F, Vaselli, O., 2002. Geochemistry of Quaternary travertines in the region north of Rome (Italy): structural, hydrologic and paleoclimatic implications. Earth Planet Sci Lett 203:709–728. doi:10.1016/S0012-821X(02)00875-0.

Minissale, A. and Sturchio, N.C., 2004. Field Trip Guide Book: "Travertines of Tuscany and Latium (central Italy)".32nd International Geological Congress, 4, 14-36.

Minissale, A., 2004. Origin, transport and discharge of CO2 in central Italy. Earth-Science Reviews, 66 (1-2), 89-141.

Minissale, A., Evans, W.C., Magro, G., Vaselli, O., 1997: Multiple source components in gas manifestations from north-central Italy. Chem. Geol., 142, 175 - 192.

Minissale, A., Vasellia, O., Tassi, F., Magro, G. and Grechi, G.P., 2002. Fluid mixing in carbonate aquifers near Rapolano (central Italy): chemical and isotopic constraints Applied Geochemistry, 17, 1329-1342.

Molli, G., 2008. Northern Apennine–Corsica orogenic system: an updated overview. Geological Society, London, Special Publications January 1, 2008, 298, 413-442.

Mongelli, F., Zito, G., Ciaranfi, N. and Pieri., P., 1989. Interpretation of heat flow density of the Apennine chain, Italy. Tectonophysics, 164, 267-280.

Moore, J., Adams, M., Allis, R., Lutz, S. and Rauzi, S., 2000. Mineralogical and geochemical consequences of the long-term presence of CO2 in natural reservoirs: An example from the Springerville-St. Johns Field, Arizona, and New Mexico, USA. Chemical Geology, 217 (3-4), 365-385. Doi: 10.1016/j.chemgeo.2004.12.019.

Müller, G., Irion, G. and Förstner, U., 1972. Formation and diagenesis of inorganic Ca-Mg carbonates in the lacustrine environment. Naturwissenschaften, 59, 158-164.

NASA, 1995. An exobiological Strategy for Mars Exploration, SP-530. National Aeronautics and Space Administration, Washington, DC.

O'Neil, J.R. and Barnes, I., 1971. C13 and O18 compositions in some fresh-water carbonates associated with ultramafic rocks and serpentinites: Western United States: Geochimica et Cosmochimica Acta, 35, 687-697, doi: 10.1016/0016-7037(71)90067-6.

Olavi Kajander, E., Björklund, M. and Çiftçioglu, N., 1999. Suggestion from observations on nanobacteria isolated from blood. In: Size Limits of Very Small Microorganisms (Proceeding) Space Studies Board and National Research Council, National Academy Press, Washington, DC, 50-55.

Ordònez, S., and Garcia del Cur, M.A, 1983. Recent and Tertiary fluvial carbonates in central Spain. In: J.D. Collinson and J. Lewin (Editors): Ancient and Modern Fluvial Systems. Int. Assoc. Sedimentol., Spec. Publ., 6: 485-497.

Özkul, M., Varol, B. and Alçiçek, M. C., 2002. Depositional environments and petrography of the Denizli travertines. Bulletin of the Mineral Research and Exploration, 125, 13-29.

Pasquarè, G., Chiesa, S., Vezzoli, L. and Zanchi, A., 1983. Evoluzione paleogeografica e strutturale di parte della Toscana meridionale a partire dal Miocene superiore. Mem. Soc. Geol. Ital., 25, 145-157.

Pazdur, A., Drobrowolski, R., Durakiewicz, T., Piotrowska, N., Mohanti, M., Das, S., 2002. d13C and d18O time record and palaeoclimatic implications of the Holocene calcareous tufa from south-eastern Poland and eastern India (Orissa). Geochronometria 21, 972108.

Peccerillo, A. and Manetti, P., 1985. The potassium alkaline volcanism of central-southern Italy: a review of the data relevant to petrogenesis and geodynamic significance. Trans. Geol. Soc. S. Afr., 88, 379-394.

Peccerillo, A., 2003. Plio-Quaternary magmatism in Italy. Episodes 26 (3), 222–226.

Pécsi, M., Scheuer, G. and Schweitzer, F., 1982. Geomorphological position and chronological classification of Hungarian travertines, in: M. Pécsi (ed.), Quaternary Studies in Hungary, Geographical Research Institute, Budapest (Hungarian Academy of Sciences), 117-133.

Pedley, H.M., 1987. The Flandrian (Quaternary) Caerwys tufa, North Wales: an ancient barrage tufa deposit, Proc. Yorks. Geol. Soc., 46, 141–152.

Pedley, H.M., 1990. Classification and environmental models of cool freshwater tufas. Sedimentary Geology, 68, 143-154.

Pedley, H.M., 2009. Tufas and travertines of the Mediterranean region: a testing ground for freshwater carbonate concepts and developments. Sedimentology, 56, 221-246.

Pedley, H. M., 2000. Ambient temperature freshwater microbial tufas. In: Riding, R.E., Stanley, M.A. (Eds), Microbial Sediments. Springer-Verlag, Berlin, 179–185.

Pedley, H.M., Hill, I., Denton, P. E, Brasington J., 2000. Three-dimensional modelling of a Holocene tufa system in the Lathkill Valley, north Derbyshire, using ground-penetrating radar. Sedimentology 47, 721-737.

Pedley, M. and Hill, I., 2003. The recognition of barrage and paludal tufa systems by GPR: case studies in the geometry and correlation of Quaternary freshwater carbonates. In: Ground Penetrating Radar in Sediments (Eds C.S. Bristow and H.M. Jol), Geol. Soc. (London), Spec. Publ., 211, 207–223.

Pedley, M., Rogerson, M., and Middleton, R. 2008. Freshwater calcite precipitates from in vitro mesocosm flume experiments: a case for biomediation of tufas. Sedimentology doi: 10.1111/j.1365-3091.2008.00983.x

Pentecost, A. and Viles, H.A., 1994. A review and reassessment of travertine classification. Géogr. Phys. Quatern., 48, 305–314.

Pentecost, A. and Coletta, P., 2007. The role of photosynthesis and CO2evasion in travertine formation: a quantitative investigation at an important travertine-depositing hot spring, Le Zitelle, Lazio, Italy. Journal of the Geological Society, London, 164, 843-853.

Pentecost, A., 1990. The formation of travertine shrubs: Mammoth Hot Springs, Wyoming. Geological Magazine, 127, 159.

Pentecost, A., 1995a. The Quaternary travertine deposits of Europe and Asia Minor, Quaternary Science Reviews, 14, 1005–1028.

Pentecost, A., 1995b. The microbial ecology of some Italian hot-spring travertines, Microbios, 81, 45–58.

Pentecost, A., 1996. Moss growth and travertine deposition: the significance of photosynthesis, evaporation and degassing carbon dioxide. Journal of Bryology, 19, 229-234.

Pentecost, A., 2005. Travertine. Springer-Verlag, Berlin.

Pentecost, A., and Lord, T., 1988. Postglacial tufas and travertines from the Craven District of Yorkshire. Cave Sci., 15(1), 15-19.

Pentecost, A., Bayari, S. and Yesertener, C., 1997. Phototrophic microorganisms of the Pamukkale travertine Turkey: their distribution and influence on travertine deposition. Geomicrobiol. J., 14, 269–283.

Perri E., Tucker, M.E and Spadafora, A. 2012. Carbonate organo-mineral micro- and ultrastructures in sub-fossil stromatolites: Marion lake, South Australia. Geobiology, 10, 105–117.

Perri, E. and Spadafora, A., 2011. Evidence of microbial biomineralization in modern and ancient stromatolites. In: Tewari, V., Seckbach, J. (Eds.), Stromatolites: Interaction of Microbes with Sediments: Cellular Origin, Life in Extreme Habitats and Astrobiology. Springer, 633–649.

Perri, E., Tucker, M., 2007. Bacterial fossils and microbial dolomite in Triassic stromatolites. Geology 35, 207–210

Platt, N.H. and Wright, V.P., 1992. Palustrine carbonates and the Florida Everglades; towards an exposure index for the fresh-water environment? Journal of Sedimentary Research, 62, 1058-1071.

Poli, G., Peccerillo, A., Donati, C., 2002. Genesis of Miocene–Quaternary acid rocks form the Tuscan Magmatism Province: some implications for structure of the Apennine lithosphere. Boll. Soc. Geol. It. Spec. 1, 129–140.

Popa, R., Kinkle, B.K. and Badescu, A., 2004. Pyrite framboids as biomarkers for iron–sulfur system. Geomicrobiol. J., 21, 193-206.

Popp, B.N. and Wilkinson, B.H., 1983. Holocene lacustrine ooids from Pyramid Lake, Nevada. In: Peryt, T.M. (Ed.), Coated Grains. Springer, Berlin, 142-153.

Rainey, D.K and Jones, B., 2009. Abiotic versus biotic controls on the development of the Fairmont Hot Springs carbonate deposit, British Columbia, Canada. Sedimentology, doi: 10.1111/j.1365-3091.2009.01059.x

Reid, R.P., Visscher, P.T., Decho, A., Stolz, J.K., Bebout, B.M., Dupraz, C., MacIntyre, I.G., Paerl, H.W., Pinchney, J.L., Prufert-Bebout, L., Steppe, T.F. and Des Marais, D.J., 2000. The role of microbes in accretion, lamination and early lithification of modern marine stromatolites. Nature, 406, 989-992.

Renaut R.W, Morley C.K, and Jones B., 2002. Fossil hot spring travertine in the Turkana Basin Northern Kenya: structure, facies and genesis. In: Renaut, R.W. and. Ashley (eds.), G.M., Sedimentation in Continental Rifts, SEPM Special Publication 73, 123-141.

Renaut, R.W. and Jones, B., 1996. Controls On Aragonite And Calcite Precipitation In Hot Spring Travertine At Chemurkeu, Lake Bogoria, Kenya: Canadian Journal Of Earth Sciences, 34, 801-818.

Renaut, R.W., Jones, B., 2000. Microbial precipitates around continental hot springs and geysers. In: Riding, R.E., Awramik, S.M. (Eds), Microbial Sediments. Springer, Berlin, 1872195.

Riding, R., 1991. Classification of microbial carbonates. In: Calcareous Algae and Stromatolites (Ed. R. Riding), Springer-Verlag, New York, 21-51.

Riding, R., 2000. Microbial carbonates: the geological record of calcified bacterial-algal mats and biofilms. Sedimentology 47, 179–214.

Riding, R., 2002. Structure and composition of organic reefs and carbonate mud mounds: concepts and categories. Earth-Science Reviews, 58, 163-231.

Riding, R., 2002a. Structure and composition of organic reefs and carbonate mud mounds: concepts and categories. Earth Science Reviews 58, 163–231.

Riding, R., 2002b. Biofilm architecture of Phanerozoic cryptic carbonate marine veneers. Geology 30, 31–34.

Riding, R., 2008. Abiogenic, microbial and hybrid authigenic carbonate crusts: components of Precambrian Stromatolites. Geologia Croatica 61/2-3, 73-103.

Riding, R., 2009. An atmospheric stimulus for cyanobacterial bioinduced calcification ca. 350 million years ago? Palaios, 24, 685-696.

Riding, R., 2009. Microbialites, stromatolites, and thrombolites. In J. Reitner and V. Thiel (eds), Encyclopedia of Geobiology. Encyclopedia of Earth Science Series, Springer, Heidelberg, 635-654.

Riding, R., 2010. The Nature of Stromatolites: 3,500 Million Years of History and a Century of Research. In Advances in Stromatolite Geobiology (eds Reitner J et al..). Lecture Notes in Earth Sciences, 131, 29–74.

Riding, R., 2011. Microbialites, stromatolites, and thrombolites. In Encyclopedia of Geobiology (eds Reitner J, Thiel V), Encyclopedia of Earth Science Series, Springer, Heidelberg, 635–654.

Riding, R. and Liang, L., 2005. Geobiology of microbial carbonates: metazoan and seawater saturation state influences on secular trends during the Phanerozoic. Palaeogeography, Palaeoclimatology, Palaeoecology, 219, 101-115.

Riding, R and Tomàs, S, 2006. Stromatolite reef crusts, early cretaceous, Spain: bacterial origin of in situ-precipitated peloidmicrospar? Sedimentology 53, 23–34.

Rozenbaum, A.G., Zilberman, E., Bar-Matthews, M., Ayalon, A., Agnon, A., 2005. Tufa deposits in the Bet Shean Valley- stratigraphic analysis of the tufa plateau.Geological Survay of Israel.

Sagri, M., Martini, I.P. and Pascucci, V., 2004. Sedimentology and tectonic evol.ution of selected Neogene-Quaternary basins of the Apennines (Italy). Field Trip Guide Book P15. In: Field Trip Guide Books, 32nd International Geological Conference, Florence 20–28 Agosto 2004 (Eds L. Guerrieri, I. Rischia and L. Serva). Memorie Descrittive della Carta Geologica d'Italia, 14-36, 63(4), 1-46.APAT, Roma.

Sanz-Montero, M.E., Rodríguez-Aranda, J.P., and Calvo, J.P., 2006. Mediation of endoevaporitic microbial communities in early replacement of gypsum by dolomite: a case study from Miocene lake deposits of the Madrid Basin, Spain. Journal of Sedimentary Research, 76, 1257–1266.

Sanz-Montero, M.E., Rodríguez-Aranda, J.P., and García del Cura, M.A, 2009. Bioinduced precipitation of barite and celestite in dolomite microbialites. Examples from Miocene lacustrine sequences in the Madrid and Duero Basins, Spain. Sedimentary Geology 222, 138–148.

Schneider, J., Schröeder, H.G, 1983. Le Campion-Alsumard Th., In Peryt, T. M.(Editor) Coated Grains. Springer- Verlag Berlin Heidelberg, 284-298.

Seong-Joo, L., Browne, K.M. and Golubic, S., 2000.On stromatolite lamination. In : Riding R.E and Awramik S.M (Eds). Microbial sediments. Springer-Verlag Berlin Heidelberg.

Serri, G., Innocenti, F., Manetti, P., 1993. Geochemical and petrological evidence of the subduction of delaminated Adriatic continental lithosphere in the genesis of the Neogene-Quaternary magmatism of central Italy. Tectonophysics 223, 117-14.

Shipton Z.K., Evans, J.P., Kirschner, D., Kolesar, P.T., Williams, A. P., Healt, J., 2004. Analysis of CO2 leakage through 'low-pearmeability' faults from naturals reservois in the Colorado Plateau, east-central Utah. In: Geological Storage of Carbon Dioxide (eds Baines S.J, Worden RH), Geological Society of London Special Pubblication, 233, 43.58.

Smith, A.J., 1982. Modes of cyanobacterial carbon metabolism. In : Carr N.G., Whitton B:A. (Eds). The biology of cyanobacteria. Blackwell, Oxford. Bot Monogr 19, 47-85.

Soligo, M., Tuccimei, P., Barberi, R., Delitala, M.C., Miccadei, E. and Taddeuci, A., 2002. U/Th dating of freshwater travertine from Middle Velino Valley (Central Italy): paleoclimatic and geological implications, Palaeogeogr. Palaeoclim. Palaeoecol., 184, 147–161.

Spadafora, A., Perri, E., McKenzie, J.A., Vasconcelos, C., 2010. Microbial biomineralization processes forming modern Ca:Mg carbonate stromatolites. Sedimentology 57, 27–40.

Spiro, B. and Pentecost, A., 1991. One day in the life of a stream – a diurnal inorganic carbon mass balance for a travertine-depositing stream (Waterfall Beck, Yorkshire), Geomicrobiol. J., 9, 1–11.

Sprachta, S., Camoin, G., Golubic, S., Le Campion, T., 2001. Microbialites in a modern lagoonal environment: nature and distribution (Tikehau atoll, French Polynesia). Palaeogeography, Palaeoclimatology, Palaeoecology 175, 103–124.

Stirn, A. 1964. Kalktuffvorkommen und Kalktufftypen der Schwabischen Alb. Abh. Karst HoeShlenknd., E, 1-91 pp. structural, hydrologic and paleoclimatic implications. Earth Planet Sci Lett 203:709–728. doi:10.1016/S0012-821X(02)00875-0.

Stumm, W. and Morgan, J.J., 1996. Aquatic Chemistry. 3rd Edn., New York (J. Wiley and Sons).

Symoens, J.J. and Van der Werff, A. 1951. Note sur les formations de tuf calcaire des environs de Consdorf (Grand DucheÂ du Luxembourg). Bull. Soc. Roy. Bot. Belgique, 83, 213±218.

Tekin, E., Kayabalı, K. and Ayyıldız, T., 2000. Evidence of microbiologic activity in modern travertines: Sıcakgermik geothermal field, central Turkey: Carbonates and Evaporites, 15, 19-27.

Tucker, M. E., 1981, Sedimentary Petrology: An Introduction: New York, John Wiley and Sons (Halsted Press), 252.

Tucker, M.E. and Wright, W.P, 1990. Carbonate Sedimentology . London, Blackwell

Turi, B., 1986. Stable isotope geochemestry of travertines. In: P. Fritz and J.C. Fontes (Eds) - Handbook of Environmental Isotope Geochemestry. 2. Terrestrial Environment, B. Elsevier, Amsterdam, 207-238.

Turner, E.C., Jones, B., 2005. Microscopic calcite dendrites in cold-water tufa: implications for nucleation of micrite and cement. Sedimentology, 52, 1043–1066.

Usdowski, E., Hoefs, J. and Menschel, G., 1979. Relationships between “C and “0 fractionation and changes in major element composition in a recent calcite-depositing spring: a model of chemical variations with inorganic CaCO, precipitation. Earth Planet. Sci. Lett., 42, 267-276.

Vai, G.B. and Martini, I.P., 2001. Geomorphologic setting. In: Anatomy of an Orogen: the Apennines and adjacent Mediterranean basin (G.B. Vai and I.P., Martini Eds.). Kluwer Academic Publishers, Dordrecht, 1-4.

Van Lith, Y., 2001. The role of sulphate-reducing bacteria in dolomite formation: a study of a Recent environment, bacterial cultures, and dolomite concretions. PhD Thesis, Geological Institute, Swiss Federal Institute of Technology, ETH, Zürich, Switzerland.

Van Lith, Y., Warthmann, R., Vasconcelos, C. and McKenzie, J.A., 2003b. Microbial fossilization in carbonate sediments: a result of the bacterial surface invol.vement in dolomite precipitation. Sedimentology, 50, 237–245.

Vasconcelos, C, McKenzie, J.A, Bernasconi, S., GrujicD, Tien, A.J, 1995. Microbial mediation as a possible mechanism for dolomite formation. Nature 377, 220–222.

Vàzquez-Urbez, M., Arenas, C., Sancho, C., Osàcar, C., Auqué, L. and Pardo, G., 2009. Factors controlling present-day tufa dynamics in the Monasterio de Piedra Natural Park (Iberian Ranges, Spain): depositional environmental settings, sedimentation rates and hydrochemistry. International Journal of Earth Sciences, 99, 1027–1049.

Verwer, K., Eberli, G.P., and Weger, R.J, 2011, Effects of pore structure on electrical resistivity in carbonates: AAPG Bulletin, 95/2, 175-190.

Visscher, P.T, Stolz, J.F, 2005. Microbialmats as bioreactors: populations, process, and products. Palaeogeography, Palaeoclimatology, Palaeoecology 219, 87–100.

Weed, W.H., 1889a. The formation of travertine and siliceous sinter by the vegetation of hot springs, Ann. Report. U.S. Geol. Surv. 1887–1888, 9, 619–676.

Weed, W.H., 1889b. The diatom marshes and diatom beds of the Yellowstone National Park, Bot. Gaz., 14, 117–120.

Weed, W.H., 1889c. On the formation of siliceous sinter by the vegetation of thermal springs, Am. J. Sci., 37, 351–359., D.F. 1984. Towars a new oxygen isotope chronostratigraphy of early to middle Pleistocene deep-sea sediments (abstract). Geological Society of America Abstracts with Program, 6, 6.

Winsborough, B.M., 2000. Diatoms and benthic microbial carbonates. In: Riding, R.E., Stanley, M.A. (Eds), Microbial Sediments. Springer-Verlag, Berlin, 76–83.

Wolicka, D. and Borkowski, A., 2008. Participation of sulphate reducing bacteria in formation of carbonates. International Kalkowsky-Symposium Göttingen, Germany. Abstract Vol.ume (Göttingen University Press) Special Vol.ume in a Geobiological Journal, 130-131.

Wray and Daniels, 1957. Precipitation of calcite and aragonite, J Amer. Chem. S oc.. 79. 2031-2034.

Wright V. P.,1992. A revised classification of limestones. Sedimentary Geology, 76, 177-185

Yagiz, S., 2010. Geomechanical properties of construction stones quarried in South-western Turkey. Scientific Research and Essays, 5(8), 750-757.

Yoshimura, K., Liu, Z., Cao, J., Yuan, D., Inokura, Y. and Noto, M., 2004. Deep source CO2 in natural waters and its role in extensive tufa deposition in the Huanglong Ravines, Sichuan, China, Chem. Geol., 205, 141–153.

Zanchi, A. and Tozzi, M., 1987. Evol.uzione paleogeografica e strutturale recente del bacino del Fiume Albegna (Toscana meridionale). Geologica Rom., 26, 305-325.

Zhang, D.D., Zhang, Y., Zhu, A. and Cheng, X., 2001. Physical mechanisms of river waterfall tufa (tra vertine) formation. Journal of Sedimentary Research, 7, 205-216

Zhang, C.L, Huang, Z., J. Cantu,Pancost R.D, BrigmonR.L, LyonsT. W., Sassen R, 2005. Lipid Biomarkers and Carbon Isotope Signatures of a Microbial (Beggiatoa) Mat Associated with Gas Hydrates in the Gulf of Mexico. Applied and Environmental Microbiology, 71, 2106-2112